Universitat Autònoma de Barcelona

TUNING OF THE POLY(P-PHENYLENEVINYLENE) DERIVATIVES EMISSION PROPERTIES BY PHASE CHANGE MATERIALS AND SONOCHEMISTRY

CHRISTIAN BELLACANZONE

Universitat Autònoma de Barcelona

TUNING OF THE POLY(P-PHENYLENEVINYLENE) DERIVATIVES EMISSION PROPERTIES BY PHASE CHANGE MATERIALS AND SONOCHEMISTRY

CHRISTIAN BELLACANZONE

THESIS DIRECTORS

Daniel Ruiz-Molina

Claudio Roscini

TUTOR

Jordi

PROGRAMA DE DOCTORAT EN CIÈNCIA
DE MATERIALS
DEPARTAMENT DE QUÍMICA
FACULTAT DE CIÈNCIES

2018

ICN2 Institut Català de Nanociència i Nanotecnologia

EXCELENCIA SEVERO OCHOA

Table of Contents

To my mother and my wife

for their continuous support

ABSTRACT

Conjugated polymers (CP) are interesting materials with peculiar optoelectronic properties which make this class of polymers good candidate for several applications such as OLEDs, organic photovoltaics, but also for bioimaging and drug delivery. In the last decades, increasing attention has been directed to the tuning of the emission properties of CP to fully exploited their application in several fields. The aim of this thesis work is to achieve a fine emission tuning of a polyphenylene vinylene (PPV) derivatives. Two main strategies have been adopted. I) Nanoparticles of PPV oligomers with different conjugation length was obtained through sonochemical synthesis. Ultrasound irradiation of PPV polymer heterogenous solution was employed to induce the activation of radical species which cut the polymer chain forming PPV oligomers. The copresence of surfactant leads to a simultaneous nanostructuration of such oligomers producing water-soluble nanoparticles which exhibited a progressive hypsochromic shift of absorption/emission compared to the parental polymer. These nanoparticles that emitted in a wide range of the visible electromagnetic spectrum are promising materials for application such as polymers LEDs and bioimaging. II) The PPV polymers and oligomers were mixed with phase change materials with different melting point. Upon heating, solid-to-liquid phase transition is induced in the PCM/PPV system and its fluorescence is blue shifted. Once the system is cooled down the initial emission is recovered. Such system could be applied as multicolour emitting temperature sensor, or for thermoregulated white organic light emitting diode, thanks to the red, green and blue emission of the PPV derivatives obtained in this work.

RESUMEN

Los polímeros conjugado (CP) son un material muy interesante con propiedades optoelectrónicas peculiares que hacen de estos polímeros óptimos candidatos por distintas aplicaciones cuáles OLEDs y celdas organicas fotovoltaicas y también por bioimagen y liberación de fármacos. En los últimos años creciente atención se ha dirigido hacía la modulación de las prioridades ópticas de los CP para poderlos emplear en distintos ámbitos. El objetivo de este trabajo es de lograr un ajuste fino de la emisión de los derivados de polifenileno vinileno (PPV) . Dos estrategias principales se han adoptados. I) Nanoparticulas de oligomeros de PPV con distintas longitudes de conjugación se han producido mediante síntesis sonoquímica. La irradiación con ultrasonidos ha sido aplicada a una solución heterogénea de polímero PPV para inducir la activación de especies radicales que rompen los enlaces doble del polímero cortándolo y generando oligomeros de PPV. La copresencia de un tensioactivo dirige la simultánea nanostructuración de los oligomeros generando nanoparticulas soluble en agua que presentan un progresivo cambio hipsocrómico de las bandas espectrales en absorción y emisión comparado con el polímero inicial. Tal nanoparticulas pueden ser utilizadas en OLEDs y bioimagen. II) los oligomeros y el polímero de PPV fueron mezclados con materiales a cambio de fase de distinto punto de fusión. Cuando tal sistema mixto es calentado, se induce la transición de solido a liquido en el PCM provocando un cambio de fluorescencia hacía el azul. Una vez que el sistema se enfríe y solidifica la emisión inicial es recuperada. Semejante sistema se puede utilizar por la fabricación de sensores de temperatura florecientes y multicolores. También podrías destinar a la realización de diodos orgánico de luz blanca termoregulados aprovechando de la emisión roja, verde y blue de los oligomeros obtenidos en este trabajo

CHAPTER

1

INTRODUCTION

1.1.BRIEF HISTORY OF CONJUGATED POLYMERS

The story of conducting polymers (CP) dates back to the 70s thanks to the pioneering work of Alan MacDiarmid, Alan J. Heeger and Hideki Shirakawa, who were recognized with the Nobel Prize in Chemistry (year 2000). In fact, the discovery of electric conduction in polyacetylene was a fortunate confluence of circumstances mixing an accidental discovery with a suitable scientific collaboration. In 1975 MacDiarmid and Heeger were both collaborators at the University of Pennsylvania working on polymeric sulfur nitride $(SN)_x$, an unusual polymer exhibiting electrical properties. This same year, MacDiarmid gave a talk at the Tokyo Institute of Technology (Japan) where he had the chance to meet Shirakawa. At that time and by mistake, scientists at Shirakawa's group had added too much Ziegler-Natta catalyst to a polymerisation reaction of acetylene resulting in pieces of a silvery polyacetylene film, instead of the usual black powder found most often. Attracted by the metallic sheen of the film characteristic of electrical conductors, MacDiarmid immediately invited Shirakawa to the University of Pennsylvania for a year to work with him and Heeger on conductive polymers. Here started a very successful collaboration. MacDiarmid and Heeger, had already discovered that the addition of bromine atoms in a doping procedure similar to that used in silicon transistor increased 10-fold the conductivity of $(SN)_x$. Therefore, they applied the same procedure to Shirakawa's polyacetylene, which is an organic polymer unlike $(SN)_x$ that however showed an increase in conductivity 10 million times higher than before doping. From here, the relevance of conductive polymers is well-known.

Initially, there were suggestions to replace (copper) electrical wiring in the different applications, from printed circuit boards to home, and even grid, power distribution with inexpensive, light-weight polymeric conductors. With the time, the "plastic" semiconductors showed up some issues of processability, limits on conductivity, and environmental stability. Nevertheless, conducting polymers were employed in some industrial applications, for example, as the antistatic coating in the roll-to-roll processing of polymer webs. Photographic film is an excellent example of the latter application and is the reason why Bayer initiated, in conjunction with Agfa, their development of series of products (Baytron) based on poly(ethylene dioxythiophene) (PEDOT) doped with poly(styrene sulphonate) (PSS). H. C. Starck Corp. currently markets PEDOT-PSS as their Clarion line of conductive coatings.

In the 90s the emphasis shifted to the optical properties exhibited by undoped conjugated polymers, which are often highly coloured and fluorescent, since there is typically large

oscillator strength in their HOMO–LUMO transition. In 1990, the group of R. Friend at University of Cambridge was investigating the electro-optical response of poly(phenylene vinylene) (PPV). They applied a dc voltage to a sandwich-structured device containing PPV film as active layer observing for the first time the electroluminescence of a conjugated polymer.[1] The publication of this observation spawned an enormous worldwide research effort to optimise the materials and device structures (polymer light-emitting diodes or PLEDs) for use in flat-panel displays and lighting.

Simultaneously, conjugated polymers were also investigated for solar-energy conversion. The photon of the solar radiation is absorbed by the polymer generating an exciton (a bound electron-hole pair). This exciton does not readily dissociate to create free electron and hole (contrary to what happen in inorganic semiconductors), because the exciton binding energy in the conjugated polymer is a tenth of an electronvolt, many times larger than the thermal energy (kT) at ambient temperature. Since the electron and the hole must be separated in order to generate electricity in the solar cell, a second organic semiconductor is added in the active layer of the organic photovoltaic devices. In this way, the exciton bond is broken thanks to the favourable electron transfer from the conjugated polymer (the electron donor material) to the second semiconducting organic material (the electron acceptor material), which must have an energetically lower lying LUMO-level. The separated charges (the electron and the hole) are subsequently collected at the electrodes of opposite polarities. Sariciftci *et al.* realised the first conjugated polymer based photovoltaic cells, using the fullerene C_{60} as acceptor material and the conjugated polymer polyl-2-methoxy, 5-(2'-ethyl-hexyloxy)-p-phenylenevinylene] (MEH-PPV) as donor material.[2] Also in this successful story, the collaboration within scientists had a crucial role. Sariciftci was studying the possibility to use the conducting polymer for the conversion of solar energy into electricity, and he asked his colleague Fred Wudl for a compound to use as acceptor material. By pure chance, Wudle was working on fullerene molecules, which are very good electron acceptors. Therefore, he opened his drawer and gave Sariciftci a black powder, saying: “take it! This is a great electron acceptor. You will like it. It looks just like a soccer ball.” (cit. Sariciftci).[3] To date, fullerene compounds are still widely employed in organic solar cells since no better alternatives have been found.

Since this pioneer works, the conjugated polymers have been applied in several fields, from energy to biology, and devices such as field effect transistors, electrochromic panels, charge storage devices, actuators, biosensors and lab-on-chip systems.

1.2. CHEMICAL STRUCTURE AND PROPERTIES OF CONJUGATED POLYMERS

In common polymers, such as polyethylene (PE), carbon atoms have a sp^3 hybridisation with C-atoms forming four strong σ-bonds. Accordingly, the electronic structure consists mainly of bonding and antibonding molecular σ and σ* orbitals, which present large energy gap. This difference explains why the common polymer materials are electrically insulating, and generally do not absorb visible light. On the contrary, conjugated polymers exhibit unsaturated carbon atoms. The strong bonds that form the molecular backbone arise from sp^2 hybridised atomic orbitals of adjacent carbon atoms that overlap yielding a bonding and anti-bonding molecular σ and σ* orbitals. The remaining atomic p_z orbitals overlap to a lesser degree, so that the resulting molecular π and π* orbitals possess less bonding or anti-bonding character, thus forming the frontier orbitals of the molecule that accounts for the optical absorption of the conjugated polymers in the visible part of the spectra. Neutral excited states can be formed for instance by light absorption of a molecule, when an electron is promoted from the HOMO to the LUMO. In general, any configuration with an additional electron in an antibonding orbital and a missing electron in a bonding orbital, i.e., a hole, corresponds to a neutral excited state. Due to the low relative dielectric constant in the organic semiconductors (on the order of $\varepsilon \approx 3$), Coulomb attraction between electron and hole is strong, resulting in an exciton binding energy ranging from of 0.5 eV to more than 1 eV. As it happens in smaller molecules, once the electron is promoted to the LUMO, it can maintain the spin it had in the HOMO, generating a singlet excited state (S). Molecular orbital diagrams corresponding to the configurations in the ground or neutral excited states are shown in Figure 1.1.

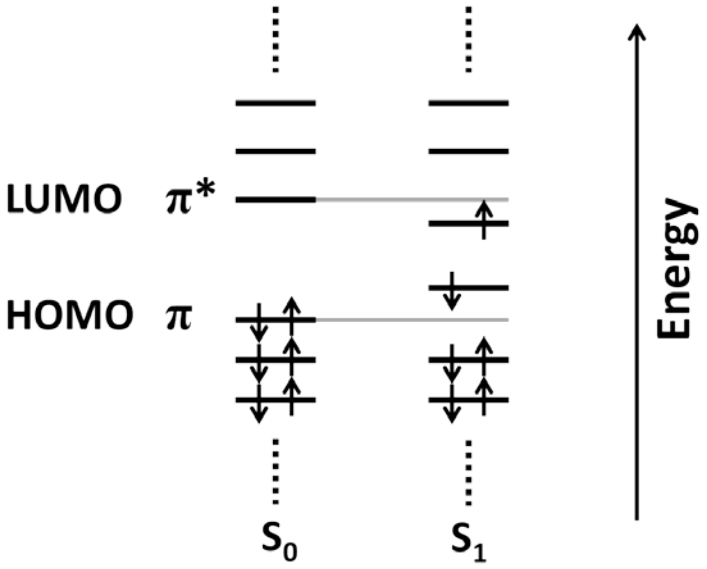

Figure 1.1. Molecular orbital diagram showing the electronic configuration for the ground state (S_0), for the first spin-singlet excited state (S_1). The arrows indicate the electron spin, and the thin horizontal grey line indicates the HOMO and LUMO boundary.

1.2.1. Chemical structure

The peculiar properties of conducting polymers are mainly derived from the conjugated structure of the polymer backbone, where the π-electrons delocalise over the whole polymer chain. The backbone of such polymers can have different molecular structures, ranging from the linear chain of polyacetylene to more complex aromatic units, as in the copolymers of poly(2,7-carbazole) derivatives. In Figure 1.2 are reported the constitutive units of the most representative conjugated polymers. Worth to mention, the introduction of heteroatoms in the structure, as for instance sulfur in polythiophene, has also a significant impact in the optical and photophysical properties of the conjugated polymers. The electron-withdrawing or electron-donating abilities of such groups lead to the modulation of the HOMO and LUMO energy levels of a conjugated system. Furthermore, the side chains of the aromatic units are also critical to both control the solubility of the resulting polymers and modulate the optical properties by determining the polymer conformation and/or inter-/intramolecular interactions.

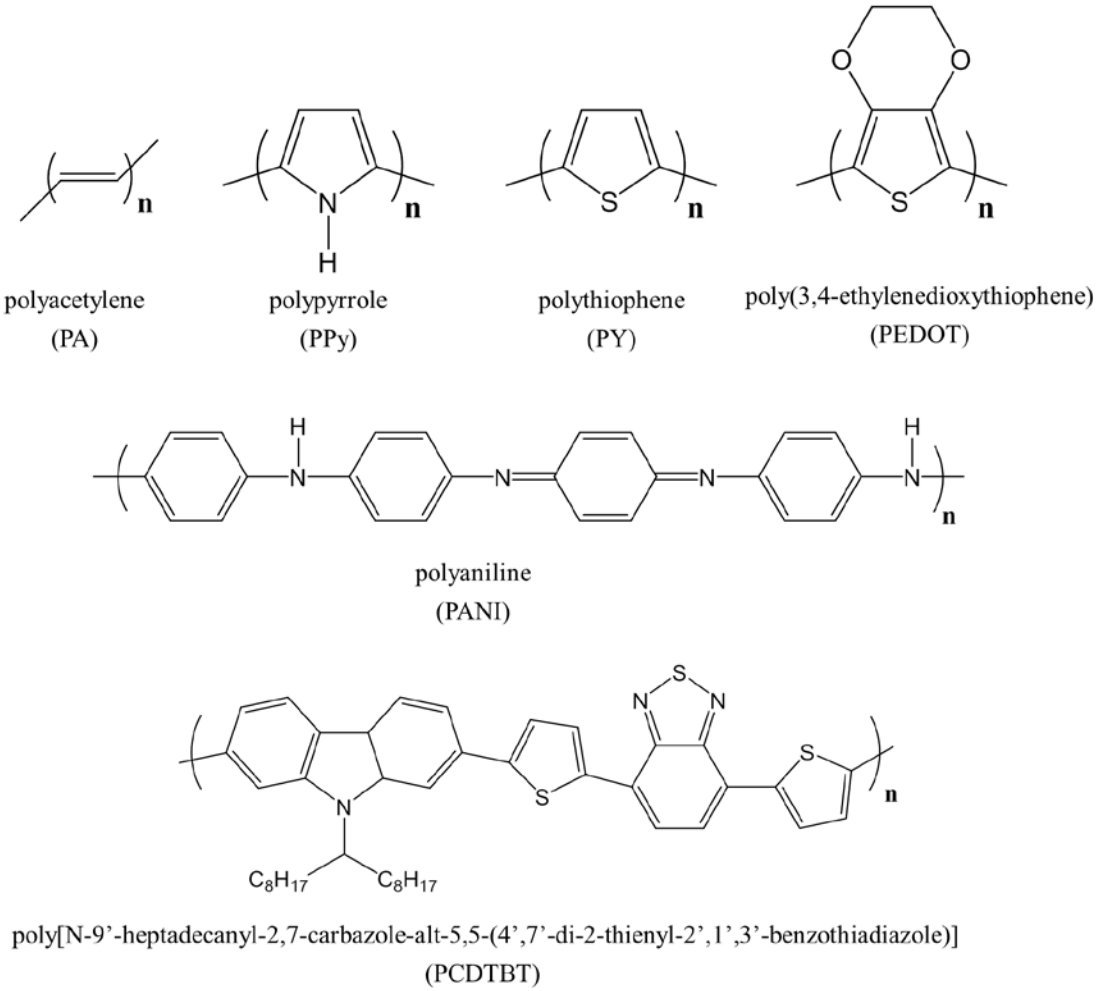

Figure 1.2. Chain structure of several representatives conjugated polymers.

1.2.2. Optical properties

In an ideal conjugated polymer delocalisation of the π-electrons should take place along the whole polymer chain. However, a more realistic picture entails the subdivision of the polymer in short conjugated segments, called chromophores, where the π-electrons are delocalised. These segments contain several monomer units with a distribution of conjugation lengths, and therefore energies, that arise from the presence of defects such as twist and kinks of the polymer chain. The distribution of chromophore energies creates an electronic band structure, where the HOMO and LUMO correspond to the valence and conduction bands, respectively. For this reason, the π-π* transition in a conjugated polymer is often referred to as band gap (E_g), and the conjugated polymer is considered to behave like one-dimensional semiconductors.[4] The E_g values of most conjugated polymers are in the range 1.5–3.0 eV, therefore, these polymers are organic semiconductors.

Comprehensive studies on the nature of these chromophores are present in literature with the aim to understand the photophysical processes which control the optical properties of the conjugated polymers. Numbered of theoretical and experimental works have been reported using polyphenylenevinylene (PPV) derivatives as a model. Oligomers of PPV with a defined number of monomeric units have been synthesised and studied, confirming that the absorption spectra shifts to higher energies on decreasing the number of monomeric units. Figure 1.3 reports the theoretically calculated UV-vis spectra for the different chain length of the MEH-PPV oligomers and the corresponding HOMO-LUMO gap.[5]

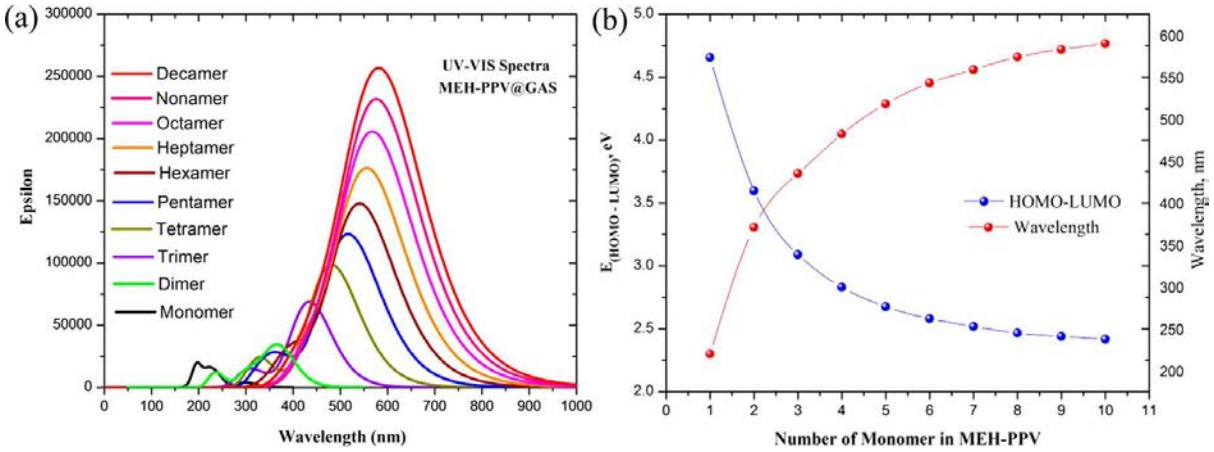

Figure 1.3. *a)* Theoretically calculated UV–vis spectra and *b)* HOMO–LUMO gap with absorption maxima wavelength for the different chain length of MEH–PPV oligomer. [5]

To explain such behaviour it is essential to understand the electronic structure and optical excitation of the corresponding phenylene vinylene units. With this aim, the chemical structure of the repetitive unit and a sketch of the distribution of the π-electrons is shown in Figure 1.4. The resonance interaction between the π bonds (the conjugation) results in delocalised π-electron states, which are occupied by the eight π-electrons of a phenylene vinylene unit. In the ground state, the π-orbital with the eight electrons constitute the HOMO level, while the antibonding π*-orbital constitute the LUMO level, where no electrons are present.

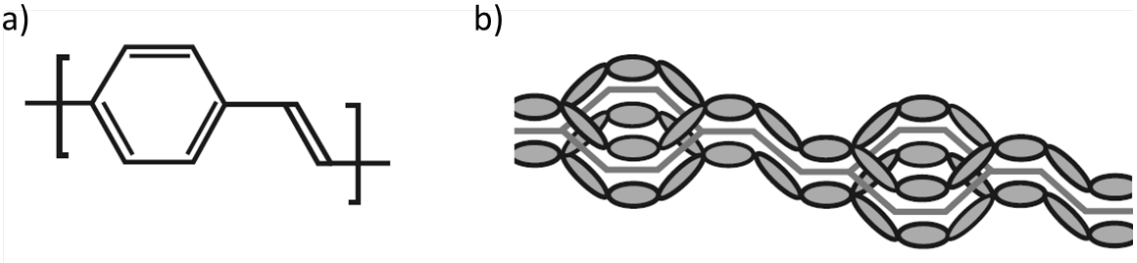

Figure 1.4. *a)* chemical structure of the monomer and *b)* a sketch of the distribution of the π-electrons.[6]

The absorption spectra of Figure 1.3 are assigned to the lowest one-electron excitation from the electronic ground state (S_0) in the HOMO level to an intermediate state, forming an exciton. The attractive Coulomb force between the hole and the electron reduces the excitation energy, which falls below the energy gap.

In order to be optically active, the transition must have which is not the LUMO level. The promotion of the electron creates a positively charged vacation in the HOMO level (hole), as it happens for other molecular electronic transitions, the spin multiplicity must be maintained during the absorption process. Since these polymers have S_0 as ground state, the absorption must produce singlet excited states.[6] As can be seen from the absorption spectra in Figure 1.3a (and the band-gap energy), the energy of the $S_0 \rightarrow S_1$ transition decreases with the increase of the monomers number. This red-shift is due to the extent of the conjugation length over a higher number of monomers units, which results from the continuous interaction between the π-electrons of the coupled monomers. Such interaction further stabilises the π-electrons, and the levels S_1 drop and, as a consequence, the energy difference between S_0 and S_1 is lowered. Thus, in short oligomers, up to a certain number of monomers, the $S_0 \rightarrow S_1$ transition energy is a direct consequence of the number of the constituent monomeric units. However, there is a limit to the energy decrease (usually up to 10-15 monomers) after which further increase of the number of units does not result in more red-shift of the absorption and emission band. This is related to the mobility of the exciton. The absorption of a photon creates an exciton in a monomer unit, which is not stationary, but propagates and could be found on each monomeric unit of the chain with equal probability. This propagation occurs through two mechanism:[7]

I. Singlet exciton with positive electron-hole parity undergo to energy transfer between neighbour monomers through the Förster mechanism.
II. For all the exciton, there is a through bond mechanism where the delocalisation depends on the mean distance between excited electron and hole, which, in

conjugated polymer, typically is of the order of few monomers length. Such distance is lower than the electron-hole distance present in inorganic semiconductors, where the bound pairs is addressed as Mott–Wannier excitons, and larger than the distance observed in molecular crystal (Frenkel excitons).[8]

In a perfectly ordered macromolecule, excitons move like wave packet, according to quantum-mechanical kinetics, and the hole-electron pair together can migrate along the polymer backbone in a so-called coherent motion. This coherent motion of the exciton requires strict phase relationship in space and time, which is perturbed by all deviations from regularity. In conjugated polymer these deviations are always present as a consequence of various defects such as kinks and torsions, inducing the break of the conjugation. The typical extension of regular segments (i.e. sequences without defects) is around ten monomers, and it explains why in the more extended polymers the band-gap is not affected anymore by the number of units.[9] For this reason, the optical properties of conjugated polymers are described in terms of effective conjugation length, which is an estimation of the average chromophores length present in the polymer. Thereby, the absorption of the conjugated polymers is the result of the sum of the absorption of all the chromophores with different effective conjugation length present in the polymer and explain the typical broad absorption band observed in these polymers.

Conjugated polymers are semicrystalline systems, built up of crystalline and amorphous regions, containing a high number of defects. Thus, the coherent mode of motion is only found within ordered crystalline domains with size in the nanometer range. In the conjugated polymer in the solid state, there is an ensemble of domains of varying sizes, ranging from the ordered assemblies of regular chain sequences down to single monomers incorporated in the coiled chain parts in the amorphous regions. In such structures, long-range energy transfer is possible thanks to a slower incoherent exciton motion, described as diffusive hopping process.

The diffusion of the exciton also explains the typical substantial Stokes shift in emission observed in the conjugated polymer. In these polymers, the radiative decay of the excited electron always takes place from the lower energy sites, i.e. chromophores with larger conjugation lengths. Even if the photogeneration of the exciton occurs in chromophores with short conjugation length (high energy), the energy of the exciton is rapidly transferred to longer adjacent chromophores, from where a low energy photon is emitted.

The ability of the exciton to diffuse provides the basis for many conjugated polymers properties, having an important consequence in several applications, such as in photovoltaics. T. Förster first treated the exciton migration.[10] In his model, he derived an analytical expression for the exciton diffusion constant (D) on a lattice of chromophores:[11]

$$D = \eta \left(\frac{4\pi C}{3}\right)^{\frac{4}{3}} \frac{R_0^6}{\tau_{fl}} \quad (1)$$

Where C is the chromophore number density, τ_{fl} is the fluorescence lifetime of the donor in the absence of electronic energy transfer, R_0 is the Förster radius (distance required for the energy transfer to occur), while η is a correction factor that accounts for the molecular details of the system. This equation for D leads to an expression for the diffusion length (L_D):[12]

$$L_D = \sqrt{6D\tau_{fl}} = \sqrt{6\eta}\left(\frac{4\pi C}{3}\right)^{\frac{2}{3}} R_0^3 = 6.36\sqrt{\eta} C^{2/3} R_0^3 \quad (2)$$

Equations 1 and 2 provide a straightforward way to predict the diffusion of electronic excitations through the material using experimentally available quantities such as the overlap of the absorption and fluorescence spectra. Equation 2 suggests that optimising specific material parameters (C, R_0 and τ_{fl}) it would be possible to have L_D values as high as 100 nm, which it would increase the efficiency of devices such as OLEDs or organic photovoltaics.

In real systems, the Förster model breaks down, since most of the materials exhibit a L_D of the order of 5-10 nm. This divergence from the theoretical L_D value can be explained taking in account different effects present in the real systems.

- The first problem concerns the increase of chromophores number (high C values), which can open up new non-radiative pathways that drastically shorten τ_{fl}.[13] The most common imply the formation of low energy, non-radiative aggregate states that act as traps that quench the monomer fluorescence.[14]
- The second difference regards the spatial dependence of the energy transfer coupling between the chromophores. When the chromophores separation approaches the molecular dimensions, the energy transfer rate can be significantly slower than that predicted by Förster theory, due to the point-dipole approximation used in theory.[15]
- The slowdown of the diffusion rate is also affected by the disorder and heterogeneity of the microenvironments, characteristic of these materials. The presence of this disorder produce a more difficult energy transfer events, since the exciton moved to

lower energy sites where its Förster overlapping integral with adjacent high-energy sites decreased.[12]

The presence of such divergences from the model system, affect the exciton diffusion in conjugated polymers, making the elaboration of quantitative models more complicated. However, such models are useful to better understand and control the charge transport in conjugated polymers and, consequently, to improve the performances of these materials for applications such as photovoltaics, OLEDs and OFETs.

Spectral broadening

As shown by Figure 1.3 the oligomers, that could be treated as the chromophores of the conjugated polymers presents an inhomogeneous broadening of the absorption and emission spectra. This universal property of the chromophores originates from the random local variations of the contribution to the transition energy that is governed by the interaction of the excited state with its polarizable environment.

In such molecules, it is expected to see the vibronic structures derived from the transition to different vibrational states of a different electronic state. According to the Franck-Condon principle, upon electronic excitation, the charge distribution of a molecule changes and so do the molecular forces. As a response to that change, the molecular skeleton will vibrate and relax into a new equilibrium configuration. The new equilibrium position is generally shifted of ΔQ respect to the ground state position, as illustrated in Figure 1.6.

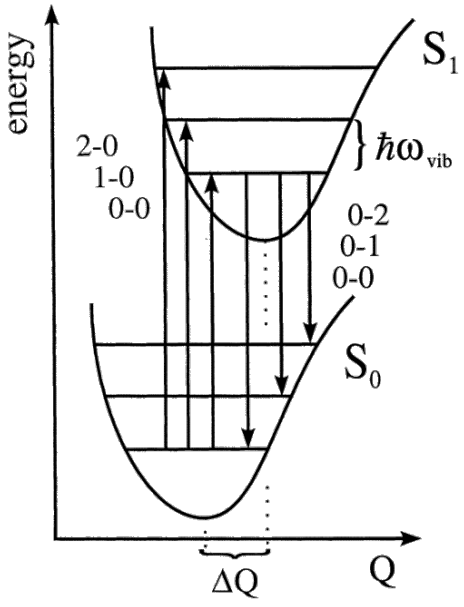

Figure 1.5. Schematic illustration of the Franck Condon principle for absorption $S_0 \rightarrow S_1$ 0-0 and emission $S_1 \rightarrow S_0$ 0-*n*. The configurational displacement ΔQ between S0 and S1 determines the intensity of the particular transitions.

If during the HOMO-LUMO optical transitions there were no readjustment of the bond lengths, which means no displacement of the potential energy curve in the excited state relative to the ground state, only a single absorption lines corresponding to the $S_0^{v=0} \rightarrow S_1^{v=0}$ transitions (0-0 transition) would be allowed due to the orthogonality of the vibrational wave functions.

Since readjustment of the bond lengths takes place, the Huang-Rhys factor is used to describe the strength of the coupling to a single harmonic oscillator of reduced mass M (which is the representation of two body-sytem as single-boody, $M=m_1m_2/(m_1+m_2)$) and angular frequency ω:

$$S = \frac{M\omega}{2\hbar}(\Delta Q)^2 \tag{3}$$

With ΔQ being the displacement of the minima of the potential curve along the configurational coordinate upon electronic excitation. In this case, the absorption spectrum consists of an electronic transition, the $S_0 \rightarrow S_1$ 0-0 vibronic line, followed by a vibronic replica, $S_0 \rightarrow S_1$ $0 \rightarrow n$, whose normalised intensity distribution (I_n), is a Poissonian distribution, mapping the overlap between the vibrational wave functions:

$$I_n = S^n e^{-S}/n! \tag{4}$$

For S > 1 it has a maximum at an energy $S\hbar\omega$ above the electronic origin band. For large values of S, I_n approaches a Gaussian with variance $\hbar\omega S^{1/2}$. Thus, S is a crude measure of the number of vibrations generated when the excited molecule relaxes from its ground state configuration to the new equilibrium configuration in the excited state and $S\hbar\omega$ is the relaxation energy. The value of S can be inferred from:

$$I_{0\rightarrow1}/I_{0\rightarrow0} = S \tag{5}$$

In general, ω is different in the ground and excited states, and potentials are not precisely parabolic, and for large molecules the concomitant modifications in the above scheme are small.

The most important information to consider about an electronic transition is the presence of several vibrational modes that are coupled to such transition. Equations 3 and 4 can be applied to each vibrational mode i associated with the Huang-Rhys factor S_i, the total Huang-Rhys factor being $S=\sum_i S_i$. If a particular vibronic line carries the same intensity as the 0-0 line, the S_i value of that mode would be 1. It should be noted that observing the 0-0 line

in an absorption/emission spectrum is all but a signature of no configurational relaxation occurring. The total relaxation energy is:

$$E^{rel} = \sum S_i \hbar\omega_i \quad (6)$$

Experimental works on π-conjugated molecules in gas phase reveal the structured absorption/fluorescence vibrational spectrum,[16] in accord with the above notion. Contrary, aromatic molecules in a fluid or solid non-crystalline matrix exhibit much broader spectra, with the loss of the fine vibronic structure. Often only a single vibronic feature can be distinguished, which is the convolution of several strong modes such as phenyl ring vibrations.

This loss of the fine vibronic structure can be ascribed to different phenomena:

- The interaction of the excited state dipole with the solvent molecules. Due to the changes in the polymer chains dipole moments after electronic excitation the solvent cage surrounding a chromophore reorganises. The statistical nature of this effect leads to broadening while the relaxation of the solvent cage induces new equilibrium configurations which also generate Stokes shifts in both absorption and emission. In frozen solutions in which solvent molecules are randomly distributed, yet spatially fixed, inhomogeneous spectral broadening reflects the locally varying van der Waals interaction energy of the excited chromophores with the neighbour.[17]
- Another contribution may result from some configurational disorder of the chromophore itself. As already mentioned above, the conjugation in conjugated polymers is interrupted by kinks, twists or local chemical modification, forming segments of varying length. The statistic arrangements of lengths translate into a distribution of transition energies.[18]
- Another reason is the spectral diffusion or relaxation due to either some slow molecular reorganisation occurring even in solid matrices at low temperatures or energy transfer. In a dense ensemble, an excited chromophore will be coupled to its nonexcited neighbours through a strong multipole and exchange coupling. This coupling leads to energy transfer and spectral relaxation because energy transfer is a downhill process.

  Another reason is the spectral diffusion due to the combination of conformational relaxation (some slow molecular reorganisation occurring even in solid matrices at low temperatures) and energy transfer.

All types of the disorder can be superimposed and give rise to an inhomogeneous broadened distribution of site energies, in the ground as well as in the excited states. Absorption and emission spectra map the convolution of both distributions. If their width becomes comparable to the vibrational spacing, vibronic structure of the spectra will be lost. In that case absorption and emission band maxima no longer represent $S_0 \rightleftharpoons S_1$ 0-0 transition energies but rather map the energy dependence of the Franck-Condon factor.

Bathochromic shift of the emission

A further peculiar optical property of the conjugated polymers is the regular bathochromic shift of the fluorescence spectra observed in their solid state, compared to the correspondent bulk solution. Molecular packing critically impacts on the electronic structure of conjugated oligomers and polymers and the resulting luminescence and charge-transport properties. When conjugated polymer chains get in contact, as in the films, excited interchain species are formed. Thus, the exciton finds new electronic pathways through the migration on conjugated segments of other polymers chains resulting in increasing delocalisation of the π– electrons, which lowers the energy of the electronic excited state. This interchain migration is slower than the intrachain migration (which typically occurs in few picoseconds), accounting for the longer lifetimes emission (in the order of the nanoseconds) exhibited by the conjugated polymers film.[19] The presence of interchain electronic species has significant implications on the performance of devices based on these materials: interchain species may be responsible for quenching a conjugated polymer's luminescence but also may be beneficial for promoting charge transport.[20]

The red-shifted emission provides only vague information on the possible interchain species that can form in conjugated polymers. Interchain emission is not always easy to detect because the overlap of the delocalized interchain excited state with the single-chain ground state wave function is usually poor, leading to long radiative lifetimes.[21-22] There is a continuum of possible interchain excited states of different nature, and probably all are possible in the inhomogeneous environment of a conjugated polymer film. For these reasons, the identification of the different interchain species is quite difficult leading to a lot of controversy in the literature about the nature of such species.[23]

1.3.APPLICATIONS OF CP

After a first period (spanning approximately from mid-70s to the 90s) of frenetic activity to gain fundamental knowledge and understanding of conducting polymers, these materials started to find pioneering applications in different fields. First industrial application focused on the antistatic properties with the development of the PEDOT-PPS polymer by the chemical company Bayer AG. The electroactive properties of the conducting polymers were also exploited for anticorrosive coatings, which nowadays represents a significant percentage of the polymer production.[24] Alternatively, conducting polymers were also proposed as electrodes in flexible flat-panel displays by replacing the rigid indium tin oxide (ITO)-coated glass, though the conductivity of the polymers revealed insufficient. However, it was found that a layer of various polyanilines or PEDOT on top of ITO led to improved devices performance and greatly enhanced lifetime. This 'hole-injection layer' is now one of the primary uses of PEDOT-PSS.

Since these seminal applications, the research on conducting polymers has made enormous progress. Intrinsic, i.e. undoped, conjugated polymers are now of great interest thanks to the fine control of their chemistry that minimizes defects and impurities, improving therefore performances and lifetimes. One of the main research lines on these materials regards the development of organic photovoltaic devices. The flexibility, lightweight and low cost of these conducting polymers enhances their use as the active layer in the organic solar cell, reaching nowadays good efficiencies and stabilities, close to those required by the industrial production and commercialisation.[25–27]

Semiconducting polymers are also of use in thin-film organic field-effect transistors (OFETs). The earliest materials examined were polyacetylene, polythiophene and an oligomer of thiophene.[28,29] In these devices, the polymer forms the channel between the source and drain electrodes of the device. The conductance of the channel is proportional to the number of charge carriers and their mobility, being the number of charge carriers modulated by the voltage applied to the gate electrode. Hence, charge-carrier mobility is the primary metric in screening materials for use in OFETs of relevance in applications such as RFID and electronic price tags or electronic paper, among others.

Beyond applications based on the conductive properties of these materials, this family of polymers have also been of relevance on different devices associated to their optical properties. For instance, conjugated polymers are one of the most attractive electrochromic materials used nowadays because of advantages such as high colouration efficiency, rapid

switching ability, and diverse colours.[30] Therefore they are of great relevance in electrochromic devices for smart windows and flexible displays.

In the last decades, many efforts have also been directed towards the development of polymer light emitting diodes (PLED). In the PLED technology the emissive electroluminescent layer is a polymer film, which emits light of particular wavelength (colour) in response to an electric current. The potential advantage of the PLEDs are lightweight, flexibility, low cost, availability of full-spectrum colour displays, high brightness at low drive voltage and good printability.[31] Finally, the high degree of biocompatibility of conducting polymers also makes them particularly interesting materials for biosensing and implantable electrodes. With the recent advance in nanotechnology, water dispersion of conjugated polymer nanoparticles has been synthesised and used as fluorescent probes for cellular detection as well as for photothermal and photodynamic therapy.[32]

Therefore, the interest of semiconductive polymers goes beyond the electronic/electric field, for which they were initially thought and extends to their use in the fabrication optical sensors and devices. However, for this field to be fully mature, several novel studies that allows for an easier, cost-effective, controllable and precise fine-tuning of their optical (absorption and emission properties) has become a real need. Besides all this, the establishment of suitable protocols that allow for their nanostructuration without compromising their properties and characteristics will definitely fuel the number of applications and its integration into devices. This is mainly the objective of the present Thesis, being the resulting micro/nanomaterials used as a proof-of-concept for new fluorescent materials and thermofluorochromic sensors.

1.4.REFERENCES

1. Burroughes, J. H. *et al.* Burroughes1990 Light-emitting diodes based on conjugated polymers.pdf. *Nature* **347,** 539–541 (1990).

2. Sariciftci, N. S., Smilowitz, L., Heeger, A. J. & Wudl, F. Photoinduced Electron Transfer from a Conducting Polymer to Buckminsterfullerene. *Science (80-.).* **258,** 1474–1476 (1992).

3. Perlin, J. Pacific Standard_Inventor of Plastic Solar Cells sees Bright Future. 1–5 (2011). Available at: https://psmag.com/environment/inventor-of-plastic-solar-cells-sees-bright-future-27718.

4. Pakbaz, K., Lee, C. H., Heeger, A. J., Hagler, T. W. & McBranch, D. Nature of the primary photoexcitations in poly(arylene- vinylenes). *Synth. Met.* **64,** 295–306 (1994).

5. Giri, S., Moore, C. H., McLeskey, J. T. & Jena, P. Origin of red shift in the photoabsorption peak in MEH-PPV polymer. *J. Phys. Chem. C* **118,** 13444–13450 (2014).

6. Strobl, G. R. *The Physics of Polymers: Concepts for Understanding Their Structures and Behavior*. (Springer Science & Business Media, 2007). doi:9783540684114

7. Barford, W. Excitons in conjugated polymers: A tale of two particles. *J. Phys. Chem. A* **117,** 2665–2671 (2013).

8. Bässler, H. & Köhler, A. in **312,** 1–65 (Publisher: Springer, Berlin, Heidelberg, 2011).

9. Hu, D. *et al.* Collapse of stiff conjugated polymers with chemical defects into ordered, cylindrical conformations. *Nature* **405,** 1030–1033 (2000).

10. Forster, T. Energiewanderung und Fluoreszenz. *Naturwissenschaften* **33,** 166–175 (1946).

11. Gochanour, C. R., Andersen, H. C. & Fayer, M. D. Electronic excited state transport in solution. *J. Chem. Phys.* **70,** 4254–4271 (1979).

12. Bardeen, C. J. The Structure and Dynamics of Molecular Excitons. *Annu. Rev. Phys. Chem.* **65,** 127–148 (2014).

13. Al-Kaysi, R. O., Sang Ahn, T., Müller, A. M. & Bardeen, C. J. The photophysical properties of chromophores at high (100 mM and above) concentrations in polymers and as neat solids. *Phys. Chem. Chem. Phys.* **8,** 3453–3459 (2006).

14. Schlosser, M. & Lochbrunner, S. Exciton migration by ultrafast Förster transfer in highly doped matrixes. *J. Phys. Chem. B* **110,** 6001–6009 (2006).

15. Krueger, B. P., Scholes, G. D. & Fleming, G. R. Calculation of Couplings and Energy-Transfer Pathways between the Pigments of LH2 by the ab Initio Transition Density Cube Method. *J. Phys. Chem. B* **102,** 5378–5386 (1998).

16. Amirav, A., Even, U. & Jortner, J. Energetics and intramolecular dynamics of the isolated ultracold tetracene molecule in its first excited singlet state. *J. Chem. Phys.* **75,** 3770–3793 (1981).

17. Personov, R., Agranovich, V. M. & Hochstrasser, R. M. *In Spectroscopy and Excitation Dynamics of Condensed Molecular Systems*. (North Holland, 1983).

18. Bässler, H. & Sariciftci, N. *Primary Photoexcitations In Conjugated Polymers : Molecular Exciton Versus Semiconductor Band Model " Edited By N . S . Sariciftci ; ISBN 981-02-2880-5 ; World Scientific Publishing Co . Pte . Ltd ., 1997 Xv + 621 Pages ;* (World Scientific, 1997). doi:10.1080/10587250008031048

19. Samuel, W., Rumbles, G. & Collison, C. J. Efficient interchain photoluminescence in a high-electron-affinity conjugated polymer. *Phys. Rev. B* **52,** 573–576 (1995).

20. Schaller, R. D. *et al.* The nature of interchain excitations in conjugated polymers: Spatially-varying interfacial solvatochromism of annealed MEH-PPV films studied by near-field scanning optical microscopy (NSOM). *J. Phys. Chem. B* **106,** 9496–9506 (2002).

21. Conwell, E. Mean free time for excimer light emission in conjugated polymers. *Phys. Rev. B* **57,** 14200–14202 (1998).

22. Schwartz, B. J. How Chain Conformation and Film Morphology Influence Energy Transfer and Interchain Interactions. *Annu. Rev. Phys. Chem.* **54,** 141–172 (2003).

23. Nguyen, T.-Q., Martini, I. B., Liu, J. & Schwartz, B. J. Controlling Interchain Interaction in Conjugated Polymers: The Effects of Chain Morphologa Exciton-

exciton Annihilation and Aggregation in MEH-PPV. *J. Phys. Chem. B* **104,** 237–255 (2000).

24. DeBerry, D. W. Modification of the Electrochemical and Corrosion Behavior of Stainless Steels with an Electroactive Coating. *J. Electrochem. Soc.* **132,** 1022 (1985).

25. Zhao, W. *et al.* Molecular Optimization Enables over 13% Efficiency in Organic Solar Cells. *J. Am. Chem. Soc.* **139,** 7148–7151 (2017).

26. Hou, J., Inganäs, O., Friend, R. H. & Gao, F. Organic solar cells based on non-fullerene acceptors. *Nat. Mater.* **17,** 119–128 (2018).

27. Machui, F. *et al.* Cost analysis of roll-to-roll fabricated ITO free single and tandem organic solar modules based on data from manufacture. *Energy Environ. Sci.* **7,** 2792–2802 (2014).

28. Horowitz, G., Fichou, D., Peng, X., Xu, Z. & Garnier, F. A field-effect transistor based on conjugated alpha-sexithienyl. *Solid State Commun.* **72,** 381–384 (1989).

29. Ebisawa, F., Kurokawa, T. & Nara, S. Electrical properties of polyacetylene/polysiloxane interface. *J. Appl. Phys.* **54,** 3255–3259 (1983).

30. Cho, S. Il & Lee, S. B. Fast electrochemistry of conductive polymer nanotubes: synthesis, mechanism, and application. *Acc. Chem. Res.* **41,** 699–707 (2008).

31. Bhuvana, K. P. *et al.* Polymer Light Emitting Diodes : Materials , Technology and Device. *Polym. Plast. Technol. Eng.* **0,** 1–17 (2018).

32. Kuehne, A. J. C. Conjugated Polymer Nanoparticles toward In Vivo Theranostics - Focus on Targeting, Imaging, Therapy, and the Importance of Clearance. *Adv. Biosyst.* **1700100,** 1700100 (2017).

CHAPTER

2

OBJECTIVES

The main objective of this Doctoral Thesis has been the development of novel experimental strategies to modulate the optical properties of semiconductive polymers and the nanostructuration of the resulting materials to favour their implementation in practical demonstrators and applications. As a proof-of-concept to validate this initial idea, poly[2-methoxy-5-(2-ethylhexyloxy)-1,4-phenylenevinylene] (MEH-PPV) has been selected as a model, since it is a widely studied conjugated polymer whose optoelectronic properties are broadly and comprehensively investigated.

To achieve this general objective, the following specific objectives were established:

Strategy 1: *use of Phase Change Materials (PCMs) to reversibly modulate the emission properties of MEH-PPV*. The hypothesis behind this idea is to use the reversible temperature-induced phase (solid-to-liquid) transition of PCMs to modify the solvation of the MEH-PPV polymer, and therefore the corresponding optical properties. Such changes are expected to modulate the emission wavelength in a reversible manner and within a narrow temperature range, around the melting point of the PCM. The specific milestones for the successful development of strategy are:

1. To validate this approach in bulk MEH-PPV solutions of PCMs of different nature and melting temperatures.
2. To micro/nanostructuration the MEH-PPV/PCM mixtures maintaining the bulkswitching properties.
3. Integrate the micro/nanostructured fluorescent material into polymeric matrices to obtain easy-handling free-standing films with thermally switchable optical properties.

Strategy 2: *use of ultrasounds (US) to control the optical properties of MEH-PPV nanoparticles*. The hypothesis is that sonication of the MEH-PPV in chloroform/H_2O mixtures will generate reactive species able to break the polymer into smaller oligomeric fractions of different optical properties, while forming the nanoemulsions from which the nanoparticles are obtained. Whereas the previous approach was based on a reversible solvation process, in this case interruption of the electronic delocalization is achieved by an irreversible chemical process. To fulfil this approach the following specific objectives are:

1. To achieve the control over the length of the resulting oligomers, and therefore on the final optical properties, by fixing different experimental parameters, mainly the concentration of the polymer in the sonicated solution.

2. The nanostructuration of the resulting oligomers into nanoparticles by confining the reaction into chloroform-in-water ultrasound induced nanodroplets.
3. The integration of the resulting nanoparticles into free-standing fluorescent films with emission at different wavelengths, covering the whole visible region of the electromagnetic spectrum.

Strategy 3: *a combination of both, PCMs and US.* The hypothesis is that by appropriately selecting the oligomer emission wavelength with US and mixing it with different temperature-variable PCMs, we could develop multicolorimetric systems of use as temperature sensors and/or white light emitting material.

CHAPTER

3

TUNING OF MEH-PPV EMISSION PROPERTIES IN PHASE CHANGE MATERIALS (PCMs)

The development of novel and simple methodologies for obtaining fine -tuned reversible optical properties in conjugated polymer (CP) represents a challenging research area as it involves control over the assembly and disassembly of polymer aggregates and, consequently, over the formation of interchain emitting species. Here, using poly[2 -ethylhexyloxy) -1,4-phenylenevinylene] (MEH-PPV) as model CP, this objective is achieved BY mixing the polymer with a phase change materials (PCM). The solid-to-liquid transition of the PCM (heating above its melting point) induces a hypsochromic shift of the main emission peak together with the appearance of a new band at high energy. The initial polymer emission is then restored cooling the mixture down the PCM melting point. The change of the colour of the emitted light in a sharp temperature range, make the PCM/MEH-PPV system a good candidate for the realisation of fluorochromic temperature sensor. Finally, the prototype of such sensor is obtained by preparing solid lipid microparticles of the mixture and embedding it in a polymeric matrix to get a flexible film.

3.1 INTRODUCTION

3.1.1 MEH-PPV, PHOTOPHYSICAL PROPERTIES

The optical and electronic properties of π-conjugated materials are defined not only by the chemical structure of the molecular units but also by the nature of their intramolecular and intermolecular electronic coupling. In the chapter one has been highlighted that one of the main characteristics of these materials is the dependence of their optical properties with the polymer chain conformation. The polymer backbone tends to twist and coil leading to disruption of π-electron delocalisation. As a consequence, a series of planar conjugated segment (chromophores) composed of different number of monomer units are formed. Thus, a more precise description of the conjugated polymer chain consists of a series of linked chromophores of different extent of π-electron delocalisation and the $\pi \rightarrow \pi^*$ energy gap will increase as the length of the segment decrease. When an exciton is formed in one of these chromophores, the intermolecular interaction between them lead to a rapid energy transfer which allows the migration of the exciton from high energy segments to low energy segments. As a result, in conjugated polymers the emission resulting from the exciton recombination always takes place from the chromophores with lower energy (high conjugation length).

The photoexcitation followed by the formation of intrachain exciton in isolated conjugated polymer is well accepted by the scientific community. The same could not be said for the effect on the chromophores when they are in close proximity and start to interact (e.g. films or aggregates), whether they reside on physically distinct chains or are tethered together in the same polymer backbone. The reason of this difficult in the detection of the interchain emission lies on the poor overlapping of the delocalized interchain excited state with the single-chain ground state wave function, which leads to long radiative lifetimes.[1]

The interaction between polymer chromophores, which enables the formation of interchain species, can occur in many ways leading to different types of π-electron interactions, defined as: aggregates, excimer, exciplex and polaron pair:[2]

- with **aggregates** are referred to multiple chromophores which share delocalise π-electrons both in the ground and excited state;[3,4]
- When the excited state is shared equally between multiple chains, the species is referred to as an **excimer**;[5–7]

- An **exciplex** is formed when the interchain excited states presents an unequal sharing of π-electron density;[8–10]
- The photoinduced charge transfer lead to the formation of radical cation, or hole polaron, in one segment and a radical anion, or electron polaron, on the other. The **polaron pairs are** interchain charge separated species.[11,12]

The most evident spectral signature of ground and excited interchain species in conjugated polymer is the bathochromic shifted emission due to the delocalization of the π-electrons between conjugated segments. The increased degree of π-electrons delocalization leads to an interchain electronic energy lower than that of the single chain exciton. The type of the interchain species is difficult to determine, especially in films of such polymer where excimers and aggregates can coexist.

In MEH-PPV diluted solution (of good solvents such as $CHCl_3$, CH_2Cl_2, toluene and tetrahydrofuran), the emission spectrum is made by the vibronic progression (originated on the C-C vibrational stretching modes of the aromatic rings) coming from the single exciton emission. The intensity of the weaker shoulder at 600 nm is the photophysical signature of interchain species that could be either aggregates or excimers.[13] Indeed, as it is well known, highly concentrated solutions, poor solvents solutions (e.g. DMSO, MeCN) and MEH-PPV film present red-shifted emission spectra (from λ_{max} = 560 nm to 600 nm), with the complete absence of the high energy band (λ_{max} = 560 nm), the increase of 600 nm band, explained by polymer aggregation or other interchain species, and a weaker shoulder at 640 nm.[9,14,15] Samuel *et al.*[7] observed that the emission band of the films did not experience any significant broadening nor loose of the vibronic structure with an emission lifetime, at low excitation intensity, longer than in solution. They therefore suggest that MEH-PPV in films forms interchain excimers in its excited state together with other types of interchain species.

Schwartz *et al.* comprehensively investigated the emission of MEH-PPV film[13]. They studied the solvatochromic spectral shift of the surface emission keeping in contact different regions of the film with solvent of different polarity. They found that the majority of the investigating regions present interchain species that are excimer-like in nature. However, the film also presented localized regions where the emission was consistent with exciplex and a charge-separated polaron pair. Based on experimental data, they suggest that there is a continuum of possible interchain excited states with differing extents of charge delocalization that depend sensitively on the local chain packing.

Such works have shown that the close packing of the polymer chains of MEH-PPV in the film led to the formation of new interchain species with the extended π-electrons delocalisation which leads to a drastic emission red-shift as high as 50 nm.

The formation of these new species is not only a direct consequence of the aggregation in the films. The different conformations assumed by the polymers in different solvent also influence the type of the interchain species formed in the resulting solid material. Schwartz's group demonstrated that the conformation of polymer chains in solution influences the morphology, and hence the interchain photophysics in films cast from different solvents.[14] Thus, the degree of interchain interactions in conjugated polymers in the final film can be controlled varying solvent (Figure 3.1).

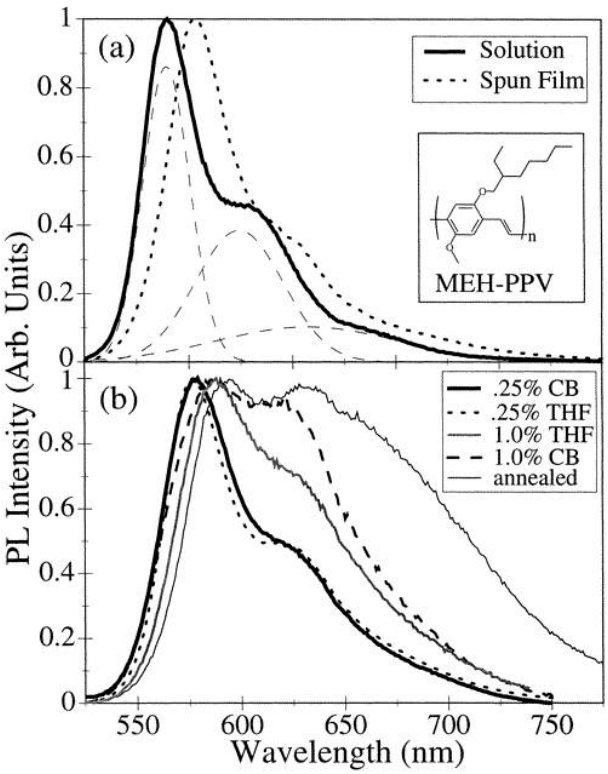

Figure 3.1. Normalised photoluminescence (PL) spectra of MEH−PPV in different environments. *a)* PL of a 0.25% w/v solution of MEH−PPV in chlorobenzene, CB (solid curve), and the film resulting from spin-casting the solution (dotted curve). The small dashed curves show Gaussian fits to the three visible peaks of the solution PL. *b)* PL of MEH−PPV films cast from a 0.25% w/v solution in CB (solid curve, same as dashed curve in *a*), a 0.25% w/v solution in THF (dotted curve), a 1.0% solution in THF (grey solid curve), a 1.0% solution in CB (dashed curve) and the film cast from the 1.0% CB solution after annealing (thin solid curve). The inset shows the chemical structure of MEH−PPV.[16]

The change in the optical properties associated to interchain species showed by MEH-PPV in films is also induced in solution. Collison *et al.* were the first to studying changes in the photophysical properties of conjugated polymers in solution as a result of their conformational and morphological (i.e. aggregation) changing induced by the addition of a

proper poor co-solvent.[17] Together with Yang *et al.* they showed that is possible to gradually induce the red-shift of MEH-PPV in solution tuning the ratio between a good and poor solvent thereby controlling the degree of aggregation and self-coiling of the polymer chains (Figure 3.2).[18]

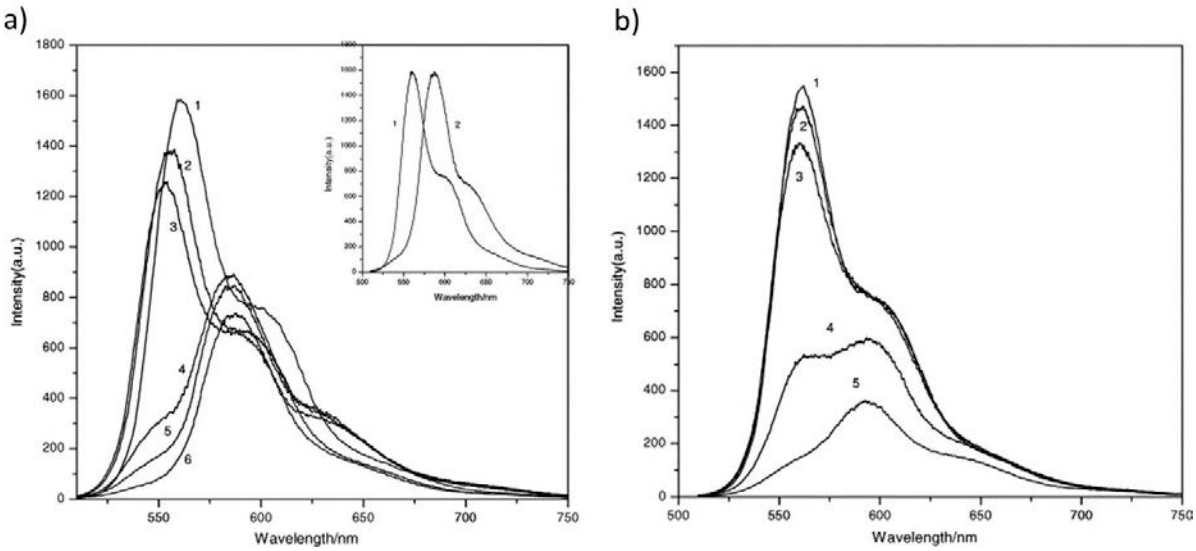

Figure 3.2. Emission spectra of *a)* MEH-PPV in chloroform–cyclohexane. Solution with chloroform content: (1) 100%, (2) 50%, (3) 30%, (4) 20%, (5) 15%, (6) 10% (Inset: normalised emissions of MEH-PPV in pure chloroform (1) and in the mixture with 10% chloroform (2), respectively); *b)* MEH-PPV in chloroform–methanol solution with chloroform content: (1) 100%; (2) 80%; (3) 70%; (4) 65%; (5) 60%. Excitation wavelength: 500 nm.[18]

In summary, the formation of interchain species in conjugated polymer (e.g. MEH-PPV), whether in solution or the solid state, induce essential variations of the emission properties. The largest spectral differences for MEH-PPV are observed between diluted solutions of the polymer in good solvents (blue-shifted structured spectrum with vibronic bands) and conditions where interchain interactions are established, producing red-shifted spectra. Therefore, by properly designing the solvent and the casting conditions of these polymers, materials with specific optical properties are obtained.

However, though this is a powerful tool to obtain materials with tuneable absorption/emission properties, in most of the case it takes place in an irreversible manner. The applicability of these materials could be further extended to optical switches if the variations of the optical properties can be reversibly and controlled by an external stimulus.

A few works report on the intrinsic thermochromic[19] and/or thermos(electro)fluorescent[20] properties of MEH-PPV and derivatives[21] in solutions[19] and as solid films.[22,23] However, all these examples produced a continuous change of the optical

properties (absorption and/or emission) and significant spectral variations were achieved upon spanning over range of temperature of 200-300 K.

Recently, in our group we exploited Phase Change Materials (PCMs) to modify the physical (solid to liquid) or chemical (different interactions are established) environments to dissolved dyes, which responded with important variations of the optical properties once the PCMs were passing from the solid to the liquid state.

In this work, we hypothesise that the variation of the environment provided by the phase transition of PCMs, could be used to reversibly tune the optical properties of conjugated polymers, such as MEH-PPV.

3.1.2 PHASE CHANGE MATERIALS (PCMS)

PCMs generally refer to a class of compounds having large latent heats of fusion with regards to melting and solidifying at a nearly constant temperature. Latent heat of a substance is the amount of thermal energy absorbed or released by the material during a change in its physical state. Specifically, the latent heat of fusion (or enthalpy of fusion) refer to the amount of energy necessary for the phase transition from solid to liquid for unit of mass of the substance at a nearly constant temperature. Therefore, PCMs:

I. store and release large amounts of heat energy in response to small temperature change (they present a heat storage capacity about 5 to 14 times higher than conventional thermal storage materials);[24]
II. are low cost materials with high heat storage density and excellent chemical stability;
III. have the prominent feature that the temperature remains almost constant during the phase change process, which can be used in a temperature control system.[25]

Based on these interesting properties, PCMs have been explored for thermal energy storage, solar energy applications, isolation in automotive industry, textile industry, containers for temperature sensitive food and medical devices, among others.

PCMs can be classified, according to their chemical nature, into organic, inorganic, and eutectic PCMs. Organic PCMs can be further divided into paraffin and non-paraffin, which gather together fatty acid, fatty alcohols, ester, and glycols.

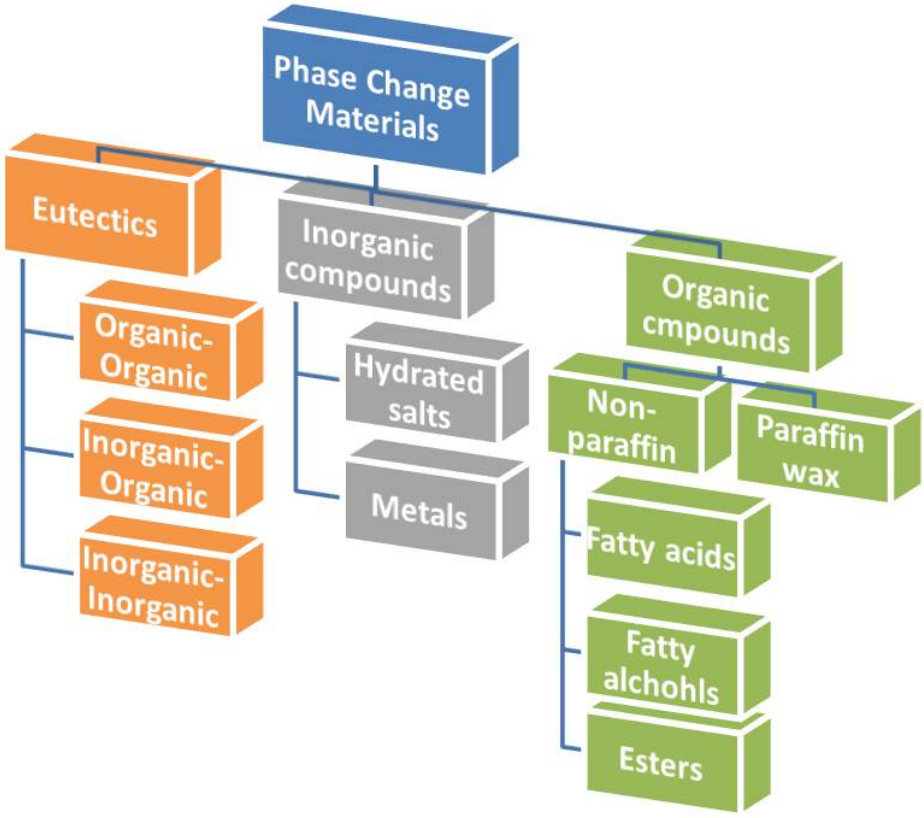

Scheme 3.1. Common classification of the PCMs based on their chemical nature.

3.1.2.1 Inorganic and Eutectics PCMs

The category of inorganic PCMs is commonly referred to water, hydrated salts, molten salts and metals or alloys. They have a precise melting point, high heat of fusion, high thermal conductivity, and high latent heat storage capacity per unit mass. Hydrated salts are some of the oldest and most studied heat storing PCMs. They consist of a salt and water, which combine in a crystalline matrix when the material solidifies. The major drawbacks with hydrated salt are their incongruent melting (i.e. the melting behaviour is not homogeneous through the material) and their compatibility with organic materials together with a lower cycling stability.[26] The other broad category of inorganic PCMs includes the metals, which are not very practical because of their high density and relatively high melting points. Also the toxicity and environmental concerns limit the employment of such materials. Alternatively, eutectic PCMs represent a minimum melting mixture of two or more components, each of which melt and freeze congruently (i.e. it maintains homogeneous composition and thermal properties).[26] The components do not normally interact to form a new chemical compound, but at certain ratios, inhibit crystallization processes resulting in a system having a lower melting temperature than its separated components.[24]

3.1.2.2 Organic PCMs

Organic PCMs have been widely studied in the last few years because of their interesting properties: I) they cover a large range of melting points that goes from -20 to 200 °C, II) they are chemically stable, non-corrosive and recyclable,[26] III) they can melt and freeze repeatedly without any phase isolation and IV) exhibit self-nucleation, which means they crystallize with little or no super cooling. Limitation, they are not usually stable at higher temperatures and typically have smaller heats of fusion per volume than inorganic PCMs, as a consequence of their lower densities ($<10^3$ Kg/m^3).[26]

Paraffins

These are saturated hydrocarbon with general formula C_nH_{n+2}. Those with number of carbon atom between C_5 and C_{15} are liquids at room temperature, while hydrocarbon with higher number of carbon in their chains (> C_{15}) are waxy solids. In general the longer the average length of hydrocarbon chain the higher the melting temperature and heat fusion.[27] Paraffins are available in a broad range of T_m. Furthermore, they are chemically inert and stable resulting in a reliable and predictable material. Their drawback derives from the fact that paraffin waxes are obtained from petroleum distillation and achieving pure products is really expensive, and thereby only technical grades are generally available. Such paraffins are mixtures of hydrocarbons with different chain lengths, with a broader phase-transition temperature.[28] Besides, paraffin waxes have low thermal conductivity in their solid state, which might represent a problem in those applications where high heat transfer rates are required during freezing.

Non-Paraffins

There include a large number of compounds with highly varied properties. To this category belong esters, fatty acid and alcohols, molecules with different chemical structures and properties. They presents large heats of fusion and no or limited supercooling (e.g. fatty acids). Their drawbacks are inflammability, low thermal conductivity, and instability at high temperatures.[24] Of particular interest are fatty acids and fatty alcohols, which are biocompatible, low toxic and renewable materials, since the raw materials are derived from vegetable and animal sources. These bio-based PCMs can be considered “food grade”, meaning that they have no effects when ingested, unlike paraffins. Such properties have led to the successful use bio-based PCMs in the cosmetic and food industries.[29] Fatty acids,

characterized by the chemical formula $CH_3(CH_2)_{2n}COOH$, possess some superior properties over other PCMs. These compounds, in their liquid phase, have a high surface tension of 2-3 x 10^{-4} N cm^{-1}, which is high enough to be retained in a host material.[30] They have large latent heats of transition and high specific heats (1.9-2.1 J g^{-1} $°C^{-1}$), exhibit only small volume changes during melting or freezing (for example melting dilatation is around 0.1-0.2 ml g-1),[31] and little or no supercooling occurs during the phase transition. Additionally, because of the protected carboxyl group, this class of PCMs are chemically, heat and colour stable. Fatty alcohols are the reduced forms of fatty acids in which the carboxylic acid has been reduced to give a primary alcohol. They have a chain length ranging from 8, with a T_m= -15 °C, to 20 carbon atoms T_m= 65 °C. Fatty alcohols with a chain length up to C_{18} are known to be biodegradable.

		Materials	Melting point (°C)
organic	paraffin	*n*-Tetradecane (paraffin C_{14})	5.5
		n-Hexadecane (paraffin C_{16})	18.2
		n-Eicosane (paraffin C_{20})	36.5
		n-Docosane (paraffin C_{22})	44.0
		n-Octacosane (paraffin C_{28})	61.6
	Non-paraffin	Nonanoc acid	12.5
		Octanoic acid	16.3
		Dodecyl alcohol	24.0
		Butyl stearate	19.0
		Dodecanoic acid	43.0
		Octadecanoic acid	67.8
inorganic	hydrated salt	$Na_2(SO^4)_2 \cdot 10H_2O$	32.0
		$Ca(NO_3) \cdot 4H_2O$	47.0
	metals	Ga	30.0
		Bi-Cd-In alloy	61.0
eutectic	inorganic-inorganic	$Na_2SO_4 + NH_4Cl + NaCl + H_2O$	10.9
	organic-organic	Dodecanoic acid + Hexadecanoic acid	32.7

Table 3.1. In the table are reported some PCMs compounds for each category with the respective T_m.

3.1.2.3 PCMs as thermal switch to control optical properties

So far, examples of the use of PCM used to control the optical properties are only described for molecular dyes. The majority of the reported switchable optical materials based on PCMs are thermochromic materials that undergo colour change upon temperature variations.[32,33]

To our knowledge, the control of emission properties of conjugated polymer dissolved in PCMs, on the contrary, has not been explored in the past. In our group organic PCMs have been employed to achieve thermally switchable emission from photon upconversion systems based on highly conjugated organic molecular dyes (energy donors and acceptors). In the solid PCMs, the aggregation of the dyes enhances the inter-chromophoric energy transfer processes leading to upconversion with a blue emission from the acceptor. When the PCM is melted, the distance between the dyes is too high to favour the energy transfer and a red phosphorescence emission from the donor compound is observable.[34]

In order to fully exploit the solid-liquid transition of PCMs in practical applications, it is necessary to overcome the problems related to the loss of mechanical properties of the PCMs in its liquid state as leakage. Recently, growing interest has been showed for the micro-/nano-confinement of PCMs has a possible solution to such drawbacks.

3.1.3 MICRO-/NANO-CONFINED PCMs

In order to increase the versatility and applicability of PCMs, these materials have been structured in the form of solid lipid micro- (SLMs) and nanoparticles (SLNs), or as core-shell micro-/nanocapsules.

Microcapsules of PCMs

Over the last, decades micro-/nanoencapsulation technology has been employed to physically confine PCMs material within the solid shell. Micro-/nanocapsules consist of tiny containers in which a liquid or solid core material is encased by a hard shell made of polymeric material. Encapsulated PCMs present several advantages:

- micro-/nanocapsules can be processed as aqueous dispersion or powder leading to a better manipulation of the final material for several application;
- prevent the leakage of PCM in the host material when it is in its liquid state;[35]
- reduction in reaction of the surrounding materials with PCMs;
- increase in heat transfer rate;[36,37]

- enhancement in thermal and mechanical stability of the PCM.[38]
- addition of functionalities on the surface of the micro-/nanocapsules for new application

Micro-/nanoencapsulation can be achieved by several techniques, involving chemical method and/or physical method. Capsules presenting different types of structures and properties can be obtained, depending on the employed techniques, on the wall composition and the physicochemical properties of the wall (Figure 3.3).[39]

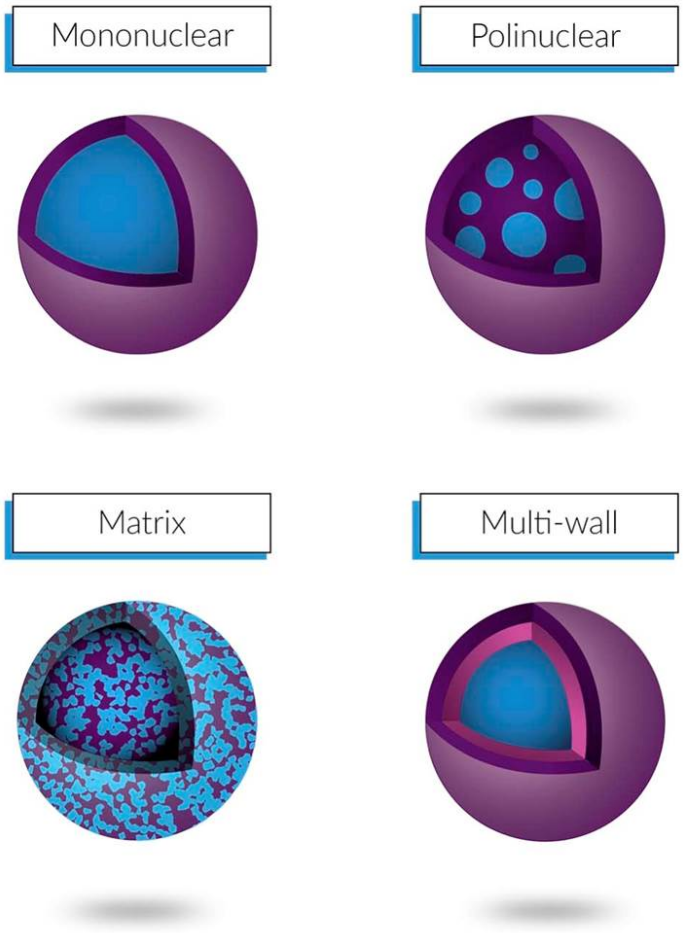

Figure 3.3. Morphology of different types of microcapsules.[39]

Currently the main method developed for the preparation of micro-/nanocapsules of PCMs are based on the formation of the shell material by either the polymerisation of monomeric/oligomeric species (e.g. interfacial polymerisation, *in situ* polymerisation) or the precipitation of the preformed polymers upon modification of the mixture conditions (such as pH changes and solvent evaporation).

In this thesis, the solvent evaporation method was the most used strategy since it does not require chemical reactions, thereby avoiding eventual side reactions with the encapsulated materials (such as PCMs, dyes, and conjugated polymers).

In this method, the preformed polymer, which forms the shell, is dissolved in water-immiscible volatile organic solvent with low boiling point, typically dichloromethane and chloroform, whereby the core material is also dissolved or dispersed. The organic solution is then added to the aqueous phase where a surfactant is present. The method involves two steps: in the first step oil-in-water emulsion (o/w emulsion) is formed using a dispersing agents and high-energy homogenisers. The size of the resulting oil droplets depends on the energy produced by the homogeniser (e.g. stirring rate and ultrasonic energy), type and amount of dispersing agent, the ratio between the organic and water phase, and viscosity. During the second step the organic solvent is evaporated, inducing the precipitation of the polymer which entraps the core material in its matrix (Scheme 3.2).

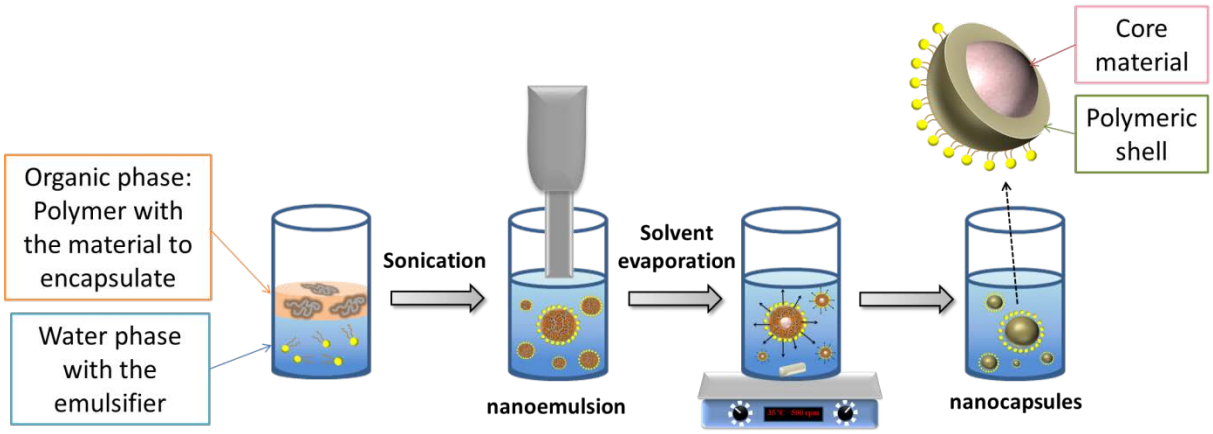

Scheme 3.2. Schematic representation of the synthesis of PCM nanocapsules by solvent evaporation method (yellow sphere represents the surfactant molecules and the grey lines the polymer).

In the design of the synthesis of core-shell capsules of PCMs, it must be taken into account the miscibility between the PCM and the polymer of the shell. Very miscible components would prevent the formation of a core-shell structure in favour of a matrix type structure when both the PCM and the polymer materials are homogeneously mixed in the particles. On the contrary, non-miscible components are more likely that favour the formation of core-shell structures. The functionality of the final particles may be affected significantly depending on which structure they present.

This method is primarily used in the pharmaceutical industry to encapsulate both hydrophobic and hydrophilic drugs. Usually, a biodegradable polymer such as poly(lactic-co-glycolic acid) is used as the shell material.[40] In the last few years, microcapsules of PCM

have been also synthesised through this method. Encapsulation of stearic acid has been achieved by solvent evaporation method using polycarbonate for the polymeric shell.[41] The resulting microcapsules showed good thermal and chemical stability with high encapsulation capacity, together with excellent thermal properties. Such microcapsules are a promising material for the energy storage.[41] Recently, in our group photochromic dyes dissolved in fatty acids have been encapsulated. The resulting material presented switchable photochromism depending on the applied temperature and without the need for chemical additives. Moreover, the confinement of dye-PCM mixtures in solid shell capsules avoided the leakage and loss of the encapsulated material guaranteeing the reversibility of the system.[42]

Solid Lipid Micro-/Nanoparticles

As an alternative to the encapsulation route, the micro- or nano-confinement of phase change material can be achieved through the synthesis of solid particles (SLPs), named as solid lipid microparticles (SLMs) or solid lipid nanoparticles (SLNs), depending on the particles size. During the last few years, increasing attention has been directed towards the synthesis of such structures mainly as carriers for drug delivery in pharmaceutical applications, but, recently, also as encapsulating systems in the cosmetic and dermatology fields.

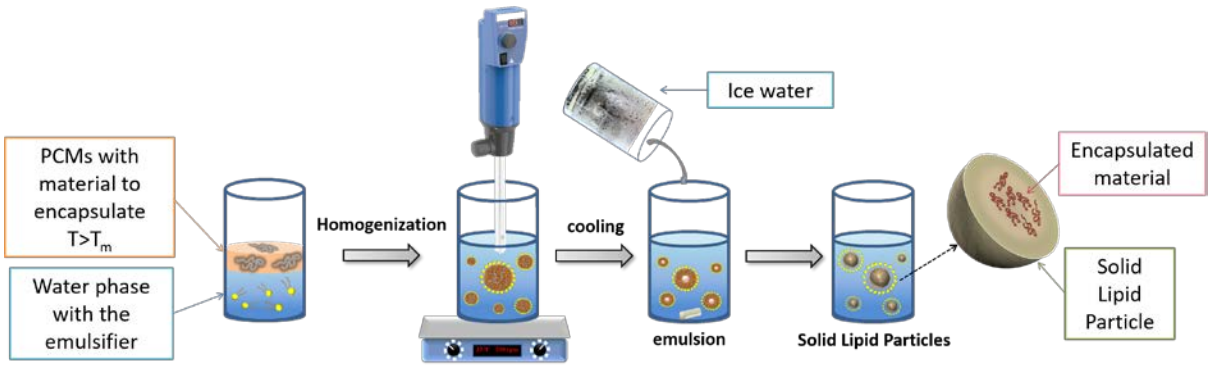

Scheme 3.3. Schematic representation of the emulsion/cooling method to synthesise SLPs (yellow sphere represents the surfactant molecules and the grey lines the material to encapsulate).

Respect to the core-shell structure of the micro-/nanocapsules, SLPs are made by PCM exclusively and do not need a polymeric shell. This structure made SLPs a simpler system and avoids the need for selecting the components in order to maintain the separation between the PCM and the polymer. Moreover, the lack of the shell material avoids that encapsulated components (e.g. drugs and dyes) spread between the PCM and the cortex material, thereby preventing the two different undesired behaviours of the final particles.

Finally, given their simple structure, SLPs are ease to produce and manufacture at an industrial scale.

In the past, several techniques have been developed to obtain SLPs. So far one of the simplest approach is the emulsion/cooling method, which involves the formation of oil-in-water emulsion by adding melted PCMs to a hot solution of water and surfactant. After the emulsification at $T > T_m$ and the formation of the droplets, micro-/nanoparticles are induced by cooling down the emulsion. If a lipophilic material needs to be encapsulated in the SLPs, this is dissolved or dispersed in the melted PCM before the emulsification. This method, also called hot melt microencapsulation technique, was developed by Bodemeir *et al.* for the encapsulation of ibuprofen in microparticles of different waxes (carnauba, paraffin, beeswax, and the semisynthetic glyceryl esters—Gelucire 64/02 and Precirol AT05).[43]

3.2 OBJECTIVES

The purpose of this work was to obtain temperature sensors based on PCM micro-/nanostructures (SLPs or capsules) loaded with the conjugated polymer MEH-PPV. It is supposed that changes of the intra- and interchain interactions experienced by the conjugated polymer MEH-PPV in solid/liquid PCMs should provide important variations of the emulsion properties of the emission properties of the polymer.

In the design of this reversible optical switch, it is assumed that while in the solid PCM it is induced the red-shifted emission of the aggregated MEH-PPV, in the liquid phase the normal emission of the separated polymeric chains is expected.

For this study three different classes of PCMs (fatty acid, paraffins, and fatty alcohols) were tested to study the behaviour of the polymer changing the polarity of the environment. Depending on the specific melting point of the diverse PCMs employed the sensor would be sensitive to different temperatures in the range of 5-100 °C. The micro-/nano-confinement of the system for the integration in flexible polymeric films could be achieved by the synthesis of micro/nanocapsules and/or solid lipid microparticles.

The final sensing material will be obtained embedding the micro-/nanostructures of PCMs loaded with MEH-PPV in polymeric matrices, as shown schematically in Scheme 3.4.

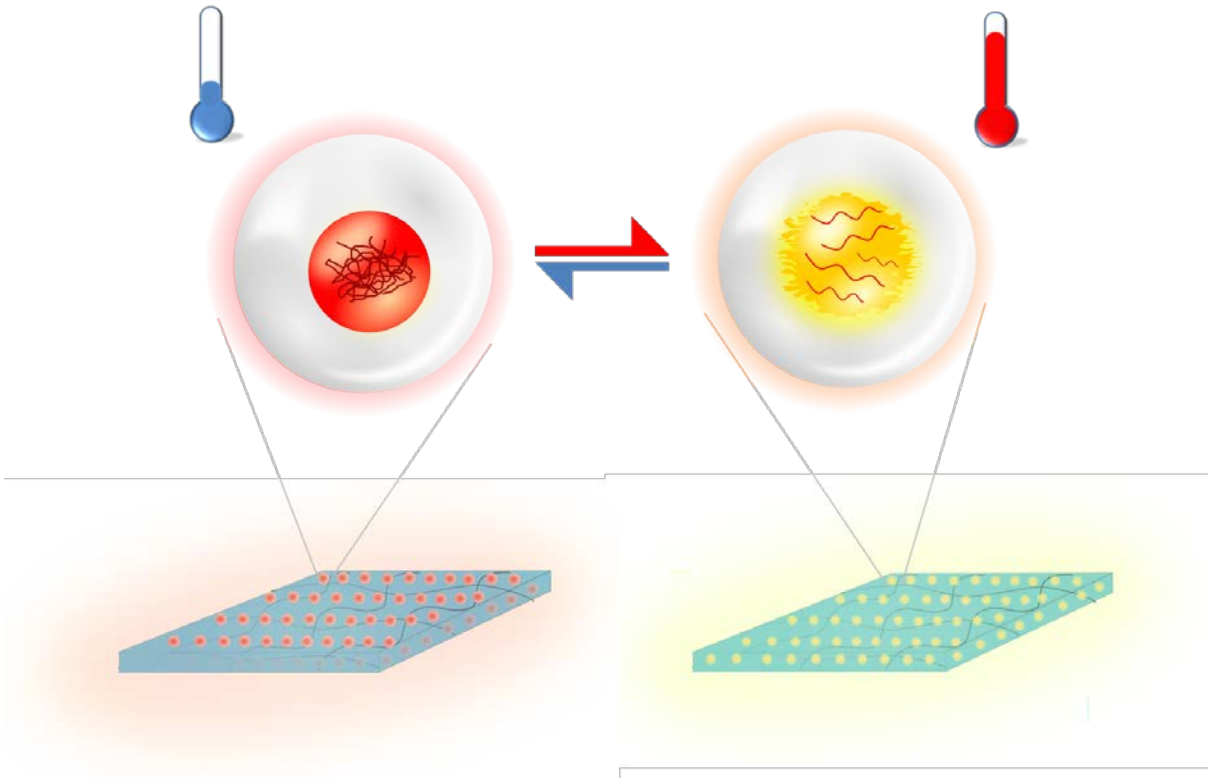

Scheme 3.4. Schematic representation of the hypothesised behaviour of the encapsulated PCMs with MEH-PPV embedded in polymeric film.

3.3 RESULTS AND DISCUSSION

3.3.1 REVERSIBLE FLUORESCENCE SWITCH OF MEH-PPV IN BULK PCMs SOLUTIONS

The behaviour of the MEH-PPV in different PCMs was first studied for bulk PCM solutions. Temperature-dependent fluorescence spectroscopy was used to measure the emission properties of the polymer at different temperatures, in particular below and above the PCM melting point. In order to maintain the same experimental setup for the fluorescence measurements of the liquid (transparent) and solid (opaque) mixtures, the measurements were carried out in reflectance mode in a triangular 1 x 1 cm cuvette, set at 45º with the incident light and the detection unit. This study was carried out for:

- PCMs of different nature (i.e. paraffins, fatty alcohols, and fatty acids) to investigate the effect of the polarity of the medium (and its solvation effect) on the emission properties of the MEH-PPV;
- at least two PCMs of each type, presenting different $T_{m,}$ in order to demonstrate the universality of the system;

- when possible, two MEH-PPV concentrations for each PCM to determine the magnitude of variation of the emission properties.

Showing the switch in PCM with different T_m would allow to demonstrate that the switch is produced by the phase transition of the PCM and not by the intrinsic thermofluorescent properties of the MEH-PPV. Moreover, if the phase change-induced switch is confirmed, the selection of PCMs of different T_m would allow an easy and straightforward strategy to tune the switching temperature of the system.

The PCM solutions of MEH-PPV (generally defined as PCM/MEH) were prepared by mixing a pre-prepared dichloromethane solution of the polymer (at a given concentration) with the suitable amount of PCM and then evaporating the volatile solvent while heating above the PCM T_m (T_m^{PCM}). When it was possible, for each PCM, two different mixtures (PCM/MEH 0.1% and PCM/MEH 0.01%) of two polymer concentrations (0.1 wt.% and 0.01 wt.) were prepared (see Experimental Section). High MEH-PPV concentrations were used to ensure the aggregation of the polymer. For each sample, temperature-dependent steady-state fluorescence measurements were carried out below and above the T_m^{PCM} to investigate the emission of MEH-PPV in the solid and liquid PCM. The reported temperatures are those set in the heating/cooling thermostat, which could be slightly different from the temperature of the sample chamber. To assure that the thermostat and the sample temperatures were as close as possible, the mixture was let to equilibrate to the set temperature for at least 10 minutes before running the fluorescence measurements.

3.3.1.1 MEH-PPV dispersed in paraffin PCMs

Initially, we aimed to investigate the behaviour of the MEH-PPV in the solid and liquid phase of non-functionalized and non-polar PCMs, like paraffins. The lack of functionality, should avoid any type of interaction with the polymer. Therefore, the possible variations of the optical of the polymer in the two phases should derive from the change of the solvation degree of the MEH-PPV in the solid and liquid phase of the PCMs. This variation of the solvation should produce different interchain interactions (e. g. formation of aggregation, excimers, exciplex, atc.) and/or intrachain effects (e. g. polymer chain torsions), with consequent changes of the mixture optical properties. A similar approach was already exploited in a precedent work carried out in the NANOSFUN group, in collaboration with the group of Prof. L. Latterini (Perugia University), where the solid-to-liquid transition of

paraffins was used to reversibly tune the intermolecular interactions between highly conjugated fluorescent aromatic molecular dyes, inducing switchable emission. [28]

Study of eicosane mixtures of MEH-PPV

The first investigated paraffin was eicosane (from now on EC), an alkane with a 20-carbon atom chain presenting a melting point of 36.5 °C.[44] After the samples preparation, it was realized that the final EC/MEH 0.1% and EC/MEH 0.01% mixtures presented large polymer aggregates deriving from the non-dissolved MEH-PPV polymer. Despite this, the mixtures were analysed by fluorescence spectroscopy (Figure 3.4).

The solid EC/MEH 0.1% mixture (20 ºC) presented a broad emission band with λ_{max} = 608 nm and a shoulder at 637 nm. This spectral feature resembles the reported emission spectrum for MEH-PPV in nanoparticles,[45,46] in poor solvents[9,17,47]or MEH-PPV solid films.[13,23,48] The red-shifted spectrum (compared to that of the polymer in good solvent) and the lack of the high-energy band (λ_{max} ~ 550 nm) confirmed that the polymer in solid EC is not fully dissolved and the emission is the contribution of aggregates or other interacting species. Unfortunately, upon heating above T_m^{EC} (60 ºC), the spectral feature only suffered little variations: just a few nanometers of blue-shift of the main peak (from 608 nm to 602 nm) and no significant change in the emission intensity, though the shoulder of the melted sample, also blue shifted by a few nanometers (637→631 nm), became more pronounced.

The EC/MEH 0.01% mixture also showed the broad emission with λ_{max} = 603 nm and the shoulder at 640 nm. Its melting, though produced a considerable decrease of the emission intensity (by half, from 7.55×10^4 to 3.79×10^4 arb. units), only induced a little blue-shift from 603 nm to 591 nm, confirming what was already observed by naked-eye, the lack of emission switch upon melting.

The lack of optical changes was ascribed to the presence of large polymers aggregates that do not dissolve neither by melting or diluting the mixture. The aggregation was due to both low polarity and large aliphatic chain of the PCM, which prevent good solvation of the polymer.

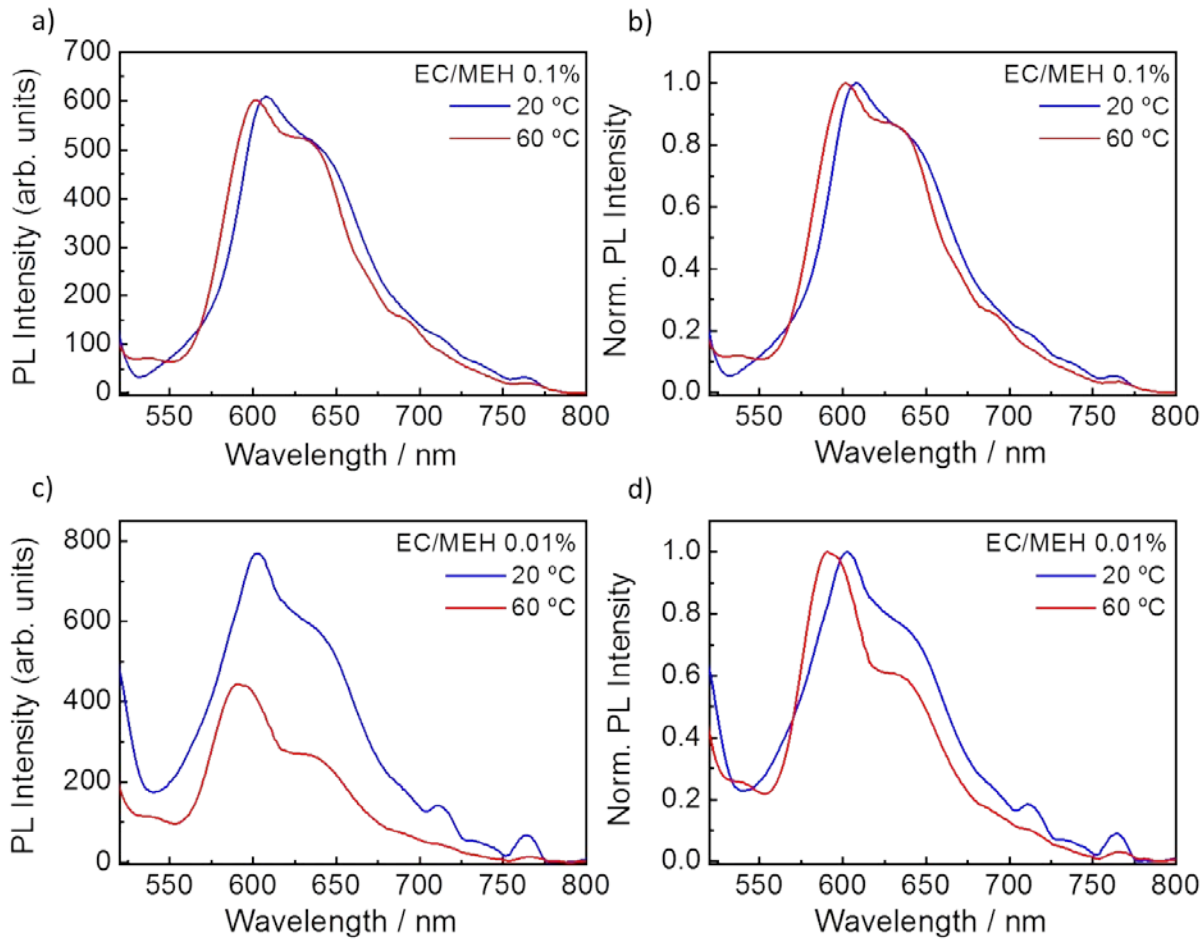

Figure 3.4. *a)* Emission and *b)* normalised emission spectra of sample EC/MEH 0.1% measured at 20 °C and 60 °C; *c)* emission and *d)* normalised emission spectra of sample EC/MEH 0.1% measured at 20 °C. All the spectra have been obtained irradiating at λ_{exc} = 490 nm.

Use of shorter parrafins

Hexadecane (HD, T_m = 18.2 ºC)[44] and tetradecane (TD, T_m = 5 ºC),[44] shorter alkanes with a 16 and 14-carbon atom chains, respectively, were then used to improve the polymer solubility. Based on the low solubility of MEH-PPV in EC, the HD/MEH, TD/MEH solutions were prepared only at the lowest polymer concentration (0.01 wt.%). The final liquid solutions appeared clear and red coloured, whereas when they were cooled down below their T_m, red solid mixtures were obtained and phase segregation between the polymer and the PCMs was not observed.

However, the low solubility of the polymer showed in EC is maintained in HD/MEH-PPV 0.01% and TD/MEH-PPV 0.01% mixtures, as it confirmed by emission spectra. Both samples presented a low blue-shift of the main peak (from 602 nm to 596 nm) upon melting the PCMs (Figure 3.5). The lack of the intrachain exciton band (λ_{max} ~ 550 nm) still confirms that the main contribution to the emission derives from interchain species interactions.

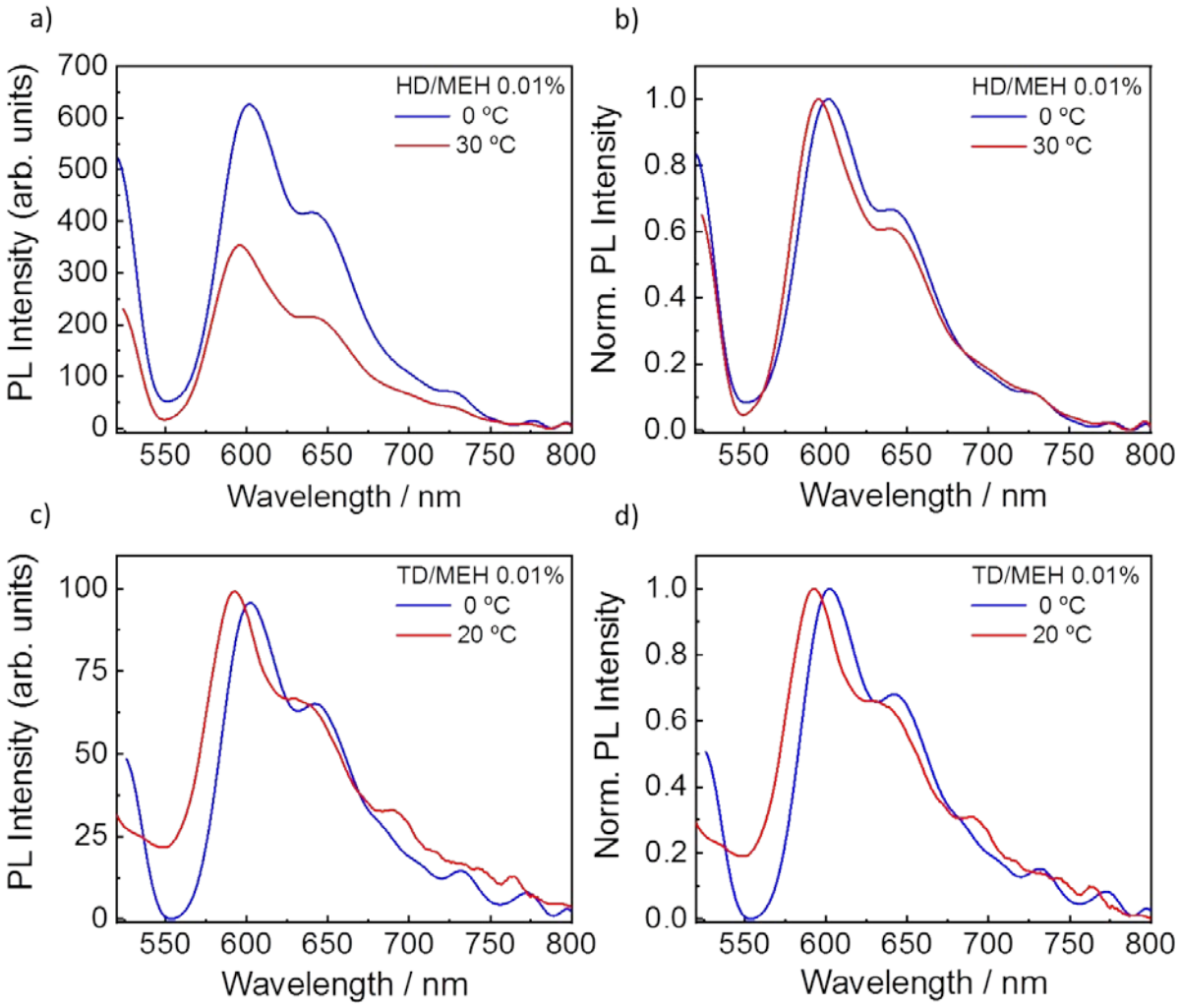

Figure 3.5. *a)* emission and *b)* normalised emission spectra of the sample HD/MEH 0.01% measured at 0 °C and 30 °C; *c)* emission and *d)* normalised emission spectra of the sample TD/MEH 0.01% measured at 0 °C (blue line) and 20 °C (red line). All the spectra have been obtained irradiating at λ_{exc} = 490 nm.

The melting of the mixtures produced a drastic decrease (approximately by half, from 6.48×10^4 to 3.92×10^4 arb. units) of the emission intensity of HD/MEH-PPV 0.01% and a little increase of the TD/MEH-PPV 0.01% emission. The different behaviour of the emission intensity variation of the paraffin mixtures is still unclear. Usually, the quantum efficiency of emission of the polymer in solution is higher than in solid films. In this case the opposite effect is observed and this is a common feature presented by many of the samples are going to be presented. One of the hypotheses for this behaviour was related to the experimental setup. The measurements were carried out in reflectance mode with the cuvette set at 45 º with the incident light and the detection beam. Even though a triangular cuvette was used, it is possible the light emitted from the solid and liquid samples comes from different depths of the cuvette (from the cuvette surface for the solid opaque samples, while from deeper region of the cuvette for the liquid mixtures). The emitted beam might have not been well focused to

the detector directions for the two (solid and liquid) conditions. The use of an integrating sphere, not available at this stage, would have allowed better conclusions on the emission intensities variations. The inner filter effect was also considered as possible cause for the decrease of intensity in liquid solutions, though the triangular cuvette was supposed to reduce this effect. Importantly, the normalised spectra of both mixtures highlight the similarity in the bands in their solid and liquid phase, with slight blue-shifts of about 6 nm (602→596 nm) and a small decrease in the intensity of the shoulder at 640 nm. These results confirm that in both solid and liquid states of the paraffin mixtures, the emissions were produced by interacting species (e.g. aggregates) formed for the low solubility of the polymer in these media. Overall, we can accomplish that no important optical variations of the MEH-PPV in different solid/liquid paraffin waxes were observed. This could be ascribed to:

- the lack of solubility of the polymer in the paraffin material in both its solid and liquid state, which makes the phase transition not relevant for the switch,
- the lack of any functionality which could provide a variation of the environment properties (e.g. polarity, molecular interactions, etc.) that should affect the emission properties of the polymer.

These results let us discard paraffin PCMs for producing thermal optical switches based on PCMs/MEH-PPV mixtures.

3.3.1.2 MEH-PPV dispersed in Fatty alcohol and ester PCMs

The next step consisted of using functional PCMs (non-paraffin PCM), whose functionalities should provide *a)* an improvement of the solubility, at least in the liquid state and *b)* variation of the environment properties (e.g. polarity) during the phase transition.

For these we proposed PCMs based on ester, long-chain alcohols and long chain acids, all of them presenting a higher polarity than the paraffin.

Tetradecanol

Tetradecanol (TDol), is a fatty alcohol with a 14-carbon atom chain presenting a melting point of 37.7 °C.[44] TDol/MEH-PPV 0.01% presented as a red solid or liquid solution (depending on the temperature) with no evidence of phase segregation between the polymer and the PCM. The fluorescence spectrum showed a broad emission band with λ_{max} = 606 nm and a shoulder at 644 nm (Figure 3.6a). Upon melting of the mixture, the intensity of the

emission is drastically reduced (approximately by half, from 1.13×10^5 to 0.46×10^5). The normalised spectra show the little blue-shift (a few nm) of the main band and of the shoulder which also became more pronounced and the appearance of a weak peak at 543 nm, possibly related to the isolated chain emission. Encouraged by this new structure, a second cooling and heating cycle was performed and the fluorescence of the corresponding liquid mixture showed an important change in the structure of the emission band. The intensity drastically decreased due to the formation of large polymer aggregates, which precipitated. Interestingly, a further blue-shift of the main band (600→591 nm), a decrease of the relative intensity of the shoulder at 635 nm and the increase of the high energy shoulder at 543 nm indicated that in the second heating cycle the emission deriving from the isolated polymer chain increased its contribution. Probably, a very low percentage of the polymer remains in solution as isolated chain, reducing the formation of the aggregates. These results showed a low solubility of the MEH-PPV polymer also in the fatty alcohols.

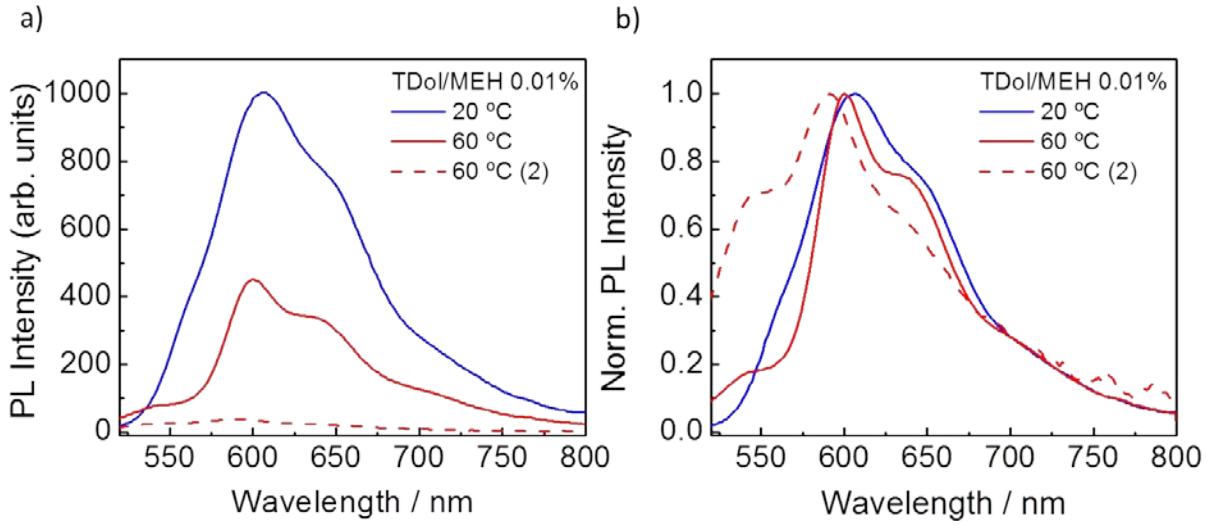

Figure 3.6. *a)* emission and *b)* normalised emission spectra of the sample TDol/MEH 0.01% measured at 20 °C, 60 °C and at 60 °C after cooling down the mixture and heated again (λ_{exc} = 490 nm).

Trilaurin

As alternative to the paraffins, it was tested the more polar glyceryl tridodecanoate (or trilaurin, abbreviated as TL), a glycerol esterified with three 1-tetradecanoic acids, (T_m = 46.5 °C).[44] In the prepared mixtures (TL/MEH 0.01%), no phase segregation between the polymer and the PCMs was observed, indicating that the polarity of the PCM allowed increasing the polymer concentration without forming macroscopic aggregates. In the solid mixture the emission spectrum showed a structure of the band resembling the one observed in EC/MEH 0.01%, with λ_{max} = 610 nm. Moreover, upon melting, the emission intensity of TL/MEH

0.01% suffered a drastic quenching (approximately by half, from 0.76×10^4 to 0.34×10^4)., as observed in eicosane (Figure 3.7a). Notably, the normalised spectra showed a blue-shift of 19 nm (610→591 nm), with the red-shift shoulders (633 nm) becoming more defined and decreasing their relative intensities (Figure 3.7b). Such larger shift suggested a better solubility of the polymer, so a more concentrated TL/MEH mixture was prepared (TL/MEH 0.1%). The solid mixtures showed broad and less structured emission spectra with λ_{max} = 614 nm and shoulders at 636 and 638 nm, respectively, characteristics of aggregated species. Upon melting, the emission intensity of TL/MEH 0.1% slightly increased (Figure 3.7c). Again, without the integrating sphere it was not possible to assign the different intensity changes. The normalised of the more concentrated sample also presented a large blue-shift of 17 nm (614→597 nm) together with a more defined res-shift (636 nm) shoulder (Figure 3.7d). The observed changes of the spectral features account for a reduction of the contribution of the aggregated species emission after melting. As expected, these changes were more evident for the TL/MEH 0.01% solution, which evidenced a higher relative intensity decrease of the longer wavelength shoulder, a larger blue-shift of the main band and the appearance of the high-energy shoulder at 545 nm. So far this TL/MEH 0.01% produced the largest blue-shift and spectral changes among all mixtures tested until now.

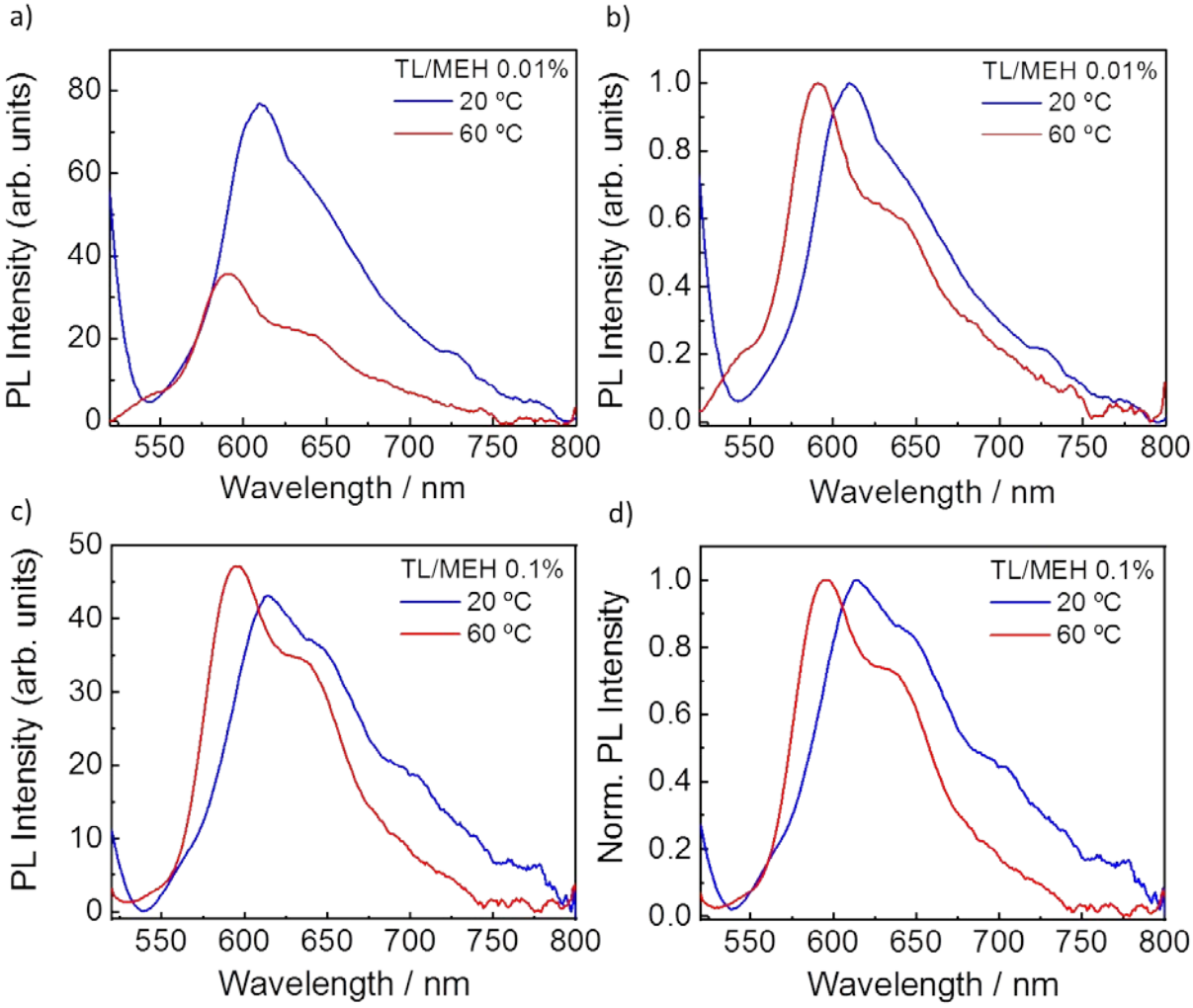

Figure 3.7. *a)* Emission and *b)* normalised emission spectra of the sample TL/MEH 0.1% measured at 20 °C and 60 °C; *c)* emission spectra and *d)* normalised emission spectra of the sample TL/MEH 0.01% measured at 20 °C and 60 °C. All the spectra have been obtained irradiating at λ_{exc} = 490 nm.

The addition of functionalities and the increase of the polarity of the medium produced better spectral changes during the solid-liquid transition of the PCM. For this reason, at this point, we hypothesised that the use of other families of PCM that could increase even more the effect on the MEH-PPV emission properties during the melting process.

3.3.1.3 MEH-PPV dispersed in Fatty acid PCMs

As alternative to paraffin, different fatty acids were also proposed as PCM to produce larger spectral changes. The study in paraffin PCMs showed that reducing the length of the alkyl chain, the solubility of the MEH-PPV could be improved. Therefore fluorescence studies were carried out in saturated fatty acids of different alkyl chain length: stearic acid (SA), dodecanoic acid (DA) and nonanoic acid (NA), of 18, 12, and 9-carbon atom chains and different melting points (T_m^{SA} = 69.3 °C, T_m^{DA} = 43 °C, T_m^{NA} = 12 °C).[44]

MEH-PPV fluorescence properties in Stearic Acid

The solid SA/MEH-PPV 0.1% mixture presented a broad emission band with λ_{max} = 617 nm and a weak shoulder at 550 nm. Once the system was heated above T_m^{SA} (80 ºC), the phase transition induced a slight increase of the emission intensity. More importantly, the normalised spectra of the melted mixture evidence a hypsochromic shift of the emission maximum of 13 nm (617→604 nm) and the appearance of an intense shoulder at 542 nm, which was strong enough to contribute on the shift of the emitted colour (Figure 3.8a-b). The colour change is so large that becomes to be visible by also naked-eye (Figure 3.8c), as showed by digital camera images of the sample in the solid (on the left) and liquid phase (on right) irradiated by UV-lamp.

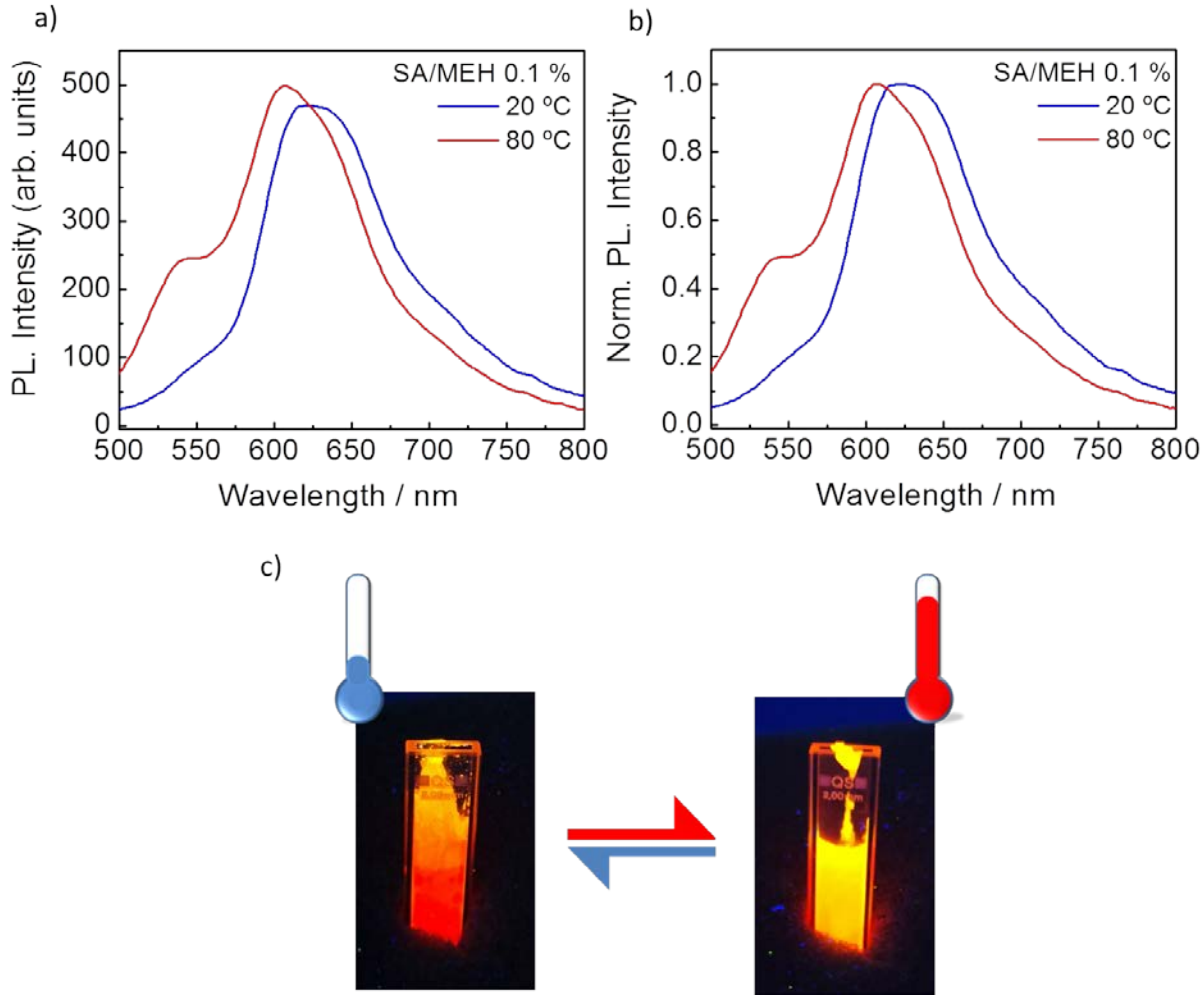

Figure 3.8. *a)* Digital camera image of sample NA/MEH 0.1% at 0 °C (left) and RT (right) irradiated by UV-lamp (365 nm); *b)* emission spectra and *c)* normalised emission spectra of sample SA/MEH 0.1% measured at 20 °C and 80 °C irradiating at λ_{max} = 490 nm.

The switch of the fluorescence provided by the lower concentrated SA/MEH 0.01% mixture was even more important. Upon melting, the broad emission band (with λ_{max} = 580 nm and a pronounced shoulder at 617 nm) recorded at 20 °C changed to a double picked spectrum (of half intensity) with a band at 580 nm and a new high-energy one at 544 nm (Figure 3.9b). The rise of this band and the decrease of the relative intensity of the low-energy shoulder is a clear indication that in this melted mixture there is a strong contribution of the emission deriving from the intrachain exciton. Actually, the spectral profile of this mixture resembles the 0-0, 0-1 and 0-2 vibronic progression characteristic of the spectra of low concentrated solutions of MEH-PPV in good organic solvents, for which it is reported that the emission is mainly given by the intrachain exciton and in less amount by interchain interacting species.[14] The high temperature required to melt the SA could also contribute to the improvement of the solvation of the MEH-PPV.

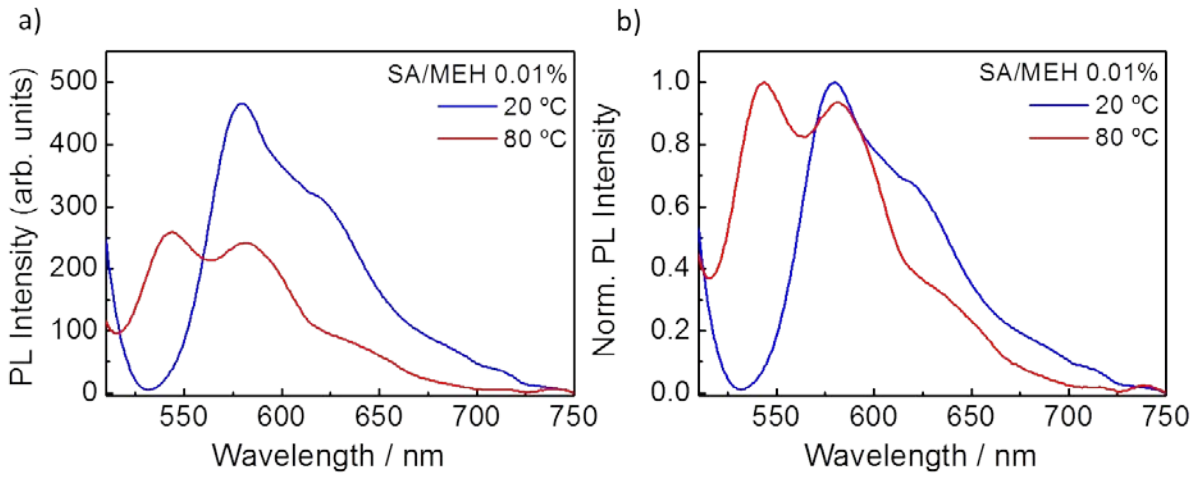

Figure 3.9. *a)* Emission and *b)* normalised emission spectra of sample SA/MEH 0.01% measured at 20 °C and 80 °C irradiating at λ_{max} = 490 nm.

MEH-PPV fluorescence properties in dodecanoic acid

The solid DA/MEH 0.1% mixture presented a broad and intense emission band with λ_{max} = 614 nm and two weak shoulders at 564 nm and 650 nm. Once the mixture was heated above the T_m^{DA} (60 °C), *i)* the (integrated) emission intensity was reduced by about half, (from 2.91×10^4 to 1.65×10^4 arb. units), *ii)* the emission maximum was blue-shifted of 19 nm (614→595 nm), as confirmed by the normalised spectra (Figure 3.10c) and *iii)* the high-energy band appeared at λ = 546 nm together with a pronounced shoulder at λ = 634 nm.

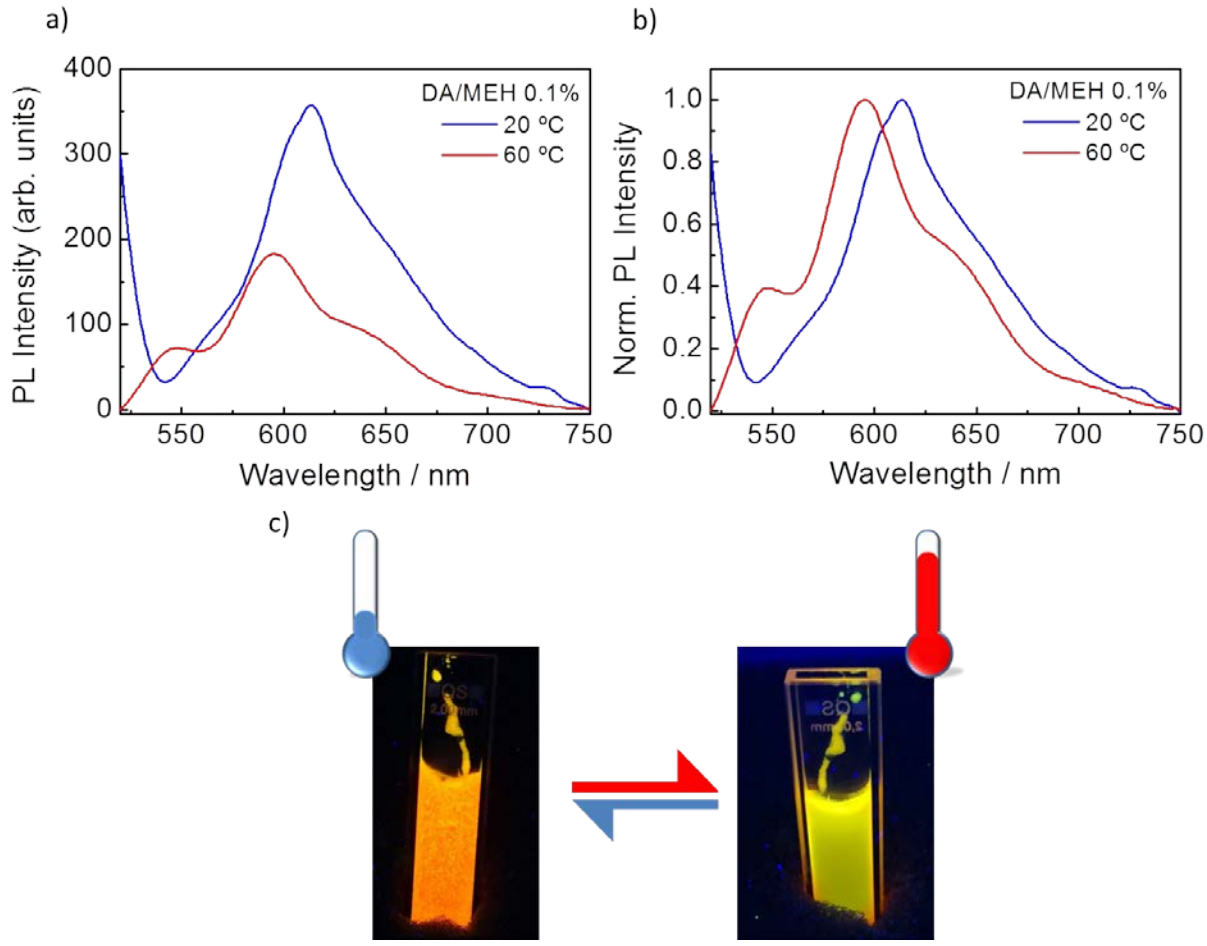

Figure 3.10 *a)* Emission spectra and *b)* normalised emission spectra of sample DA/MEH 0.1% measured at 20 °C and 60 °C; *c)* digital camera image of sample NA/MEH 0.1% at 0 °C (left) and RT (right) irradiated by UV-lamp (365 nm).

The contribution of the high-energy band to the bulk emission of the mixture was strong enough to produce a colour emission change from orange to yellow, as showed by the digital camera images of DA/MEH 0.1% in the solid (on the left) and liquid phase (on right), irradiated by UV-lamp (Figure 3.10a).

Similar results were observed with the DA/MEH 0.01% mixture, which at 20 ºC presented a broad and intense emission band with maximum at λ_{max} = 611 nm and a weak shoulder at 567 nm (Figure 3.11a). Once the solution was heated above T_m^{DA}, (60 ºC) the emission intensity was reduced by half (from 1.29×10^5 to 0.60×10^5 arb. units). Worth to mention that the phase change produced a shift of the main band as high as 30 nm (611→581 nm) and the appearance of the strong high energy band at λ_{max} = 548 nm, related to the 0-0 vibronic transition of the intrachain exciton of the polymer. The weak shoulder appearing at 643 nm confirms the lower contribution of species deriving from polymer the interchain. Notably, in this case, the spectral shift (of 30 nm) produced by this mixture during the phase

change was 10 nm larger than what obtained by the concentrated sample and the largest among all PCM investigated samples. Moreover, considering that the strong high-energy band quickly appeared at 548 nm with also higher relative intensity than the concentrated sample, the colour-shift effect is even larger.

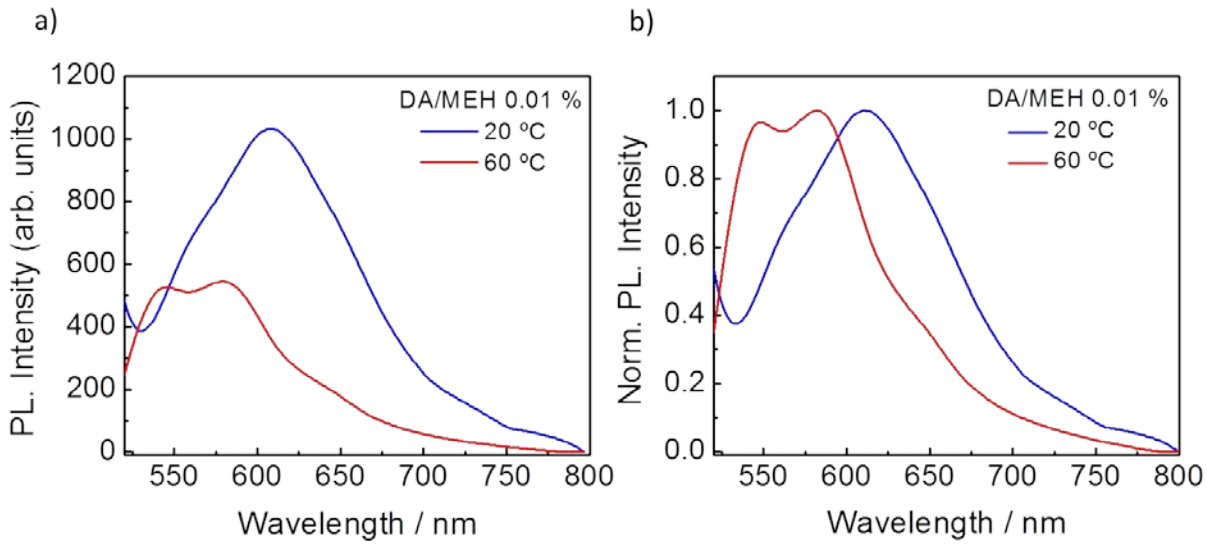

Figure 3.11. *a)* Emission spectra and *b)* normalised emission spectra of sample DA/MEH 0.01% measured at 20 °C and 60 °C. All the spectra were obtained irradiating at λ_{max} = 490 nm.

MEH-PPV fluorescence properties in Nonanoic Acid

The solid NA/MEH 0.1% and NA/MEH 0.01% mixtures, measured at 0 ºC presented a broad, unstructured and intense emission band with a maximum at λ_{max} = 610 nm and 589 nm, respectively and shoulders at 648 nm. The blue-shifted (21 nm) emission maximum of the diluted sample was ascribed to the better solvation of the polymer chains by the shorter aliphatic moiety of NA, even in the solid phase.

Once the solutions were heated at 30 °C, the emission intensities of the main bands decreased (more than half for the concentrated solution, a bit less for the diluted one), similarly to what observed for the previous samples (Figure 3.12a and Figure 3.12c). The normalised spectra evidenced a 18 nm hypsochromic shift (610→592 nm) of the main emission band of the concentrated sample (Figure 3.12b). No shift was observed for the NA/MEH 0.01% (Figure 3.12d), since the solid NA was already solvating enough the MEH-PPV to provide a blue-shifted band. In both solutions a strong high-energy band appeared at λ_{max} = 549 nm and 550 nm, together with the pronounced shoulders at 641 and 645 nm, respectively. The structured bands of the spectra obtained in the liquid NA could be

associated to the 0-0, 0-1 and 0-2 vibronic transitions characteristic of the polymer in good organic solvents.

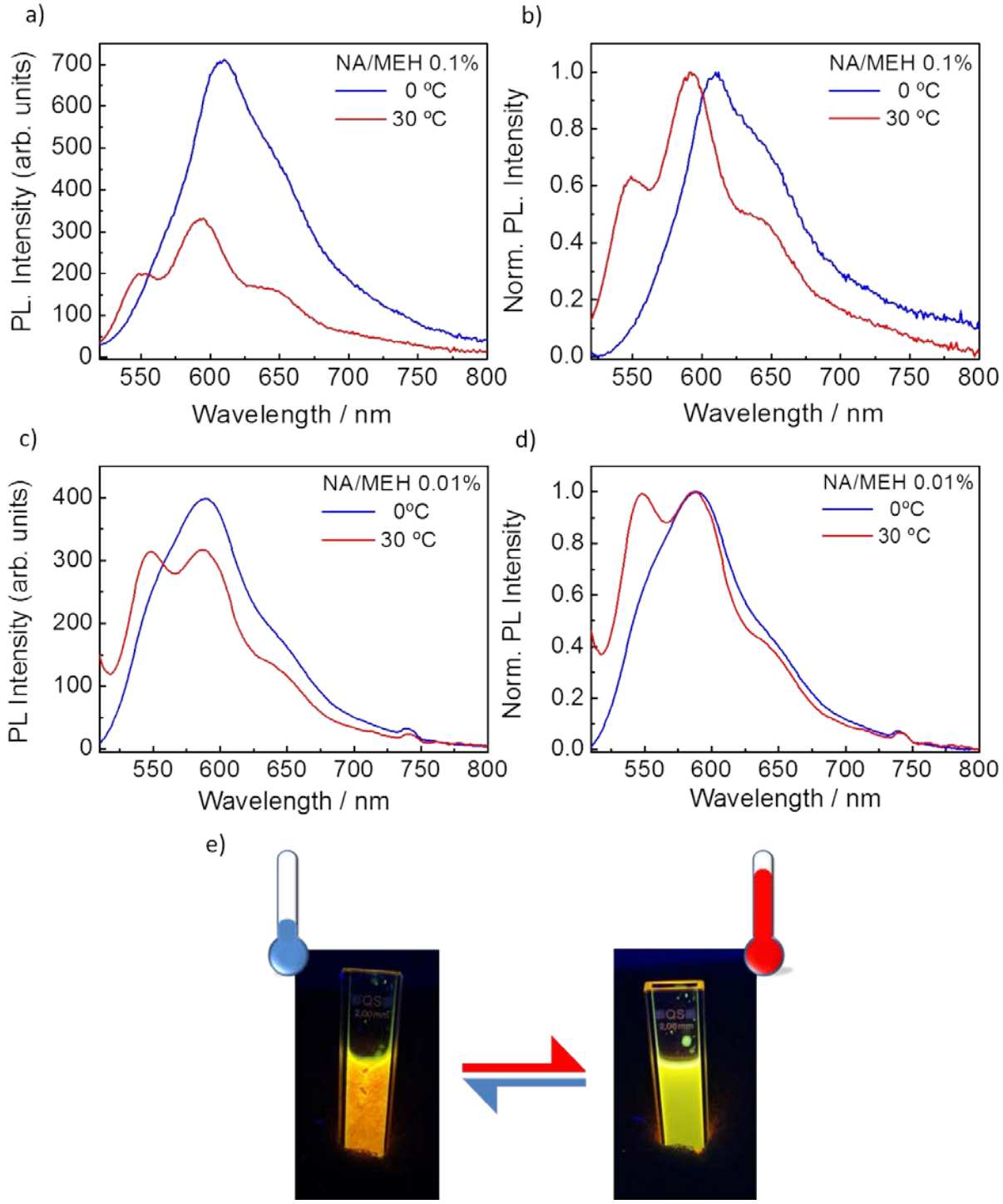

Figure 3.12. *a)* Emission spectra and *c)* normalised emission spectra of sample NA/MEH 0.1% measured at 0 °C and 30 °C; *c)* emission and *d)* normalised emission spectra of sample NA/MEH 0.01% measured at 0 °C and 30 °C. (All the spectra were obtained irradiating at λ_{max} = 490 nm). *e)* Digital camera image of sample NA/MEH 0.1% at 0 °C (left) and RT (right) irradiated by UV-lamp (365 nm).

The colour change of the solutions was so evident that it could be detected by naked-eye, as showed by digital camera images of the NA/MEH 0.1% mixture in the solid (on the left) and liquid phase (on right) irradiated by UV-lamp (Figure 3.12e).

Solvent polarity effect on MEH-PPV fluorescence

MEH-PPV showed better solubility in fatty acids PCM, as proved by the previous results, probability due to the different polarity of the fatty acids compared to the paraffins. To confirm such hypotheses, we planned an additional experiment where an organic acid was slowly added to the EC/MEH-PPV 0.01% solution to increase in a controlled manner the polarity of the medium. More precisely, acetic acid (AA) was selected as the organic acid.

The addition of AA to the melted sample (1 mL) induced a remarkable variation of the emission of the polymer, after adding 100 µl a new band at 539 nm appeared. This band was not present in the melted EC/MEH 0.01% mixture. The emission intensity of such band, associated to the intrachain exciton, increased raising the amount of AA from 100 to 500 µl (Figure 3.13). The increased polarity of the media due to the presence of the acetic acid favour the disaggregation and stabilising the polymer in the elongated chain conformation.

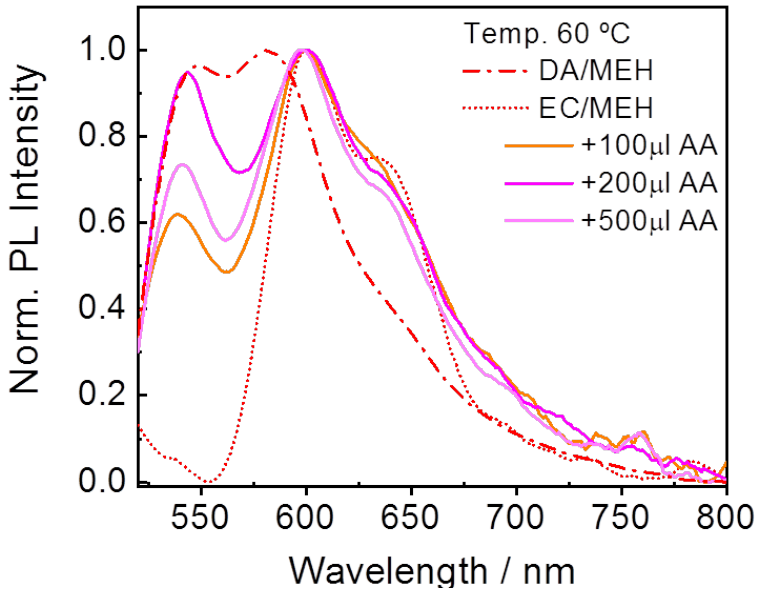

Figure 3.13. Emission spectra of DA/MEH 0.01% (red dash dot line) and EC/MEH 0.01% (red dot line) mixtures measured at 60 °C and after addition of increasing amount of acetic acid (AA) to the EC/MEH mixture.

3.3.1.4 Detailed study of the DA/MEH 0.1% and NA/MEH 0.1% mixtures

Temperature-dependence study of the PCM/MEH mixtures

To get finer information on the variation of the optical properties of the mixture above and below T_m^{DA}, temperature-dependent fluorescence measurements were carried out in a range of temperature of interest (from 20 to 90 °C for DA/MEH 0.1% and from 0 to 40 ºC for NA/MEH 0.1%), every 10 °C (Figure 3.14). First, both samples were stabilized at 0 °C for 10 minutes, after which the emission was measured at this temperature.

Below T_m^{DA}, when the temperature was increased up to 40 °C the emission intensity of DA/MEH diminished significantly, though the position of the emission maximum (λ_{max} = 614 nm) suffered no variations. At 50 °C, just above T_m^{DA}, the spectral variation follows the same trend as that observed until 40 ºC, with a further decrease of the intensity and a slight blue shift (5 nm) of the emission band. However, the most dramatic changes of the spectral features are observed only above this temperature, when the melting of DA was completed melted. The phase transition of the mixture induced a decrease of the fluorescence intensity (possibly associated to the experimental setup) and, more importantly, a prominent blue shift (19 nm) of the main band and the appearance of new defined bands, characteristic of the vibronic transitions 0-0, 0-1, and 0-2 observed in liquid solution of good organic solvents.[14] Heating above the T_m^{DA}, from 60 ºC to 90 °C, no significant changes of the emission intensity and bands positions were observed, apart from the little variation of the ratio between the bands at 546 nm and 595 nm. Quenching of the emission caused by the temperature increase (from 20 to 60 ºC) was excluded, since heating from 60 °C to 90 °C the emission intensity did not lead to a further decrease of the emission (Figure 3.14a and Figure 3.14b). Notably, while in a large range of temperatures below or above the T_m^{DA} there is almost no change of the spectral properties, a dramatic variation is verified in only 10 ºC, during which the melting of the PCM is produced.

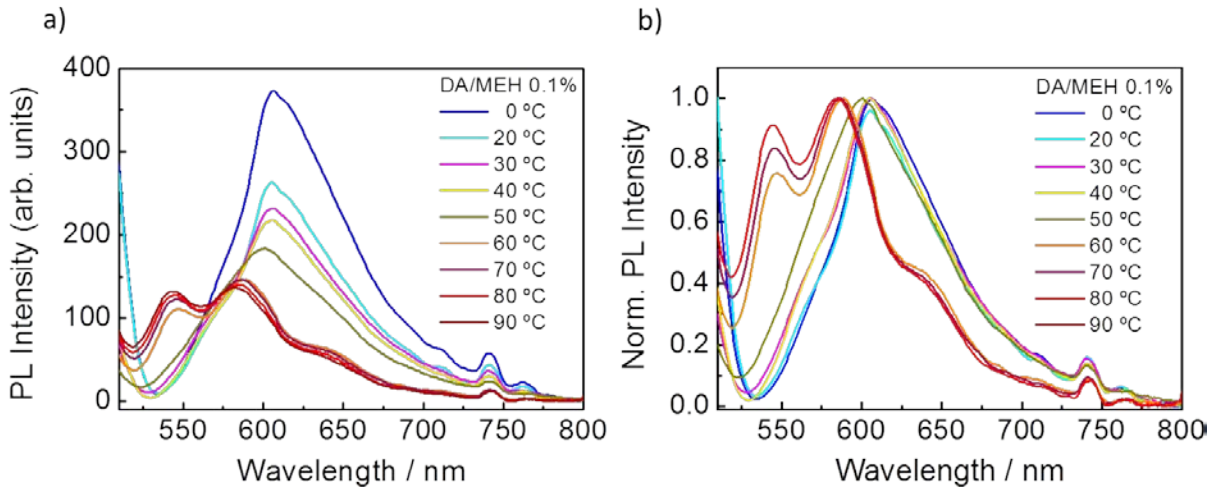

Figure 3.14. *a)* emission spectra and *b)* normalised emission spectra of sample DA/MEH 0.1% measured at 0 °C and each 10 °C from 20 °C to 90 °C (coloured solid line). All the spectra were obtained irradiating at λ_{exc} = 490 nm.

Similar results were obtained for NA/MEH 0.1%. The spectral changes (intensity, shift and appearance of the high-energy band) were produced heating the sample from 0 to 10 ºC. Above this temperature there is a negligible variation of the relative intensity of the high-energy band and no further hyposchromic shifts or new bands formation are observed. Again, the major variations of the spectral features (position and shape) are observed around the T_m^{NA} and follow the same trend observed in DA samples, with the only difference that the spectral changes were observed around 0-10 ºC, instead of around 50-60 ºC, clearly indicating that they are strictly related to the T_m^{PCM}. Also in this case, the fact that this variation is produced passing from 0 to 10 ºC rather than from 10 to 20 ºC (T_m^{NA} = 12 ºC) was ascribed to the cooling efficiency of the sample chamber, which probably was at slightly higher temperature than the set in the thermostate.

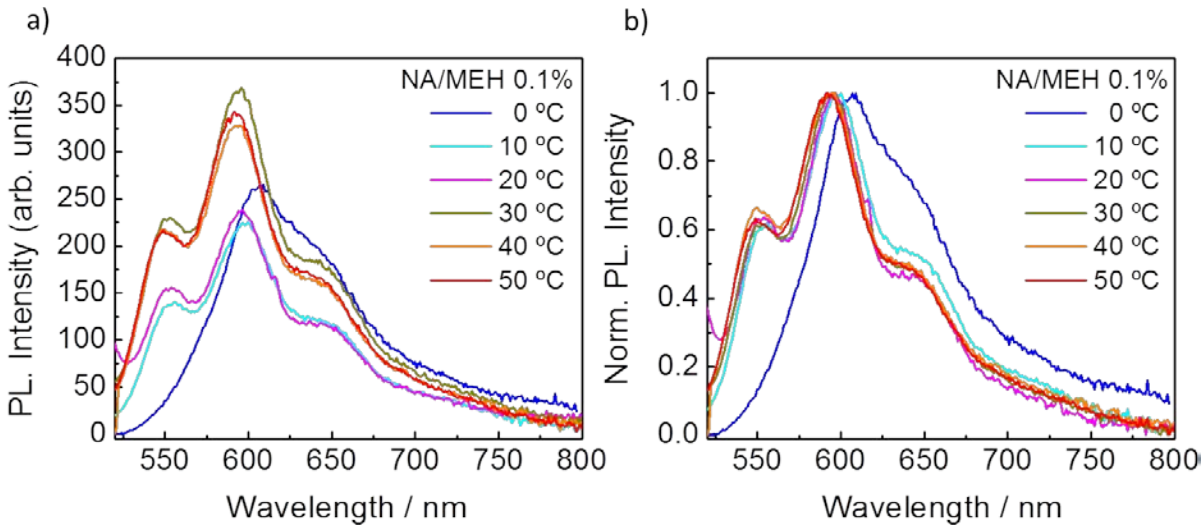

Figure 3.15. *a)* Emission spectra and *b)* normalised emission spectra of sample NA/MEH 0.1% measured each 10 °C from 0 °C to 50 °C (coloured solid line). All spectra were obtained irradiating at λ_{max} = 490 nm.

It must be mentioned that the bands ratios (between the 0-0 and 0-1 bands) of the sample DA/MEH 0.1% studied every 10 ºC was different from those obtained measuring the fluorescence just at two temperatures, below and above the T_m^{PCM} (Figure 3.12a and b). This behaviour was ascribed to the fact that for these temperature-dependent fluorescence measurements, the sample was previously subjected to heating and cooling cycles. The repeated heating possibly guaranteed a better solubilisation (and disaggregation) of the polymer chains and an increase of the contribution of the intrachain exciton (higher relative intensity of the high-energy 0-0 vibronic band) to the final spectra.

From these experiments, it can be stressed that in DA/MEH 0.1% and NA/MEH 0.1% mixtures, the main changes in the emission of MEH-PPV are primarily produced by the phase change of the PCM, rather than by the variation of temperature itself, confirming the hypothesis that the phase of the PCM (specifically the fatty acids) can be used to tune the optical properties of the conjugated polymer. The fact that the most pronounced variation of the fluorescence in DA/MEH-PPV is observed between 50-60 ºC, rather than between 40-50 ºC (where it would be expected since the T_m^{DA} = 42 ºC), and between 0-10 ºC, rather than between 10-20 ºC (T_m^{DA} = 12 ºC), was ascribed to the effective temperature of the sample chamber, which was possibly slightly lower than the 50 ºC or higher than the 10 ºC set in the thermostat.

Study of the reversibility of the PCM/MEH mixtures

To verify the reversibility of the DA and NA-based switches, repeated heating-cooling cycles from below to above the respective T_m^{PCM} were carried out (Figure 3.16). This study was performed for the DA-based (DA/MEH 0.1% and DA/MEH 0.01%) and NA-based (NA/MEH 0.1%) switches. For all samples, the corresponding spectral shifts were reproduced after each cycle (band positions fully recovered), confirming in all cases the reversible behaviour. Emission intensity variations were observed, without following a specific trend after each cycle. The random oscillations of the emission intensity in both solid and liquid mixtures is still not clear, though degradation of the MEH-PPV was excluded since *a)* the intensity does not decrease after each cycle and *b)* the mixtures were all highly fluorescent after months of storage. Finally, normalising the spectra respect to the respective 0-1 vibronic transition band it could be observed an increase (no shift) of the 0-0 vibronic transition band in liquid PCMs. The variation of the relative band intensity was an indication of the presence of fewer polymer aggregates after each cycle, possibly due to the increased solvation degree of the polymer chains after each melting process.

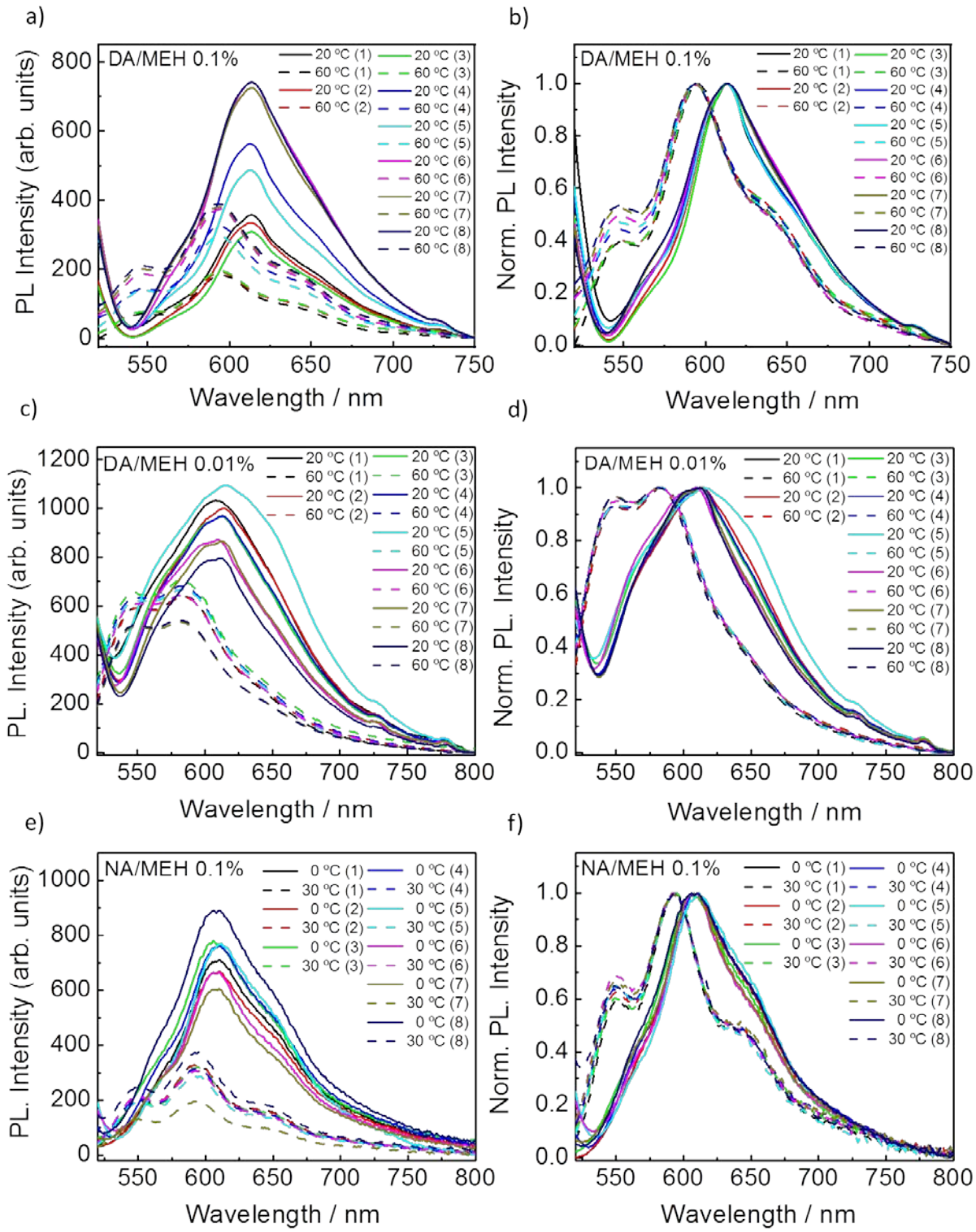

Figure 3.16. *a)* emission and *b)* normalised emission spectra of DA/MEH 0.1% measured at two different temperatures, 20 °C (solid lines) and 60 °C (dashed lines) performing a total of eight cycles of heating and cooling; *c)* emission and *d)* normalised emission spectra of DA/MEH 0.01% measured at two different temperatures, 20 °C (solid lines) and 60 °C (dashed lines) performing a total of eight cycles of heating and cooling; *d)* emission spectra of NA/MEH 0.1% measured at two different temperatures, 0 °C (solid lines) and 30 °C (dashed lines) performing a total of eight cycles of heating and cooling; *e)* emission spectra of the heating-cooling cycles normalised. (All spectra were obtained irradiating at λ_{max} = 490 nm).

Study of the MEH-PPV solubility in fatty acids PCM

The fluorescence of the polymer changed from DA to NA and also in the same PCM between the two concentrations (0.1% and 0.01%). In particular, the emission spectra of the MEH-PPV showed an increase in the relative intensity of the high energy peak in liquid PCM, passing from dodecanoic to nonanoic acid and also in the same fatty acids decreasing the concentration. Such band come from solution-like polymer chain, and the changing in the intensity indicates better solubility of it. To confirm the better solubility of the polymer in NA, deduced from the fluorescence spectra, dynamic light scattering (DLS) analysis of the NA/MEH 0.1%, DA/MEH 0.1% and 0.01%, was performed (Figure 3.17). The polymer in $CHCl_3$ was also studied for comparison. The mixture NA/MEH 0.1% presented a single peak to 23.61 nm, while for the mixture DA/MEH 0.1% was found a bimodal distribution with the two peaks at 287.1 and 1237 nm. The drastic reduction in the hydrodynamic radius of the MEH-PPV in NA compared to DA proved the low aggregation, thereby the better solubilisation of the polymer in NA. The bimodal distribution was still present in DA upon lowering the concentration, but the peaks shifted to lower dimension (255 nm and 37 nm) as a result of the increased polymer dispersion. Interestingly, MEH-PPV in CHCl3 (with 0.1 wt.% concentration) showed a multimodal size distribution with three peaks at 655.3, 99.8, and 19.3 nm, which are smaller than the ones in DA, whereas larger than the single peak in NA, suggesting the solvation of NA to be even higher that $CHCl_3$.

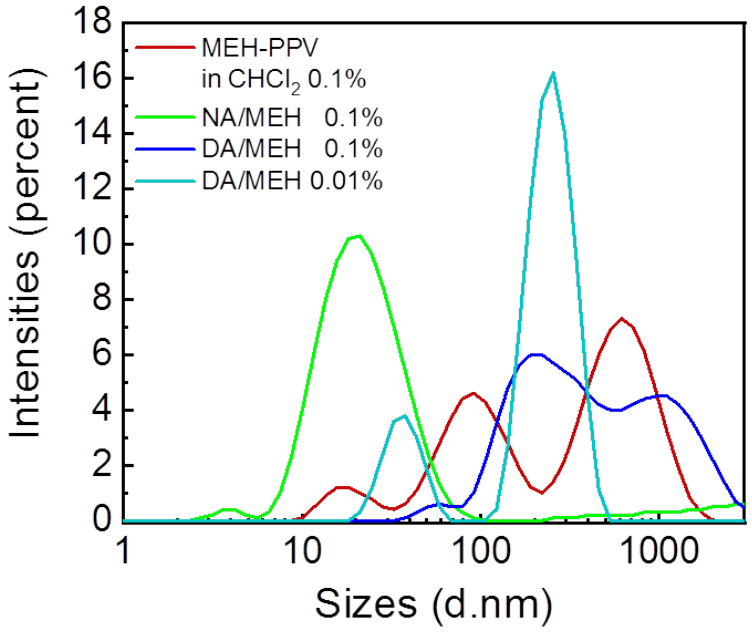

Figure 3.17. DLS analysis of the mixtures NA/MEH 0.1% (green line), DA/MEH 0.1% (blue line), DA/MEH 0.01% (turquoise line), and MEH-PPV in $CHCl_2$ 0.1%.

In summary, PCMs of different families were tested as medium providing switchable fluorescent property of the dissolved MEH-PPV polymer. Paraffin PCMs were not solvating enough the polymer in both solid and liquid phase, fact that prevented the switching of the optical properties of the polymer. Non-paraffin PCMs, with more solvating properties, allowed observing larger switch. The PCM type and the concentration revealed to be important parameters to obtain mixtures with large spectral shifts. Fatty acid PCMs of three different melting points were far better than the others to achieve larger spectral shift, with the record belonging to the DA/MEH 0.01% mixture which provided 30 nm of shift of the main band. Moreover the colour shift effect is enhanced by the appearance of the strong high-energy band at 548 nm. The use of the three fatty acids would allow the fabrication of multi-temperature sensors, providing spectral changes around the respective melting points. Fine temperature-dependent experiments proved that while little spectral variations were detected in a wide range of temperature changes, above or below the T_m^{PCM}, abrupt modifications were induced in only 10 ºC, crossing the T_m^{PCM}. The abrupt spectral change observed within a narrow range of temperature, makes the fatty acids/MEH mixtures potential precise temperature sensors. Moreover, the fact that the switch is always produced around the T_m^{PCM}, excludes that the emission colour change is related to the intrinsic thermofluorochromism of the polymer which, though it is reported, it provides a continuous (not abrupt) variation of the spectral properties and requires 100 of ºC of temperature change.[19,20] Finally, two of the investigated mixtures proved to provide reversible spectral shifts upon several cooling/heating cycles. The random variation of the intensity it is still not completely understood (possibly related to the experimental setup), though degradation was excluded.

3.3.1.5 Analysis of the spectral signature

Liquid PCMs

As discussed above, fatty acid were the PCMs that induced the largest spectral changes of the MEH-PPV emission. In particular, upon melting of the solutions of MEH-PPV, the main effects produced were:

- Structuration of the emission spectra in three main features (2 bands and one shoulder),
- Hypsochromic shift of the main emission band.
- Formation of high-energy band around ~ 550 nm.

The structured spectra are composed by progressions of possible vibronic bands, which are summarized in the Table 3.2.

DA MEH-PPV conc.	PCMs state	λ_{0-0}	λ_{0-1}	λ_{0-2}
0.1%	Solid	564 nm	614 nm	650 nm
	Melted	546 nm	595 nm	634 nm
0.01%	Solid	567 nm	610 nm	-
	Melted	548 nm	581 nm	643 nm
NA MEH-PPV conc.	PCMs state	λ_{0-0}	λ_{0-1}	λ_{0-2}
0.1%	Solid	-	610 nm	648 nm
	Melted	549 nm	592 nm	641 nm
0.01%	Solid	-	589 nm	640 nm
	Melted	548 nm	588 nm	638 nm
SA MEH-PPV conc.	PCMs state	λ_{0-0}	λ_{0-1}	λ_{0-2}
0.1%	Solid	550 nm	617 nm	650 nm
	Melted	542 nm	604 nm	629 nm
0.01%	Solid	567 nm	580 nm	617 nm
	Melted	544 nm	580 nm	640 nm

Table 3.2. λ_{max} of the bands corresponding to the vibronic transition 0-0, 0-1, 0-2 of the DA/MEH, NA/MEH, and SA/MEH mixtures at 0.1% and 0.01% concentrations in the solid and liquid PCMs phase.

Below the spectral features of the mixtures are analysed in more details. The analysis mainly focuses on DA/MEH 0.1 mixture, though similar observations can be extrapolated for the other fatty acid mixtures.

DA liquid solutions of MEH-PPV (above T_m^{DA}) showed structured emission spectra at both polymer concentrations, with quite well defined bands (Figure 3.10 and Figure 3.11). The presence of such bands (and shoulders) can be explained by the co-existence of different interchain and intrachain emitting species. The structured emission spectra of DA/MEH mixtures (made of two defined bands and a longer wavelength shoulder) resemble, in spite of the bands ratio differences, the one obtained from dichloromethane (CH_2Cl_2) solutions of MEH-PPV (Figure 3.18b), in which both the bands and the shoulder are at similar positions

(λ = 562, 605 and 660 nm). These bands are well documented in the literature for diluted solutions of MEH-PPV in good solvents (e.g. CH_2Cl_2) and are assigned mainly to the intrachain exciton vibronic transitions of an extended polymer chain.

To better understand the spectral composition, the emission spectra of DA/MEH 0.1% obtained at 60 °C and of the DCM solution were deconvolved into 4 Gaussian bands (Figure 3.18a). This procedure is reported in the literature, though in some cases, Lorentzian or a mixture of both is also used.

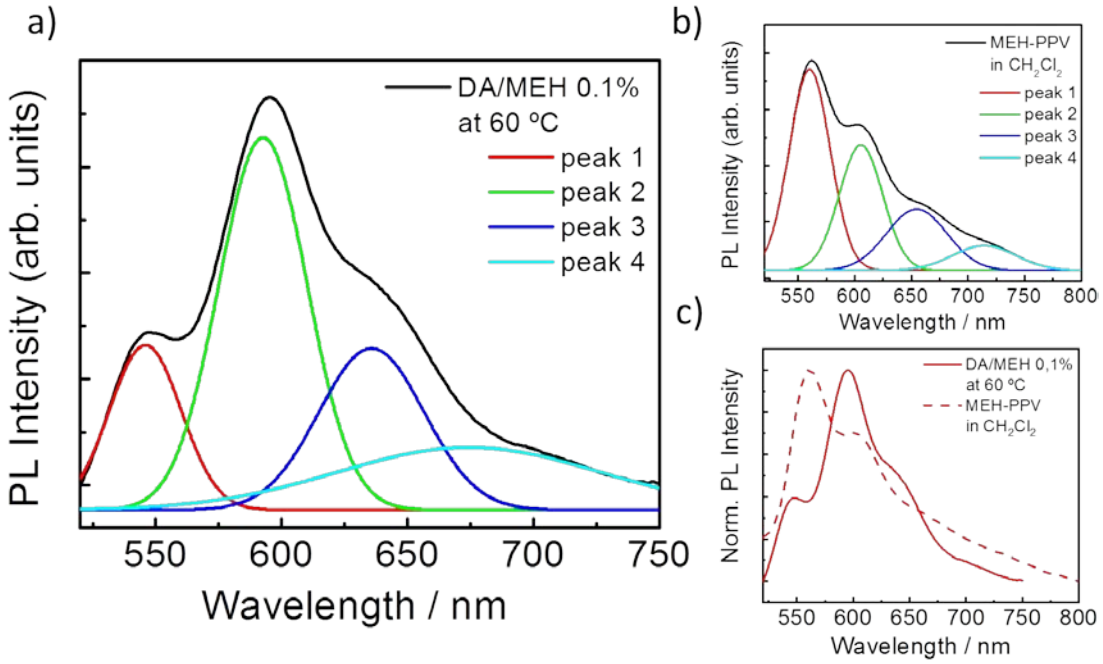

Figure 3.18. *a)* Emission spectra of DA/MEH-PPV 0.1% measured at 60 °C (black line) deconvolved into four Gaussian bands. The red (maxima at 545 nm), green (maxima at 595 nm) and blue (maxima at 636 nm) bands correspond to the vibronic transitions 0-0, 0-1 and 0-2 respectively. The cyan band (maxima at 670 nm) represents the emission from polymers aggregates. *b)* Emission spectra of MEH-PPV dissolved in DCM (black line) measured at room temperature also deconvolved into four Gaussian bands. The red (maxima at 560 nm), green (maxima at 606 nm) and blue (maxima at 654 nm) bands correspond to the vibronic transitions 0-0, 0-1 and 0-2 respectively. The cyan band (maxima at 710 nm) represents the emission from polymers aggregates. *c)* emission spectra of sample DA/MEH-PPV 0.1% measured at 60 °C (solid red line) and MEH-PPV in DCM measured at room temperature (red dashed line).

The deconvolved bands of the DA/MEH 0.1% mixture with maxima at λ_{max} = 545 nm, 595 nm and 636 nm were associated to the vibronic transitions 0-0, 0-1, and 0-2 respectively. The band at 670 nm was, instead, related to the emission of large aggregates, which are also present in concentrated MEH-PPV solutions[14] or solid films[49].

Upon comparison of the normalised fluorescence spectra of MEH-PPV dissolved in CH_2Cl_2 and in liquid DA, significant differences of the relative intensities of the four peaks were detected (Figure 3.18c). Two possible effects can arise for such difference:

- the simultaneous presence of the polymer as a single elongated chain (isolated solution-like chains) and as domains of packed chains (aggregated film-like chains).[47]
- the variation of the vibronic structure of the intrachain exciton depends on the polarity change experienced by the polymer in different environments, as reported by Schwartz and co-workers.[14] The change in the relative intensities of the emission bands are assigned to variations of the vibronic coupling: the alteration of the interactions between adjacent chromophores changes both the Franck-Condon emission envelope and the number of sequence and combination bands underlying the main vibronic structure.[14] We could hypothesise that the polar head of the fatty acid influences the dipole moment of the different interchain excited state of the polymer. When the DA is liquid, the polymer chains experience a local surrounding environment with different dielectric properties, which induces geometry modifications with a consequent energy reorganisation.[50]

In order to analyse the spectra *liquid fatty acid* (SA, DA, NA) mixtures with MEH-PPV at different concentrations (0.1 wt.% and 0.01 wt.%) it was taken into account the relative intensities ratio between the 0-0 and 0-1 vibronic transition bands ($I_{0\text{-}1}/I_{0\text{-}0}$). This intensities ratio is correlated with the Huang-Rhys factor, *S*, which is actually given by the expression:

$$I_{0-1}/I_{0-0} = S \quad (1)$$

This parameter is a measurement of the displacement of the minimum energy positions of harmonic vibrational potentials associated with ground and excited electronic states. *S* describes the difference between ground and excited state geometries which affect the linear vibrational coupling to electronic excitations. In works reported in the literature it has been demonstrated that the Huang-Rhys factor correlates with the conformational disorder: larger *S* values are associated to increased disorder and, thus, to the formation of aggregates.[3] The variation of the relative intensity of 0-0 and 0-1 vibronic bands, ($I_{0\text{-}1}/I_{0\text{-}0}$), with the polymer concentration, is reported in the literature to be an evidence of aggregation and normally it diminishes upon increasing polymer concentration.[51] This relative increase is explained taking into account that the aggregates of MEH-PPV emit around 598 nm. Such emission coincides with the vibronic 0-1 band of the intra-chain isolated chromophore. Thus, the overlap of the emission of the polymer aggregates and that deriving from the 0-1 vibronic transition of the isolated chains leads to higher intensity emission in this spectral region (and lower $I_{0\text{-}1}/I_{0\text{-}0}$ value) when more aggregates are formed. Its higher value at lower temperatures

and higher concentrations is evidence that supports the coexistence of single elongated polymer chains and domains of packed chains.

From the $I_{0\text{-}1}/I_{0\text{-}0}$ ratio of the normalised spectra of the fatty acid mixtures, it is observed that (Table 3.2):

- *the temperature increase above the T_m^{PCM} gives lower $I_{0\text{-}1}/I_{0\text{-}0}$ values*. This is valid for the DA/MEH mixture, where the $I_{0\text{-}1}/I_{0\text{-}0}$ ratio passes from 1.32 (60 ºC), 1.19 (70 ºC), 1.10 (80 ºC), and 1.03 (90 ºC), indicating a decrease of the aggregate emission. By applying more energy to the system (as heat), the motion of the molecules increases, and the polymers aggregates redissolve, leading to a variation of the emission spectra (Figure 3.14). In the case of the NA/MEH mixture, upon phase change transition the higher degree of disaggregation is already reached and does not vary rising the temperature. This behaviour cab assigned to a better solubility of the polymer in NA.
- *dilution of the mixtures gives lower $I_{0\text{-}1}/I_{0\text{-}0}$ values*. The $I_{0\text{-}1}/I_{0\text{-}0}$ ratio passes from 2.54 (DA/MEH 0.1%), 1.66 (NA/MEH 0.1%) and 2.04 (SA/MEH 0.1%) to 1.04 (DA/MEH 0.01%), 1.01 (NA/MEH 0.01%) and 0.94 (SA/MEH 0.01%). In all the cases the relative intensity of the 0-0 vibronic transitions band increases upon dilution. Less concentrated solutions favour the dissolution of the aggregates and the emission from the intrachain exciton (Table 3.3).
- *the $I_{0\text{-}1}/I_{0\text{-}0}$ changes with the length of the alkyl chain of the PCM*. The $I_{0\text{-}1}/I_{0\text{-}0}$ ratio of the melted NA/MEH 0.1% is 1.66, much smaller than the DA/MEH 0.1% value (2.54), indicating a lower presence of aggregates. On the other hand, the $I_{0\text{-}1}/I_{0\text{-}0}$ ratio for the liquid SA/MEH 0.1% (2.04) is higher than for NA/MEH 0.1% (1.66) but smaller than that of DA/MEH 0.1% (2.54). This indicates that longer alkyl chains induce more formation of polymer aggregates. The $I_{0\text{-}1}/I_{0\text{-}0}$ higher value of SA/MEH 0.1% (less aggregates) than the solution of the shorter fatty acid DA/MEH 0.1% could be explained by the fact that to achieve liquid SA it must be reached a higher temperature, which should favour the dissolution of the polymer and the decrease of the aggregates. This is also observed in the less concentrated SA/MEH 0.01%, whose $I_{0\text{-}1}/I_{0\text{-}0}$ = 0.94 means that the high-energy 0-0 vibronic band is stronger than the 0-1 one. This is the highest value obtained for all fatty acid solutions, though it is made by SA, which as longest alkyl chain. The high temperature required to melt the PCM and the lower concentration of the polymer guarantee a much better solvation of the polymer.

	0.1%			0.01%		
	$I_{0\text{-}0}$	$I_{0\text{-}1}$	$I_{0\text{-}1}/I_{0\text{-}0}$	$I_{0\text{-}0}$	$I_{0\text{-}1}$	$I_{0\text{-}1}/I_{0\text{-}0}$
DA/ MEH-PPV	71.93	182.74	**2.54**	526.01	544.89	**1.04**
NA/ MEH-PPV	200.30	331.64	**1.66**	313.98	316.44	**1.01**
SA/ MEH-PPV	243.87	498.49	**2.04**	258.77	242.27	**0.94**

Table 3.3. Emission intensities of the peaks for the transition 0-0 and 0-1, and the ratio between these two peaks for the MEH-PPV in three different fatty acid and at two different concentrations.

Solid PCMs

The emissions from the *solid mixtures* are also studied in details. Usually, the increase of the interaction between polymer chains results in the red-shift of the emission spectra and, often, in the decrease of the emission intensity of the polymer system. This phenomenon is due to the energy transfer processes among the polymer chains allowing the higher excited state to access longer conjugated segments. In this way, the emission comes from lower energy states. This phenomenon is dominated by Foster energy transfer, which implies a non-radiative energy transfer between a donor and acceptor sites separated by certain distance r.[52] The energy transfer rate is proportional to the inverse of the sixth power of the distance ($1/r^6$) between two sites; thus decreasing rapidly with the increase of the distance.

The red-shifted emission of the solid DA/MEH 0.1%, compared to the liquid mixture, was ascribed to both an environment with higher dielectric constant, as other polymer chains surrounding the emitting polymer chain, and an increased Forster energy transfer. Furthermore, the reduction of the vibronic structure of the spectra recovered in the solid state of the PCM is another sign of the polymer aggregation. These data are in accordance with the photoluminescence studies of MEH-PPV solid films.

The emission band of SA/MEH 0.1% presents a very broad band with maximum at 620 nm, which is probably due to the superimposition of the emission from different species. Figure 3.19c shows the emission of SA/MEH 0.1% at 20 °C deconvolved into four Gaussian bands. The deconvolution highlights that the intensities of the emission from the 0-1 (607 nm) and 0-2 vibronic transition (642 nm) are comparable, indicating that it is likely to have a higher contribution to the emission from aggregates states than in the other mixtures. Indeed,

DA/MEH 0.1 and NA/MEH 0.1 mixtures in their solid state show a less intense emission around 650 nm which appear, instead, as weak shoulders.

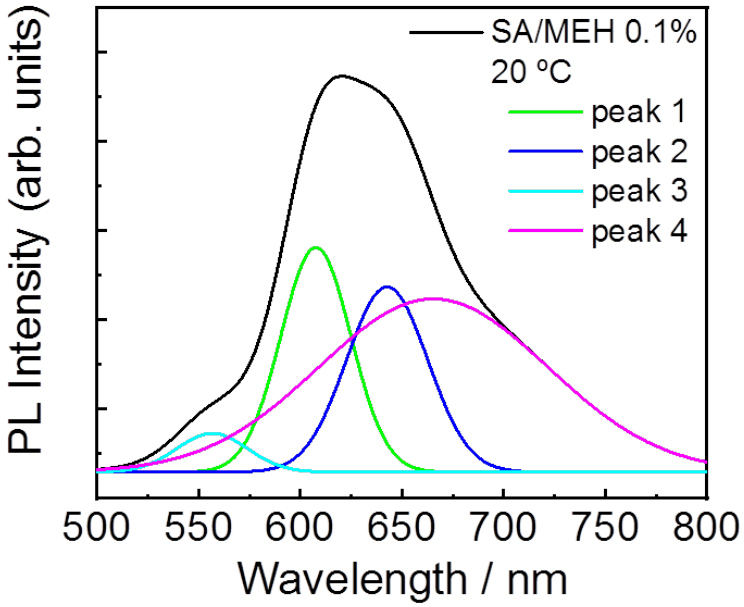

Figure 3.19. Emission spectra of SA/MEH 0.1% measured at 20 °C (black line) deconvolved intofour Gaussian bands with λ_{max} = 555 nm (cyan), 607 nm (green), 643 nm (blue) and 667 nm (magenta).

3.4 IMPLEMENTATION AND PROTOTYPE

The change in the colour of the emitted light upon the heating of the system DA/MEH-PPV is noticeable even at naked eyes. Figure 3.20 reports a picture where on the left there is a piece of cellulose filter paper soaked with the liquid sample NA/MEH 0.1% (top), DA/MEH 0.01% (middle), and SA/MEH 0.01% (bottom) and then cooled to 4ºC, while on the right there is a second piece of paper soaked with the sample heated above T_m of the respective fatty acids. The mixtures were chosen at the concentrations where the largest shift in the emission properties of the MEH-PPV, passing from solid to liquid, was providing. All samples were irradiated with a UV-lamp at 365 nm. The red to yellow emission colour change, also observable at naked-eye, matched with the emission spectra of the corresponding system in solid (DA λ_{max} = 611 nm, Figure 3.10 and SA λ_{max} = 617 nm, Figure 3.8) and liquid state (DA λ_{max} = 548 nm + 581 nm, Figure 3.10 and SA λ_{max} = 604 nm + 542 nm, Figure 3.10). The changing in the NA/MEH soaked paper was less evident, probably due to the rapid melting of the NA at room temperature. Upon heating and cooling the soaked cellulose filter paper, the yellow and red emissions were repeatedly formed.

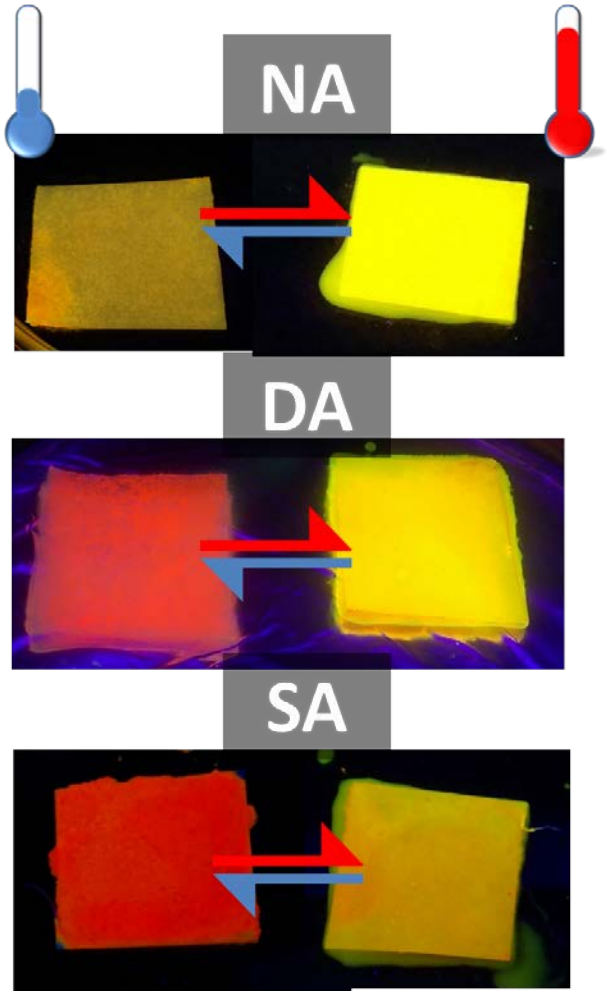

Figure 3.20. Digital camera image of two pieces of cellulose filter paper soaked with the mixture NA/MEH 0.1% (top), DA/MEH 0.01% (middle), and SA/MEH 0.1% (bottom). The piece on the left is kept at room temperature, while the one on the right is heated above T_m^{DA}. Both samples were irradiated with a UV-lamp at 365 nm.

The previous experiments have demonstrated the ability of all systems made by fatty acid PCMs and MEH-PPV to provide reversible the emitted colour switch around a defined temperature, through the variation of the emission properties of the polymer in solid/liquid PCM. Also, the versatility of the system was proved employing different fatty acids, together with the stability showed performing several heating/cooling cycles. Finally, the suitability of such system as temperature sensor has been tested in cellulose paper where the mixture was absorbed, maintaining the thermally switchable optical properties showed in bulk solutions.

Further improvement of such sensor implies the fabrication of flexible films that could be obtained integrating the mixture PCMs/MEH-PPV in a polymeric matrix. From the data reported above, the system DA/MEH 0.01% is the one showing the most drastic change in emission during the phase transition. In the first tentative to obtain such films, the system DA/MEH-PPV 0.01% was added to a water solution of chitosane (1% w/v) while heating at

50 °C. The mixed solution was magnetically stirred to generate an oil-in-water emulsion. Afterwards, the mixture was poured in a plastic Petri dish to let the water evaporating so to obtain a chitosan film (for more details see the experimental section). The resulting film was not homogenous, mainly due to a low stabilization of the emulsion.

The fluorescence of the resulting film was studied at 20 °C and 60 °C (Figure 3.21a). At room temperature, the emission spectrum of the chitosan film showed a main band at 598 nm, and a second one at 571 nm with similar intensities. When the temperature was raised to 60 °C, the film showed an increase of the emission intensity (3-folds, from 230 to 627) Moreover, the relative intensity of the two bands change, with the band at higher energy becoming slightly more intense (632) that the peak at lower energy (627). As expected a blue-shift of the bands (the main band shifts from 598 nm to 583 nm and the second one from 571 nm to 549 nm). Cooling down the film, the starting emission is restored, though maintained the higher intensity (Figure 3.21b). The response to the temperature variation of the chitosane films resembles what observed with the system DA/MEH 0.01% in bulk.

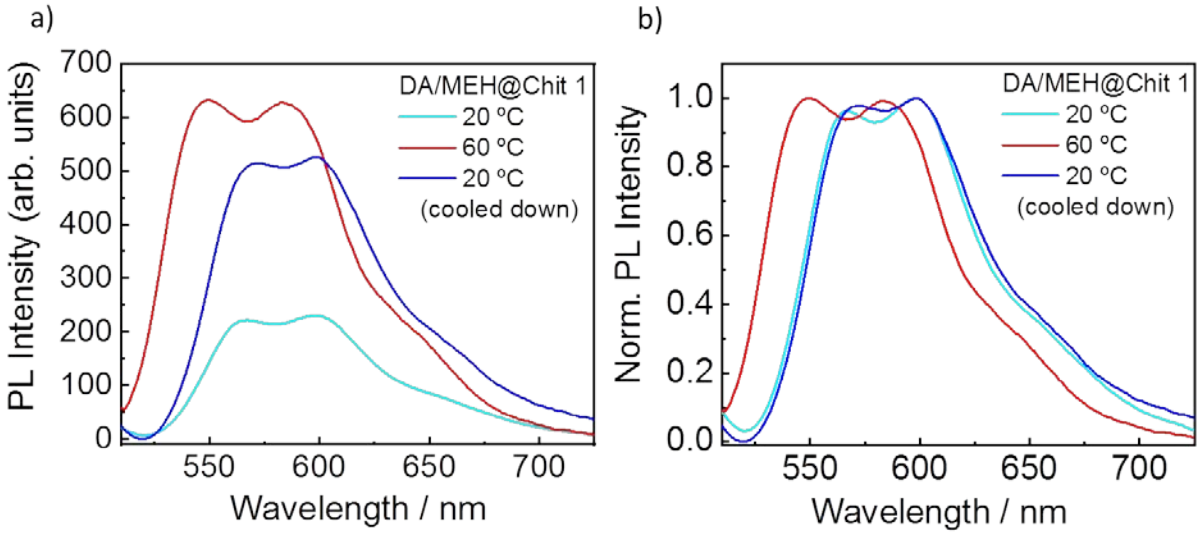

Figure 3.21. *a)* emission and *b)* normalised emission spectra of the DA/MEH-PPV chitosan film measured at 20 °C (blue line), 60 °C (red line) and the film cooled down to 20 °C (cyan line). Spectra obtained irradiating at λ_{exc} = 490 nm.

3.4.1 SWITCHABLE OPTICAL MATERIAL BASED ON MICROCONFINED SYSTEMS

Despite the promising results, as proof of concept, obtained with the soaked cellulose and the chitosan films, the leakage of the PCMs in its molten state is a a key limitation for the final application. Both the cellulose and the polymeric film could not retain the liquid PCMs leading to a loss of the active material and irreversibility of the process.

In our group, we already solved the issue of transferring optical properties of bulk systems (e.g. solutions) into solid materials, through the micro/nanoencapsulation strategy. Micro-/nanoconfinement of the mixtures, as polymeric micro-/nanocapsules or solid lipid microparticles, should resolve this issue, leading to a more versatile material that can be used in real applications.

3.4.1.1 Micro-/nanoencapsulation of PCMs/MEH-PPV solutions

*Poly(methyl methacrylate) (**PMMA**)*

Initially it was decided to prepare core-shell polymeric microcapsules through the emulsification/solvent evaporation method. This has been already used in the NANOSFUN group for the encapsulation of photoactive dyes, since it avoids chemical reactions and in principle should preserve the optical properties of the encapsulated materials. Two shell polymers were selected for these microcapsules: poly(methylmethacrylate) (PMMA), a standard polymer (T_g = 105 ºC) usually used in these syntheses and poly(2,6-dimethyl-1,4-phenylene oxide) (PPO), a high T_g polymer (T_g = 205 ºC) which should guarantee high thermal resistance of the capsules shell, allowing the use of the capsules for the fabrication of high temperature sensors. As core materials DA/MEH 0.1% and NA/MEH 0.1% were selected since were the PCM systems providing the largest shifts. Though the MEH concentration was not the one providing the largest shift, the more concentrated system was selected to assure enough signals in the fluorescent experiments with the microcapsules powder, whose emission was expected to be reduced significantly by the light scattering produced during the measurements in reflectance mode. The first syntheses were limited to microcapsules, which generally are easier to isolate and characterize than the nanocapsules.

The syntheses of the 4 types of capsules were carried out using the same protocol, as described in the experimental section. The only difference consisted in the use of different volatile organic solvents in PPO and PMMA capsules, replacing the CH_2Cl_2 with $CHCl_3$ for the PPO capsules, since the latter is not soluble in the CH_2Cl_2.

The resulting microcapsules (hereafter named as MC PMMA DA/MEH and MC PPO DA/MEH) were analysed by scanning electron microscopy (SEM) to study the morphology and size distribution. Figure 3.22a shows two SEM images, captured at different magnitudes, where it is possible to observe the successful formation of both PMMA (0.4-5.1 µm) and PPO (0.25-2.55 µm). PMMA microcapsules presented smooth surface and a bi-modal distribution, with two main populations of mean size of 1.25 µm and 3.67 µm (inset in Figure 3.22a). The core-shell structure of the microcapsules can be deduced by the internal cavity observable in the partially formed microcapsules (Figure 3.22a).

MC PPO DA/MEH presented a rough and irregular surface. SEM image obtained at high magnification (Figure 3.22b) showed the presence of multiple cavities and suggested that the surface was made by small nanoparticles.

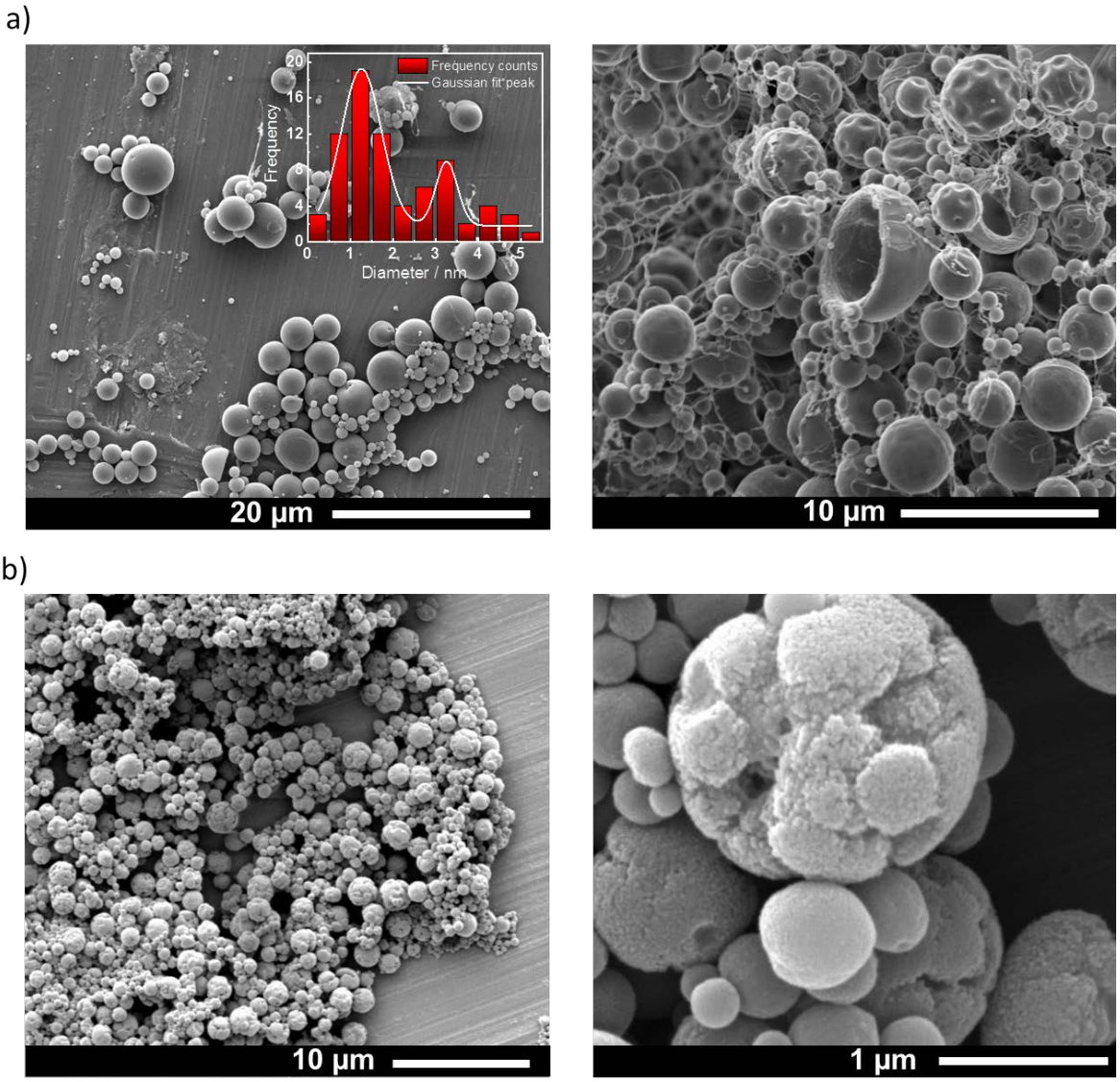

Figure 3.22. SEM images of *a)* MC PMMA DA/MEH and *b)* MC PPO DA/MEH captured at two different magnitudes. Inset of Figure *a*: size distribution of the capsules determined by ImageJ analysis software.

The stability of such microcapsules was also tested performing temperature-dependent SEM analysis. Figure 3.23 shows the SEM images of the PMMA and PPO microcapsules taken after increasing the temperature from 26 °C to above the T_g of the respective shell materials. PMMA microcapsules were stable up to 101 °C, after which the temperature led to the loss of the microcapsules structure, due to the overcome of the T_g^{PMMA} (105 °C).[44]

PPO microcapsules were stable up to 250 °C, showing a much higher stability than PMMA microcapsules. Such high temperature stability was unexpected, taking into account that the reported T_g^{PPO} is 210 °C. Furthermore, no leaking from the microparticles was observed until the capsules deformation, which suggested a good encapsulation of the DA. This experiment confirmed that both PMMA and PPO are suitable polymers to for these PCMs microcapsules, since they guarantee good stability far above the phase transition temperature of the contained PCM, with no apparent leakage of the liquid DA. From this series of images, it could be also stated that SLMs made only by DA (without shell material) were not present.

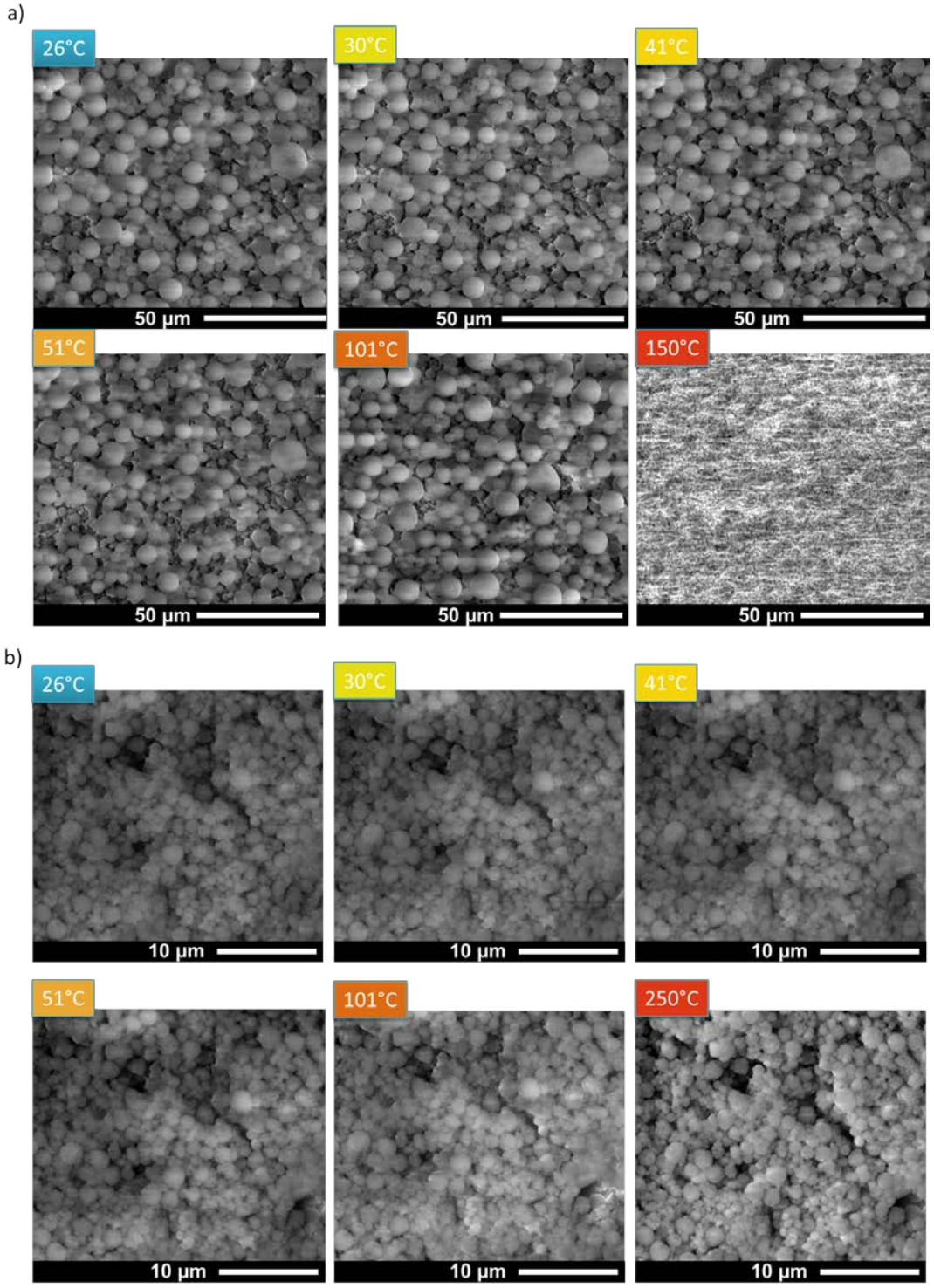

Figure 3.23. Images of *a)* MC PMMA DA/MEH and *b)* MC PPO DA/MEH, captured at different temperatures using the SEM equipped with a heating stage.

SEM analysis did not exclude the possibility that the microparticles were made of only polymers (polymer nanoparticles).

The presence of DA inside the capsules was confirmed, instead, by Differential Scanning Calorimetry (DSC) analysis of the lyophilised MC PMMA DA/MEH and MC PPO DA/MEH capsules (Figure 3.24). In both heating traces of the two types microcapsules it was observed an endothermic band around ~42.0-44.0 ºC, very close values to what was measured in the two heating steps of the bulk DA/MEH sample (43.5 ºC and 42.6 ºC). The fact that the same T_m^{DA} was observed for DA confined in the microcapsules and in bulk, allowed the following conclusions:

- DA was successfully encapsulated within the PMMA and PPO cortex,
- The MEH-PPV was not affecting the T_m^{DA}, neither in bulk and inside the capsules, otherwise it would have been lower than the reported value (43.8 ºC),[44]
- The PMMA or PPO and the DA are present in the capsules, mainly as separated phases (i.e. core-shell structures), rather than as homogeneously mixed material. If this was not the case, the T_m^{DA} would have not been significantly affected.

Attempts to detect the T_g of the shell polymers failed, possibly for the little amount of the material.

a)

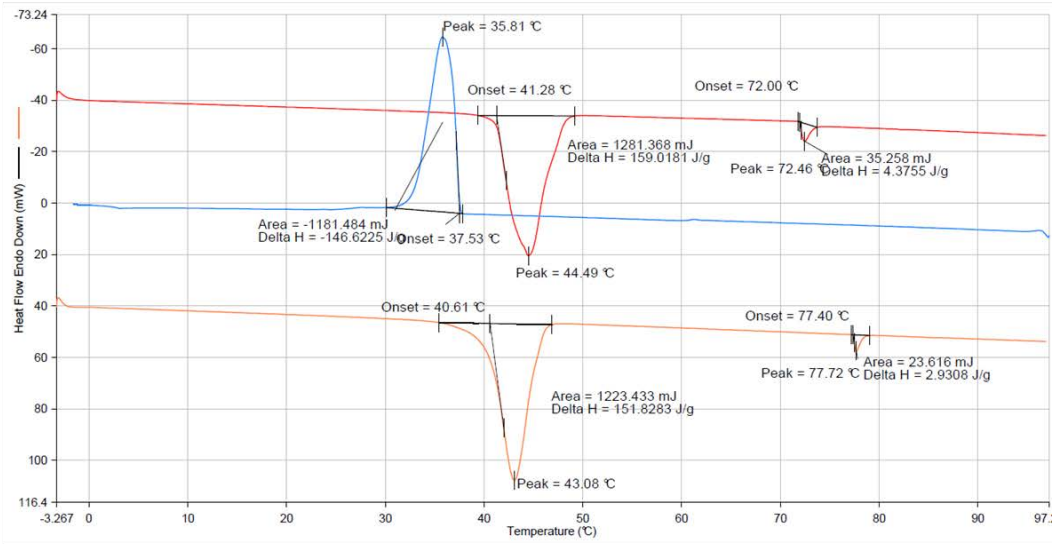

b)

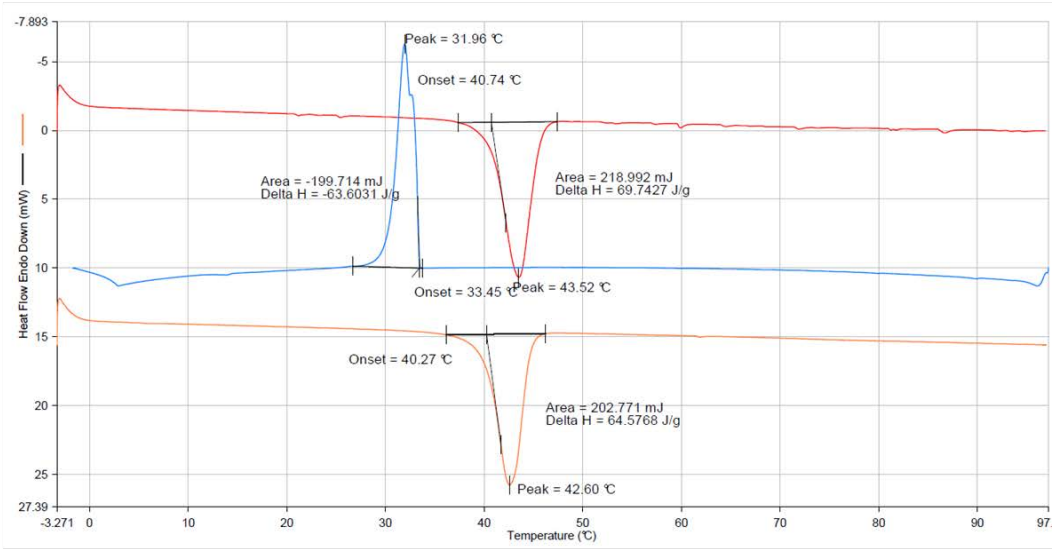

c)

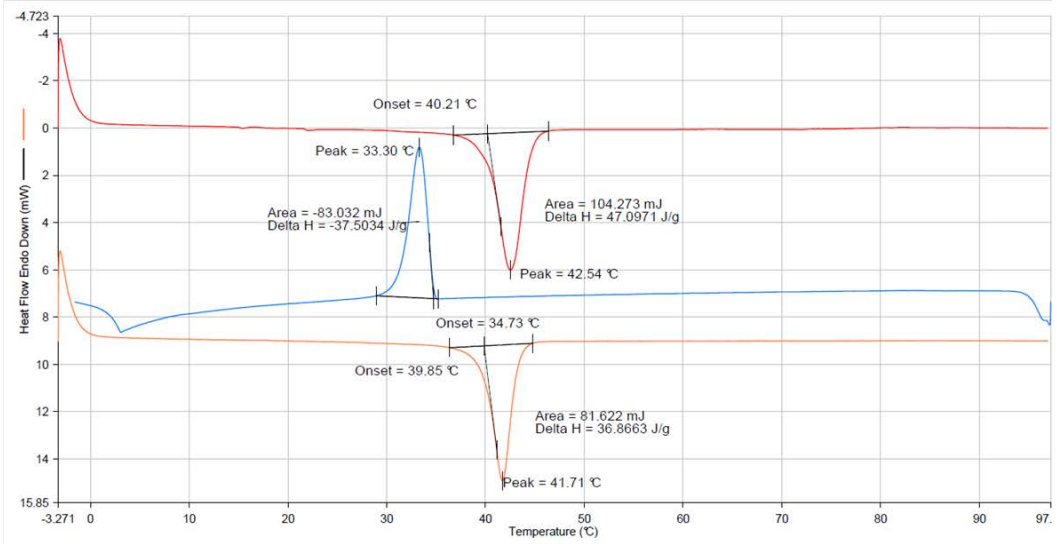

Figure 3.24. DSC analysis of *a)* DA/MEH, *b)* MC PMMA DA/MEH and *c)* MC PPO DA/MEH performing cycles of heating (red line), cooling (blue line) and heating again (orange line), from 0 °C to 100 °C at rate of 10 °C/min.

A further confirmation of the presence of DA inside the capsules came from ^{1}H-NMR analysis of the capsules. For this PMMA (MC PMMA DA) microcapsules of DA were prepared again, in the same way, but without the MEH-PPV. Such microcapsules, once lyophilised, were dissolved in deuterated chloroform ($CDCl_3$), magnetically stirring for several hours. Since both DA and PMMA are completely soluble in chloroform, the redissolved microcapsules in the deutered solvent, provided a homogeneous solution that could be analysed by ^{1}H-NMR (Figure 3.25a). PMMA and DA were also analysed by ^{1}H-NMR to have assignable reference peaks (Figure 3.25b and Figure 3.25c). The presence of the proton signals (0.88, 1.26, 1.63 and 2.31 ppm) coming from DA in the NMR spectrum of the MC PMMA DA confirmed the presence of the fatty acid inside the capsules. In order to determine the payload of the microcapsules, a certain amount of DMSO was added in the MC PMMA DA solution, as internal reference. The presence of DMSO produced a little shift of signals of DA protons in the NMR spectrum of the microcapsules. From the ratio between the integral of the DMSO signal (2.62 ppm) and the integral of the DA signal (2.31 ppm) in the microcapsules sample it was determined a payload of ~30% (for more details see the experimental section).

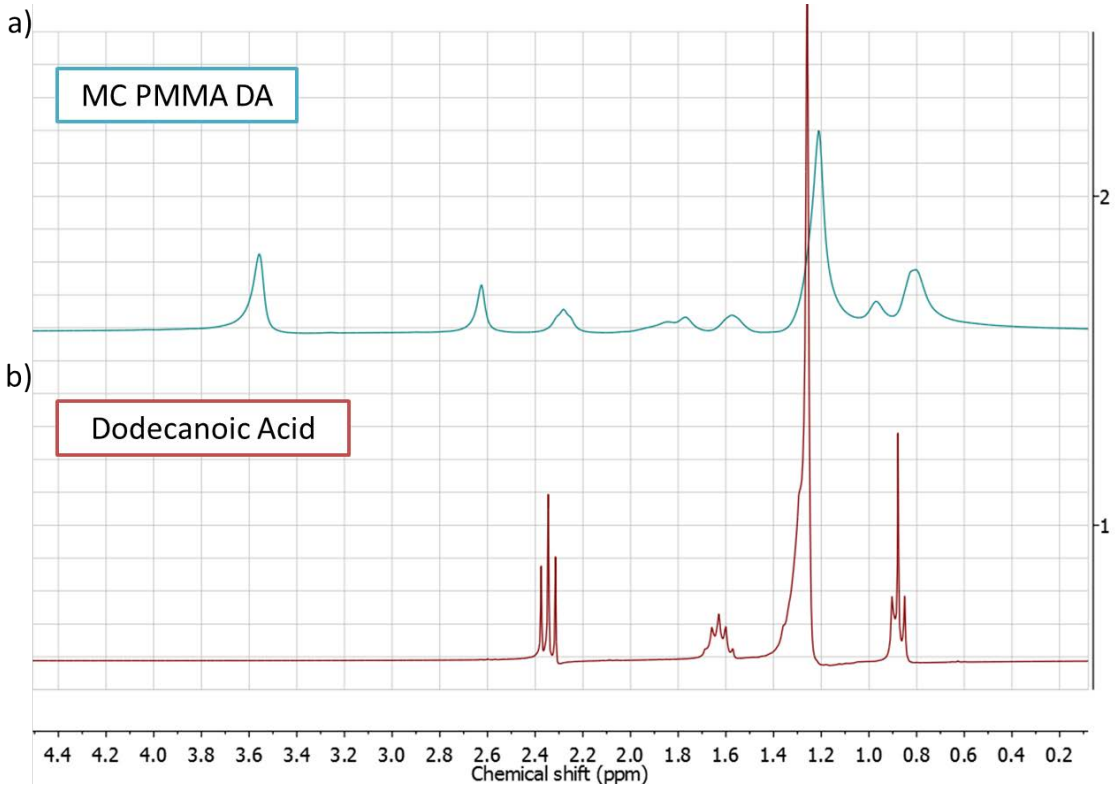

Figure 3.25. ^{1}H-NMR spectra (250 MHz, $CDCl_3$) of dissolved MC PMMA DA and DA. The spectrum of pure DA was recorded for comparison. The capsules present the characteristic peaks of PMMA at δ_H/ppm = 3.56 (s, 3H, OCH_3), 2.00-1.57 (m, 2H, CH_2), 0.97-0.80 (m, 3H, CH_3) and of DA at δ_H/ppm = 2.31 (t, 2H, $COCH_2$), 1.63 (m, 2H, CH_2), 1.26 (m, 16H, $(CH_2)_8$), 0.88 (t, 3H, CH_3). DMSO (δ_H/ppm = 2.62 (s, 6H, $(CH)_2$) was used as an internal reference.

PMMA and PPO microcapsules were also obtained, using the same method, with the NA/MEH as internal core (MC PMMA NA/MEH and MC PPO NA/MEH). SEM showed the successful encapsulation of the mixture with both polymers (Figure 3.26). Again, while PMMA capsules (0.5-3.5 µm) had smooth surface, the nanoparticles of the shell of PPO capsules provided the rough surface.

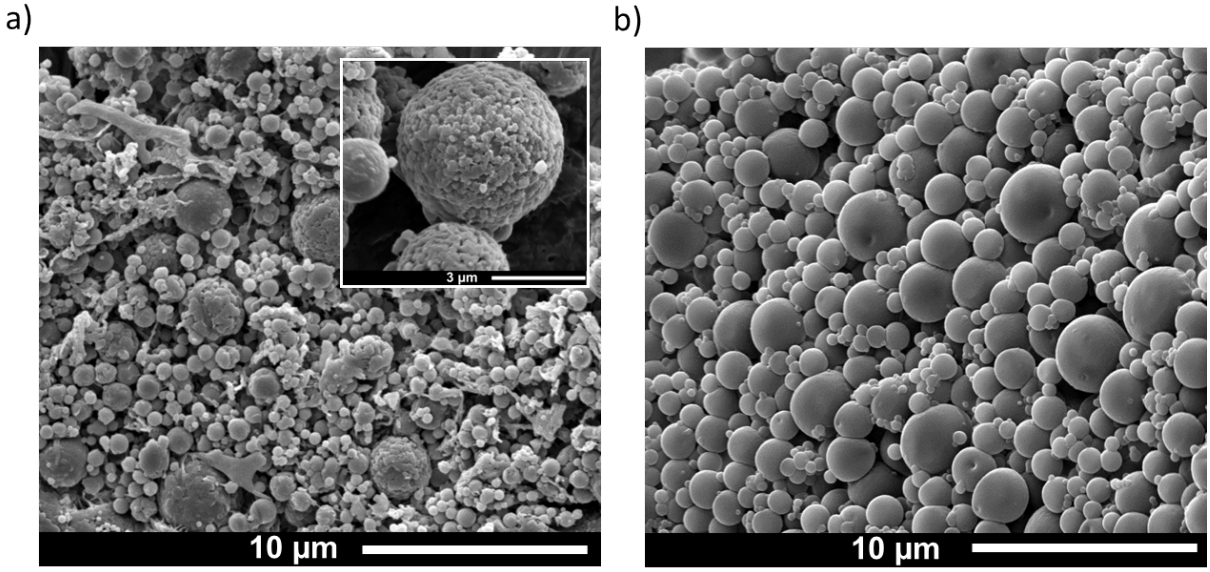

Figure 3.26. SEM image of *a)* MC PMMA NA/MEH and *b)* MC PPO NA/MEH. Inset: zoom of MC PPO NA/MEH.

In order confirm the presence of NA inside the PPO capsules, ^{1}H-NMR analysis was carried out on a batch of PPO capsules, prepared in the same manner as before, but without including the MEH polymer (MC PPO NA). The dissolved MC PPO NA showed the proton signals of NA (by comparison with the spectrum of NA), confirming its presence in the capsules. The NA was retained in the microstructures despite the rough structure of the shell. By using DMSO as internal standard, it was determined a payload of ~20%.

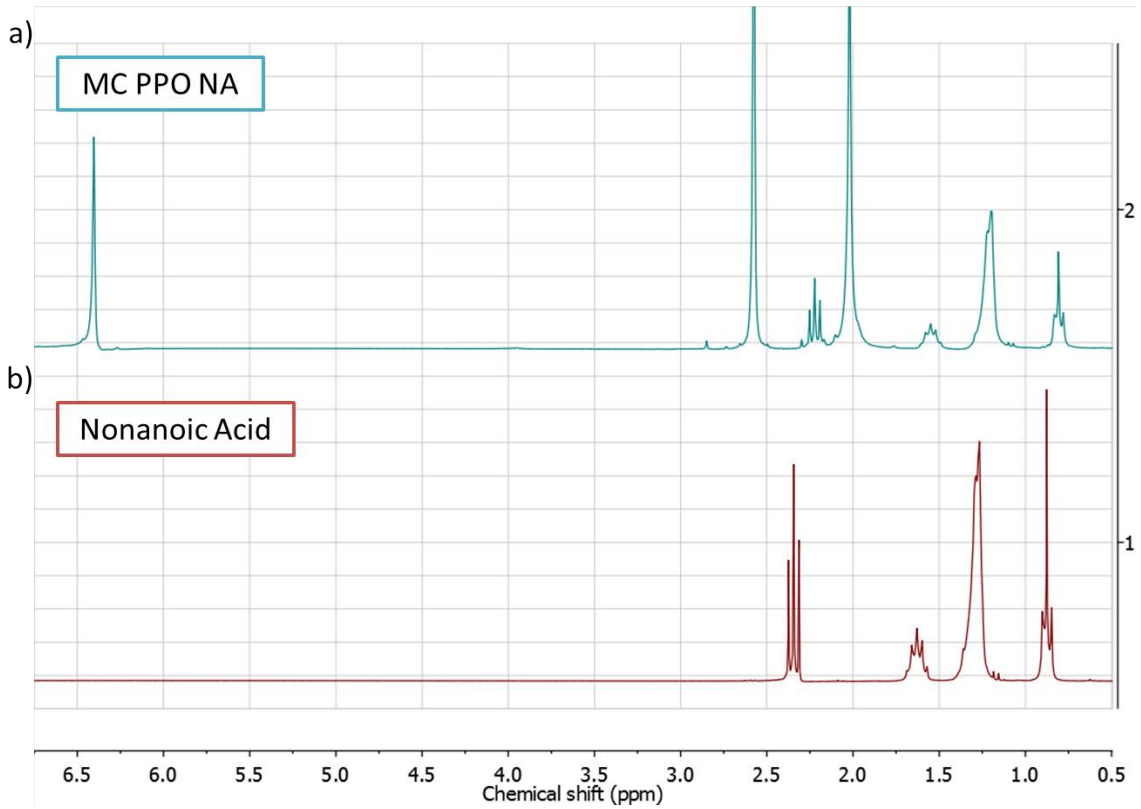

Figure 3.27. ^{1}H-NMR spectra (250 MHz, $CDCl_3$) of dissolved MC PPO NA capsules, and NA. The spectra of pure NA were recorded for comparison. The capsules present the characteristic peaks of PPO at δ_H/ppm = 2.07 (s, 6H, $(CH_3)_2$), 6.4 (s, 2H, Ar) and of NA at δ_H/ppm = 2.34 (t, 2H, $COCH_2$), 1.62 (m, 2H, CH_2), 1.27 (m, 16H, $(CH_2)_5$), 0.88 (t, 3H, CH_3). DMSO (δ_H/ppm = 2.62 (s, 6H, $(CH)_2$) was used as an internal reference.

Once the core-shell microcapsules of different shell (PMMA and PPO) and core materials (DA/MEH, NA/MEH) were successfully obtained and characterized, it was decided to also investigate the synthesis of core-shell nanocapsules. Thus PMMA nanocapsules with the MEH-PPV 0.1% as a core material, were prepared through the miniemulsion solvent evaporation technique, a variation of the method applied in the microcapsules synthesis, with the difference that in order to obtain smaller droplets in the O/W emulsion higher energy (ultrasonication) was applied during the emulsification step. SEM of the resulting nanocapsules (NC PMMA DA/MEH) confirmed the formation of nanocapsules with size ranging between 20 to 120 nm (Figure 3.28a). The size distribution was extrapolated (Figure 3.28c) obtaining a population with a mode of 37.6 nm and a mean diameter of 45 ± 16.3 nm. TEM on a single particle showed a marked lower contrast inside the particle than in the shell (Figure 3.28b), supporting the core-shell structure of the nanocapasules.

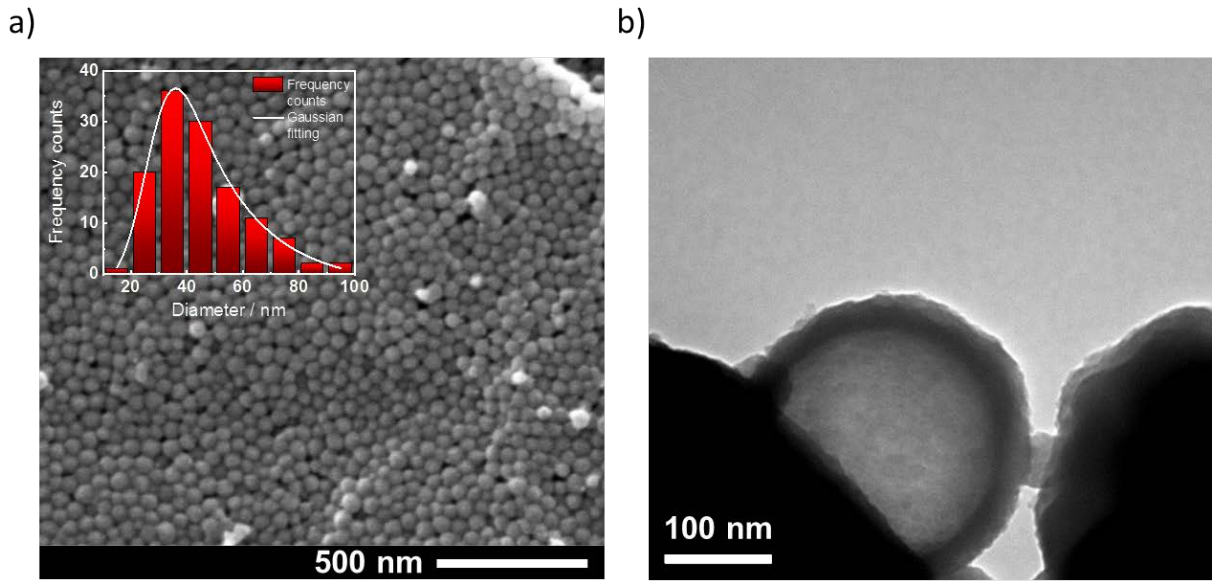

Figure 3.28. *a)* scanning and *b)* transmission electron microscopy images of NC PMMA DA/MEH. Inset in *a)*: size distribution of the microcapsules determined by ImageJ analysis software.

Study of the optical properties of the capsules.

Once the different types of micro-/nanocapsules were obtained, their optical properties were investigated to verify if the behaviour of the polymer in bulk DA solutions was also retained in the micro-/nanostructures. All capsules (MC-PMMA DA/MEH, MC-PMMA NA/MEH, MC-PPO DA/MEH, MC-PPO NA/MEH and NC-PMMA DA/MEH) were lyophilised and their fluorescence spectra were recorded in reflectance mode at two different temperatures, below and above the T_m^{PCM}.

Analysing the emission behaviour of the obtained capsules it was observed that:

- the spectra of the capsules suffered important modification respect to those obtained for the respective bulk solutions and in most of the cases the band ratios were not matching. At room temperature, MC-PMMA DA/MEH presented the main band centred at 602 nm and a weak shoulder at 640 nm, similar (just a few nm of shift) to the bulk emission. However, the high-energy band (556 nm) present in the microcapsules emission, did not appear in the bulk DA/MEH solution. Similar discussion is valid for the NC-PMMA DA/MEH that presented the maximum at 590 nm and also the prominent high-energy band at 550 nm. MC PPO DA/MEH also showed a broad band with maximum at 600 nm, and a shoulder in at xxx nm. Similar results were obtained for the PMMA and PPO capsules containing NA/MEH mixture.

- When the temperature was raised above T_m^{PCM}, all investigates capsules, showed a very little hypsochromic shift, only 4-6 nm, (Figure 3.29d), compared to the one showed by bulk solutions.

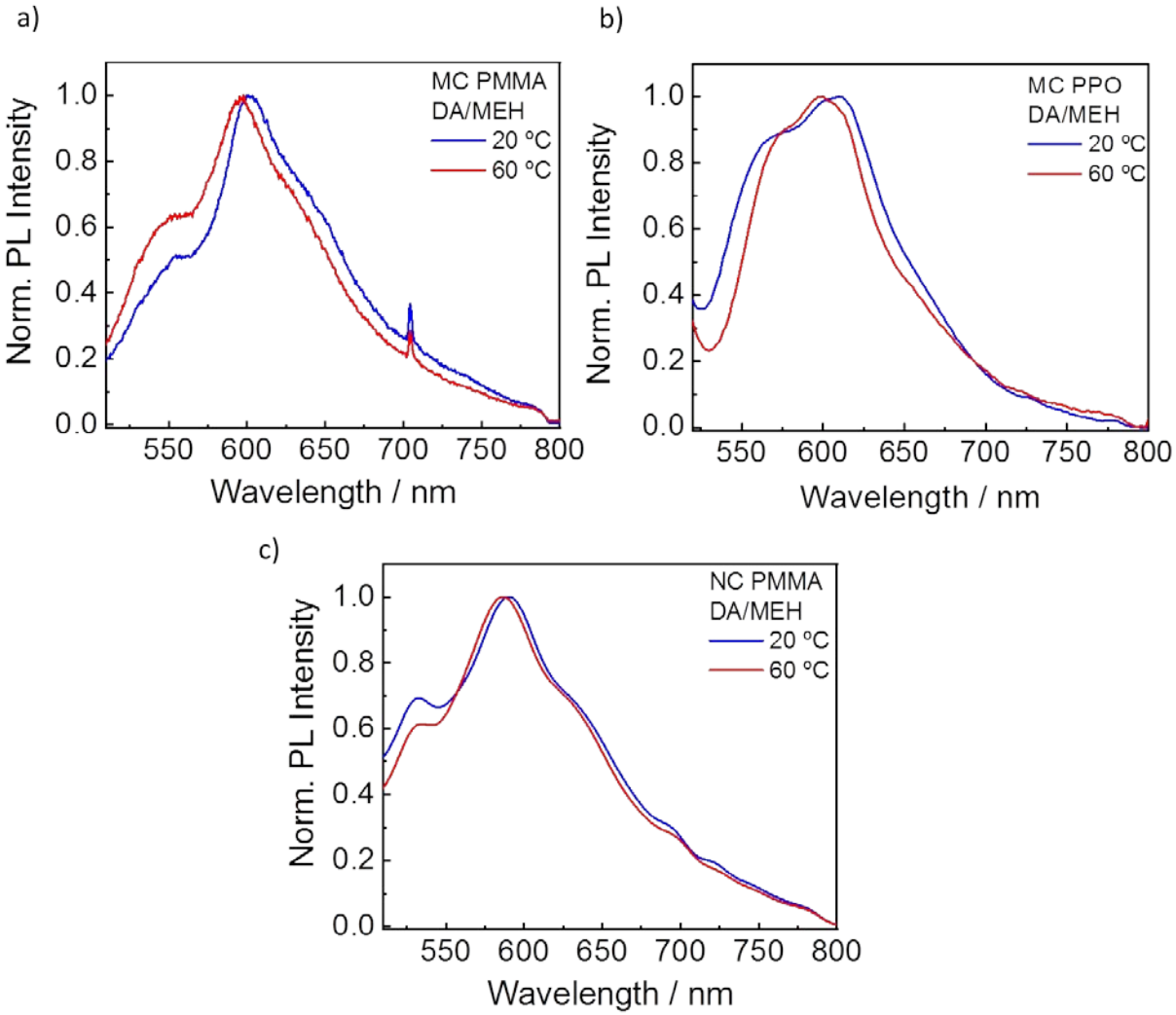

Figure 3.29. Normalised emission spectra at 20 °C and 60 °C of *a)* MC-PMMA DA/MEH, *b)* MC-PPO DA/MEH, and *d)* NC-PMMA DA/MEH exciting at 490 nm.

- In addition to the discrepancy of the optical properties of the micro-/nanocapsules compared to the bulk systems, it was realized that all structured samples turned yellow and lost their fluorescence after storing them in the laboratory for several days, while the bulk solutions maintained their color for several weeks. As example, it is reported the normalised emission spectra of the MC PPO NA/MEH and of bulk NA/MEH-PPV, which shows how the emission of the microcapsules undergo a large blue-shift of about 35 nm, respect to the bulk solution, after several days of storage.

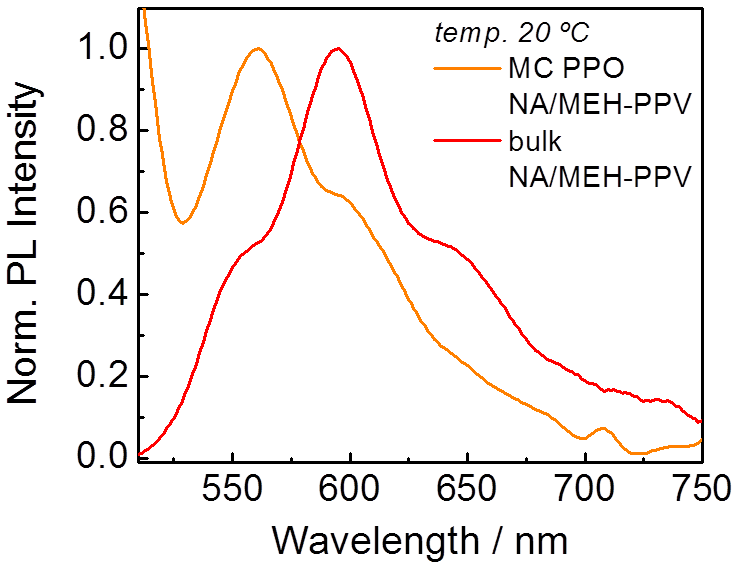

Figure 3.30. Normalised emission spectra of ample MC PPO NA/MEH-PPV after several days from the synthesis (orange line) compared with the normalised emission of the bulk system NA/MEH-PPV (red line).

With these results, we supposed that the lack of activity of the encapsulated thermal switch could be due to:

- side interactions/reactions occurring during the synthesis between the surfactant (PVA) with the core materials (DA and MEH-PPV), which would prevent the switch of MEH-PPV in the solid/liquid PCM,
- the distribution of the MEH-PPV into the polymer shell (PMMA or PPO), which would stop the role of the PCM in the switching process.

In order to understand the cause of the lack of the optical activity of the capsules, a series of experiments were carried on, selectively changing the emulsifier, the PCMs (to understand the cause of such side reactions) or removing the shell material. Such studies were conducted in the microscale, since the obtained microstructured particles were simpler systems to characterize.

Effect of the surfactant.

The microcapsules were synthesised following the process reported for the sample MC PMMA DA/MEH, using sodium dodecyl sulphate (SDS), instead of PVA, as surfactant (hereafter named as MC PMMA DA/MEH *SDS*). The microcapsules morphology was analysed by SEM, and no significant changes were detected (Figure 3.31a). The only effect of the substitution of the surfactant regarded average size of the microcapsules which was

reduced. Figure 3.31b shows the bimodal distribution of the average microcapsules diameter, exhibiting a global maximum of 0.7 µm and a local maximum one of 1.3 µm.

Unfortunately, MC PMMA DA/MEH *SDS* also exhibited, with time, the shift of the emission to yellow, or the complete loss of the fluorescence. Because of this no further investigation were carried out on these capsules and the surfactant was excluded as effect for the MEH-PPV degradation.

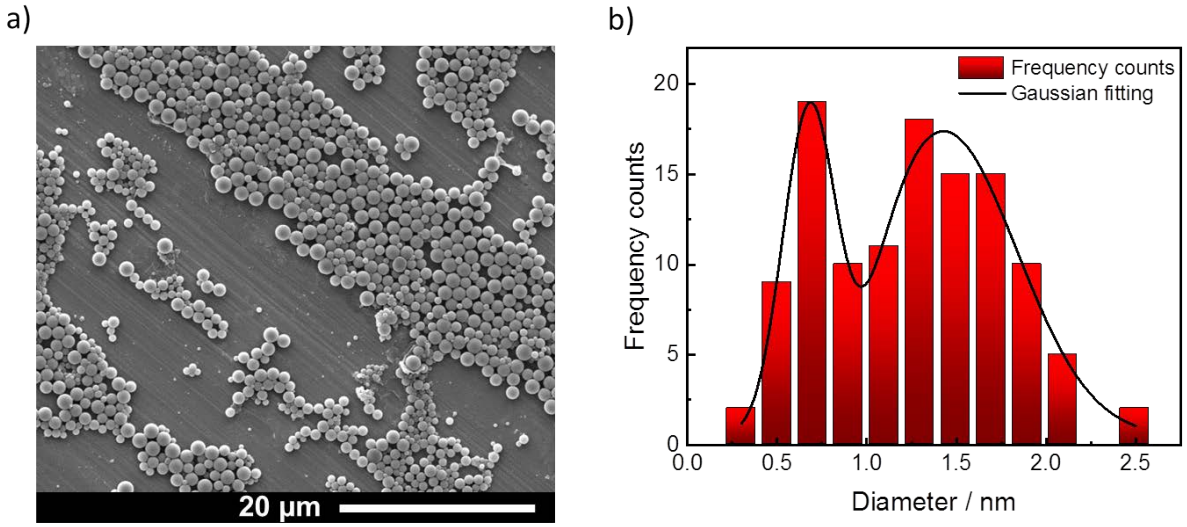

Figure 3.31. *a)* SEM images of MC PMMA DA/MEH-PPV *PVA*; *b)* size distribution of the microcapsules determined by ImageJ analysis software.

Replacement of fatty acids by paraffin

Based on such results, we hypothesised that the degradation of MEH-PPV could be the consequence of the fatty acid reactivity. The bulk mixtures of fatty acids (DA or NA) and MEH-PPV were stable for a long time, so the phenomenon observed in the microcapsules preparation derived from some reactions of the PCM with some compounds involved in the synthesis.

Therefore, a less reactive PCM was tested as core material for PMMA and PPO microcapsules. The mixture EC/MEH 0.1% was encapsulated through the solvent evaporation method, as described above (MC PMMA EC/MEH and MC PPO EC/MEH). SEM of the resulting samples showed, in both cases, the successful formation of the capsules whose core-shell structure could be confirmed by the presence of the cavities in the partially formed capsules (Figure 3.32a and b). Moreover, both PMMA and PPO capsules presented, in this case, a similar smooth surface, indicating that the fatty acids (DA or NA) were responsible of the formation of the nanoparticles on the shell of the PPO capsules.

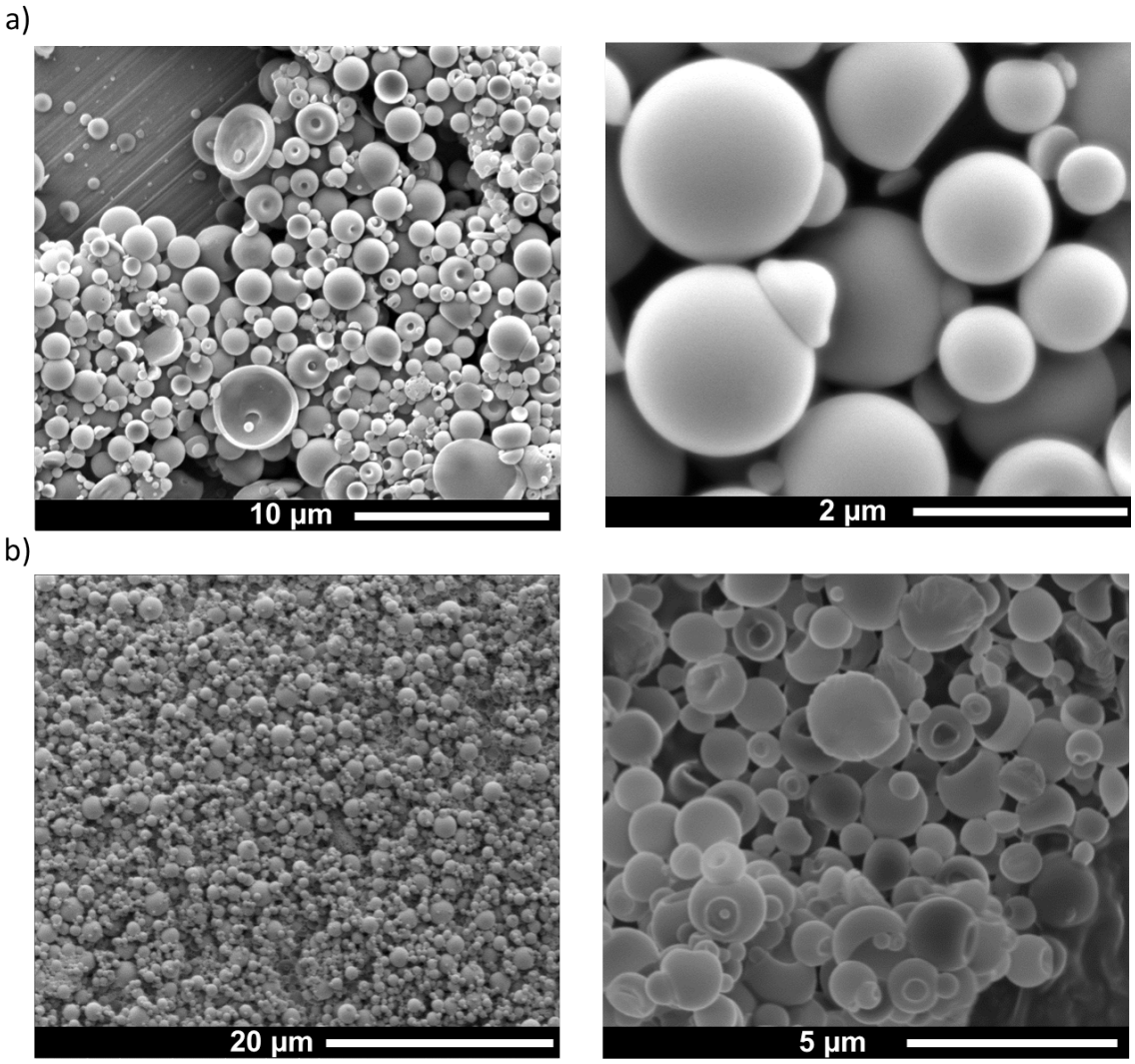

Figure 3.32. SEM of *a)* MC PMMA EC/MEH and *b)* MC PPO EC/MEH.

The capsule powders were analysed by fluorescence spectroscopy (Figure 3.33) after several months from the synthesis. The emission spectra obtained from the microcapsules resemble those observed in the bulk EC/MEH 0.1% mixture. At room temperature, the MC PMMA EC/MEH presented an emission spectrum with the main band at 594 nm (Figure 3.33a). Increasing the temperature, the intensity of the emission slight increased (red line) and a shoulder at 546 nm appeared. For the MC PPO EC/MEH a drastic increase of the emission intensity was observed when the sample was heated. In both cases, the normalised spectra (Figure 3.33b) highlighted the expected negligible blue-shift of the emission when the sample was heated above the T_m^{DA}.

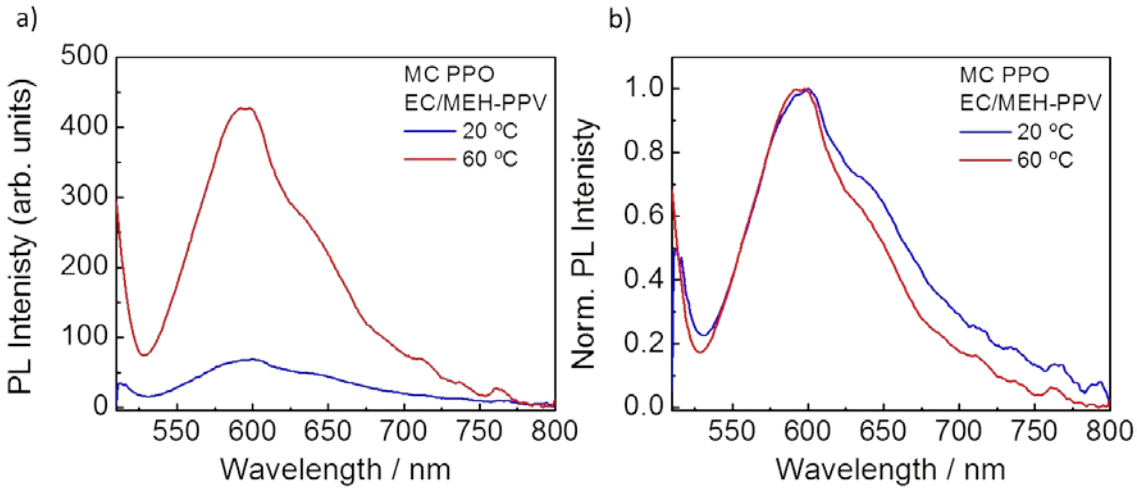

Figure 3.33. Emission *a)* and *c)* and normalized emission spectra *b)* and *d)* of *a)* and *b)* MC PMMA EC/MEH and MC PPO EC/MEH measured at 20 °C and 60 °C, exciting at 490 nm.

Notably, both samples did not show any colour change or quenching of the fluorescence over time, confirming that the use of non-acid PCMs provided higher polymer stability. However, this PCM did not provide the suitable medium for the switch, since EC did not induce any emission colour change upon melting, as already observed in bulk experiments.

However, these results corroborated that the fatty acids could be the direct cause of the degradation of the conjugated polymer during the synthesis and/or the storage.

The bulk mixture DA/MEH possessed excellent stability, with no changes the emission after several heating-cooling cycles and after months of storage after the preparation. Therefore, we could speculate that reactions within the fatty acids and the components of the microcapsules are responsible for the change in the optical properties of MEH-PPV. Since the surfactant was already demonstrated to not be the responsible for this degradation, the only other component present in all the syntheses was the water. It was deduced that the degradation of MEH-PPV could be related to the acidity of fatty acids in water. Indeed, in water, the carboxylic group of the fatty acids partially dissociate in H_3O^+ cations and $RCOO^-$ anions, according to the equilibrium:

$$RCOOH + H_2O \rightleftarrows RCOO^- + H_3O^+$$

Thus, even if fatty acids are weak acids, we supposed that the low concentration of such ionic species was sufficient to react with MEH-PPV. In order to corroborate our hypothesis, two different experiments were carried on.

The mixture NA/MEH 0.01% (0.5 g) was added to 2 ml of H_2O in a glass vial. In a second vial, the same amount of NA/MEH-PPV 0.01% was added to 2 ml of H_2O acidified with HCl to a final pH = 4. Both mixtures were left magnetically stirring for several days at room temperature. The selected fatty acid was NA because it is liquid at room temperature and it was easier to mix the NA/MEH mixture with water without needing heating. Figure 3.32 shows the fluorescence measured for these two samples after a different time from the mixtures preparation. The lack of variation of the emission properties of the acidified mixture demonstrated that the deprotonation of fatty acid in the presence of water is the cause of the degradation of MEH-PPV.

Indeed, the mixed solution of water with NA/MEH-PPV turned yellowish after 4 days of stirring, with the main emission band of the bulk system NA/MEH-PPV 0.01% shifting from the 596 nm to 536 nm (dash grey line). When NA/MEH-PPV 0.01% was stirred with the acidic water (solid red line), no changes of the emission properties of MEH-PPV was observed, even after 30 days of continuous stirring.

The addition of strong acid in the water/fatty acid mixture displaced the equilibrium of the weak carboxylic acid towards the protonated form:

$$AH + H_2O \rightleftarrows A^- + H_3O^+ \tag{2}$$

The fraction of the deprotonated (f_{A^-}) carboxylic acid can be estimated using the Cratin model[53] developed to describe stearic acid dissociation at the oil–water interface:

$$f_{A^-} = \frac{10^{(pH-pK_a)}}{1 + 10^{(pH-pK_a)}} \tag{3}$$

So, taking in account the dissociation constant of NA (pKa = 4.9), it is possible to estimate the fraction of deprotonated carboxylic acid at the two different pHs of the H2O in the NA/H_2O mixture. At pH 7 (neutral pH of the water), the estimated f_{A^-} is 0.99, meaning that 99% of the NA is deprotonated. Lowering the pH to 4, the estimated f_{A^-} is 0.11, meaning that only 11% of the NA is deprotonated. Thus, also the calculations using this model show the huge decrease of the deprotonated NA in acidic water confirming the reactivity of the acid in presence of neutral water.

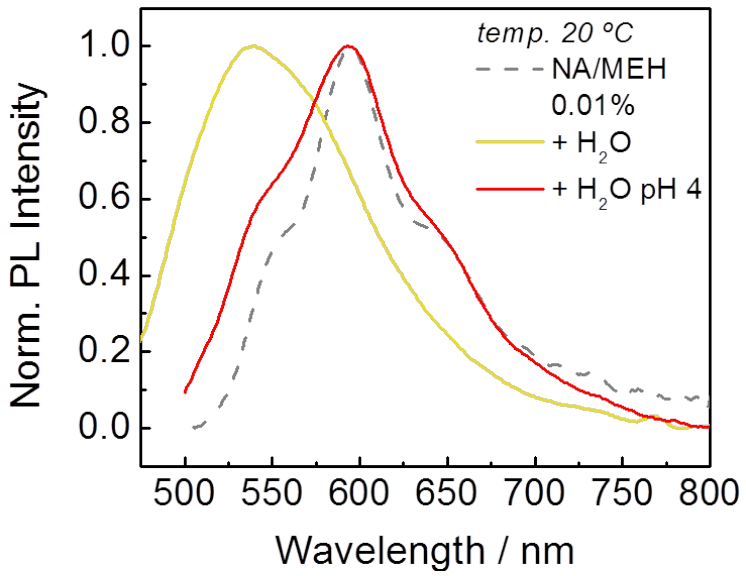

Figure 3.34. Normalised emission spectra of the bulk system NA/MEH 0.01% (grey dash line) compared with the normalised emission of the system NA/MEH 0.01% stirred in the presence of H_2O (yellow solid line) and the normalised emission of the system NA/MEH 0.01% stirred in presence of acidic (pH4) H_2O (red solid line).

Once our hypothesis was confirmed by the experiments reported above, a new synthesis of microcapsules was performed. The system DA/MEH-PPV 0.01% was encapsulated using PMMA as shell polymer material (MC PMMA DA/MEH pH4). The synthesis was carried on as before, with the only difference that the aqueous phase was acidified to pH = 4. The SEM analysis confirmed the formation of the particles (Figure 3.33a-b), indicating that the acidic pH did not affect the structuration of the PMMA in the shell. The fluorescence of the MC PMMA DA/MEH-PPV pH4 was studied at two temperatures (20 °C and 60 °C).

The emission spectra showed a broad band at 590 nm, which did not shift over time, indicating that the synthesis in acidic conditions, provided stability to the MEH-PPV (Figure 3.35c). Heating the sample from 20 °C to 60 °C the intensity doubled. Also, the normalised spectra (Figure 3.35d) highlighted the blue-shift of the sample, from 580 nm to 565 nm, passing from room temperature to 60 °C. However, though the shift of the main band reproduced quite well the bulk behaviour (it was just little less than in bulk), there were other features that confirmed different effects between the bulk and the capsules: the high-energy band did not appear in the heated microcapsules and cooling down the capsules, the spectra did not recover the starting feature.

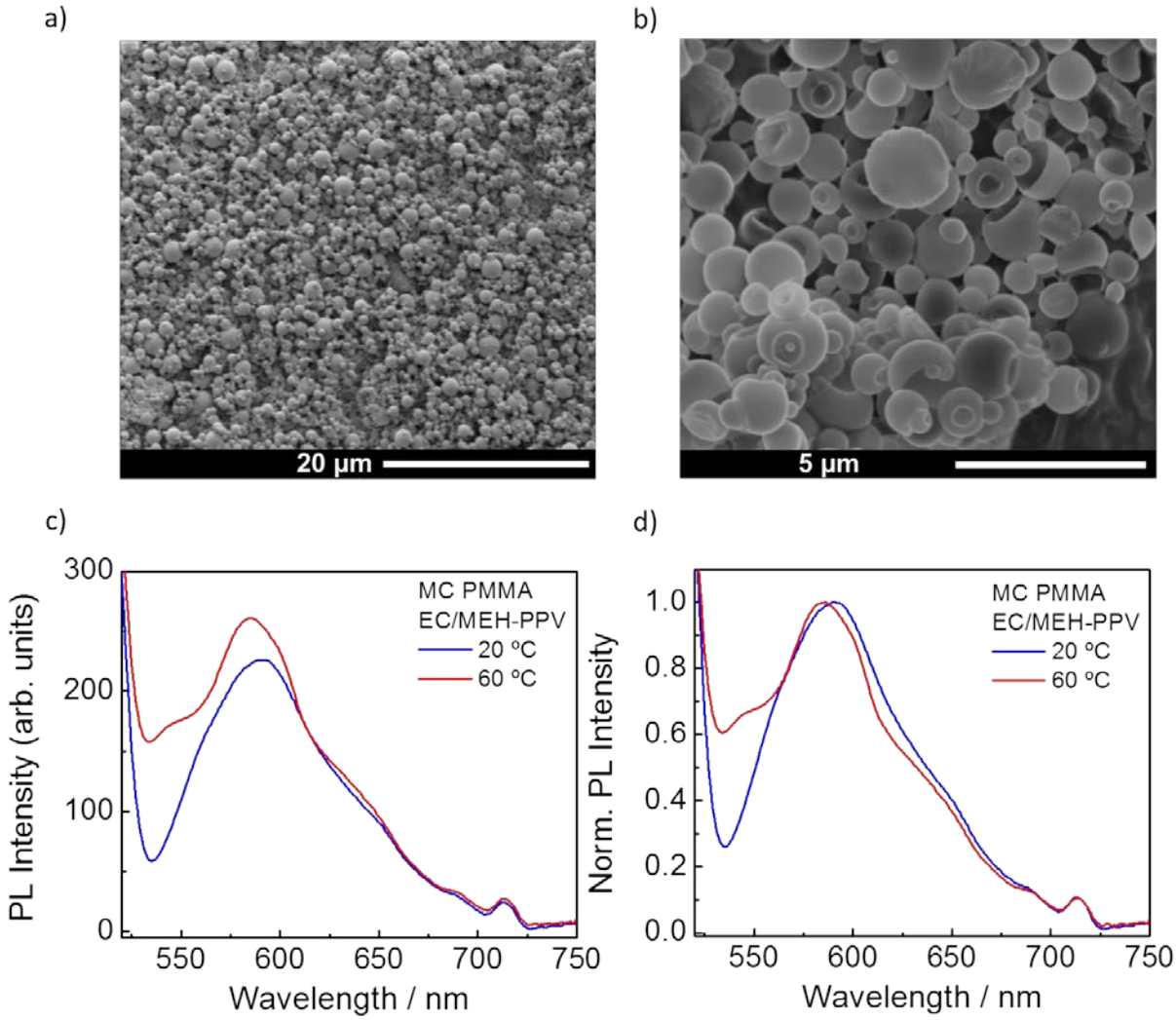

Figure 3.35. *a) - b)* Scanning electron microscopy images of sample MC PMMA EC/MEH-PPV captured at a different magnitude. *c)* emission spectra and *d)* normalised emission spectra of the sample MC PMMA EC/MEH-PPV measured at 20 °C (blue line) and 60 °C (red line), exciting at 490 nm.

Thus, even if the microcapsules were formed and the MEH-PPV was stable, the optical behaviour of the capsules still did not reflect what found in bulk mixtures, indicating that the microconfinement was affecting, somehow their optical properties.

In order to simplify the system, it was proposed to investigate the optical behaviour of solid lipid microparticles loaded with the MEH-PPV.

3.4.1.2. Solid lipid microparticles (SLMs)

Solid lipid microparticles (SLMs) could be the right alternative to the polymeric microcapsules. In such particles, the PCMs are microstructured with the help of an emulsifier without being covered with other polymeric materials. These structures are the closest system to bulk mixtures, since the SLPs would be only made by the PCM, the MEH-PPV polymer and the surfactant that is used during the particles synthesis. The advantage of using these

SLMs consists on the fact that the possible interactions of PCMs and the loaded MEH-PPV the MEH-PPV, with the shell polymer materials are avoided. The SLMs are expected to exhibit the same properties of the bulk material. SLMs of three different materials were prepared to investigate the optical behaviour. For synthesis of these SLMs, only PCMs, solid at room temperature can be used.

Eicosane

To optimize the process of fabrication of the SLMs, it was decided to start with the EC/MEH 0.1% mixture. Though EC did not provide any switch of the optical properties, it is a highly hydrophobic material, which would facilitate the formation of the SLMs, providing a starting point for the fabrication of SLMs of other more complex PCMs.

As a first step, an oil-in-water (O/W) emulsion was prepared by adding the EC/MEH mixture heated above the T_m^{EC} into a water solution containing the surfactant and also heated above the melting point of the PCM. Once the emulsion was formed, the addition of cold water induced the solidification of the PCM droplets. The resulting SLMs dispersion was lyophilised for two days, to obtain a solid sample (for more details see experimental section). SEM images (Figure 3.36a) show the formation of microparticles with a large average size (between 10 to 30 µm). The sample appeared clean with the absence of unstructured material.

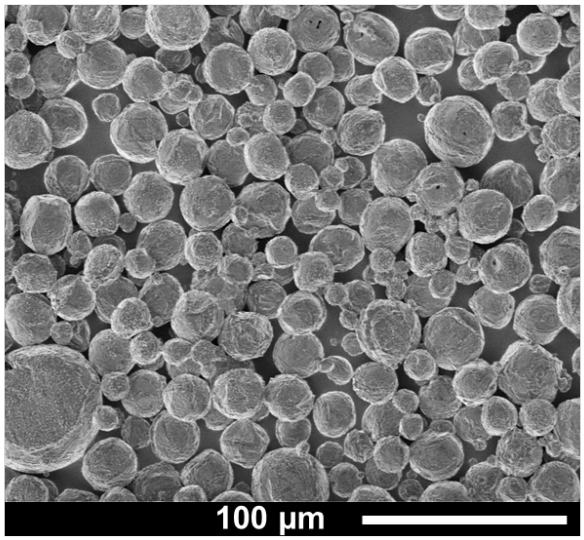

Figure 3.36. *a)* Scanning electron microscopy images of the sample SLMs EC/MEH.

Stearic acid

Once the formation of the SLMs was confirmed, the EC was replaced with a fatty acid, where the MEH-PPV showed pronounced changes of the optical properties, upon

crossing its T_m. The system of MEH-PPV dispersed in stearic acid was the first tested. The polar head could represent a problem at the moment of preparing the emulsion, since it could interact with the emulsifier, destabilizing the emulsion. However, the long alkyl chain, made SA quite good PCM to emulsify in stable droplets.

The synthesis procedure was the same reported above, with some variation. First, the aqueous phase was acidified to pH 4 in order to avoid the deprotonation of the carboxylic group, and then the temperature needed to be increased up to 75 °C, due to the high melting point of the stearic acid. The resulting microparticles (SLM SA/MEH) were washed then lyophilised for two days (for more details see experimental section). The microparticles suspension was studied by optical microscopy, while the powder obtained after the lyophilisation was analysed by SEM (Figure 3.37a-b), which corroborated the formation of microparticles with a large average size (between 10 to 50 μm). The sample appeared clean with the absence of unstructured material.

The fluorescence of the microparticles was studied at two different temperatures of 20 °C and 80 °C, at this last temperature the stearic acid melted destroying the microparticles structure. At room temperature, the microparticles showed two bands at 563 nm and 599 nm, slightly less intense, (Figure 3.37c). When the sample was heated, the emission band of the conjugated polymer retained the same structure presented at low temperature, with a slightly decreased intensity. Moreover, the normalised spectra (Figure 3.37d) showed the blue-shift of the emission band of the melted sample, with the bands shifting to 543 nm 579 nm respectively. The emission of the microparticles showed similarities with the bulk system, especially the one at high temperature, which is practically the same as in the heated bulk. This was expected, since the melted particles are basically a bulk mixture of the SA and MEH-PPV. The room temperature spectrum presented, instead, a small blue-shift compared to the emission of the solid bulk (from 579 nm to 563). Besides, in the emission band of the bulk system is present a weak shoulder at 619 nm, while in the microparticles is present an intense and defined peak.

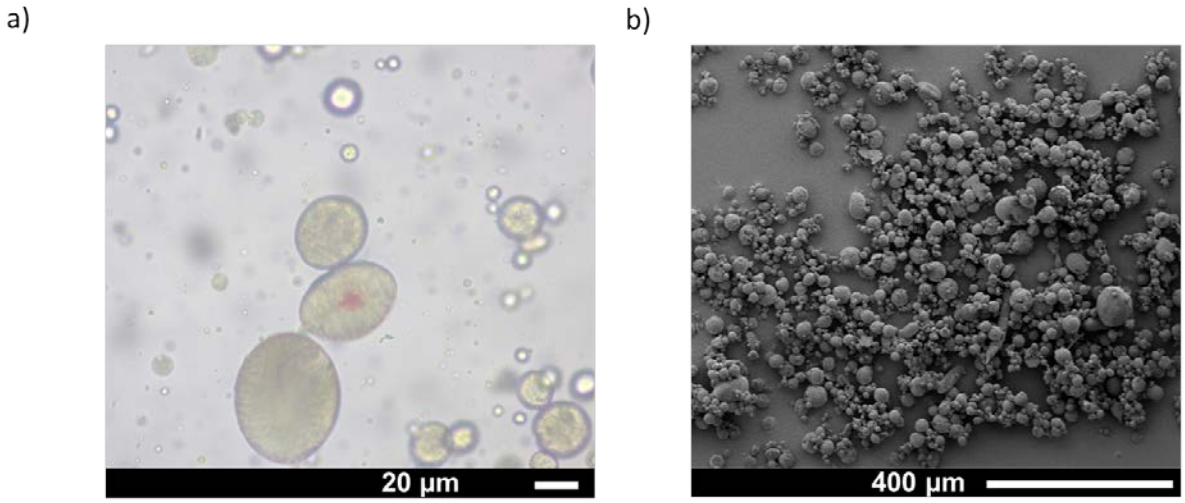

Figure 3.37. *a)* Optical microscope image and *b)* scanning electron microscopy image of the sample SLMs SA/MEH.

Dodecanoic acid

Based on the good results of the synthesis of the SLMs of SA, the system of MEH-PPV dispersed in DA was also structured in microparticles, since it was the most interesting in terms of optical shift upon heating, at least in bulk systems.

In a first experiment, the same procedure used for the sample SLM SA/MEH was followed trying to obtain SLMs of DA/MEH 0.01% (SLMs DA/MEH) with the only variation of the temperature of oil and the aqueous phases, which were set to 55 °C (just above the T_m^{DA}. The resulting suspension was observed by optical microscope (Figure 3.38) which showed mainly unstructured material.

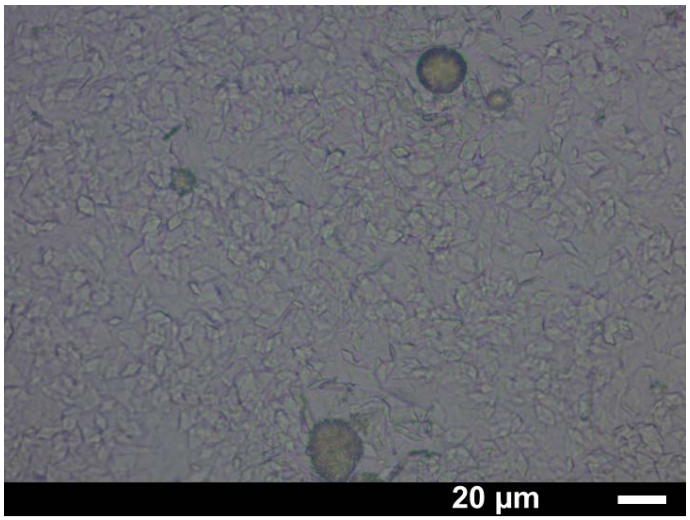

Figure 3.38. Optical microscope image of the sample SLMs DA/MEH.

The failure in the formation of the microparticles in the previous synthesis was ascribed to a lousy stabilisation of the emulsion provided by the emulsifier Tween®20 and to the higher amphiphilic properties of DA respect to the SA, which could destabilize the emulsion. Thus, a new synthesis was performed replacing Tween®20 with PVA and maintaining all the others parameters unchanged. The SEM of the resulting SLMs (SLMs DA/MEH *PVA*) suspension, confirmed the formation of the SLMs (Figure 3.39a). However, SEM of the lyophilized SLMs showed the presence of a large amount of unstructured material, with the microparticles present only in low concentration (Figure 3.39b). The fact the unstructured material in the water suspension was not observed at the optical microscope, was ascribed to a good homogenization in the water phase or to the loss of the particles structure during the preparation of the SEM samples. In any case, the presence of the unstructured material in the final particles was undesired and another synthesis was attempted.

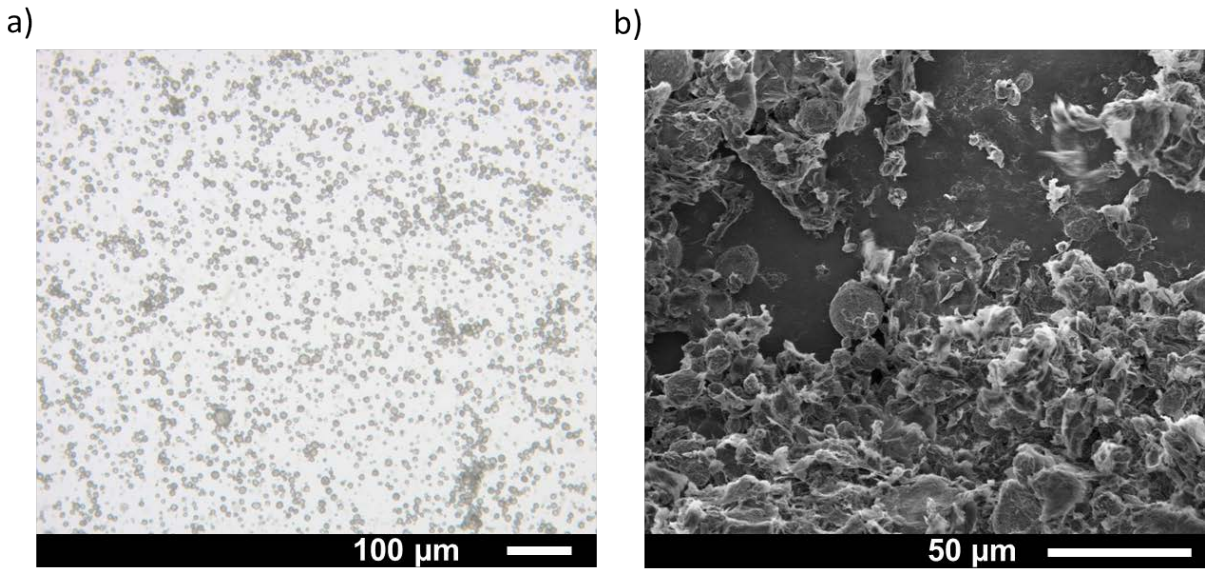

Figure 3.39. *a)* optical microscope image and *b)* scanning electron microscopy image of the sample SLMs DA/MEH *PVA*.

A new synthesis was performed by using dioctyl sulfosuccinate sodium salt (AOT) as emulsifier. Also, diversely to the previous syntheses, in this case the cold water added to the emulsion contained the surfactant AOT in order to maintain the particles stabilisation during the cooling process (for more details see experimental section). The resulting SLMs (SLMs DA/MEH *AOT*) were analysed by both optical microscopy (Figure 3.40a) and SEM which showed the formation of microparticles and their maintenance also in dry conditions, in which a low amount of unstructured material was observed.

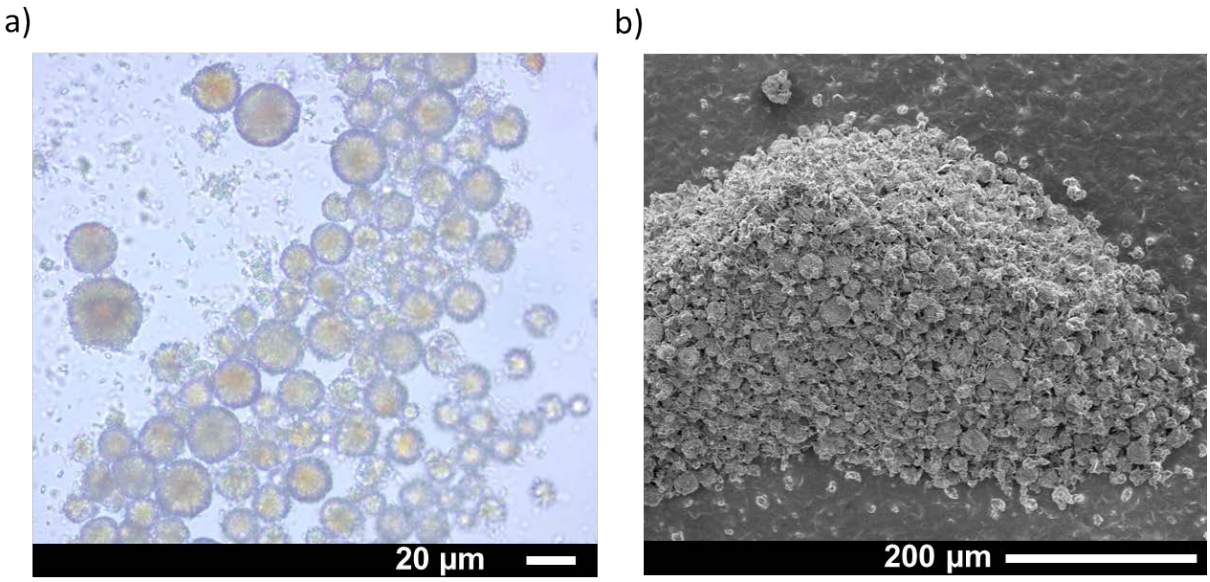

Figure 3.40. *a)* optical microscope image and *b)* scanning electron microscopy image of the sample SLMs DA/MEH-PPV *AOT*.

3.4.1.3. Study of the optical properties of the SLMs

Once the SLMs of different PCMs were successfully obtained, their fluorescence properties were investigated at below and above the respective T_m^{PCM}. Since there is no shell material, the temperature dependent fluorescence experiments will induced the loss of the SLMs once they were heated above the T_m^{PCM}. Though this would not be practical for real applications, it will be useful to see if upon removing the shell material and using the optimized conditions to avoid the MEH-PPV degradation, we were able to observe the switch in the structured materials upon heating.

The fluorescence of the SLMs EC/MEH was studied at 20 °C and 60 °C. At the upper temperature the EC melted and microparticles structure were obviously destroyed. As expected, upon heating a very small change of the emission position was observed (Figure 3.41), reproducing the results observed in bulk materials highlight a small blue shift (from 598 to 588 nm).

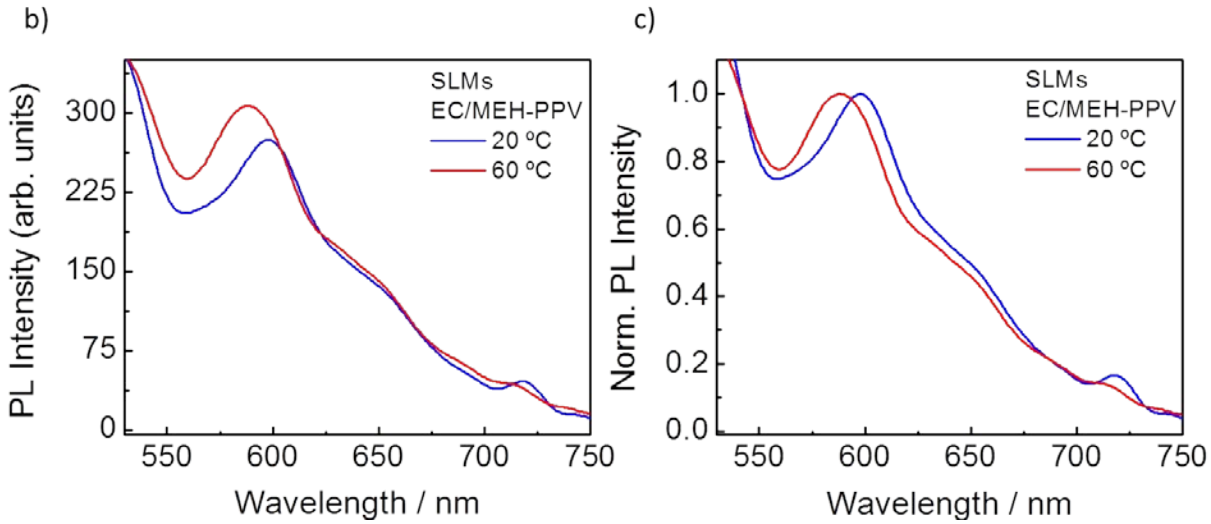

Figure 3.41. *a)* emission and *b)* normalised emission spectra of the sample SLMs EC/MEH measured at 20 °C and 60 °C, exciting at 490 nm.

At room temperature, SLMs SA/MEH showed a band at 563 nm and another one, slightly less intense, at 599 nm (Figure 3.42b). When the sample was heated, the emission band of the conjugated polymer retained the same structure presented at low temperature, with a slightly decreased intensity. The emission of the microparticles showed similarities with the bulk system, especially for the spectrum obtained at high temperature (80 ºC), which practically overlaps the spectrum of the heated bulk mixture. This was expected, since the melted particles are basically a bulk mixture of the SA and MEH-PPV. The room temperature spectrum presented, instead, a small blue-shift compared to the emission of the solid bulk (from 579 nm to 563). Besides, in the emission band of the bulk system is present a weak shoulder at 619 nm, while in the microparticles is present an intense and defined peak. Very importantly, the normalised spectra (Figure 3.42b) showed a significant blue-shift of the emission upon melting, with the bands shifting to 543 nm 579 nm respectively.

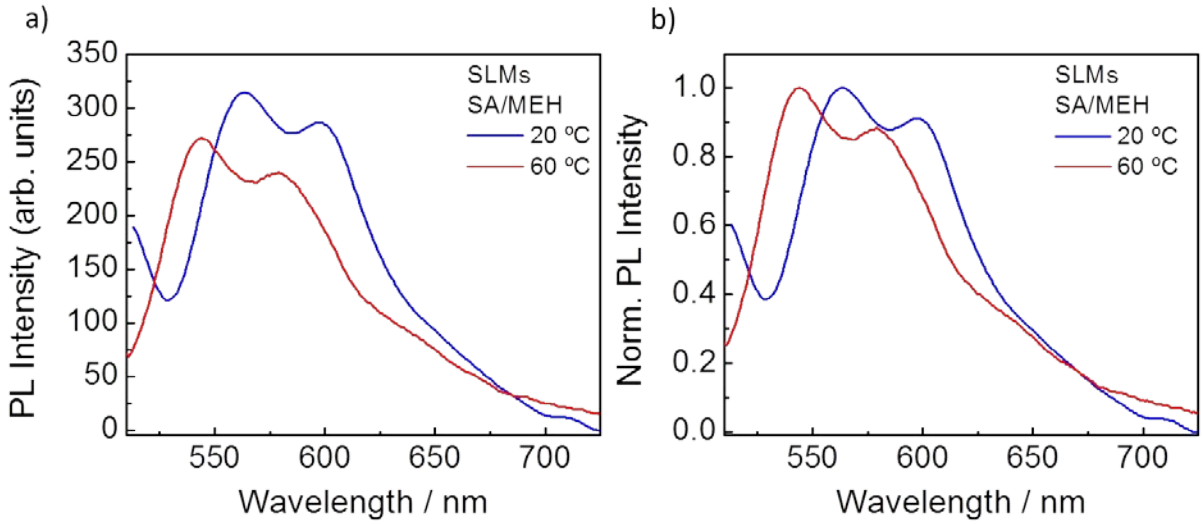

Figure 3.42. *a)* Emission and *b)* normalised emission spectra of the sample SLMs SA/MEH measured at 20 °C and 60 °C, exciting at 490 nm.

3.4.1.4. Thermally switchable optical sensors based on thin films and SLMs/MEH

With SLMs of SA it was finally obtained an optical switch whose behaviour resembled the one observed in bulk. Moreover, no degradation was observed during storage, making these SLMs of fatty acids MEH-PPV a very promising system to obtain thermally switchable optical materials. In order to obtain an optical material, with reversible properties, the SLMs needed to be embedded in a polymeric film, which would trap the particles and maintain their confined structure below and above the T_m^{PCM}.

The films were prepared by dropcasting the suspension of the SLMs previously mixed with a solution containing a large amount of a film-forming polymer, which precipitates upon the water evaporation, trapping the SLMs.

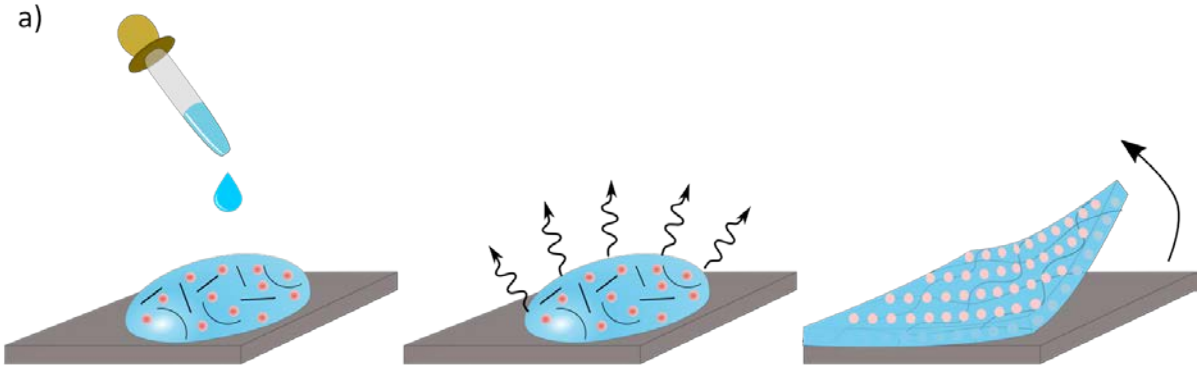

Scheme 3.5. Scheme of the dropcasting method used to prepare polymeric films.

For this the suspension of the SLMs DA/MEH *AOT* were used without freeze-drying the SLMs to avoid possible damages of the SLMs and their aggregation. PVA was selected as

film forming polymer, a material largely used in our group since it provides flexible and colourless films.

The obtained film (hereafter named as SLMs DA/MEH AOT@PVA) and the dried SLMs DA/MEH *AOT* (used for the film) were studied by DSC and their thermal properties were compared to those of the bulk PCM. The DSC profile of the SLMs DA/MEH *AOT* (Figure 3.43a) was similar to the bulk system, showing T_m of ~44 °C. The structuration did not affect the thermal properties of the material.

When the microparticles were incorporated in the PVA film, their DSC profile changed (Figure 3.43b) showing two different endothermic peaks: one, with lower intensity, corresponding to ~49 °C, and the second one, more intense, corresponding to ~40 °C. Both transitions were associated to the melting of DA. The presence of two T_m was ascribed to the presence of two different dominium for the DA. due to the presence of PVA, during the melting of the microparticles, the polymer may interact with the DA at the PVA/SLMs interface, modifying the crystallinity of the fatty acid, resulting in the formation of two crystalline structures presenting two different T_m.

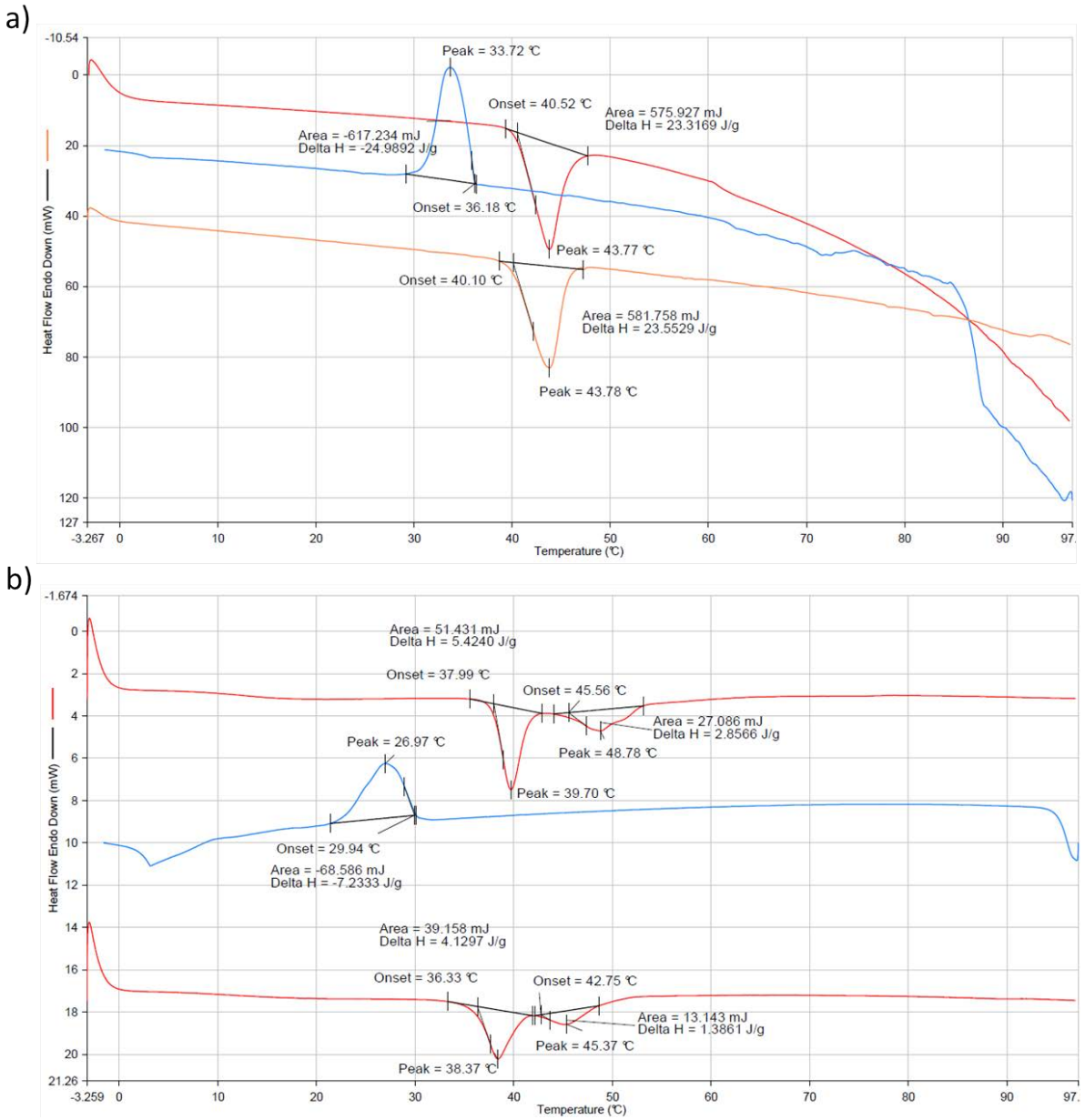

Figure 3.43. DSC analysis of sample *a)* SLMs DA/MEH *AOT* and *b)* SLMs DA/MEH *AOT*@PVA performing three cycles of: heating (red line), cooling (blue line), and heating again (orange line), from 0 °C to 100 °C at the rate of 10 °C/min.

Finally, the fluorescence of SLMs DA/MEH *AOT*@PVA film was studied at 20 °C and 60 °C. Figure 3.44a shows the film emission which, at room temperature (blue line) presents a broad emission band with the maximum centred at 602 nm. When heated to 60 °C (red line) the emission intensity slight decreased and a new band at higher energy appeared (544 nm). Furthermore, as shown by the normalised spectra in Figure 3.44b, the main peak of the emission from the heated sample is blue-shift to 586 nm. When the film was cooled down, the initial emission band was recovered, with the only difference of slight increase in intensity (cyan line).

The fluorescence of the microparticles embedded in the PVA film showed nearly the same blue-shift (20 nm) to the variation of the temperatures as that observed in the bulk DA/MEH mixture. The spectra recorded for the films were in both solid and liquid DA slightly blue shifted respect to the same spectra recorded in bulk mixtures (Figure 3.44b). However the emission switch of the film was also detectable with naked-eye. Therefore, such system made of solid lipid microparticle loaded with MEH-PPV and embedded in the polymeric matrix could be employed as a temperature fluorescent sensor.

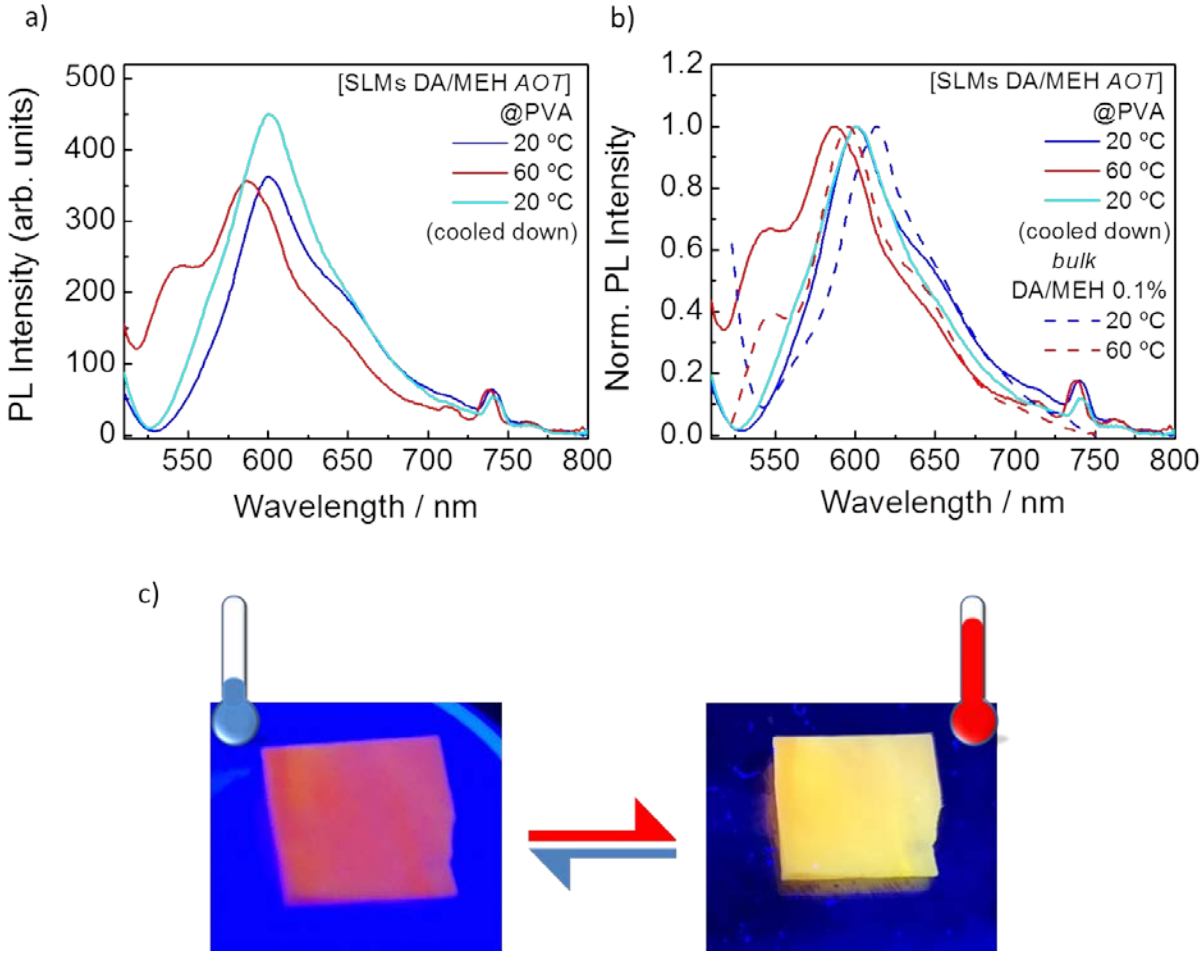

Figure 3.44. *a)* Emission spectra and *b)* normalised emission spectra of the sample [SLMs DA-MEH *AOT*]@PVA measured at 20 °C (blue line), 60 °C (red line), and at 20 °C after cooling down the sample (excitation at 490 nm). *c)* Digital camera capture of the film at two different temperatures (RT and 60 ºC).

3.5 SUMMARY

In this work we started with the hypothesis that the optical properties of the conjugated polymer MEH-PPV could be reversibly switched from the aggregation-like emission to the single chain-like emission by simply dissolving the polymer in phase change materials which reversibly modifies the optical properties of the loaded polymer upon solid to liquid phase transition. The bulk experiments performed dissolving MEH-PPV in different PCMs confirmed our hypothesis, identifying the fatty acids as the best PCMs for such switching behaviour. The large blue-shift observed in the fatty acids/MEH-PPV mixture upon phase change was ascribed to the better solvation of the polymer in the molten state than in the solid state. Probably, this solvation is the consequence of the higher polarity of the fatty acids, due to the carboxylic group, which actuates only when it is in the liquid phase. On the contrary, when the PCM is in its solid state it does not interact with the polymer. The lack of polarity in paraffin PCMs did induce significant spectral shifts.

The suitability of such system as temperature sensor was demonstrated preparing a prototype where the PCMs/MEH-PPV mixture was directly deposited onto cellulose paper. The substrate, once heated, exhibited an evident change of the emitted light, observable even by naked-eye. Though it demonstrated to be a good proof-of-concept, the lack of reversibility for the diffusion of the liquid PCM pushed us to fabricate a polymeric film embedding the PCM/MEH mixture responsible for the switch.

In the view of the implementation of the prototype, the mixture was encapsulated in micro-/nanocapsules to realise flexible polymeric films. The encapsulation of the PCMs was achieved, as showed by different characterisation techniques (SEM, DSC and NMR), but the thermal switch of the bulk mixtures was always lost. The different behaviour of the mixture PCMs/MEH-PPV exhibited in the micro-/nanocapsules was probably due to both the interaction of MEH-PPV with the polymeric shell and the reactivity of the fatty acids.

To avoid the side interactions between the polymeric shell and the core materials, the micro-confinement of the system PCMs/MEH-PPV was achieved forming solid lipid microparticles in acidic conditions. SLMs of the mixtures SA/MEH-PPV and DA/MEH-PPV was successfully synthesised and exhibited similar optical behaviour of the bulk mixtures.

Finally, the SLMs of the mixture DA/MEH-PPV were embedded in a polymeric matrix in order to obtain a polymeric flexible film. The final material exhibited reversible optical switch of the emission of MEH-PPV upon heating and cooling cycles. Thus, a final improved prototype was successfully fabricated.

3.6 EXPERIMENTAL SECTION

PREPARATION OF THE DISPERSIONS

Preparation of the PCMs/MEH mixtures.

For the solution PCM/MEH 0.1%, the suitable volume (0.1-1 mL) of the polymer stock solution in CH_2Cl_2 (0.1 wt.%) was added to the right amount of PCM in a glass vial, in order to have the final concentration of MEH in PCM of 0.1 wt.%. The organic solvent dissolved the PCM resulting in a clear liquid solution at room temperature. The solution was placed in a sonicating water bath for 30 minutes to improve the polymer dissolution. The organic solvent was evaporated placing the vial with the mixture in a hot plate heating at a temperature of 10 ºC above the T_m^{PCM} and stirring overnight. The evaporation of the CH_2Cl_2 led to a red liquid mixture. In the case of EC mixtures some aggregates were also formed. Once cooled to room temperature, the mixtures made of PCMs with T_m^{PCM} > RT turned solid with no apparent phase segregation of the polymer, while those made of PCMs with T_m^{PCM} < RT remained as red homogeneous liquids.

The PCM/MEH 0.01% mixtures were obtained weighting in a glass vial 100 mg of the solution PCM/MEH 0.1% and adding 900 mg of PCM. Successively, 2 ml of CH_2Cl_2 solution were added to the PCM/MEH solids, and the solution was placed in a sonicating water bath to improve the dissolution of the polymer in the PCM. Finally, the organic solvent was evaporated by heating at 10 ºC above the T_m^{PCM} and stirring the solution overnight.

PREPARATION OF THE MICRO/NANOSTRUCTURED MATERIALS

PMMA and PPO microcapsules

For the oil phase, 0.8 g of the system PCM/MEH-PPV (where as PCM was used DA, NA and EC) were dissolved in 5 ml of CH_2Cl_2 (or $CHCl_3$ in the case of using PPO) and placed in sonicating water bath for ~10 minutes. Separately, 0.5 g of PMMA (M_w ~120.000) or PPO were dissolved in 5 ml of CH_2Cl_2 (or $CHCl_3$ in the case of PPO) and placed in sonicating water bath for ~10 minutes. In the standard protocol PVA (1% hydrolysis M_w ~89.000) was employed as the emulsifier, dissolving it in H_2O at the concentration of 1 w/v%. Only in one case, specifically for the sample MC DA/MEH-PPV *SDS*, the PVA was replaced with SDS at the same concentration. Successively, the two organic solutions were poured in 15 ml of H_2O/PVA (or H_2O/SDS) solution and emulsified by ultra Turrax®

homogenizer at the constant speed of 8.000 rpm. After 30 minutes the homogenization was stopped, and the O/W emulsion was obtained. In order to achieve the formation of microcapsules, the organic solvent was removed inducing the precipitation of the PMMA (or PPO) to form the shell around the PCM/MEH core. The solvent evaporation was carried out stirring the mixtures (500 rpm) at 35 °C for the first 3 hours and at room temperature overnight. The final microcapsules suspensions were centrifuged three times at 10.000 rpm for 5 minutes in order to remove non-structured materials.

In the case of the sample MC PMMA DA/MEH-PPV pH4, the synthesis procedure was the same reported above, with the only difference of the addition of HCl to the H_2O/PVA solution in order to adjust the pH at 4.

PMMA nanocapsules

100 mg of the mixture DA/MEH 0.1% were dissolved in 2 ml of CH_2Cl_2 and placed in sonicating water bath for ~10 minutes. Separately, 125 mg of PMMA (M_w ~120.000) were dissolved in 2 mL CH_2Cl_2 and placed in sonicating water bath for ~10 minutes., 120 mg of SDS was dissolved in H_2O to form a homogeneous solution (1 w/v %). Successively, the two organic solutions were poured in 10 ml of H_2O/SDS solution and magnetically stirred (600 rpm) for 20 minutes to obtain a pre-emulsion. The miniemulsification was achieved by ultrasonication of the pre-emulsion for 180 seconds with a Branson sonifier W450 Digital at 70% amplitude. The nanocapsules were formed inducing the precipitation of the PMMA around the DA/MEH through the evaporation of the organic solvent achieved by magnetically stirring (500 rpm) the miniemulsion at 35 ºC for the first 3 hours and at RT overnight. The final nanocapsules suspensions were centrifuged three times at 13.000 rpm for 10 minutes in order to remove unstructured materials.

Solid lipid microparticles

In a typical synthesis of SLMs, the oil-in-water emulsion was prepared by the addition of 0.5 g of the melted PCM/MEH-PPV 0.01% in 20 ml of the aqueous phase containing emulsifier (1% w/v). As PCM EC, DA and SA were used, while Tween®20 (polyethylene glycol sorbitan monolaurate) and AOT were employed as surfactants. The aqueous phase was previously heated to 10 °C above the melting point of the PCM used to avoid the solidification. When a fatty acid was used as PCM the aqueous phase was acidified to pH = 4 adding aqueous HCl (0.01 M). The emulsion was obtained by homogenizing at 3.000 rpm using the Ultra-Turrax homogenizer. After 10 minutes, 30 ml of cold water (~5 °C) was

poured in the mixed solution and the stirring was immediately stopped. In the case of the sample SLMs DA/MEH-PPV *AOT*, the cold water also contained AOT (0.5 w/v %). The final suspension was then placed in ice bath for 10 min to further decrease the temperature and, afterwards, in the fridge for 12 hours to let it stabilize. The resulting solid lipid microparticles flocculated in the aqueous phase forming a pink and opaque compact layer floating on top of the continuous aqueous phase (creaming). The microparticles were cleaned washing three times with water and then the dispersion was freeze-dried for two days. The sample SLMs DA/MEH-PPV *AOT* was not lyophilised.

Fabrication of the film

The film was from the SLMs DA/MEH-PPV *AOT*. First, 0.8 g of the microparticles suspension were added to 8 g of PVA water solution (20 wt.%) and left magnetically stirring for 2 hours. Successively the mixed solution was drop-casted onto a plastic Petri dish and left to dry under vacuum at room temperature. The final flexible films could be easily peeled out from the Petri dish.

CHARACTERISATION

Proton nuclear magnetic resonance (^{1}H-NMR)

100 mg of microcapsules were dissolved in $CDCl_3$ and ^{1}H-NMR spectra were recorded using the spectrometer Bruker DPX250 (250 MHz for ^{1}H-NMR). The spectra are given in chemical shifts, δ (ppm). The peaks are defined as singlets (s), triplets (t) or multiplets (m). 20 µl of DMSO (δ_H/ppm = 2.62 (s, 6H, $(CH)_2$) were added to the samples, as an internal reference, for quantitative determination of the microcapsules payload.

Differential Scanning Calorimetry (DSC)

Measurements were carried out in a Perkin Elmer DSC8500 LAB SYS (N5340501) equipped with a Liquid N_2 controller CRYOFILL (N534004). Approximately 2 mg of the sample were deposited on the 0.5 cm-in-diameter aluminium pan. An empty pan was used as a reference. The scanning rate was 10 K/min for both the heating and cooling processes. The scanned temperature range depended on the sample. The melting/crystallization point were calculated from the intersection between two tangents (one is the slope of the endo- or exothermic peak and the other is the straight line of the baseline).

3.7 REFERENCES

1. Conwell, E. Mean free time for excimer light emission in conjugated polymers. *Phys. Rev. B* **57,** 14200–14202 (1998).

2. Schwartz, B. J. How Chain Conformation and Film Morphology Influence Energy Transfer and Interchain Interactions. *Annu. Rev. Phys. Chem.* **54,** 141–172 (2003).

3. Blatchford, J. *et al.* Photoluminescence in pyridine-based polymers: Role of aggregates. *Phys. Rev. B - Condens. Matter Mater. Phys.* **54,** 9180–9189 (1996).

4. Lemmer, U. *et al.* Aggregate fluorescence in conjugated polymers. *Chem. Phys. Lett.* **240,** 373–378 (1995).

5. Jenekhe, S. A. & Osaheni, J. A. Excimers and Exciplexes of Conjugated Polymers. *Science (80-.).* **265,** 765–768 (1994).

6. Samuel, I. D. W. *et al.* Picosecond Time-Resolved Photoluminescence of PPV Derivatives. *Synth. Met.* **84,** 497–500 (1997).

7. Samuel, W., Rumbles, G. & Collison, C. J. Efficient interchain photoluminescence in a high-electron-affinity conjugated polymer. *Phys. Rev. B* **52,** 573–576 (1995).

8. Osaheni, J. A. & Jenekhe, S. A. Efficient blue Luminescence of a Conjugated Polymer Exciplex. *Macromolecules* **27,** 739–742 (1994).

9. Quan, S. *et al.* Solvent and concentration effects on fluorescence emission in MEH-PPV solution. *Eur. Polym. J.* **42,** 228–233 (2006).

10. Gebler, D. D., Wang, Y. Z., Fu, D. K., Swager, T. M. & Epstein, A. J. Exciplex emission from bilayers of poly(vinyl carbazole) and pyridine based conjugated copolymers. *J. Chem. Phys.* **108,** 7842–7848 (1998).

11. Yan, M., Rothberg, L. J., Papadimitrakopoulos, F., Galvin, M. E. & Miller, T. M. Spatially indirect excitons as primary photoexcitations in conjugated polymers. *Phys. Rev. Lett.* **72,** 1104–1107 (1994).

12. Schwartz, B. J., Hide, F., Andersson, M. R. & Heeger, A. J. Ultrafast studies of stimulated emission and gain in solid films of conjugated polymers. *Chem. Phys. Lett.* **265,** 327–333 (1997).

13. Schaller, R. D. *et al.* The nature of interchain excitations in conjugated polymers: Spatially-varying interfacial solvatochromism of annealed MEH-PPV films studied by near-field scanning optical microscopy (NSOM). *J. Phys. Chem. B* **106,** 9496–9506 (2002).

14. Nguyen, T. Q., Doan, V. & Schwartz, B. J. Conjugated polymer aggregates in solution: Control of interchain interactions. *J. Chem. Phys.* **110,** 4068–4078 (1999).

15. Cossiello, R. F., Susman, M. D., Aramendía, P. F. & Atvars, T. D. Z. Study of solvent-conjugated polymer interactions by polarized spectroscopy: MEH-PPV and Poly(9,9′-dioctylfluorene-2,7-diyl). *J. Lumin.* **130,** 415–423 (2010).

16. Nguyen, T.-Q., Martini, I. B., Liu, J. & Schwartz, B. J. Controlling Interchain Interactions in Conjugated Polymers: The Effects of Chain Morphology on Exciton−Exciton Annihilation and Aggregation in MEH−PPV Films. *J. Phys. Chem. B* **104,** 237–255 (2000).

17. Collison, C. J., Rothberg, L. J., Treemaneekarn, V. & Li, Y. Conformational effects on the photophysics of conjugated polymers: A two species model for MEH-PPV spectroscopy and dynamics. *Macromolecules* **34,** 2346–2352 (2001).

18. Zhang, H. *et al.* Conformational transition of poly[2-methoxy-5-(2′-ethylhexoxy)-p-phenylene vinylene] in solutions: Solvent-induced emitter change. *J. Photochem. Photobiol. A Chem.* **147,** 15–23 (2002).

19. Köhler, A., Hoffmann, S. T. & Bässler, H. An Order–Disorder Transition in the Conjugated Polymer MEH-PPV. *J. Am. Chem. Soc.* **134,** 11594–11601 (2012).

20. Wantz, G. *et al.* Temperature-dependent electroluminescence spectra of poly(phenylene-vinylene) derivatives-based polymer light-emitting diodes. *J. Appl. Phys.* **97,** (2005).

21. Oliveira, F. A. C. *et al.* Temperature effects on the vibronic spectra of BEH-PPV conjugated polymer films. *J. Chem. Phys.* **119,** 9777–9782 (2003).

22. Jakubiak, R., Yan, M., Wan, W. C., Hsieh, B. R. & Rothberg, L. J. Description and Importance of Interchain Excited States in Conjugated Polymer Photophysics. *Isr. J. Chem.* **40,** 153–157 (2000).

23. Da Silva, M. A. T. *et al.* Identification of the optically active vibrational modes in the photoluminescence of MEH-PPV films. *J. Chem. Phys.* **128,** (2008).

24. Sharma, A., Tyagi, V. V., Chen, C. R. & Buddhi, D. Review on thermal energy storage with phase change materials and applications. *Renew. Sustain. Energy Rev.* **13,** 318–345 (2009).

25. Lin, Y., Jia, Y., Alva, G. & Fang, G. Review on thermal conductivity enhancement, thermal properties and applications of phase change materials in thermal energy storage. *Renew. Sustain. Energy Rev.* **72,** 128–145 (2017).

26. Mehling, H. & Cabeza, L. F. *Heat and cold storage with PCM. Hand book, Publisher Springer, Germany* (2008). doi:10.1007/978-3-540-68557-9

27. Himran, S., Suwono, A. & Mansoori, G. A. Characterization of alkanes and paraffin waxes for application as phase change energy storage medium. *Energy Sources* **16,** 117–128 (1994).

28. Hasnain S.M. Review on sustainable thermal energy storage technologies, Part I: heat storage materials and techniques. *Energy Convers. Manag.* **39,** 1127–1138 (1998).

29. Singh, S., Gaikwad, K. K., Lee, M. & Lee, Y. S. Temperature-regulating materials for advanced food packaging applications: a review. *J. Food Meas. Charact.* **12,** 588–601 (2017).

30. Rozanna, D., Chuah, T. G., Salmiah, A., Choong, T. S. Y. & Sa'ari, M. Fatty Acids as Phase Change Materials (PCMs) for Thermal Energy Storage: A Review. *Int. J. Green Energy* **1,** 495–513 (2005).

31. Dhanusiya, G. & Rajakumar, S. Thermal analysis of PCM based building wall for cooling. **2,** 850–857 (2013).

32. Naito, K. Amorphous-crystal transition of organic dye assemblies: Application to rewritable color recording media. *Appl. Phys. Lett.* **67,** 211 (1995).

33. Burkinshaw, S. M., Griffiths, J. & Towns, A. D. Reversibly thermochromic systems based on pH-sensitive functional dyes. *J. Mater. Chem.* **8,** 2677–2683 (1998).

34. Massaro, G., Hernando, J., Ruiz-Molina, D., Roscini, C. & Latterini, L. Thermally

Switchable Molecular Upconversion Emission. *Chem. Mater.* **28,** 738–745 (2016).

35. Fang, G., Chen, Z. & Li, H. Synthesis and properties of microencapsulated paraffin composites with SiO2shell as thermal energy storage materials. *Chem. Eng. J.* **163,** 154–159 (2010).

36. Cabeza, L. F. *et al.* Use of microencapsulated PCM in concrete walls for energy savings. *Energy Build.* **39,** 113–119 (2007).

37. Bao, B. *et al.* A controllable approach to development of multi-spectral conjugated polymer nanoparticles with increased emission for cell imaging. *Chem. Commun.* **49,** 10623 (2013).

38. Sari, A., Alkan, C., Karaipekli, A. & Uzun, O. Microencapsulated n-octacosane as phase change material for thermal energy storage. *Sol. Energy* **83,** 1757–1763 (2009).

39. Jurkowska, M. & Szczygieł, I. Review on properties of microencapsulated phase change materials slurries (mPCMS). *Appl. Therm. Eng.* **98,** 365–373 (2016).

40. Li, M., Rouaud, O. & Poncelet, D. Microencapsulation by solvent evaporation: State of the art for process engineering approaches. *Int. J. Pharm.* **363,** 26–39 (2008).

41. Zhang, T., Wang, Y., Shi, H. & Yang, W. Fabrication and performances of new kind microencapsulated phase change material based on stearic acid core and polycarbonate shell. *Energy Convers. Manag.* **64,** 1–7 (2012).

42. Juliïà-López, A. *et al.* Temperature-Controlled Switchable Photochromism in Solid Materials. *Angew. Chemie - Int. Ed.* **55,** 15044–15048 (2016).

43. Bodmeier, R., Wang, J. & Bhagwatwar, H. Process and formulation variables in the preparation of wax microparticles by a melt dispersion technique. I. Oil-in-water technique for water-insoluble drugs. *J. Microencapsul.* **9,** 89–98 (1992).

44. Lide, D. R. *Handbook of Chemistry and Physics*. (CRC Press, 2017). doi:9781498784542

45. John K. Grey, Doo Young Kim, Brent C. Norris, William L. Miller, and & Barbara*, P. F. Size-Dependent Spectroscopic Properties of Conjugated Polymer Nanoparticles. (2006). doi:10.1021/JP065990A

46. Green, M., Howes, P., Berry, C., Argyros, O. & Thanou, M. Simple conjugated polymer nanoparticles as biological labels. *Proc. R. Soc. A Math. Phys. Eng. Sci.* **465,** 2751–2759 (2009).

47. Menon, A., Galvin, M., Walz, K. A. & Rothberg, L. Structural basis for the spectroscopy and photophysics of solution-aggregated conjugated polymers. *Synth. Met.* **141,** 197–202 (2004).

48. Andersson, M. R., Yu, G. & Heeger, A. J. Photoluminescence and electroluminescence of films from soluble PPV-polymers. *Synth. Met.* **85,** 1275–1276 (1997).

49. Arnautov, S. A. *et al.* Properties of MEH-PPV films prepared by slow solvent evaporation. *Synth. Met.* **147,** 287–291 (2004).

50. Coropceanu, V., André, J. M., Malagoli, M. & Brédas, J. L. The role of vibronic interactions on intramolecular and intermolecular electron transfer in π-conjugated oligomers. *Theor. Chem. Acc.* **110,** 59–69 (2003).

51. Quan, S. *et al.* Solvent and concentration effects on fluorescence emission in MEH-PPV solution. *Eur. Polym. J.* **42,** 228–233 (2006).

52. Forster, T. Energiewanderung und Fluoreszenz. *Naturwissenschaften* **33,** 166–175 (1946).

53. Cratin, P. D. Mathematical Modeling of Some pH-Dependent Surface and Interfacial Properties of Stearic Acid. *J. Dispers. Sci. Technol.* **14,** 559–602 (1993).

CHAPTER

4

CONJUGATED POLYMER NANOPARTICLES (CPNS) WITH TUNEABLE OPTICAL PROPERTIES

The development of novel and simple methodologies for the obtaining of semiconductive polymer nanoparticles with fine-tuned optical properties represents nowadays a challenging research area as it involves a simultaneous chemical modification and nanostructuration of the polymer. Here, starting from poly[2-methoxy-5-(2-ethylhexyloxy)-1,4 ... into the one ... of oligomers with tunable conjugation length and their nanostructuration, employing a miniemulsion method. Ultrasound irradiation of heterogeneous mixtures leads to the formation of hypochlorous acid that disrupts the electronic conjugation through polymer chain cleavage. Moreover, control over the degree of the electronic conjugation of the oligomers, and therefore of the optical properties, is achieved simply by varying the polymer concentration of the initial solution. Finally, the presence of surfactants during the sonication allows for the formation of nanoparticles with progressive spectral shift of the main absorption (from λ_{max} = 476 to 306 nm) and emission bands (from λ_{max} = 597 to 481 nm). The integration of conducting polymer nanoparticles into polymeric matrices yields self-standing and flexible fluorescent films.

4.1 INTRODUCTION

In the last few years, the interest on conjugated polymers also focused on their structuration in nanoparticles which represent multifunctional nanoscale materials with great potential in the energy generation and storage, as well as for early stage diagnosis and therapy applications.

4.1.1 Advantages and properties of CPNs

Aqueous dispersions of polymers nanoparticles are critical raw materials used in an interesting variety of industrial applications. For examples, polymer dispersions are commonly used in the formulation of coatings and paints, thanks to low viscosity it represents with respects other organic solutions that facilities its processing and manipulation.[1]

Such interesting rheological properties together with the possibility to obtain water dispersions of polymers otherwise soluble exclusively in organic solvents were the motivation for the first synthesis of conjugated polymer nanoparticles back in the 80s. Initially, polyacetylene, polypyrrole, and polyaniline water suspension were generated by dispersion or emulsion polymerisation.

Nanoparticles composed of the conjugated polymer poly[3,4-(ethylenedioxy)thiophene] (PEDOT) and the polyelectrolyte poly(styrenesulfonate) (PSS) are nowadays commercially available as aqueous dispersions. Films prepared from such suspensions exhibit conductivities of up to $>10^3$ S cm^{-1}, and they are used, for example, for the preparation of hole injection layers in organic light-emitting diodes (OLEDs) or even as alternative to the common indium tin oxide (ITO) electrodes.

Conjugated polymers are known to have photophysical properties very dependent on the effective conjugation length and the conformation of the polymer chains. Since these parameters can be altered during the nanostructuration process, one of the advantages to have such conjugated polymer nanoparticles is the ability to control the final optical properties depending on the different synthesis conditions described as follows.

- ***Synthesic methodologies***

The synthesis conditions affect the conjugated polymer conformation in the resulting nanoparticles which exhibit a shift in the absorption spectra. For instance, in polythiophene nanoparticles synthesised by miniemulsion polymerisation or reprecipitation, where the

particles formation occurs rapidly, the polymer constrained in a small volume is believed to adopt a collapsed conformation. As a consequence, the polymer backbone presents kinks and bends which cause a reduction in the conjugation length and a blue-shift absorption maximum compared to the polymer in solution.[2] When the nanoparticles are prepared by self-assembly over an extended reaction time, the formation of highly ordered structures, possibly consisting of aligned, stretched polymer chains are promoted. The increased order leads to a red-shift of the absorption maximum.[3] Such shift is due to energy transfer to low-energy chromophores (the segments with larger conjugation length), which is more favoured upon increasing chain-chain interactions, and approaches the red-shifts observed in the film casted from homogeneous solution..[4]

- ***Nanoparticles dimensions***

Conjugated polymer nanoparticles also exhibit size-dependent photophysical properties. It should be emphasised that a different force drives such phenomena compared to the quantum confinement effect which controls the size-dependent absorption and emission properties in quantum dots. In CPNs, the optical properties are mainly dependent on the conformational changes of the polymers, the nature of the aggregates, and the distance between the chromophores. Masuhara and coworkers prepared 40-400 nm nanoparticles of poly(3-[2-(N-dodecylcarbamoyloxy)ethyl]thiophene-2,5-diyl) (P3DDUT) and investigated their spectroscopic and thermochromic behaviour in water. They observed a blue shift in the absorption and emission spectra of nanoparticles upon decreasing the size from 400 to 40 nm (Figure 4.1).[5]

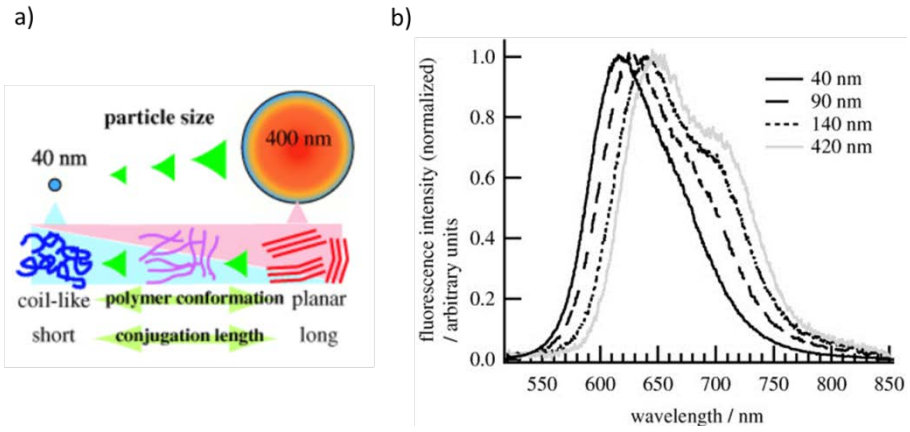

Figure 4.1. *a)* Schematic representation of the different polymer conformations adopted depending on the sizes. *b)* Fluorescence spectra of P3DDUT nanoparticles, with various mean diameters, dispersed in water. The excitation wavelength was 480 nm. (Copyright 2004 Wiley-VCH Verlag GmbH & Co. KGaA, Weinheim).[5]

The authors the optical modifications with size to three different conformations of the polythiophene derivatives into the particles:

I. In the smallest nanoparticles (~40 nm) the polymers chains assume the coil-like conformation with distortions and bendings of the C–C bonds between adjacent thiophene rings. This conformation reduces the conjugation length, which stands for the blue-shifted absorption and emission properties. Such assembly induces the formation of an amorphous phase.

II. In the largest particles (400 nm), the polymer chains adopt a planar conformation in which the thiophene rings are coplanar and tends to form π–stacked aggregates leading to a crystalline phase. The limitation in the rotation of the thiophene rings resulting from the intermolecular interactions makes the conjugation length longer, inducing the red shift in absorption and emission of the conducting polymer.

III. Between the flexible coil-like and the rigid planar conformation, there are distorted conformations which possess some degrees of freedom, allowing partial distortion in the main chain. These conformations present a conjugation length longer than the coil-like conformation and the assembly of such copolymers lead to a quasicrystalline phase.

Barbara *et al.* conducted a detailed study on the photophysical properties of poly[2-methoxy-5-(2-ethylhexyloxy)-1,4-phenylenevinylene] (MEH-PPV) nanoparticles with different sizes (10-100 nm). Interestingly, employing single-particle spectroscopy, they found out that the nanoparticles with diameters longer than 10 nm, which contain more than one polymer chain, exhibited bulk-like structure and properties, in contraposition to polythiophene based nanoparticles. The observed size-dependent spectroscopic properties were ascribed to the distance dependence of four main kinetic processes: electronic energy transfer from more to lower energy sites, triplet-triplet annihilation, singlet exciton quenching by triplets, and singlet exciton quenching polarons.[4]

These two studies demonstrate that the size-dependent photophysical properties of conjugated polymers nanoparticles are strictly connected with the polymer conformation which is controlled by the chemical structure of the polymer backbone. Thus, conjugated polymers with different chemical structure exhibit different size-dependent intermolecular interaction in the nanoparticles. As showed by the different size-dependent optical properties exhibited by polythiophene and MEH-PPV nanoparticles presented in the cited works.

- ***Use of surfactants***

Usually, the majority of the techniques employed in the synthesis of the nanoparticle involve the use of a surfactant to stabilise the emulsion and the final colloidal dispersion. Piok *et al.* investigated the effect of the surfactant on the optical properties of CPNs. Upon comparison of a film obtained from the nanoparticles dispersion with the one obtained from a surfactant free bulk solution, they did not observe any change in the basic spectroscopic properties associated to the presence of the surfactant. Nevertheless, they found interesting differences in the photoexcitation kinetics and experimentally showed that the film prepared from the nanoparticles had an influence on the generation, migration and recombination behaviour of the photoexcited species.[6]

4.1.2 Additional properties of CNPs

Further interesting properties of conjugated polymer nanoparticles are their brightness and optimised photostability by comparison to molecular dyes, as a result of a large absorption cross-section. Such properties attracted increasing interest in recent years for the use of conjugated polymer nanoparticles as a new class of highly fluorescent probes. McNeill *et al.* investigated in detail the photophysical properties of CPNs to determine their suitability as a fluorescent probe in live cells imaging. In particular, analysis of single particle photobleaching revealed excellent photostability, with as many as 10^9 or more photons emitted by each nanoparticle before irreversible photobleaching.[7] In comparison, the most photostable, dyes such as Rhodamine 6G, can emit only around 10^6 photons per molecule before irreversible photobleaching,[8] which is not ideal for long-term single molecule fluorescence tracking. In addition to such enhanced photophysical properties, many studies demonstrated that various types of conjugated polymer nanoparticles are taken up and accumulated by different types of living cells allowing an increase of the fluorescence signal. Moreover, the nanoparticles investigated in such studies did not present toxicity for the cell.[7,9–12]

Such enhanced properties also make these nanomaterials suitable for various applications, ranging from water processable inks for devices fabrication (photovoltaic[13] and electrochromic cells[14], OLEDs[15] or lasers[16]) to non-toxic fluorescent biological labels,[12,17] or even to induce photophysical processes at the nanoscale (e.g. photoinduced electron[18] or energy transfer[19]). Though, to fully exploit these limitless possibilities, further basic research is still required. One of such areas is the development of novel and simple methodologies for

the obtaining of semiconductive nanoparticles with fine-tuned optical (especially emission) properties,[20] due to its implicit technological relevance and the applications that can be derived from there.

4.1.3 Spectral tuning of conjugated polymers and CNPs

So far, spectral emission tuning of bulk semiconductive polymers has raised lots of interest and has been reported through different strategies.

The most straightforward approach to control the optical properties of conjugated polymers involves the dissolution of the polymer in solvents with different solvation power and at various concentrations. In literature, it has been well described how some media solvate preferentially the lateral groups, while others mainly solvate the polymer backbone.[21] As a consequence, the solvent affects the macromolecular conformations of conjugated polymers changing the distribution of the effective conjugation length, which results in the modification of the emission profile. Quan *et al.* did a systematic investigation of steady-state fluorescence of MEH-PPV in two solvents, toluene and tetrahydrofuran, and at several different concentrations. They showed how increasing the concentration the emission was red-shifted, with a preliminary aggregation of the polymer chains as revealed by the small change of the relative intensity of the vibronic bands 0–0 and 0–1 (I_{0-0} / I_{0-1}), which were activated by exciting the polymer at different wavelengths. The change in the ratio I_{0-0} / I_{0-1} also allowed to observe that the aggregation degree was dependent on the solvent.[22] Obviously, the tuning of the optical properties using different solvents is not viable in perspective of possible applications.

Cadby and co-workers encapsulated and confined MEH-PPV in periodic silica host with various pore sizes. The different pore sizes control the degree of aggregation of the conjugated polymer. Through (polarised) photoluminescence excitation spectroscopy, they investigated the role played by interchain aggregation and chain morphology in polaron production (Figure 4.2). They observed a blue-shift of the emission, together with changes of the polarisation ratio, upon decreasing the pore size. The data in Figure 4.2a shows that photoluminescence (PL) from the polymer incorporated into small silica pores (blue line) is qualitatively similar to data collected on a dilute solution (cyan line), while PL from polymer incorporated into medium (brown line) or large (orange line) pores looks much more like data collected on a polymer film sample (pink line). Therefore, based on the experimental data, they suggested that the polymer assumed different conformation: I) aligned and isolated

polymer chain in the small pore samples; II) closely packed, yet parallel polymer chains in medium pore samples; and III) aggregated and coiled polymer chain, resembling the film environment, in large pore samples. Thus, by guest/host chemistry, they achieved to control the inter- and intramolecular interaction of conjugated polymer and, consequently, the tuning of the optical properties of such material.[23]

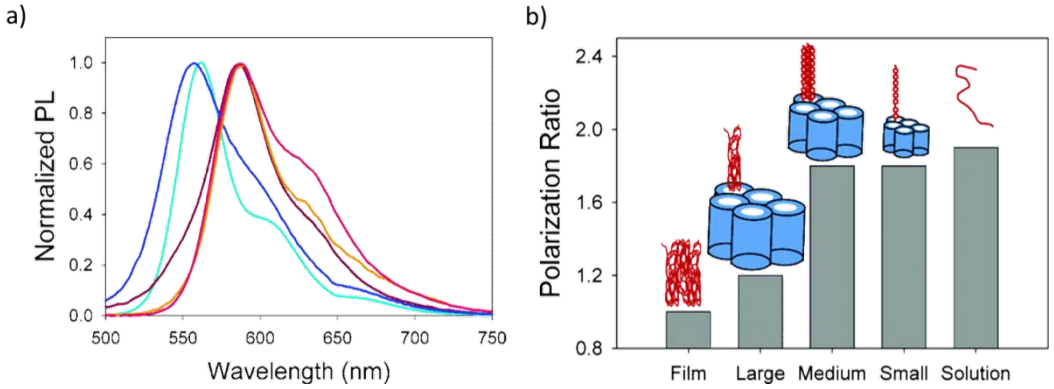

Figure 4.2. *a)* Photoluminescence spectra of diluted MEH−PPV solution (cyan), a drop casted polymer film (pink), and the three washed polymer-in-silica nanopore samples. The smallest pore material is shown in blue, the medium pore material in brown, and the large pore material in orange. *b)* Maximum polarisation ratio achieved for each sample with different pore size. (Copyright 2005 American Chemical Society).[23]

Other strategies to tune the optical properties of the conjugated polymers involve physical methods, such as post-fabrication annealing/cooling or pressure/mechanical cycles.[24–26] Alternative chemical strategies include polymer modification with different core units[27]/side substituents,[28] or the controlled synthesis of oligomeric species differing on the number of repetitive monomers (and therefore conjugation length).[29] For example, Ruiz Perez and co-workers developed a method to obtain anisotropic conjugated polymer nanoparticles with an ellipsoidal shape *via* heterophase polymerisation (Figure 4.3).[30]

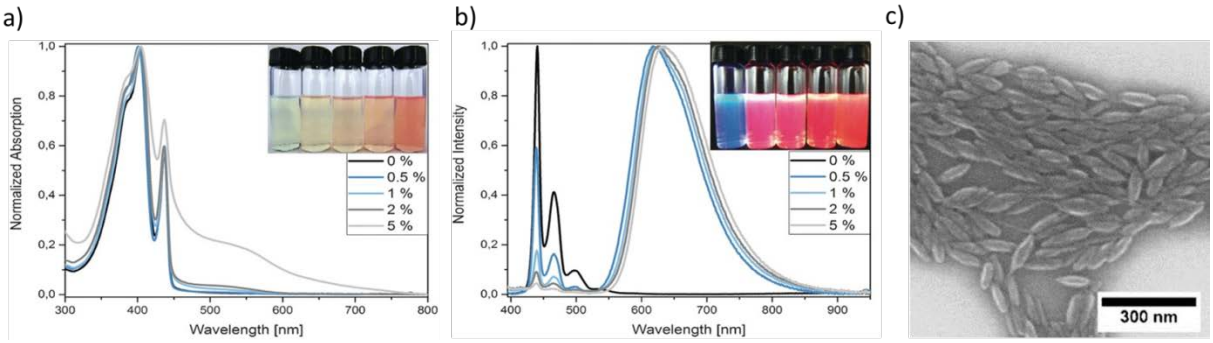

Figure 4.3. *a)* Absorption spectra and *b)* emission spectra of sample obtained by polymerising poly(9,9-dioctylfluorene) (PF8) with varying dye contents (between 0 and 5 mol %). The insert shows the aspect of the 100-fold diluted dispersions under daylight (top) and under UV-light irradiation (bottom). *c)* SEM image of the resulting nanoparticles. (Copyright 2017 Wiley-VCH Verlag GmbH & Co. KGaA, Weinheim).[30]

Through the incorporation of electron-withdrawing repeat units in the polymer backbone, they were able to tune the emission properties and colour of the resulting aqueous dispersion.[30]Tilley *et al.* reported the synthesis and the spectroscopic characterisation of a trimer, tetramer and pentamer oligomers based on the polymer backbone structure of MEH-PPV. They observed in the oligomers a sequential increase in absorption and emission maxima and a decrease in the fluorescence lifetime as the π conjugation length is increased,[29] (Figure 4.4).

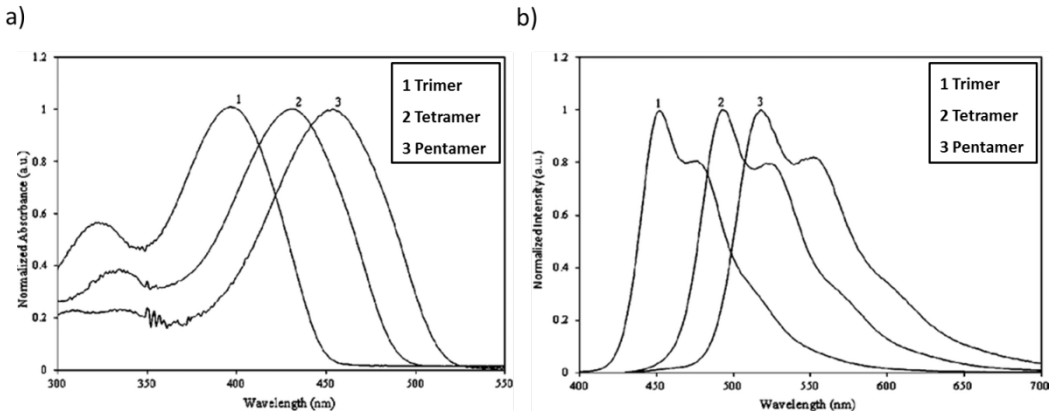

Figure 4.4 *a)* Absorption and *b)* emission spectra of the oligomers in chloroform. (Copyright 2011 American Chemical Society).[29]

Only very recently the synthesis of nanoparticles with tunable optical properties has been partially achieved through the synthesis of polymer dots with packing-dependent emission.[17,30] Piwonski *et al.* synthesised conjugated polymer dots (Pdots) of poly(1,8-carbazole)-benzothiadiazole copolymer (PCzBT), with sizes typically below 10 nm, by a reprecipitation technique where the packing of the polymers was controlled varying the conditions of the synthesis (Figure 4.5). They demonstrated that the different packing inside the nanoparticles of the polymer regulates the fluorescence brightness and the intraparticle energy migration efficiency. The Pdots synthesised with different conditions also showed a small shift in the absorption and emission.[20]

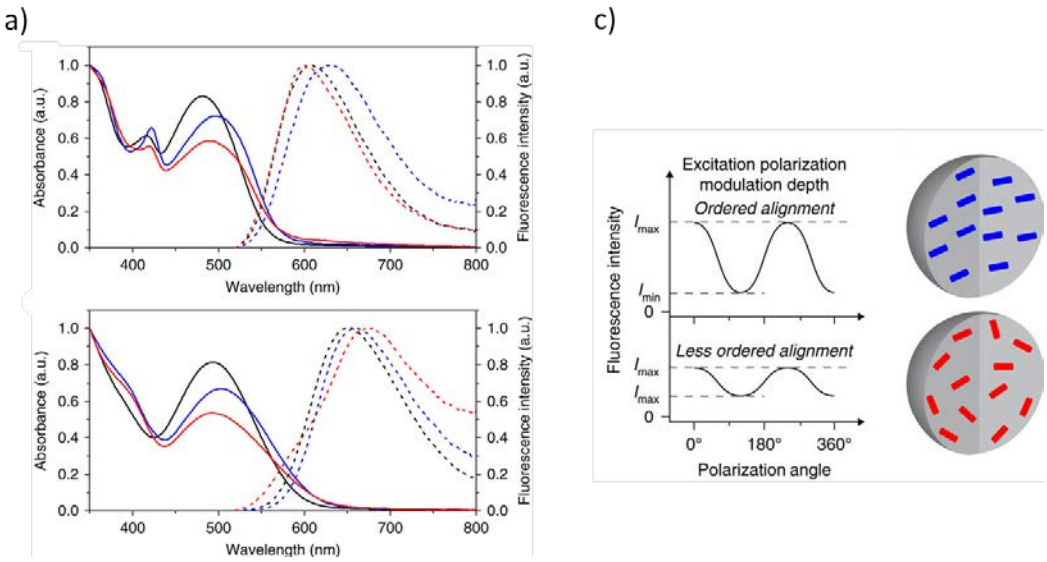

Figure 4.5 *a)* Steady-state absorption (solid lines) and fluorescence (broken lines) of the poly(1,8-carbazole)-benzothiadiazole copolymer (PCzBT) in THF (black lines) and PCzBT Pdots obtained modifying the synthesis conditions (blue and red lines), dispersed in water. *b)* Steady-state absorption (solid lines) and fluorescence (broken lines) spectra of the PCzDTBT in THF (black lines) and PCzDTBT Pdots dispersed in water (blue and red lines). *c)* Schematic illustrations of the spatial orders of the emitting sites in the Pdots fabricated varying the synthesis conditions. (Copyright Springer Nature publishing group).[20]

As already described in the previous examples, different strategies have been followed to tune the spectral properties of conjugated polymers. However, these approaches present several drawbacks, such as complex chemical reactions which involve several steps and the use of large amount of toxic solvents. In other cases, the incorporation in the polymer backbone of expensive metals is required. Furthemore, the micro-/nano-confinement of the conjugated polymers depends on the synthesis of micro-/nanostructures, such as mesopourous silica, in a separate time-consuming step. Therefore, there is a need to find novel approaches for the simultaneous spectral tuning and nanostructuration of semiconductive polymers. Herein we hypothesise that the use of ultrasounds may represents an interesting approach with this aim.

4.1.4 Irradiation by ultrasound: physical processes involved and their effects

The interest in ultrasound and cavitational effects extends for more than 100 years. The first report of cavitation was published in 1895 by Thornycroft and Barnaby when they noticed bubble formation, severe vibration, and surface damage to the propellers of their submarine, the H.M.S. Daring. Later, in 1917, Lord Rayleigh published the first mathematical model describing a cavitational event in an incompressible fluid. Since then,

the effects of ultrasonic energy on physical (e.g. homogenisation, disaggregation, emulsification) and chemical processes have been studied very deeply.

Acoustic waves travel through an elastic medium as an alternating series of compressions and rarefactions (Figure 4.6). In a fluid (such as water or air) the main effect of an acoustic wave regards the motion of the molecules. So the effect is that the molecules transmit their motion to an adjacent molecule and return to their original position, with such motion parallel to the wave propagation.

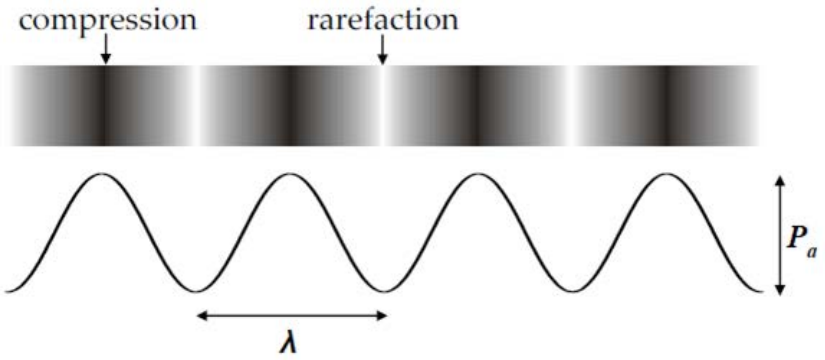

Figure 4.6. Schematic representation of a sound wave and the corresponding pressure fluctuations. (Copyright 2008, Maikel M. Van Iersel).[31]

The sound wave (in term of pressure waves) possesses two essential characteristics: the pressure and the amplitude. The wavelength (λ), is related to the frequency of the sound source (*f*), and the speed of sound (*c*), through the universal wave equation (1):

$$\lambda = \frac{c}{f} \tag{1}$$

The speed of sound is determined by the density (ρ), and the compressibility of the medium through which the wave travels. In liquids, the speed of sound is typical ~1500 m/s, while the frequency spans roughly from 15 kHz to 10 MHz. Thus, using the equation (1), the associated acoustic wavelengths results in the range of 10 to 0.01 cm, this is larger than molecular dimension. The effect of the ultrasound at the molecular level in the chemical reactions is not a direct consequence of the wave propagation, but it derives from different physical effects, in particular the cavitation. Such phenomenon is correlated with the sound intensity (I_0), which determines the maximum sound pressure amplitude (P_a), of the acoustic wave:

$$P_a = \sqrt{2\rho c I_0} \tag{2}$$

The acoustic cavitation occurs through three stages: 1) nucleation, 2) bubbles growth, 3) and implosive collapse (Figure 4.7). The alternate compression and rarefaction cycles of the sound wave in the liquid induce the start of the nucleation, which arises from weak points in the liquid, such as gas cavities, or by partial vaporisation of the liquid. In the second stage the bubble starts to grow. Initially, during the negative-pressure, the rate of expansion is fast, so the bubbles are not recompressing during the positive-pressure. This growth is the result of the slightly higher surface area of the cavity during expansion than during compression. At some point, the bubbles reach a resonant size whit the sound field leading to efficient absorption of its energy (obviously, the size is determined by the frequency of the ultrasound). This energy accelerates the bubble growth until the bubble can no longer sustain itself and the surrounding liquid rapidly flows in, producing in the cavity implosion. The dynamics of such collapse is faster than mass and heat transfer.

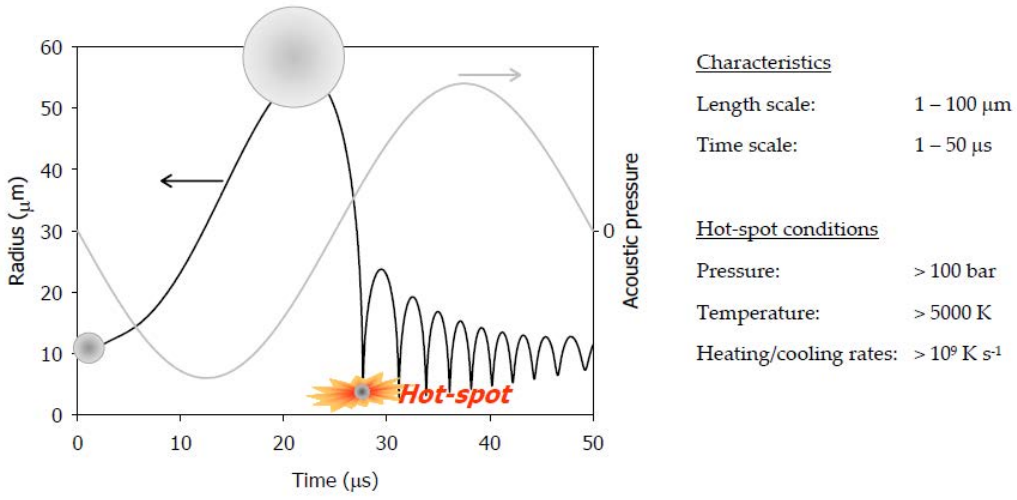

Figure 4.7. Acoustic pressure and corresponding radius-time curve for a single cavitation event, leading to a hot-spot. On the right, some characteristic values for the process and the hot-spot conditions are displayed. (Copyright 2008, Maikel M. Van Iersel).[31]

Thus the consequence of the cavity compression is an impressive increase of pressure and temperature of the cavity contents, which is often referred to as hot-spot. Calculation and experimental data showed that such hot-spot reaches temperatures of several thousands of Kelvin, and pressures of hundreds of bars. The heating and cooling rates in these hot-spots are also extremely high (Figure 4.7). The cavitation and the extreme conditions obtained inside and around these cavities can induce several physical and chemical phenomena.

4.1.5 Ultrasound induced chemical reactions

The cavity compression releases a significant amount of energy in a short period inducing a thermal excitation of the molecules which can provide high-energy chemistry. The high temperatures inside the cavities induce the excitation of molecules to their excited state, that can emit light when returning to their ground state (sonoluminescence), or form highly reactive radical species.[32] These species can be used to activate chemical reactions.

Since the first use of the ultrasound to enhance reaction rates reported by Loomis in 1927, such technique has been further developed and applied in several fields. The low-frequency, high-intensity ultrasound has been investigated and employed for decades to induce and catalyse chemical processes. An entire branch of chemistry, called sonochemistry, has been developed based on ultrasound irradiation. The ultrasound irradiation has been used to promote and accelerate numbered of different chemical reactions (homogeneous[33] and heterogeneous[34] organic reactions, organometallic reactions,[35] and polymerisation[36]). For example, ultrasound has been used to accelerate the Diels-Alder cycloaddition reaction between conjugated dienes and reactive alkenes (dienophiles), one of the most important reaction in synthetic organic chemistry. Javed *et al.* performed synthesis of different hydroquinone derivatives and lonapalene (an anti-psoriatic agent). When the reactions was assisted by ultrasound they enhanced the yield (from 77% to 97%), with a drastic reduction of the reaction time (from 35 h to 3.5 h).[37]

The formation of radical species in homogeneous and heterogeneous media induced by ultrasound has been widely investigated and, recently, it has been applied for the water disinfection and the wastewater treatment. In particular, the ultrasound has been used to remove chlorocarbons (such as chloromethane, dichloromethane, chloroform, carbon tetrachloride) compounds from water. Chloroform and carbon tetrachloride are among the most widespread contaminants in surface and underground water, and in tap water treated by chlorination, and they are difficult to remove. However, it is possible to induce the sonolytic degradation of these compounds by ultrasound. The sonochemical degradation of chlorocarbons in water has been widely studied and the resulting products have been indetified. In a recent work, Wu *et al.* reported a comprehensive characterisation of the ionic and radical species formed, proposing the following mechanism:

Cleavage of chloroform

$$CHCl_3 \xrightarrow{)))} Cl\cdot + \cdot CHCl_2 \quad (3)$$

$$CHCl_3 \xrightarrow{)))} H\cdot + \cdot CCl_3 \quad (4)$$

$$CHCl_3 \xrightarrow{)))} HCl + :CCl_2 \quad (5)$$

$$Cl\cdot + Cl\cdot \longrightarrow Cl_2 \quad (6)$$

$$Cl\cdot + \cdot CCl_3 \longrightarrow CCl_4 \quad (7)$$

$$\cdot CCl_2 + \cdot CCl_2 \longrightarrow C_2Cl_4 \quad (8)$$

Reaction with the cracked species of water

$$H_2O \xrightarrow{)))} \cdot H + \cdot OH \quad (9)$$

$$Cl_2 + H_2O \longrightarrow HOCl + HCl \quad (10)$$

$$:CCl_2 + H_2O \longrightarrow 2HCl + CO \quad (11)$$

$$H\cdot + CHCl_3 \longrightarrow H_2 + \cdot CCl_3 \quad (12)$$

$$\cdot OH + CHCl_3 \longrightarrow H_2O + \cdot CCl_3 \quad (13)$$

$$H\cdot + \cdot CCl_3 \longrightarrow CHCl_3 \quad (14)$$

Scheme 4.1. Radical species and products formed during the sonication of $H_2O/CHCl_3$ mixtures.[38] Where ")))" stands for ultrasonic radiation.

4.1.6 Ultrasound irradiation for nanoemulsion

The cavitation effect induced by the ultrasound is also used to prepare nanoemulsion from non-miscible liquids. Such nanoemulsion consists of stable and homogeneous liquid droplets of nanometric size dispersed in a non-miscible liquid (continuous phase). In oil-in-water (O/W) nanoemulsion, oil nanodroplets made of a hydrophobic phase, are dispersed in the aqueous phase. The formation of nanodroplets implies a huge increase of the surface tension, making the nanoemulsion a thermodynamically unstable system. Therefore, a high amount of energy must be provided to the system in order to form such nanoemulsion. The cavitation process induced by ultrasound can to provide this energy and the sonication of a heterogeneous mixture of two immiscible liquids allows the formation of the nanoemulsion. The addition of surfactants is critical for stabilising the nanodroplets because as it decreases the surface tension of the system allowing smaller nanodroplets to be achieved and it avoids or minimises the kinetic processes responsible for the loss of the nanodroplets, such as coalescence, flocculation and Ostwald ripening.

The size of the nanodroplets is generally tuned by controlling:

→ The chemical composition of the mixture (solvent, oil/water ratio, type and concentration of surfactants, use of co-stabilisers such as hydrophobes, that reduces the diffusion of the oil from one droplet to the other, etc.);

→ The energy applied to the system. In the nanoemulsion prepared by high energy methods, such as the high-pressure, high shear and ultrasound based homogenisers, the energy is controlled by tuning the pressure, the homogenisation rate or the ultrasound amplitude respectively.

These nanoemuslions can be used as template for the fabrication of polymeric nanoparticles. When the nanoemulsion is generated, polymeric nanoparticles can be obtained within the droplets by (a) inducing the polymerisation of monomers dissolved in the oil droplets and/or in the water phase, or (b) starting from a preformed polymers that precipitate through the modification of the properties of the mixture (such as the evaporation and/or the diffusion of a solvent previously added to the mixture to dissolve the polymer, changes of the pH, etc.).

Among the different options, solvent evaporation is a widely employed method used to prepare polymeric nanoparticles. This method maintains a high purity inside the nanoparticles, since is not required any polymerisation reaction, thereby avoiding the alteration of the excellent optoelectronic properties showed by the conjugated polymers with the presence of reactants or side product.[39]

The Scheme 4.2 shows the steps involved in the synthesis of the polymeric nanoparticles through the miniemulsion solvent evaporation technique, which has been used in this thesis. Briefly, the preformed polymer is dissolved in an organic solvent with a low boiling point. Successively, the organic solution is added to the water phase in the presence of an emulsifier and magnetically stirred to form a macro-emulsion. Then, the as-formed emulsion is irradiated by ultrasound, so that the big droplets are broken down, and a nanoemulsion is formed. Finally, the organic solvent is evaporated heating the solution to induce the precipitation of the polymer inside the droplets which results in solid polymeric nanoparticles.

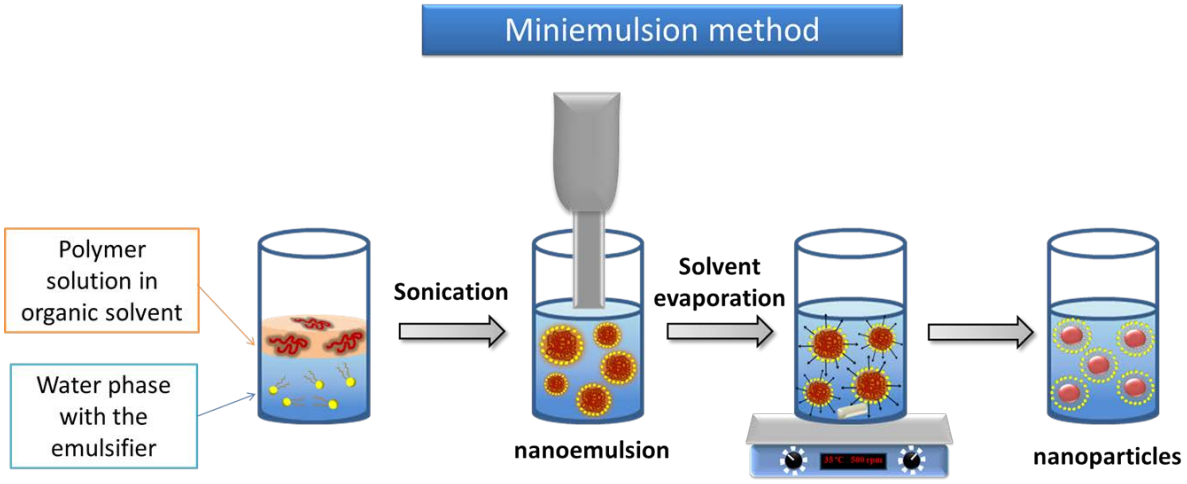

Scheme 4.2. Schematic representation of the different steps involved in the miniemulsion and solvent evaporation techniques for the synthesis of polymeric nanoparticles (the yellow sphere represents the surfactanct and the red line the polymer).

The presence of the surfactant on the final particles surface also avoids the aggregation of the nanoparticles leading to a stable suspension. The final size of the nanoparticles is controlled by the size of the nanodroplets, which, as discussed above, depends on the amplitude of the ultrasound, the ratio between the water and the oil phase, the amount of the surfactant and the amount of the polymer in the organic phase.

4.2 Objective

Chlorine radicals (·Cl, ·$CHCl_2$, ·CCl_3)[40] and hypochlorous acid (HOCl)[41] produced during the sonication chloroform/water mixture can be potentially used to systematically cleave conjugated species, and therefore to modify the final optical properties of the polymers. Actually, the action of HOCl on conjugated system is well known in biology, since the hypochlorous is generated, among other reactive oxygen species (ROS), by phagocytes cells to kill a wide range of pathogens. The hypochlorous acid is a highly oxidative species which reacts also with various components of mammalian cells, in particular with haemoglobin. In previous works, Maitra *et al.* identified several cleavage products resulting from the reaction of HOCl with the double bonds of the porphyrin of the heme group, and they propose the mechanism reported in fig—to explain the cleavage of the C=C bond mediated by HOCl (see Scheme 4. 3).[42]

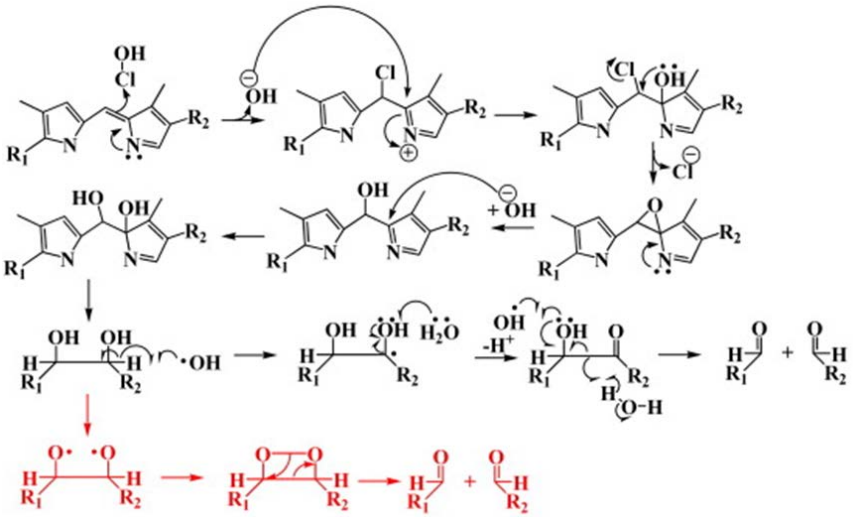

Scheme 4. 3. Proposed chemical mechanism for the HOCl-mediated cleavage of carbon–methyne bridges between the adjacent pyrrole ring of the heme moiety. (Copyright © 2011 Elsevier Inc.)[42]

Chlorine radicals obtained by different means such as daylight,[43] ɣ-radiations[44] or thermal treatment,[45,46] have also been shown to tune the properties of MEH-PPV upon polymer fragmentation.[43–46] Bronze-Uhle *et al.* studied the action of ionizing radiation on MEH-PPV, which was already known to produce a chromatic alteration of the polymers. They found that the chlorine radicals produced from the chloroform radiolysis, induced by gamma ray radiation, attack the vinyl double bond of the polymer backbone, breaking the electronic conjugation and eventually the chain (the proposed mechanism is reported in Scheme 4.4).[44]

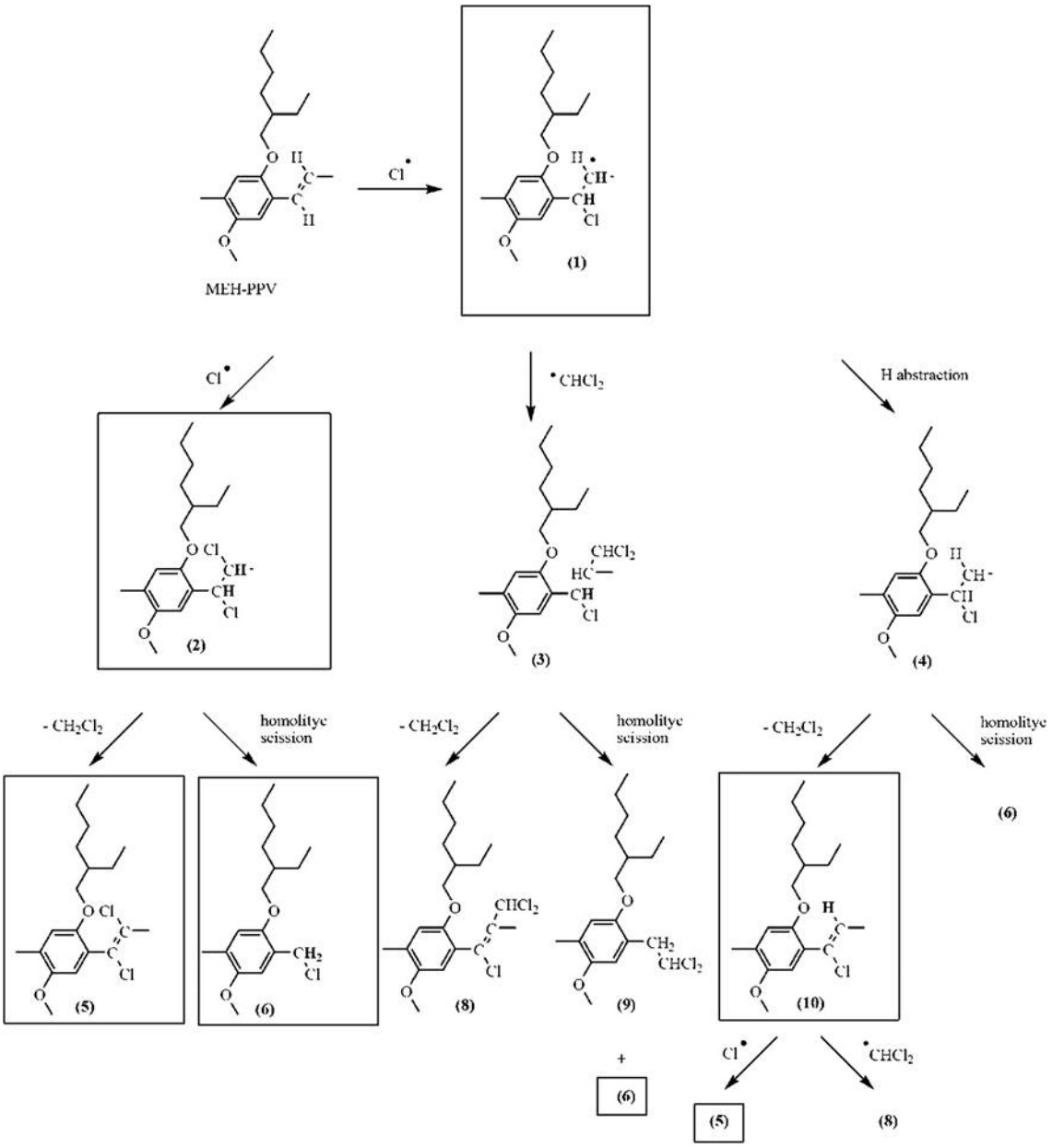

Scheme 4.4. Proposed mechanism of MEH-PPV degradation by chlorine and alkyl halide radicals, that induce blue-shifts in the absorption spectra. The radicals were formed by ɣ induced dissociation of $CHCl_3$. The products highlighted are related to H-NMR signals observed by the authors. (Copyright © 2011 AIP Publishing)[44]

However, the same results could be obtained with HOCl, which acts as strong oxidative species cleaving linear conjugated systems.[42,47,48] Conjugated polymer scission and chain shortening caused by oxidative species (i.e. H_2O_2) have been previously exploited to confer biodegradability to fluorescent CPNs suitable for bio-imaging,[12] but no controlled tuning of the emission properties has been reported.

Our objective therefore is to use ultrasound energy to induce both radical activation, i.e. chemical reaction, and the fragmentation and the formation of nanoemulsion, i.e. nanoparticles, in a chloroform/water mixture.

Sonication of the semiconductive polymer solutions of different concentrations under such experimental conditions is expected to induce different fragmentation degrees, resulting in the formation of nanoparticles with tunable optical properties. A schematic representation of this process is shown in Scheme 4.5. As a proof-of-concept to validate our approach, herein we propose the use of MEH-PPV, because of its excellent luminescence quantum yield ($\Phi_f^{toluene} = 0.34$),[21] semiconducting[49] and non-linear optical[50] properties.

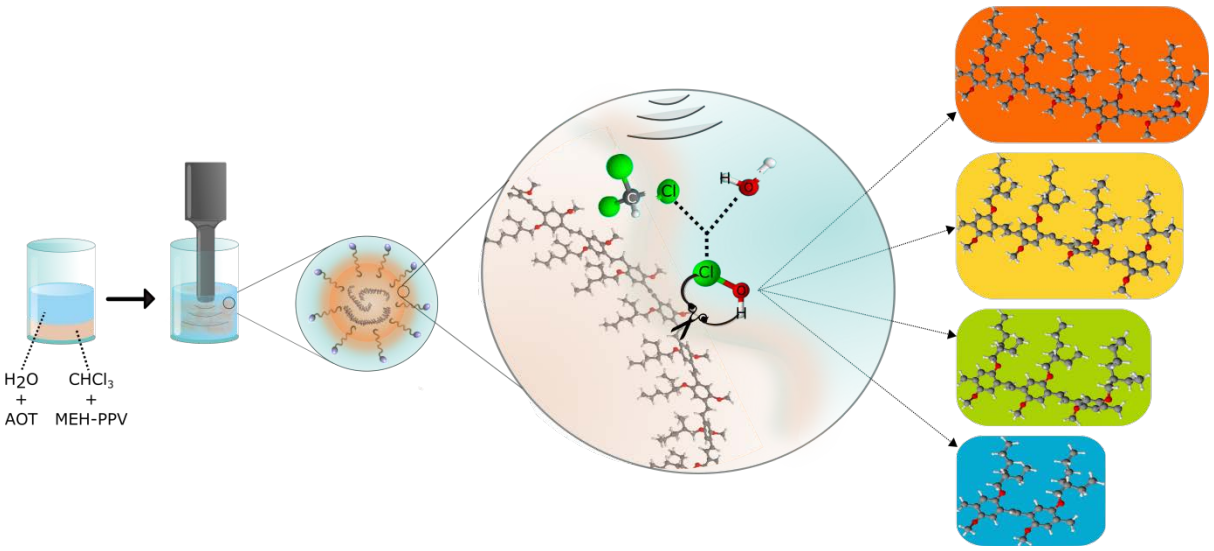

Scheme 4.5. Scheme of the sonication process of a mixture made of water and a MEH-PPV chloroform solution which produces different fragmentation units with tuneable optical properties depending on the initial polymer concentration.

4.3 RESULTS AND DISCUSSION

4.3.1 Synthesis of oligomers: Irradiation of bulk solution of MEH-PPV@$CHCl_3/H_2O$

In order to demonstrate the validity of our approach, MEH-PPV chloroform solutions were initially sonicated in Milli-Q® water. At this stage no surfactant was added, to avoid possible side reactions and allow an easier isolation of the formed products. We expected that the radicals species produced by irradiating with ultrasound the chloroform/water mixture reacts with the vinylene group of the MEH-PPV, breaks the polymer chain and generates oligomers presenting different optical properties. Two organic solutions of MEH-PPV in $CHCl_3$ were prepared with the following polymer concentrations: 2 mM (hereafter named as MEH-s X), and 8 mM (MEH-s 4X). The detailed procedure is reported in the materials and methods section.

Spectroscopic UV-Vis characterisation of the extracted organic phases after sonication (MEH-s) showed a progressive hypsochromic shift of the main absorption band, from λ_{max} = 500 nm for the parent untreated polymer to 425 and 306 nm, for MEH-s 4X and MEH-s X samples, respectively (Figure 4. 8a).

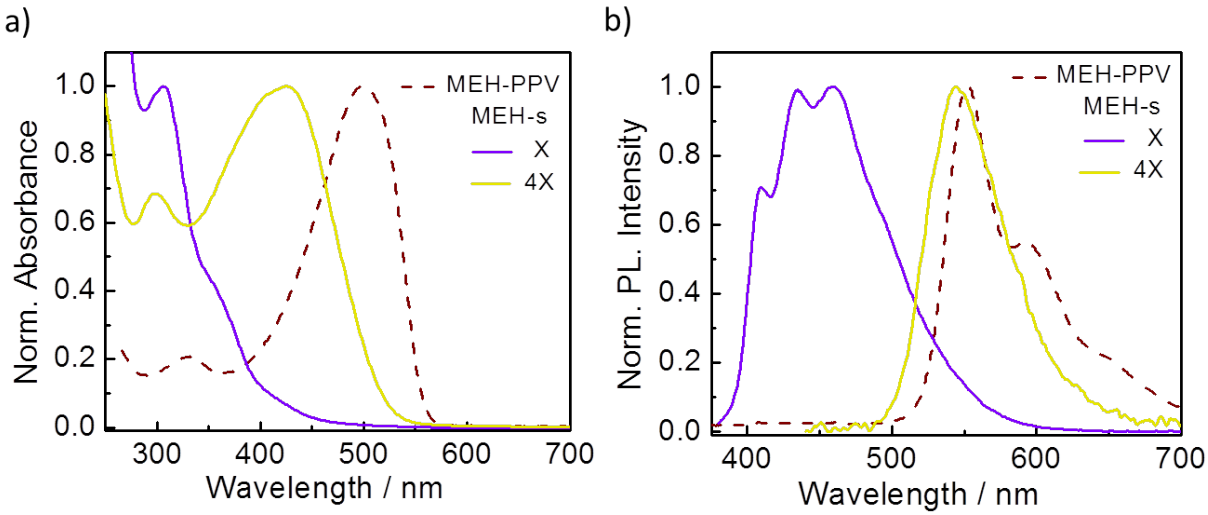

Figure 4. 8. *a)* Absorption and *b)* emission spectra of untreated (λ_{max}^{abs} = 500 nm and λ_{max}^{emis} = 552 nm, dashed lines) and sonicated MEH-PPV solutions (MEH-s 4X, λ_{max}^{abs} = 425 nm and λ_{max}^{emis} = 544 nm, purple; MEH-s X, λ_{max}^{abs} = 306 nm and λ_{max}^{emis} = 435 and 460 nm, yellow), recorded in $CHCl_3$.

Similar results were obtained for the fluorescence measurements (Figure 4. 8b). A blue-shift of the emission band from λ_{max} = 552 nm of the untreated polymer to 544 (MEH-s 4X) and 435 nm (MEH-s X). The hypsochromic shift found for both, absorption and emission spectra, was associated to the postulated formation of shorter oligomeric fragments. While

the sample MEH-s 4X presents a narrow and featureless emission band indicating the presence of a single emitting species, in the sample MEH-s X the emission band is broader, and three different peaks appear. Such a structure could be due to the formation of different emitting species, or it could be ascribed to the different vibronic transition of new single species.

This formation of shorter oligomeric fragments is also in agreement with the decrease of the quantum yield (QY) and the increase of the fluorescent lifetime upon polymer dilution (Table 4.1).

Sample	Absorption λ_{max} (nm)	Emission λ_{max} (nm)	Φ_f	τ (ns)							n_{ECL}
				τ_1	f_1	τ_2	f_2	τ_3	f_3	χ^2	
MEH-PPV	500	552	0.48	0.308	98.639	2.876	1.361	-	-	1.288	10-17
MEH-s 4X	425	544	0.28	0.428	65.813	1.136	30.731	3.921	3.456	1.141	4
MEH-s X	306	435-460	0.17	0.990	74.947	2.257	25.053	-	-	1.379	2

Table 4.1. Absorption and emission main maxima, quantum yield (Φ), lifetime (τ) values and effective conjugation lengths (ECL) of parent MEH-PPV and sonicated samples MEH-s X and MEH-s 4X.

Such trends are similar to those found for PPV oligomers, where shorter conjugation domains present longer emission lifetime.[29] The blue-shift of the absorption band also provides the variation of the effective conjugation length (ECL),[38] which decrease (Table 4.1) passing from the untreated polymer (n_{ECL}=10- 17)[51] to MEH-s 4X (n_{ECL}=4) and MEH-s X (n_{ECL} =2), which further confirms the formation of oligomeric species. The effective conjugation length (n_{ECL}) was extrapolated from the linear correlation between the energy corresponding to the long-wavelength transition *vs* the reciprocal value of the monomeric units. [38] The energy was calculated using the formula:

$$E = \frac{hc}{\lambda_A} \tag{15}$$

Where h is the Planck constant, c the speed of light, and λ_A the absorption maximum (in the case of MEH-s X the long-wavelength transition was associated to the shoulder at λ=369 nm).

The broad structureless absorption bands are attributed to an inhomogeneous superposition of absorption spectra arising from a distribution of chromophores with various chain lengths. The emission spectra, on the contrary, are assigned only to the low-energy

chromophores (*i.e.* segments with longer conjugation length). The emission from the high-energy segments is not observed since they lose their excitation through energy transfer to the low-energy chromophores. The energy transfer also explains the substantial Stokes shift observed in conjugated polymers. In the case of the oligomers, where it is present a well-defined conjugation length, one could expect a mirror-image relationship between the absorption and the emission band, which is not the case. Tilley *et al.* investigated the possible presence of a range of ground state torsional configurations to explain the broad absorption spectra observed in PPV oligomers and polymers. They studied, as a model, a trimer of PPV finding that the molecule can exist as a mixture of six different rotamers which can also have different torsional configurations. Such range of conformations is expected to have different electronic arrangements and transition energies which result in the broadening observed in the absorption spectra. So, the asymmetry of absorption and fluorescence spectra can be associated with more considerable torsional flexibility in the ground state compared to the excited state.[29]

The presence of such rotamers may explain the different fluorescence decay profile observed for the polymer and the MEH-s. The polymer presents bi-exponential decay with the longer lifetime contribution (2.876 ns) in really low percentage (1.36 %). The sample MEH-s X also exhibits a bi-exponential decay, but with the longer lifetime contribution (2.257 ns) becoming more important (25 %). This contribution may be ascribed to the presence of emitting rotamer configuration, which also could explain the multi-exponential decay of sample MEH-s 4X, which followed the same trend of sample MEH-s X.

Confirmation of the fragmentation process was also obtained by chemical means. ^{1}H-NMR spectra of both samples (Figure 4.9) showed new signals in the 7.0-8.0 ppm regions, mainly associated to modifications of the vinylene moieties in the new-formed species.

The weak signals at 9.77 and 10.42 ppm were attributed to the formation of carbonyl moieties, whose presence was also supported by new peaks in FT-IR spectra (Figure 4.10): 1730 cm^{-1}, C=O stretching of aromatic aldehydes, 1680 cm^{-1}, C=O stretching of carboxylic groups. The incorporation of these functionalities in MEH-PPV by different chemical means has already been shown to take place through oxidative cleavage,[44] which in the case of conjugated systems can be induced by HOCl.[42,47,48] No relevant intensity modifications were observed for C-H stretching of the methoxy and alkoxy groups (1037 cm^{-1}) and to the aromatic C=C stretching (1502 cm^{-1}) peaks, confirming that the sonication induced mainly chemical changes to the vinylene groups.

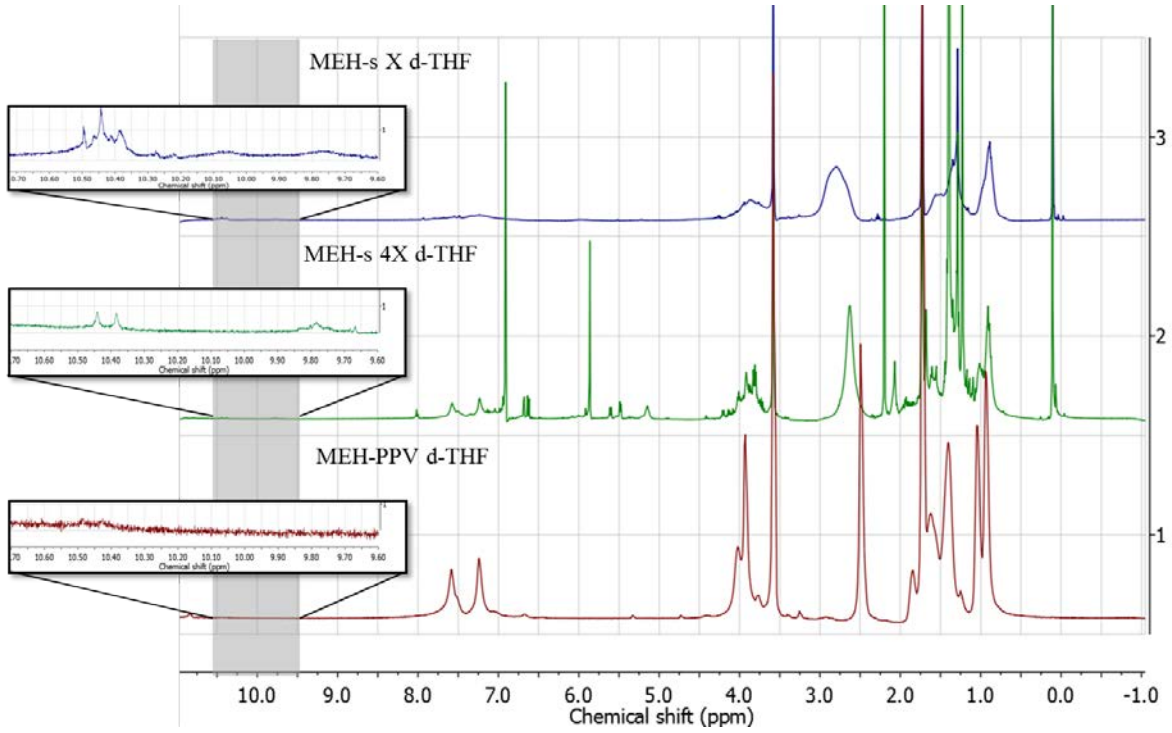

Figure 4.9. ^{1}H-NMR of samples MEH-s X, MEH-s 4X and parent MEH-PPV. All samples were recorded in THF-d_8.

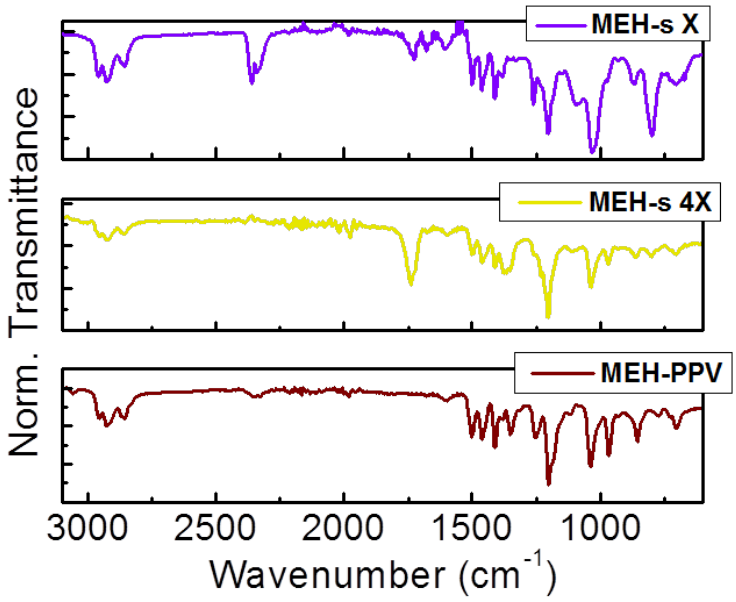

Figure 4.10. FT-IR of samples MEH-s X, MEH-s 4X and parent polymer MEH-PPV.

X-Ray photoelectron spectroscopy (XPS) of the samples revealed a concomitant increase of the oxygen (from the 11.97% of the parent polymer to 21.16% for MEH-s X) and chlorine (from the 0.61% to 2.16%), along with a decrease of the relative carbon amount

(from 87.42% to 76.67%), as the polymer concentration of the initial solution decreased, indicating a higher degree of fragmentation (Figure 4.11).

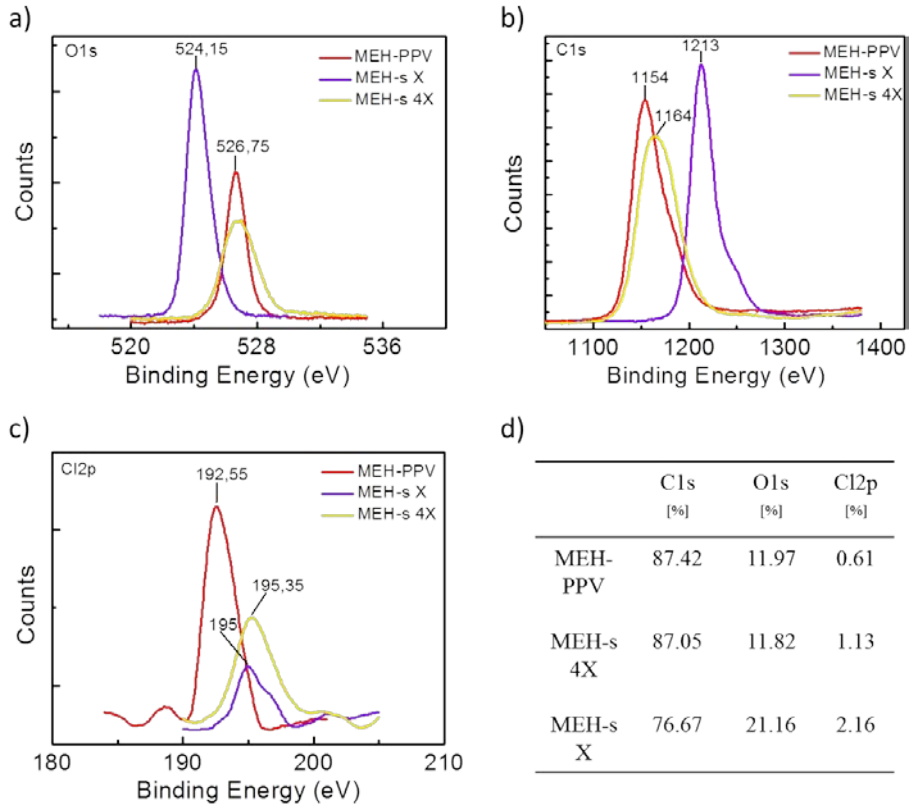

	C1s [%]	O1s [%]	Cl2p [%]
MEH-PPV	87.42	11.97	0.61
MEH-s 4X	87.05	11.82	1.13
MEH-s X	76.67	21.16	2.16

Figure 4.11. XPS spectra of samples MEH-s X (purple line), MEH-s 4X (yellow line) and parent MEH-PPV polymer (red line). *a)* O1s core level, *b)* C1s core level and *c)* Cl2p core level; *d)* table reporting relative quantities of C, O and Cl in MEH-s X, MEH-s 4X and MEH-PPV samples.

Elemental analysis of the treated samples showed a similar trend, with the relative carbon amount decreasing (MEH-s 4x, 70.0%; MEH-s X, 63.7%) as the concentration of the initial polymer solution diminishes (Table 4.2).

		C (%)	H (%)	N (%)	S (%)
MEH-s 4X	*Avg.*	71.00	9.10	0.30	<0.10
	rsd (%)	0.40	1.10	38.70	
MEH-s X	*Avg.*	63.70	8.50	0.58	<0.10
	rsd (%)	0.30	0.40	2.90	

Table 4.2. Elemental analysis of sonicated samples MEH-s X and MEH-s 4X.

FT-Raman spectra recorded for MEH-s X and MEH-s 4X samples (Figure 4.12) were quite similar. In both spectra is present an intense band located around 1580-1590 cm^{-1}, which was ascribed to C–C stretching vibration of the phenyl rings and a weaker band at a longer wavenumber, approximately at 1625 cm^{-1}, arising from the C=C stretching of the vinyl group.

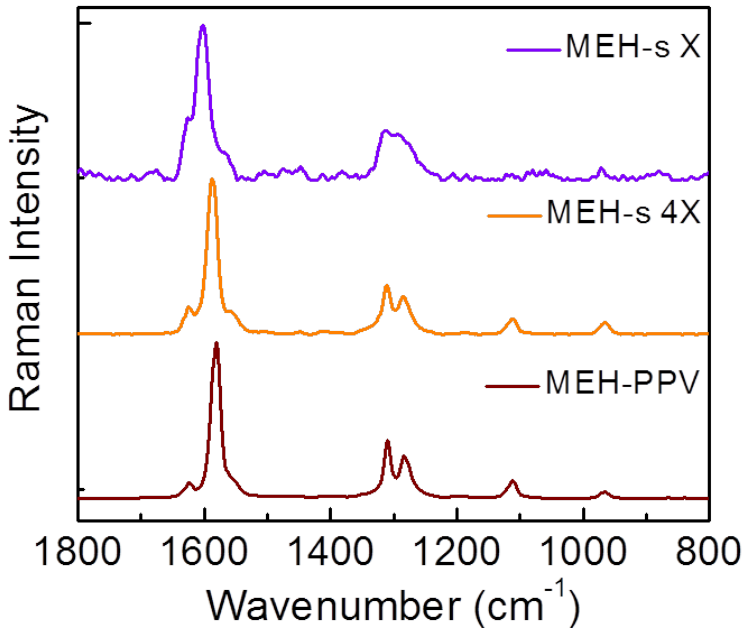

Figure 4.12. FT-Raman spectra of samples MEH-s X, MEH-s 4X and parent polymer MEH-PPV.

Two trends were found along the samples regarding these two aforementioned bands: a) there is a gradual upshift of the whole spectrum upon going from MEH-PPV to MEH-s 4X and MEH-s X, with a shift of the most intense band from 1581 cm^{-1} (MEH-PPV) to 1602 cm^{-1} (MEH-s X), and b) the intensity ratio I~1625/I~1585 increases as the concentration of the starting polymer solution diminishes. These same trends were reported for a series of PPV derivatives, with the progressive decreasing of the chain length, [52–54] and can be easily tracked down theoretically (Figure 4.13).

The molecular geometries of the PPV-based model systems were calculated at the Density Functional Theory (DFT) level. A detailed description about the parameters used to obtain the theoretical model is reported in the materials and methods section.

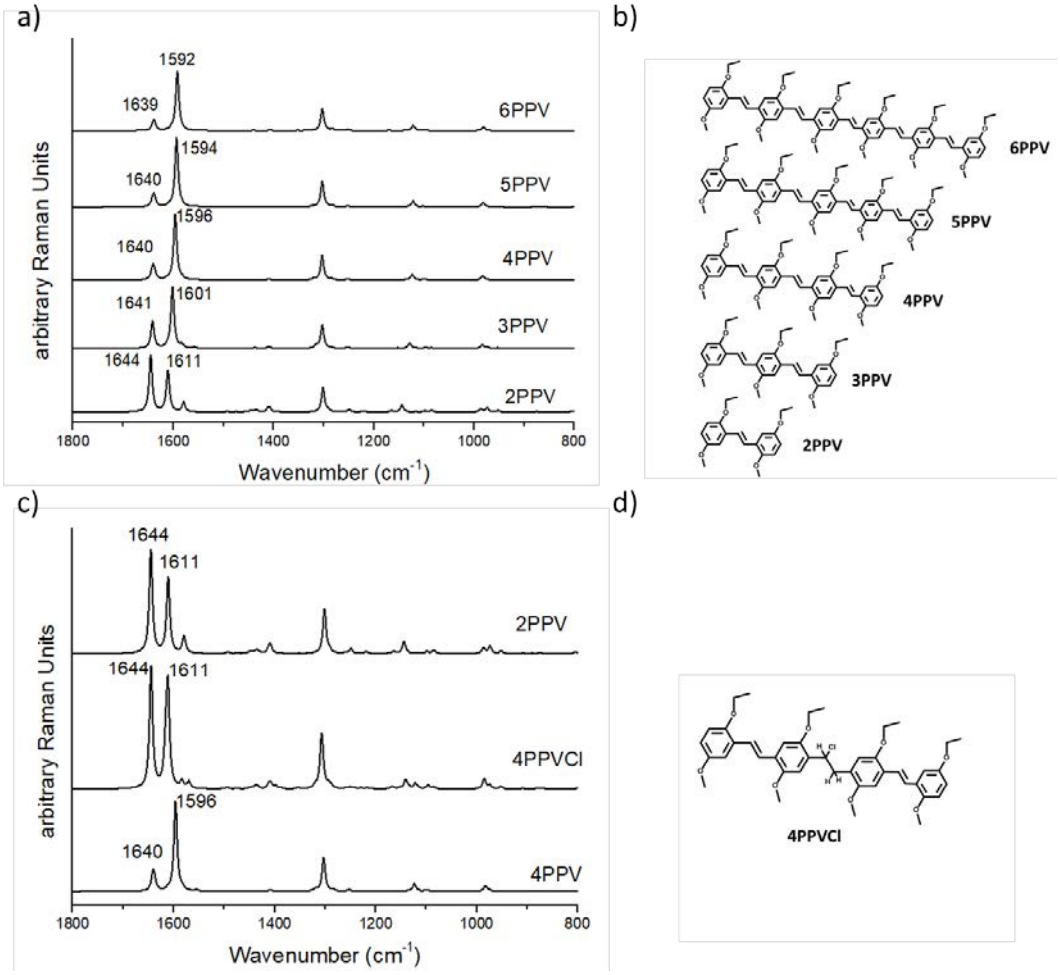

Figure 4.13. *a)* DFT-calculated (BHLYP/6-31G**) Raman spectra of the 2PPV-6PPV model systems; *b)* chemical structures of the PPV-based systems used for theoretical studies. *c)* DFT-calculated (BHLYP/6-31G**) Raman spectra of the 4PPV, 4PPVCl and 2PPV model systems; *d)* chemical structures of the PPV-based systems exhibiting the hypothesised chlorine addition to the vinylene group used for theoretical studies.

Sonication of the $CHCl_3$ solution of MEH-PPV in water induces the formation of shorter fragments and/or disruption of effective conjugation length due to a direct attack of the vinyl group. These two effects would appear similarly in Raman spectroscopy since theoretical DFT calculations predict almost superimposable spectra for a 2PPV fragment and a 4PPV in which HCl adds to the central vinylene group (4PPVCl).

Therefore, these results highlight that fragmentation of the samples, either by conjugation disruption or by selective chain cleavage, is more efficient in less concentrated samples.

The formation of oligomeric units of lower molecular weight than the untreated MEH-PPV was supported by diffusion-ordered NMR spectroscopy (DOSY) and gel permeation chromatography (GPC). Both sonicated samples, showed higher diffusion

coefficient parameters than for the untreated MEH-PPV (Figure 4.14), indicating a lower molecular weight for the obtained compounds.

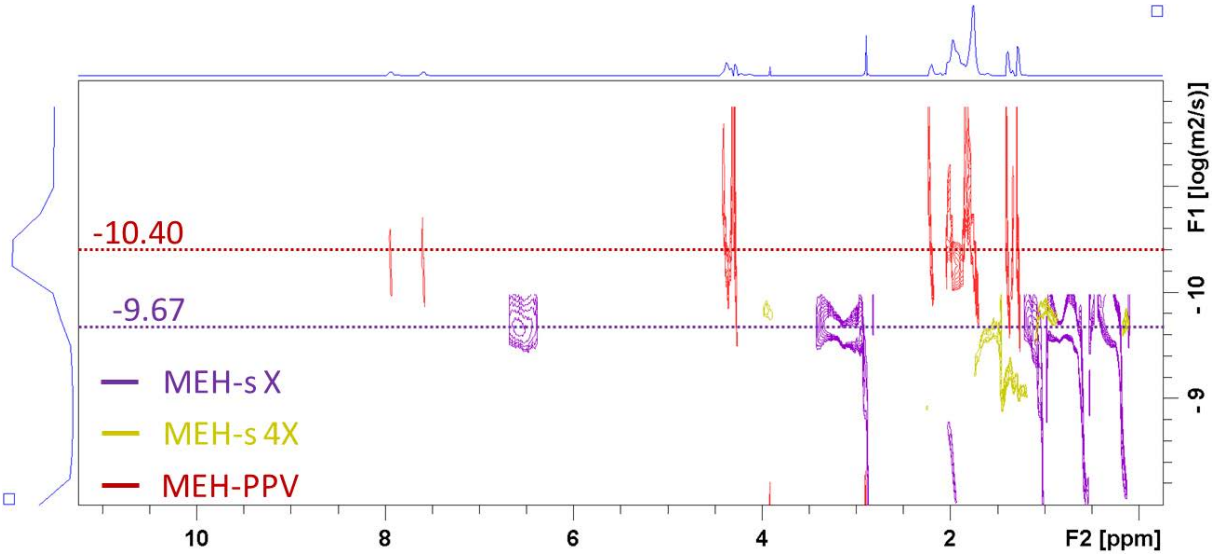

Figure 4.14. ^{1}H-NMR DOSY of samples MEH-s X, MEH-s 4X and parent MEH-PPV polymer in THF-d_8. The x-axis represents the regular ^{1}H chemical shift (ppm), and the y-axis represents the relative diffusion rate.

Accordingly, only species of lower number average molecular weight (M_n) than untreated MEH-PPV (M_n = 40.000-70.000) were detected by GPC (chain lengths decreased from an average of 211 to 18 and 60 units respectively) for the MEH-s X and MEH-s 4X samples, confirming the sonication produces shorter oligomers (with lower chain length and n_{ECL}) rather than only partial saturation of the initial polymer (Table 4.3).

	M_n (x10^4)	Mw (x10^4)	PDI	Average chain length
MEH-PPV	3.67	19.84	5.41	211
MEH-s 4X	1.58	5.25	3.33	60
MEH-s X	0.47	0.88	1.84	18

Table 4.3. Number average molecular weight (Mn) and weight average molecular weight (Mw) and polydispersity index (PDI) of untreated MEH-PPV polymer and sonicated samples MEH-s X and 4X, obtained from GPC measurements. The average chain lengths have been calculated divided the M_n values obtained by GPC for the molecular weight of the monomeric unit.

The difference between the chain length and the effective conjugation length (n_{ECL}) was ascribed to the loss of conjugation due to both bonds saturation and conformational twisting of the oligomer chain.

Finally, and to demonstrate that this process was not restricted to a few specific cases, we decided to investigate the behaviour, upon sonication, of mixtures prepared from MEH-PPV solutions with concentrations of 4 mM (2x), 6 mM (3x) and 12 mM (6x). Interestingly, sonicating these solutions with the same conditions as above, novel absorption and emission bands appeared between those obtained from the non-treated polymer and the lowest concentrated (2 mM) sonicated solution.

In this way, we fully demonstrated how by simply changing the initial concentration of the MEH-PPV polymer, we were able to fine-tune the optical properties along the whole visible region of the formed oligomeric species (Figure 4.15). This trend was observed exciting the samples at both λ = 300 nm and the corresponding lowest energy absorption maxima (λ_{max}). Moreover, the overlapping of the normalised emission spectra obtained exciting at different wavelengths (λ=300 nm and λ_{max}), indicate the emitting species is always the same (Figure 4.15c). Only in the case of MEH-s X the slight variation of the emission band upon changing of the excitation wavelength evidences the formation of different emitting chromophores.

Once the fragmentation and the electronic disruption were confirmed, further experiments were carried out to study the reaction mechanism. As initially mentioned, polymer fragmentation could be attributed to the reactivity of the polymer with different species formed along the sonication process, mainly chlorine radicals, produced directly from the sonication of $CHCl_3$, and HOCl, obtained as secondary species from the sonication of $CHCl_3/H_2O$ mixture. A series of control experiments were performed to validate our starting hypothesis about the reactivity of HOCl.

A first blank experiment consisted in the sonication of a MEH-PPV chloroform solution in the absence of water was performed. The irradiation by ultrasound of $CHCl_3$ should induce the formation of only chlorine radicals (and no HOCl) according to previous literature.[55] For this experiment, the $CHCl_3$/MEH-PPV solution was prepared with the concentration of 8 mM (corresponding to the sample MEH-s 4X). The sample was studied by absorption and emission spectroscopy, and the resulting spectra were compared with the parent polymer and the sample MEH-s 4X obtained after the sonication of the water/chloroform mixture. The absorption and emission spectra in Figure 4.16 show a perfect overlapping between the bands obtained from the MEH-PPV sample sonicated only in chloroform and the parent polymers, whereas the sample MEH-s 4X sonicated in the $H_2O/CHCl_3$ mixture exhibited a remarkable blue shift in absorption and emission. The experiment confirmed that water is needed to start the reaction and indirectly corroborate the

initial hypothesis on the HOCl activity, excluding the chlorine radicals as the main species involved in the polymer chain scission.

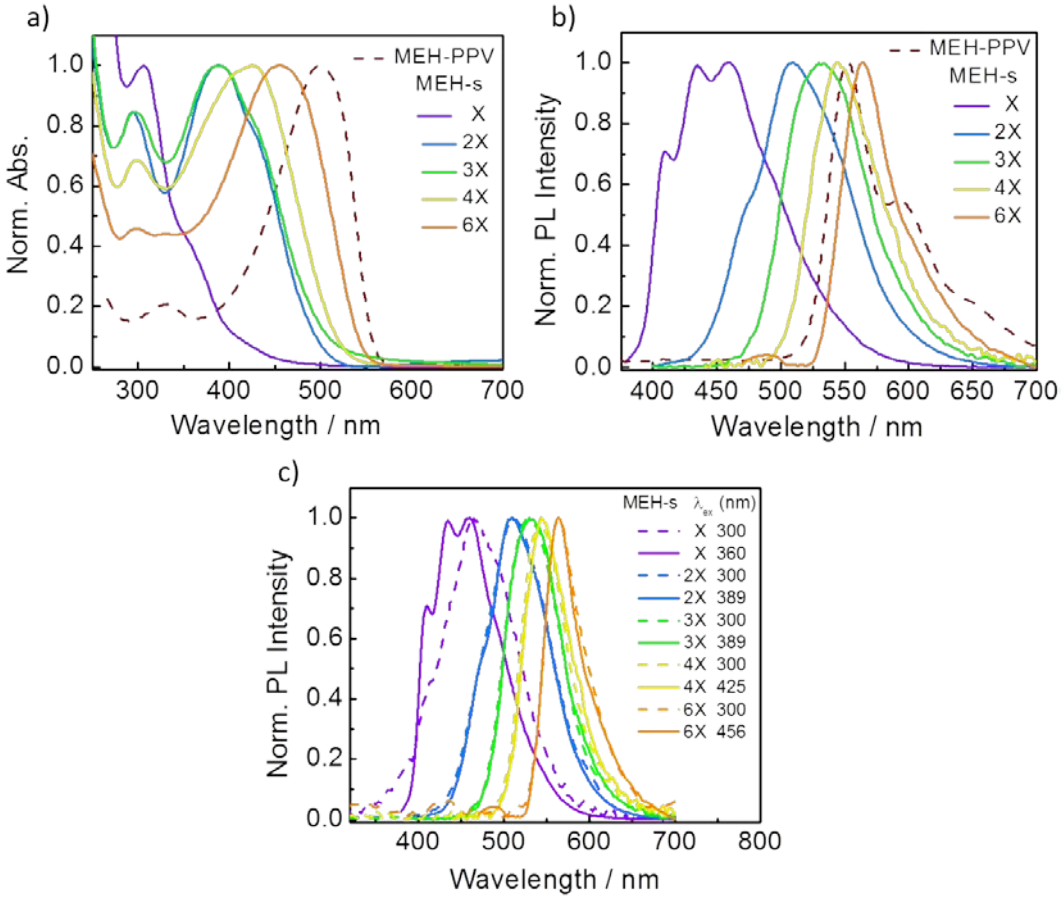

Figure 4.15. *a)* absorption and *b)* emission spectra of untreated MEH-PPV (dashed lines) and MEH-PPV solutions sonicated at different concentrations (MEH-s X, 2X, 3X, 4X, 6X). *c)* Emission spectra of the series of MEH-s X and MEH-s 4X exciting at 300 nm (dashed line) and the absorption maxima. All spectra were performed in $CHCl_3$.

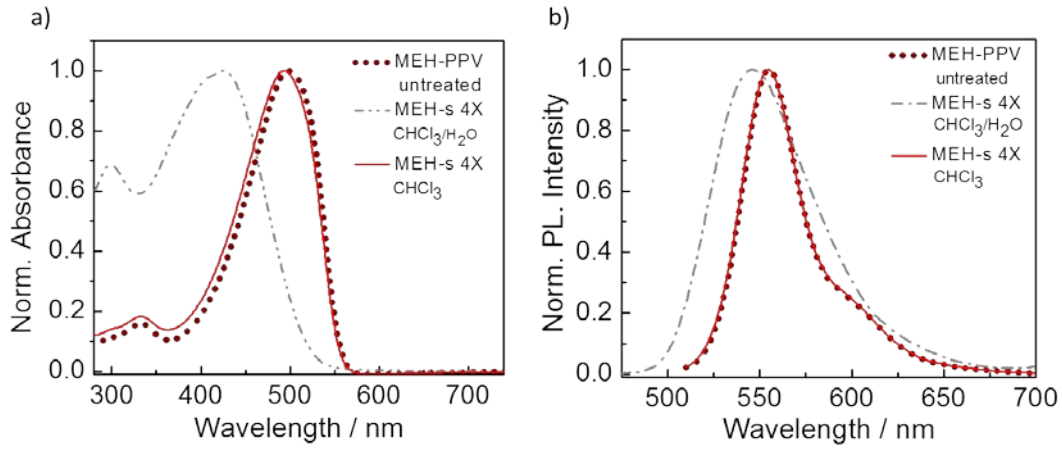

Figure 4.16. *a)* absorption and *b)* emission spectra of untreated MEH-PPV (red dotted line), MEH-PPV sonicated in $CHCl_3$ (8 mM) only (solid red line), and MEH-PPV sonicated in $CHCl_3/H_2O$ mixture (MEH-s 4X, dashed-dotted line). All spectra were recorded in $CHCl_3$.

The second blank experiment consisted in the replacement of $CHCl_3$ by toluene or CH_2Cl_2 in the nanoemulsion preparation, where chlorine radicals production is avoided or much less favoured, and no HOCl is formed. Also for this experiment, the MEH-PPV chloroform solution was prepared a MEH-s 4X concentration. Figure 4.17 shows the absorption and emission spectra obtained from MEH-PPV sonicated in a water/toluene mixture (pink solid line) and a water/dichloromethane mixture (blue solid line) compared with the spectra obtained from the parental polymer and the sample MEH-s 4X obtained in the water/chloroform mixture. No blue shift in absorption and emission was observed when the chloroform is replaced with a different organic solvent. Thus, such experiment proved that the presence of the $CHCl_3$ is essential for the fragmentation of the polymer because, when it is replaced by another solvent like dichloromethane, the oligomers was not formed. Moreover, replacing the halogenated solvent with another organic solvent such as toluene, indirectly confirm that HOCl is the active species involved in the polymer chain scission excluding the possible reaction of other radicals formed during the sonication of the water. Since from the sonication of the water/toluene mixture was formed only radicals species derived from the cracking of the water, while chlorine radicals was not present.

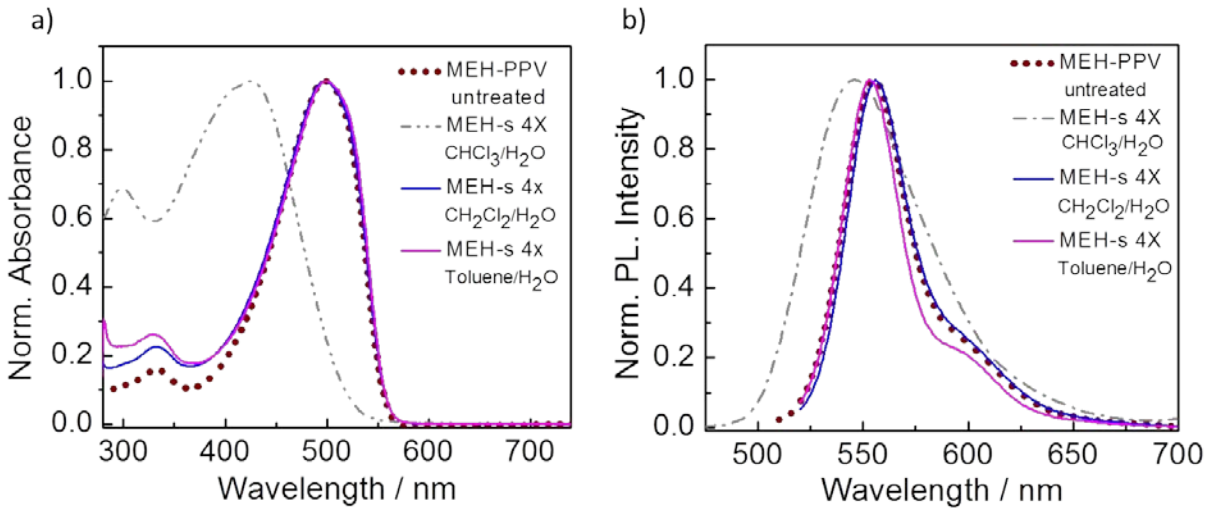

Figure 4.17 *a)* absorption and *b)* emission spectra of untreated MEH-PPV in $CHCl_3$ (dotted red line), MEH-PPV sonicated in $CHCl_3/H_2O$ mixture (MEH-s 4X, dash-dotted line), MEH-PPV sonicated in CH_2Cl_2/H_2O mixture (blue solid line), MEH-PPV sonicated in toluene/H_2O mixture (magenta solid line). The concentration of MEH-PPV in CH_2Cl_2 and toluene corresponds to the one of the sample MEH-s 4X (8 mM). The spectra were recorded in the organic solvent used for the sonication as describe in the figure.

To summarise, it is interesting to notice that the blank experiments did not show relevant modifications of the absorption and emission spectra, pointing out the crucial role played by the HOCl in the fragmentation process. In fact, the relevance of HOCl is not

surprising at all as it has already been shown to produce the cleavage of linear conjugated systems with the consequent formation of carbonyl moieties.[42,47,48]

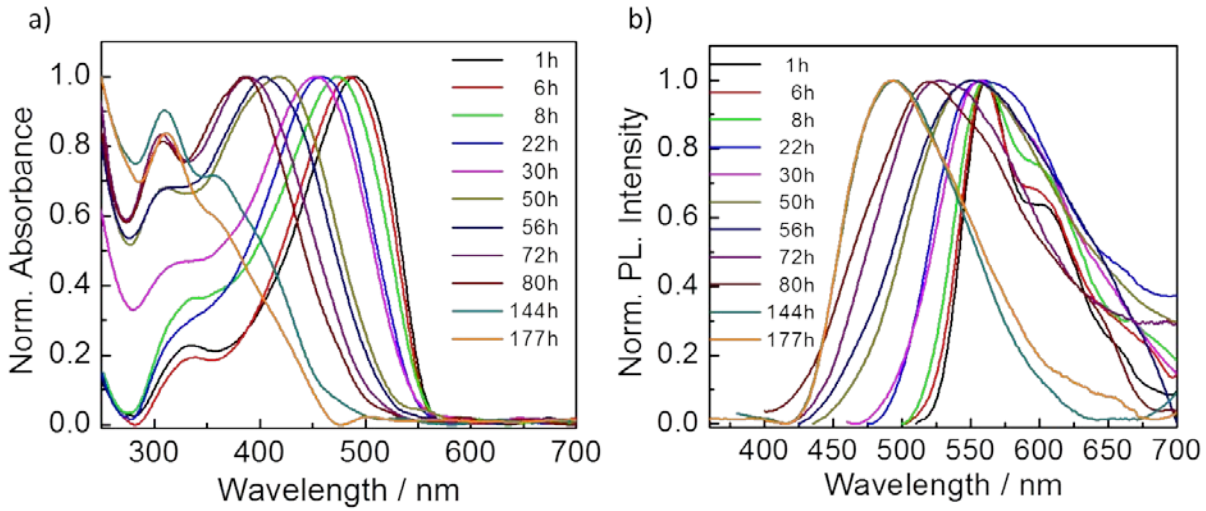

Figure 4.18. *a)* absorption and *b)* emission spectra of CH_2Cl_2 solutions of MEH-PPV treated with an aqueous solution of NaOCl (0.1 M) and HCl (0.001 M), recorded at different reaction times.

In any case, to fully confirm the role of HOCl, thereby confirming our initial hypothesis, we decide to follow the reactivity of MEH-PPV in presence of a source of HOCl, produced from NaOCl/HOCl mixture, rather than by ultrasound. For this purpose, a CH_2Cl_2 solution of MEH-PPV (8 mM) was treated with a NaOCl/HOCl acidified aqueous solution (pH = 6), without sonication. The initial MEH-PPV solution was prepared following the procedure used for sample MEH-s and similar polymer concentrations to guarantee the comparability of such mixed solution with the one irradiated by ultrasound, as detailed reported in materials and methods section. Dichloromethane has been selected as the organic solvent because in the previous experiments it has been already shown to be inert when mixed with water and irradiating by ultrasound. Sodium hypochlorite has been added because it is well known to dissociate in water producing, among other species, the HOCl, whose formation rate increases at acidic pH. Thus, we expected that the HOCl formed by NaOCl (without irradiating by ultrasound) should brake down the polymer as before, demonstrating the action of the hypochlorous acid.

Also, in this case, a progressive hypsochromic shift of the main absorption and emission bands over time was observed (Figure 4.18). Noteworthy, the absorption and emission spectra show that 6 hours after the addition of NaOCl, only a few nanometers of spectral blue-shift is observed. The reaction has to last up to 144 hours to reach the same blue-shift that is observed employing the ultrasound, where, by controlling the polymer

concentration, it is achieved in only 5 minutes. Such results reinforce the validity of our approach. The reaction was also followed by ^{1}H-NMR, as reported in Figure 4.19.

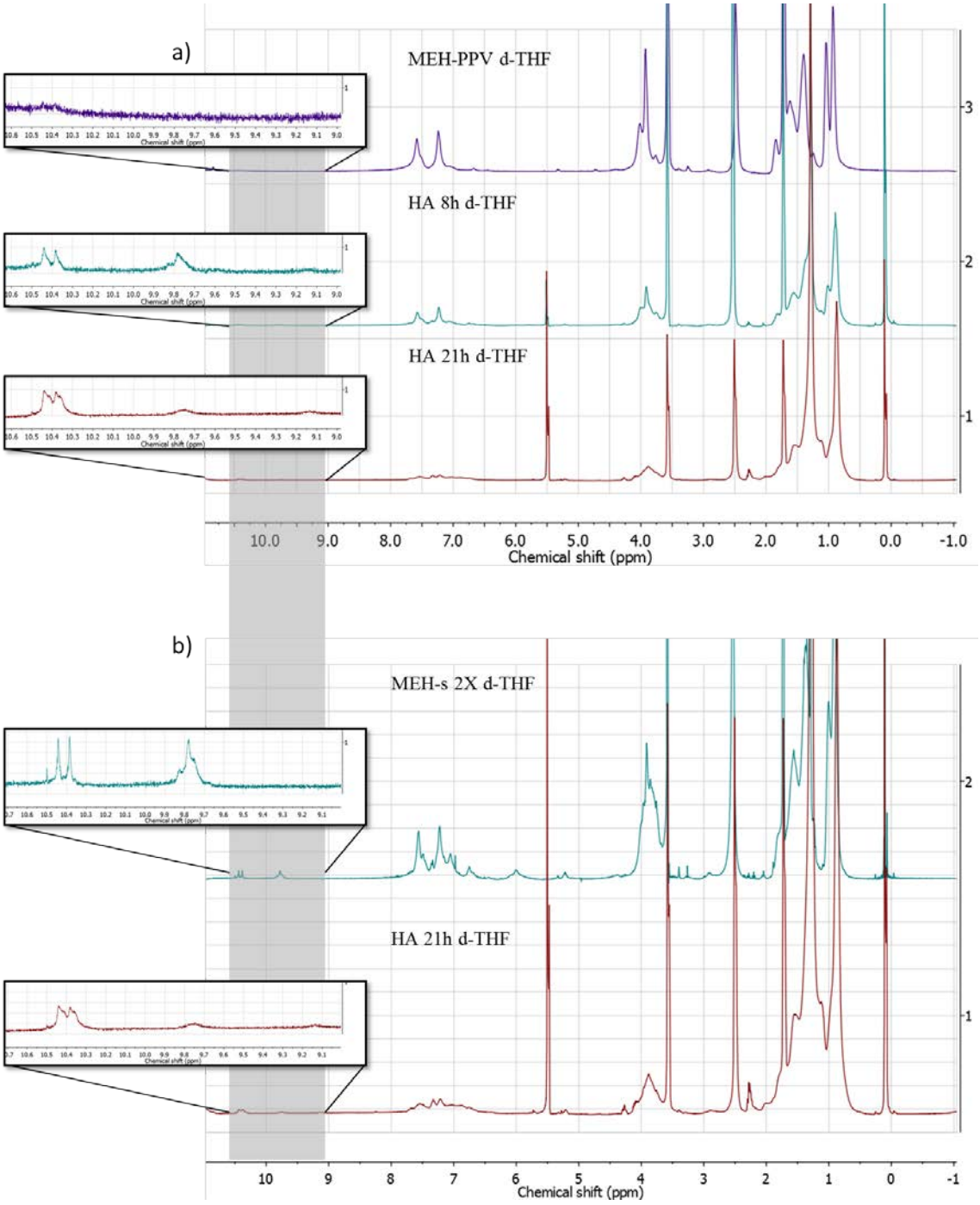

Figure 4.19. *a)* ^{1}H-NMR spectra, recorded at different reaction times, of the products obtained from the treatment of CH_2Cl_2 solution (8 mM) of MEH-PPV with an aqueous solution of NaOCl (0.1 M) and HCl (0.001 M); *b)* ^{1}H-NMR spectrum of a HOCl-treated (21 h) CH_2Cl_2 solution of MEH-PPV (8 mM). For comparison, the spectra of the sonicated sample MEH-s 2X, which presented the same absorption and emission spectra was inserted. All the samples were recorded in THF-d_8.

^{1}H-NMR spectral changes of the HOCl-treated samples measured at selected reaction times t (HA-t, Figure 4.19a) indicated the formation of new species resembling those

obtained through sonication (MEH-s). Notably, also in the HOCl-treated CH_2Cl_2 solution of MEH-PPV (e.g. HA-21h, Figure 4.19b) the signals at 10.42 and 9.77 ppm, related to carbonyl moieties resulting from the cleavage of the conjugated system, were observed.

The role of HOCl in the process was finally assessed upon: a) sonication of a MEH-PPV $CHCl_3$ solution in a basic water solution (NaOH, 1 M), which is prompted to neutralize the formed HOCl (Figure 4.20a-b) and b) sonication of MEH-PPV in a $CHCl_3/H_2O$ solution in the presence of resorcinol as a HOCl-scavenger[54] (Figure 4.20c). In this case, the polymer solution tested was the less concentrated where the hypsochromic shift and the change in the band structure are more important so to better visualise the eventual changes in the optical properties upon the addition of NaOH and resorcinol.

In all cases a dramatic reduction of the blue-shift was detected confirming the formation and/or activity of HOCl was hindered.

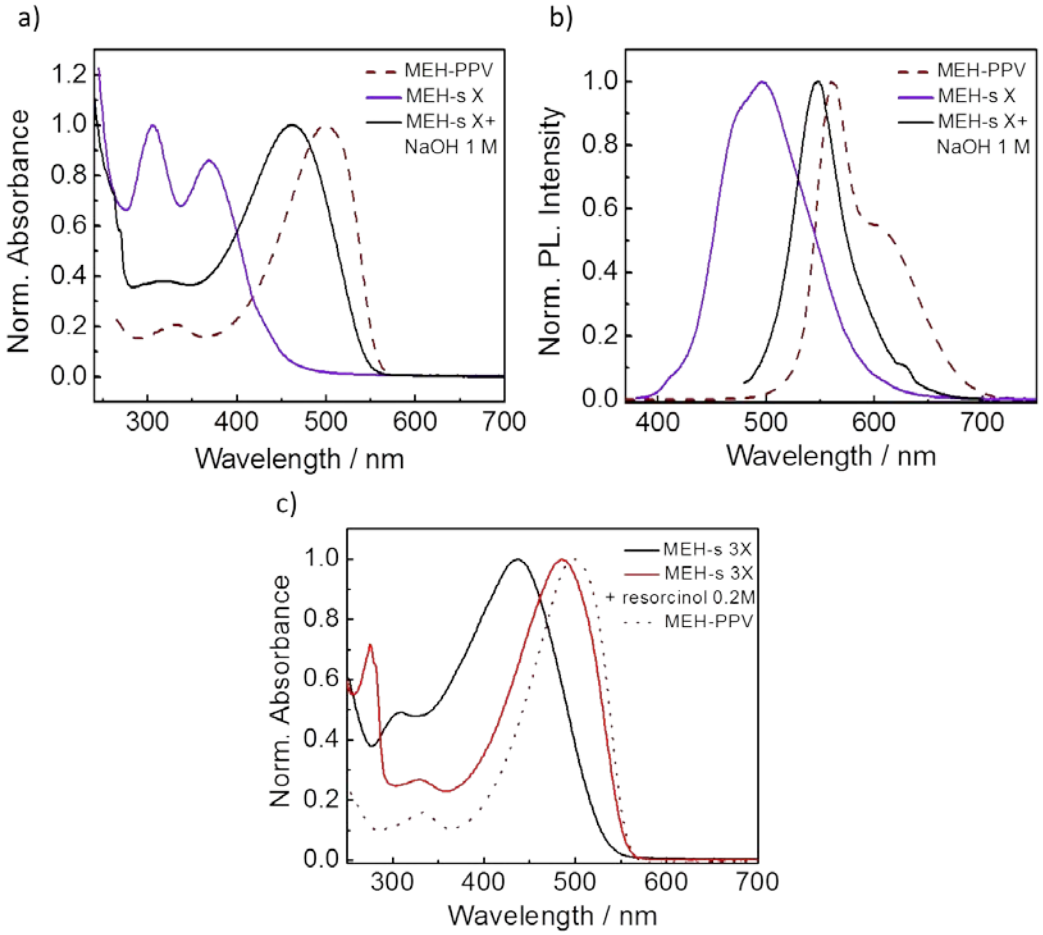

Figure 4.20. *a)* Absorption and *b)* emission spectra of parent MEH-PPV (dashed red line), MEH-PPV sonicated in the $CHCl_3/H_2O$ mixture (MEH-s X, purple solid line) and MEH-PPV sonicated in the $CHCl_3/H_2O$ mixture (MEH-s X, black solid line) in the presence of NaOH (1 M). All spectra were recorded in $CHCl_3$; c) absorption spectra of MEH-PPV sonicated in $CHCl_3/H_2O$ mixture (MEH-s 3X, black solid line) and of MEH-PPV sonicated in the $CHCl_3/H_2O$ mixture in the presence of an aqueous solution (0.2 M) of resorcinol (MEH-s 3X, red solid line).

The control experiments corroborate the effect of the hypochlorous acid on fragmentation of MEH-PPV and defined some parameters essential to obtain the oligomers, such as the co-presence of water and chloroform, and the relevance of the concentration on the optical properties of the final oligomers.

The solutions of the polymer in $CHCl_3$ used for the synthesis of the oligomers are quite diluted, fact that can contributes to the increase of the experimental errors that might affect the reproducibility of the process. Thus, in view of a future scale-up of the process and to increase its efficiency, further experiments were aimed to obtain the different oligomers from a starting concentrated solution with a fixed amount of polymer. We hypothesised that the variation of the volume of water, while keeping constant the volume of chloroform and the polymer concentration, could change both the production rate of the radical species and their diffusion in the organic phase leading to a control over the produced oligomeric species. The organic solution of MEH-PPV in $CHCl_3$ was prepared with a polymer concentrations of 5 mM, and 4 mL of this solution was added to a the following volume of aqueous phase: 8 mL, 12 mL, 16 mL, and 24 mL. The mixed solutions were sonicated following the protocol employed for the previous samples. Spectroscopic characterization of the resulting organic phase showed a progressive hypsochromic shift in absorption and emission increasing the volume of water (Figure 4.21).

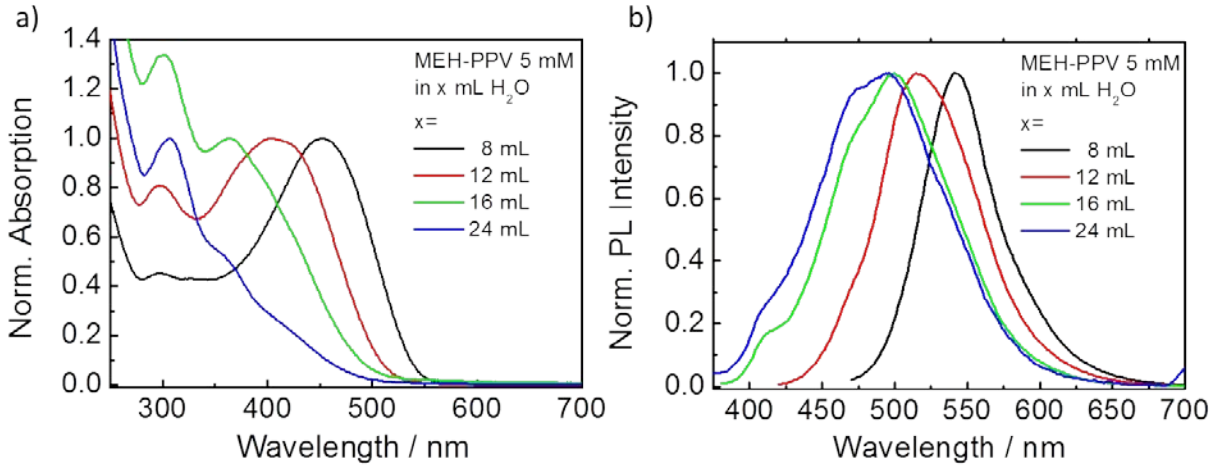

Figure 4.21. *a)* Absorption and *b)* emission of MEH-PPV 5mM sonicated in presence of increasing amounts of H_2O.

The absorption of the sonicated polymer passed from λ_{max}=452 nm of the lower water volume to λ_{max}=353 nm of the highest one. The emission passed from λ_{max}=541 to λ_{max}=494 nm. Interestingly, the polymer showed the expected variation of the optical properties upon changing the volume of water, indicating the formation of different oligomeric species. Such

dependence of the oligomer formation on the volume of aqueous phase could be ascribed to the formation of smaller oil droplets, which are formed as the ratio between the water phase and the organic phase is increased. Probably, in the presence of smaller droplets there is an increase of the surface area and thus a faster diffusion of the HOCl to the organic phase, leading to higher concentration of the acid and a more effective scission of the polymer chain.

4.3.2 Nanostructuration of MEH-s oligomers

To simultaneously achieve the optical tuning and the formation of nanoparticles (CPNs) via a modified miniemulsion method,[39] polymer solutions of six different concentrations, named 2 mM (X), 4 mM (2X), 6 mM (3X), 8 mM (4X), 12 mM (6X) and 20 mM (10X), were sonicated again in Milli-Q® water, but now in the presence of a surfactant (AOT, 0.1 wt.%) that stabilizes the chloroform-in-water nanoemulsion. As previously observed for the non-containing surfactant mixtures, the spectroscopic UV-Vis characterisation of the sonicated samples showed a progressive hypsochromic shift of the main absorption bands (from λ_{max} = 476 nm to 306 nm) as the concentration of polymer decreases (Figure 4.22a).

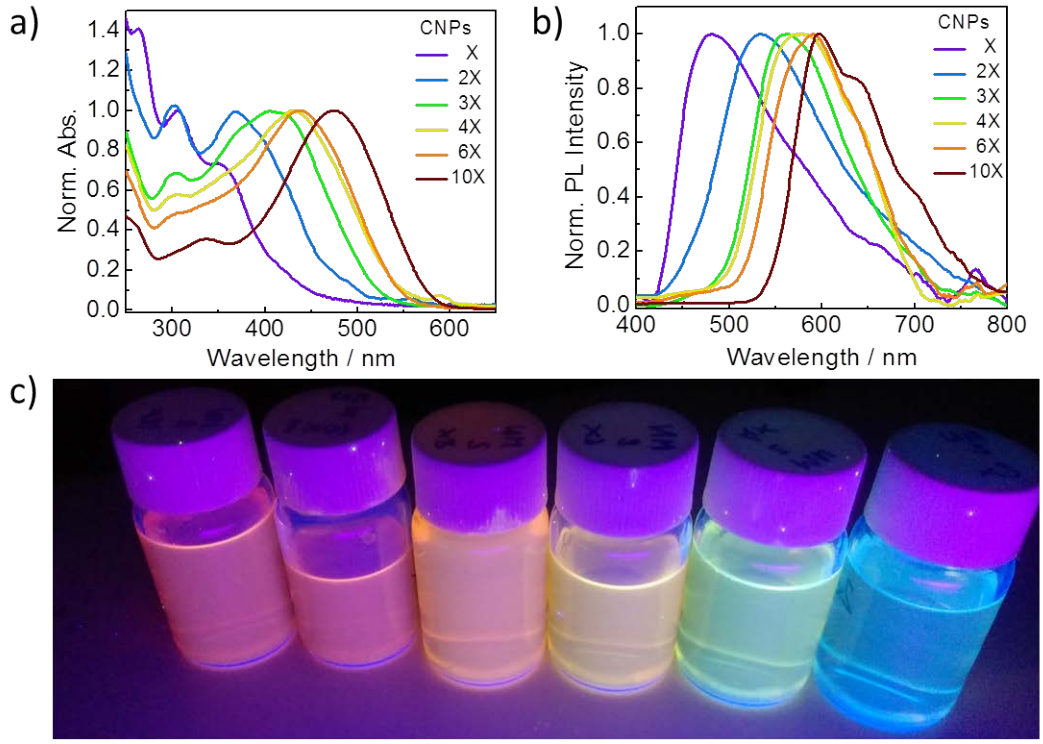

Figure 4.22. CPNs suspensions and their characterisation. *a)* absorption, *b)* emission spectra and *c)* digital camera image of the series of CPNs_X-10X.

A related blue-shift correlation of the emission bands (from λ_{max} = 597 nm to 481 nm) with the initial polymer concentration was also found for the CPNs (Figure 4.22b). Also, in this case, little or negligible differences in the emission bands were observed irradiating at 300 nm or at the corresponding low-energy absorption band maxima, indicating that the formation of mainly homogeneous oligomeric species was not affected by the presence of the surfactant (Figure 4.23).

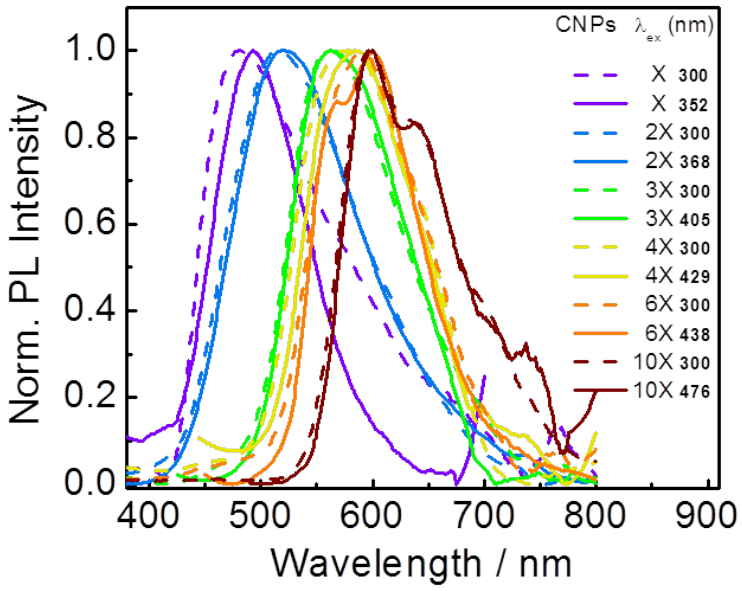

Figure 4.23. Emission spectra of the series of CPNs_X-10X exciting at 300 nm (dashed line) and at the absorption maxima.

Fluorescence quantum yield (Φ_f) (Table 4.4) values for the different samples (Φ_f=0.047-0.093) were lower than those obtained from MEH-s oligomers in chloroform, possibly due to the quenching effects typically observed for the solid CPNs.

Sample	Absorption λ_{max} (nm)	Emission λ_{max} (nm)	Φ_f	n_{ECL}
CPNs 10X	476	597	0.051	9
CPNs 6X	438	590	0.093	4.4
CPNs 4X	428	577	0.079	3.9
CPNs 3X	407	562	0.095	3.1
CPNs 2X	368	534	0.047	2.2
CPNs X	306	481	0.049	2

Table 4.4. Absorption and emission main maxima, quantum yield (Φ_f) values and effective conjugation length (n_{ECL}) of the series of CPNs_X-10X.

TEM and SEM (Figure 4.24) images showed the expected formation of nanoparticles for all the sonicated mixtures, with dimensions ranging from 62 ± 7 nm to 146 ± 23 nm.

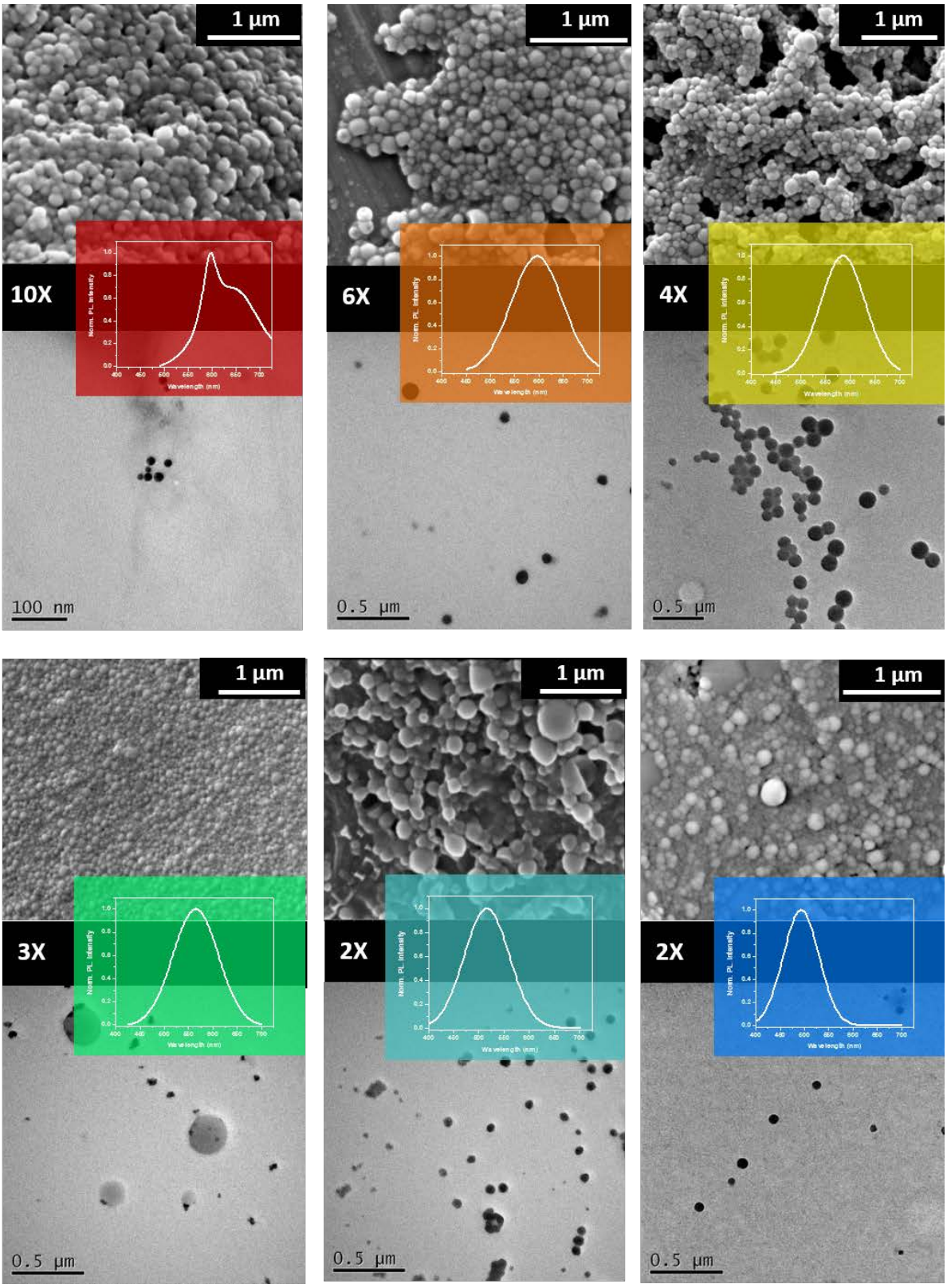

Figure 4.24. SEM and TEM images with the corresponding emission spectra of the samples CPNs_10X (up/left), CPNs_6X (up/centre), CPNs_4X (up/right), CPNs_3X (bottom/left), CPNs_2X (bottom /centre) and CPNs_X (bottom /right).

The variation in the size of the different CNPs observed by the DLS analysis showed the absence of correlations between the nanoparticles size and their optical properties since no clear trend in the variation of the size is observable. In Figure 4.25 the histogram of the size distribution obtained from DLS analysis on the samples CNPs X-2X-3X-4X are reported.

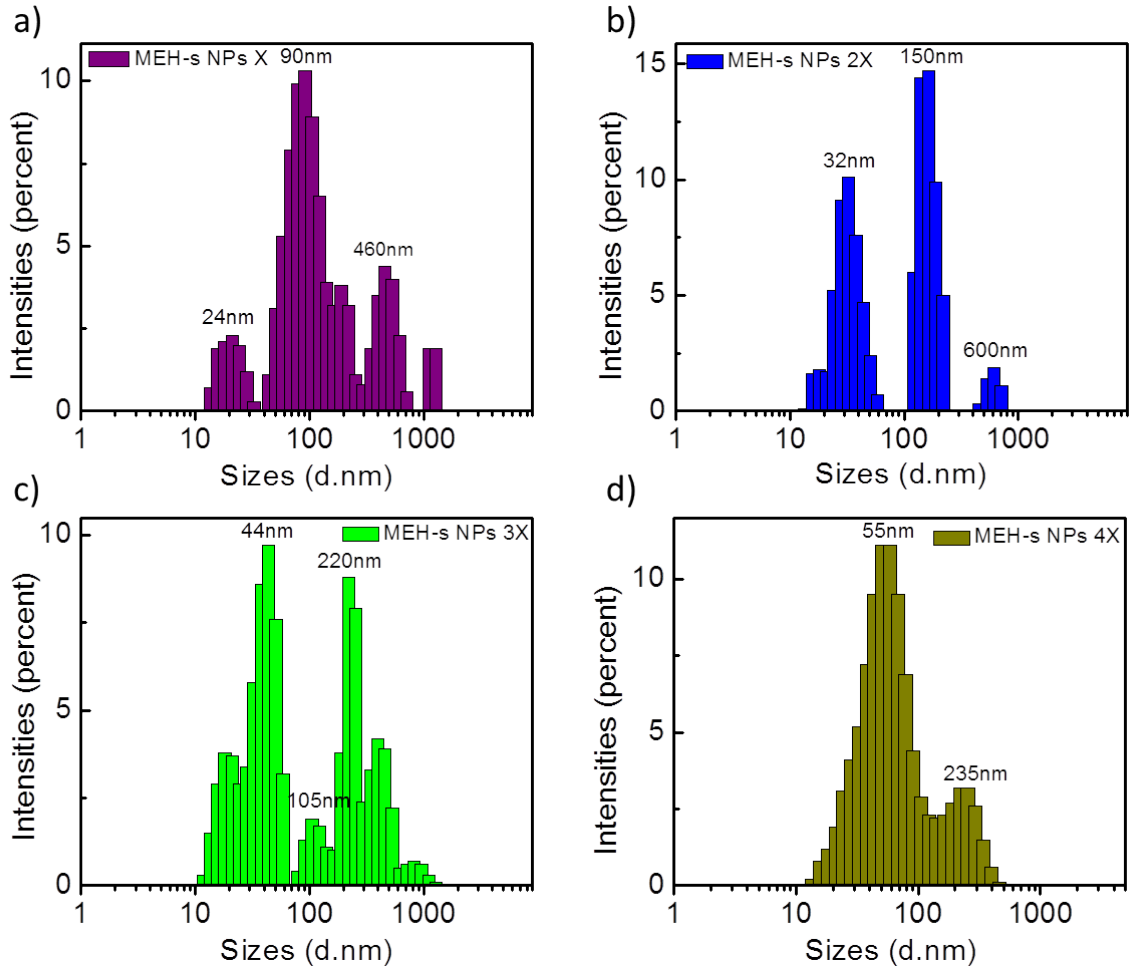

Figure 4.25. DLS analysis of the samples a) CPNs_X; b) CPNs_2X; c) CPNs_3X; d) CPNs_4X.

The nanoparticles showed red shift emission properties with respect to the fragmented species obtained upon sonication of the mixtures of the same concentration, but without surfactant (MEH-s). This red- shift can be explained on the basis of different intermolecular interactions between the oligomeric chains induced by the close packing present in the nanoparticles, as already described for several conjugated polymer nanoparticles,[4,57] rather than to the formation of different oligomeric species. The interchain interactions of the polymer within the CPNs favour the overlap between π orbitals, enlarging the conjugation, increasing the exciton diffusion and thus yielding lower energy emission.[4,57] Such explanation of the red-shift observed in the CNPs was supported by FT-Raman spectroscopy

(Figure 4. 26). The recorded data of the CPNs samples indicate similar spectra profiles as those obtained for the non-structured oligomers, indicating the presence in the nanoparticles of the same species produced without forming nanoparticles.

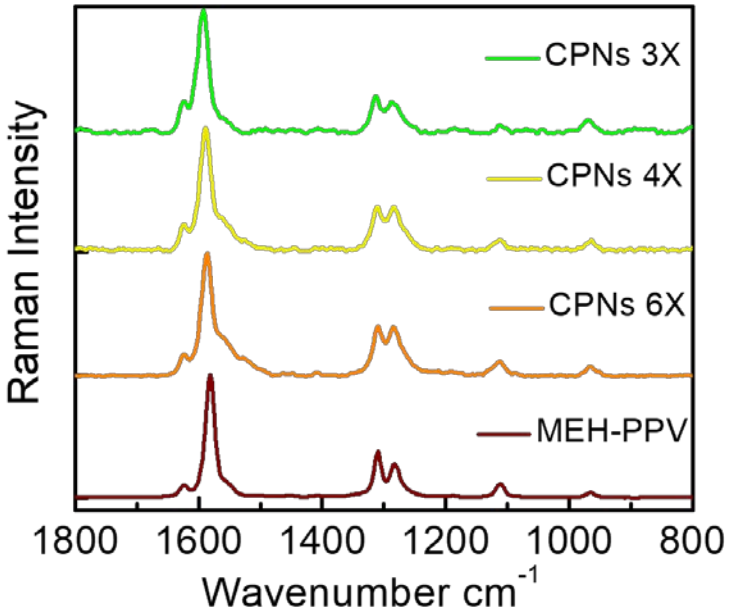

Figure 4. 26. FT-Raman spectra of samples parent MEH-PPV, CPNs_3X, CPNs_4X and CPNs_6X.

Furthermore, CPNs_3X presented its most intense Raman band (1592 cm-1) upshifted respect to CPNs_6X (1585 cm-1), and a higher I~1625/I~1585 ratio, both features indicative of shorter conjugated chains as the initial polymeric concentration decreases; that is, also supporting fragmentation into oligomers in the nanoemulsion.

Notably, minor impurities of micro/nanosized cubic crystals confirmed to be NaCl by EDX analysis, were also found in all the analysed nanoparticles sample (Figure 4.27a-b-c).

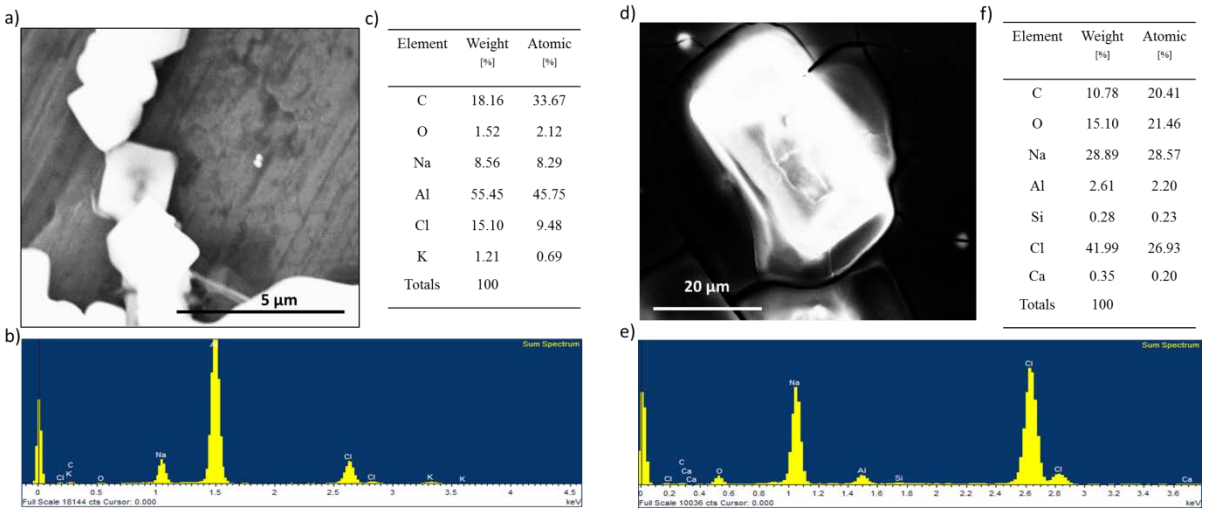

Figure 4.27. *a)* SEM image and *b)* EDX spectrum with *c)* the relative amount of the detected elements on the sample CPNs_4X, in the area where crystals are observed. *d)* SEM image and *e)* EDX spectrum with *f)* the relative amounts of the detected elements on the crystals formed after sonicating a $CHCl_3/H_2O$ mixture without MEH-PPV.

These crystals, formed after sonication even in the absence of the polymer (Figure 4.27d-e-f) and the surfactant, were most likely obtained by the recombination of chlorine species and traces of sodium found in the water as well as in the walls of the vial, and/or by decomposition of NaOCl[56] formed upon recombination of HOCl and the sodium ions traces.

4.3.3 Fabrication of fluorescent films

Finally, on the pursuit of functional materials, all CPNs suspensions (CPNs_X-10X) were used to form self-standing, flexible polyvinyl alcohol (PVA) films (CPNs_X-10X@PVA), through drop casting (Figure 4.28a).

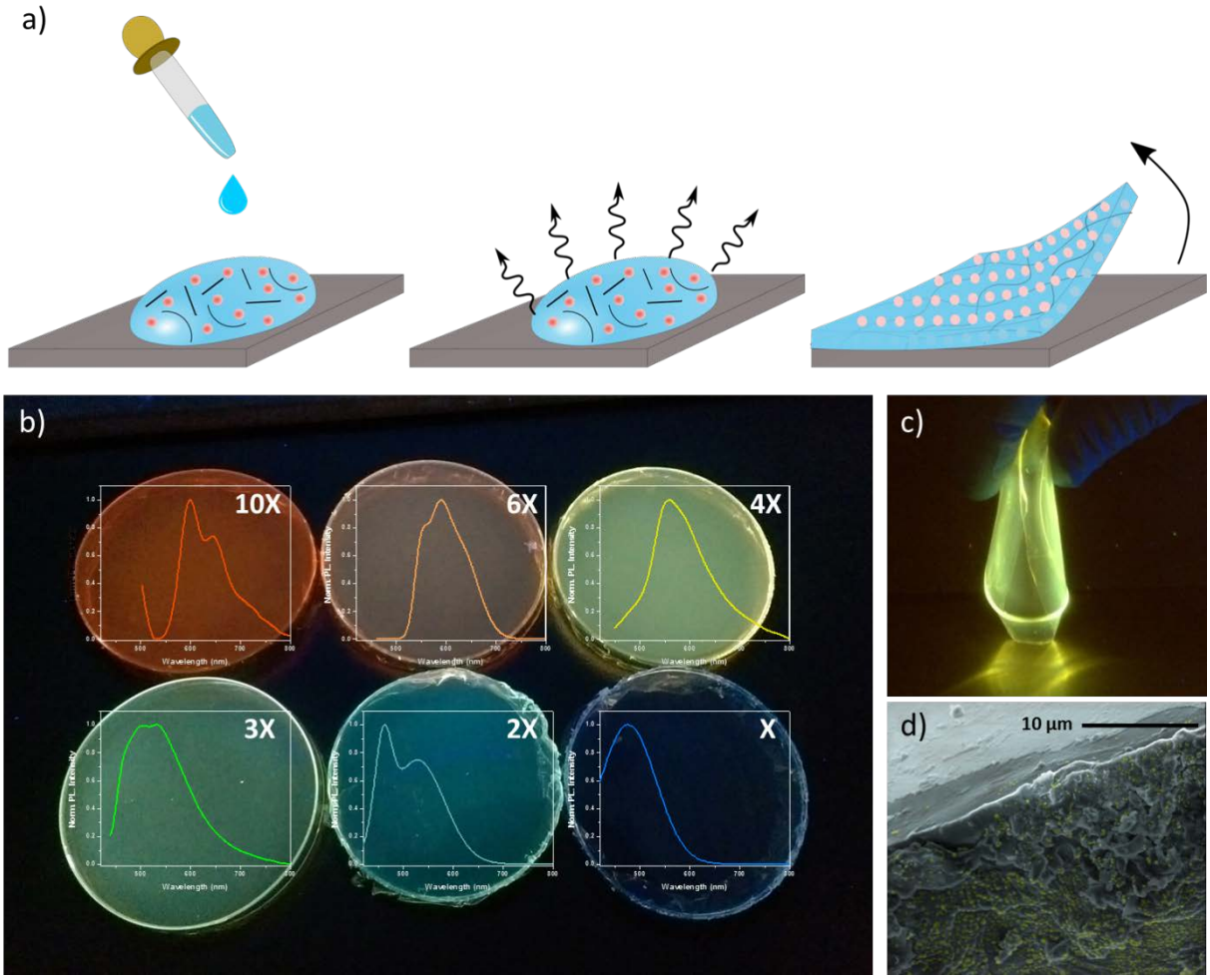

Figure 4.28. Scheme of the films formation and their characterization. a) scheme of drop-casting process of the CPNs_X-10X suspensions leading to the formation of the PVA films after H_2O evaporation; b) digital photographs of CPNs_X-10X@PVA films and corresponding emission spectra; c) digital photograph of bended CPNs_4X@PVA fluorescent film showing its flexibility; d) SEM picture of CPNs_4X@PVA film cross section.

The procedure followed to prepare the PVA film is described in the experimental section. Another suspension (containing the film forming polymer PVA) of the CNPs is

prepared and then casted onto a Petri plate. The water evaporation induced the precipitation of the PVA which formed a film while trapping the CNPs. The PVA is also acting as a stabiliser for the colloidal suspensions, preventing the aggregation of the CPNs during the film formation. Figure 4.28a describes schematically the drop-casting method used to make the polymeric films. From this process a flexible, coloured and emissive films (Figure 4.28) could be easily obtained. A cross-section of the film was analysed by SEM to confirm the presence of the nanoparticles embedded in the polymeric matrix. The absorption (Figure 4.29) and emission (Figure 4.28b) properties of the PVA films resemble those of the CPNs suspensions, indicating that the spectral features of the nanoparticles are transferred to a polymeric functional material. Only minor additional bands appear in the spectra of the films by comparison to the colloidal nanoparticles suspensions, most likely due to partial loss of NPs structure and/or mutual diffusion of MEH-PPV and PVA chains.

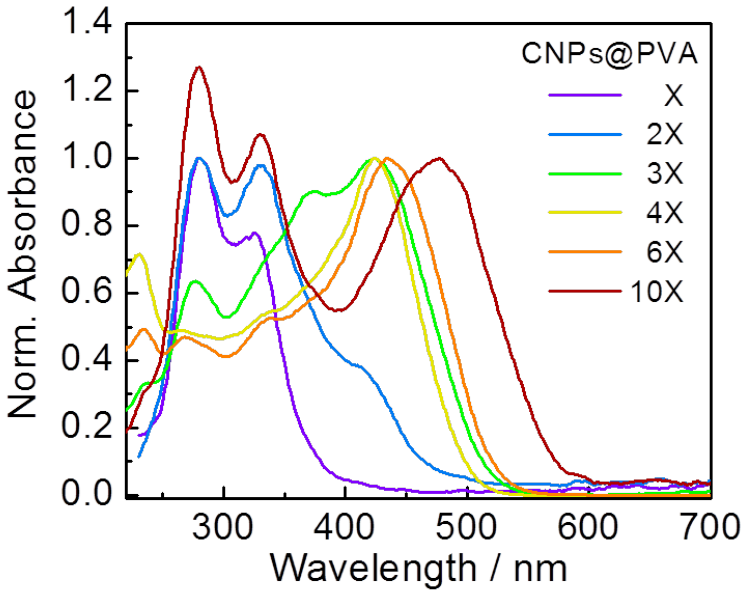

Figure 4.29. Absorption spectra of the CPNs_X-10X@PVA films formed from the corresponding suspensions CPNs_X-10X.

4.4 SUMMARY

In summary, the reactive species HOCl generated upon sonication of a chloroform/water mixture were used to fragment the MEH-PPV polymer, with a degree of fragmentation tuned by the initial concentration of the polymer in the organic solution; at lower polymer concentrations there are less polymer chains to be cleaved and therefore smaller fragments than for the more concentrated solutions are obtained over the same sonication time. The same effect can also be obtained varying the ratio between the aqueous and the organic phase

with a fixed amount of polymer. Such fragmentation accounts for the systematic tuning of the optical properties. Though, worth to mention, previous synthetic studies revealed that optical shifts are no longer effective for oligomers with 10 units or more,[29] considerably smaller than those obtained in this work. So to fully explain our experimental observation, beyond complete fragmentation, partial saturation of vinylene moieties and/or twsit of the polymer chains,[47] must also be claimed. Finally, when the sonication process is done in the presence of surfactants, the nanoemulsion is stabilized resulting in the final formation of nanoparticles with tuned optical properties. Thanks to stability of such nanoparticles, these could be further integrated into polymeric matrices leading to the obtaining of self-standing and flexible fluorescent films.

4.5 EXPERIMENTAL SECTION

4.5.1 Materials and Methods

Materials.

Poly[2-methoxy-5-(2-ethylhexyloxy)-1,4-phenylenevinylene] (MEH-PPV, average Mn 40,000-70,000), dioctyl sulfosuccinate sodium salt (AOT, 97.0%) and resorcinol (97%) were purchased from Sigma Aldrich. Aqueous NaOCl solution (available chlorine 15%) was purchased from Alfa Aesar. NaOH pellets, chloroform (synthesis grade), dichloromethane (synthesis grade), toluene (synthesis grade) and the aqueous HCl solution (37%) were purchased from Scharlau Chemicals. Tetrahydrofuran-d_8 (THF-d_8) was purchased from Euriso-top. All chemicals were used without further purification.

OriginPro 8 software was used to analyse and visualize spectral data.

Sonication of $CHCl_3/H_2O$ MEH-PPV mixtures (MEH-s).

The organic solutions of MEH-PPV in $CHCl_3$ were prepared with the following polymer concentrations: 2 mM (MEH-s X), 4 mM (MEH-s 2X), 6 mM (MEH-s 3X), 8 mM (MEH-s 4X) and 12 mM (MEH-s 6X). To assure the complete dissolution of the polymer in $CHCl_3$, the solutions were placed in a sonication bath and sonication steps of 30 minutes were applied. This sonication did not produce any optical changes on the solution. Once the homogeneous MEH-PPV solutions were obtained, mixtures of 4 mL of each polymer solution and 12 mL of Milli-Q® water were prepared in a 25 mL glass vial (diameter of 30

mm). Each mixture was sonicated for 5 minutes at 70% amplitude using the Branson Digital Sonifier 450 (400 W) with a 13 mm step horn and flat tip submerged inside the mixture. During the ultrasonication process the vial containing the mixture was placed in an ice bath to avoid an excessive heating. At the end of the process the sample was placed in a separation funnel in order to collect the organic phase from the mixed solution. The same process was repeated for each polymer solution (MEH-s).

Synthesis of conjugated polymer nanoparticles (CPNs).

CPNs were obtained using a modified miniemulsion method.[58] MEH-PPV homogeneous solutions in $CHCl_3$ were prepared at different concentrations: 2 mM (CPNs_X), 4 mM (CPNs_2X), 6 mM (CPNs_3X), 8 mM (CPNs_4X) and 12 mM (CPNs_6X). To assure the complete dissolution of the polymer in $CHCl_3$, the solutions were placed in a sonication bath and sonication steps of 30 minutes were applied. Once the homogeneous MEH-PPV solutions were obtained, mixtures of 4 mL of each polymer solution and 12 mL of a Milli-Q® water solution containing the anionic surfactant AOT (0.1 wt.%) were prepared in a 25 mL glass vial (diameter of 30 mm). Miniemulsions were prepared by ultrasonicating for 5 minutes at 70% amplitude, using the Branson Digital Sonifier 450 (400 W) with a 13 mm step horn and flat tip submerged inside the mixture. The vial containing the mixture was placed in an ice bath during the ultrasonication to avoid excess heating. After sonication, the samples were stirred in an oil bath at 35°C for 3 h in order to evaporate the organic solvent. Upon evaporation of the solvent the MEH-PPV particles were formed. The same process was repeated for each polymer solution (CPNs). In the case the powder of the CPNs was required for their characterization, the corresponding suspensions were frozen at -80 ºC and then freeze-dried during 2 days.

Films preparation.

PVA films containing the CPNs (CNPs X-10X@PVA) were prepared through drop casting method. The concentrated suspensions of CPNs were diluted in order to approximately reach a polymer concentration of 2 mM and filtered through 0.2 μm syringe filter. 5 mL of the diluted CPNs suspensions were added to 10 mL of aqueous solution of the film forming PVA (10 wt.%). The obtained suspensions were transferred onto a polystyrene Petri plate and

water was left evaporating at room temperature during 4 days. The dried film could be easily pealed out from the Petri container, obtaining self-standing flexible films.

Treatment of a CH_2Cl_2 MEH-PPV solution with NaOCl.

A 4X MEH-PPV dichloromethane solution (8 mM) was prepared by adding the polymer to the organic solvent and assuring the complete dissolution in a sonication bath. A water solution of NaOCl (0.1 M) and HCl (0.001 M) was prepared from Milli-Q® water. Once the homogeneous organic solution was obtained, 4 mL of this was added to 12 mL of NaOCl/HCl aqueous solution in a closed vial and left stirring at 500 rpm in the dark. Aliquots of the organic phase were taken at different reaction times and analysed by UV-VIS absorption, fluorescence and ^{1}H-NMR spectroscopies.

Theoretical calculations.

The molecular geometries of the PPV-based model systems were calculated at the Density Functional Theory (DFT) level using the hybrid, generalized gradient approximation (GGA) functional BHLYP1[59] and a 6-31G** basis[60–62] set, as implemented in the GAUSSIAN09 program.[63] All geometrical parameters were allowed to vary independently apart from planarity of the rings and no symmetry constraints were imposed during the optimization process. On the resulting ground-state optimized geometries, harmonic frequencies calculations were performed to ensure the finding of the global minimum. The calculated Raman frequencies were scaled by commonly used scaling factor 0.9244 for BHLYP method.[64]

4.6 REFERENCES

1. Urban, Dieter and Takamura, K. *Polymer Dispersions and Their Industrial Applications*. *Wiley-VCH 36 Verlag, Germany,* (2003). doi:10.1002/macp.200390002

2. Szymanski, C. *et al.* Single molecule nanoparticles of the conjugated polymer MEH-PPV, preparation and characterization by near-field scanning optical microscopy. *J. Phys. Chem. B* **109,** 8543–8546 (2005).

3. Ong, B. S., Wu, Y., Liu, P. & Gardner, S. Structurally ordered polythiophene nanoparticles for high-performance organic thin-film transistors. *Adv. Mater.* **17,** 1141–1144 (2005).

4. Grey, J. K., Kim, D. Y., Norris, B. C., Miller, W. L. & Barbara, P. F. Size-dependent spectroscopic properties of conjugated polymer nanoparticles. *J. Phys. Chem. B* **110,** 25568–25572 (2006).

5. Kurokawa, N., Yoshikawa, H., Hirota, N., Hyodo, K. & Masuhara, H. Size-dependent spectroscopic properties and thermochromic behavior in poly(substituted thiophene) nanoparticles. *ChemPhysChem* **5,** 1609–1615 (2004).

6. Piok, T. *et al.* The photophysics of organic semiconducting nanospheres: A comprehensive study. *Chem. Phys. Lett.* **389,** 7–13 (2004).

7. Changfeng Wu, Barbara Bull, Craig Szymanski, Kenneth Christensen & Jason McNeill. Multicolor Conjugated Polymer Dots for Biological Fluorescence Imaging. *ACS Nano* **2,** 2415–2423 (2008).

8. Eggeling, C., Widengren, J., Rigler, R. & Seidel, C. A. M. Photobleaching of Fluorescent Dyes under Conditions Used for Single-Molecule Detection: Evidence of Two-Step Photolysis. *Anal. Chem.* **70,** 2651–2659 (1998).

9. Rahim, N. A. A. *et al.* Conjugated polymer nanoparticles for two-photon imaging of endothelial cells in a tissue model. *Adv. Mater.* **21,** 3492–3496 (2009).

10. Howes, P., Green, M., Levitt, J., Suhling, K. & Hughes, M. Phospholipid Encapsulated Semiconducting Polymer Nanoparticles: Their Use in Cell Imaging and Protein Attachment. *J. Am. Chem. Soc.* **132,** 3989–3996 (2010).

11. Moon, J. H., McDaniel, W., MacLean, P. & Hancock, L. F. Live-cell-permeable poly(p-phenylene ethynylene). *Angew. Chemie - Int. Ed.* **46,** 8223–8225 (2007).

12. Repenko, T. *et al.* Bio-degradable highly fluorescent conjugated polymer nanoparticles for bio-medical imaging applications. *Nat. Commun.* **8,** 8–15 (2017).

13. Kietzke, T. *et al.* Novel approaches to polymer blends based on polymer nanoparticles. *Nat. Mater.* **2,** 408–412 (2003).

14. Wei, J. *et al.* Polyaniline nanoparticles doped with star-like poly(styrene sulfonate): Synthesis and electrochromic properties. *Sol. Energy Mater. Sol. Cells* **99,** 141–147 (2012).

15. Park, E.-J. *et al.* White-Emitting Conjugated Polymer Nanoparticles with Cross-Linked Shell for Mechanical Stability and Controllable Photometric Properties in Color-Conversion LED Applications. *ACS Nano* **5,** 2483–2492 (2011).

16. Mikosch, A., Ciftci, S. & Kuehne, A. J. C. Colloidal Crystal Lasers from Monodisperse Conjugated Polymer Particles via Bottom-Up Coassembly in a Sol-Gel Matrix. *ACS Nano* **10,** 10195–10201 (2016).

17. Feng, X., Tang, Y., Duan, X., Liu, L. & Wang, S. Lipid-modified conjugated polymernanoparticles for cell imaging and transfection. *J. Mater. Chem.* **20,** 1312–1316 (2010).

18. Schwarz, K. N. *et al.* Charge generation and morphology in P3HT : PCBM nanoparticles prepared by mini-emulsion and reprecipitation methods. *Nanoscale* **7,** 19899–19904 (2015).

19. Shen, X. *et al.* Enhanced Two-Photon Singlet Oxygen Generation by Photosensitizer-Doped Conjugated Polymer Nanoparticles. *Langmuir* **27,** 1739–1744 (2011).

20. Piwoński, H., Michinobu, T. & Habuchi, S. Controlling photophysical properties of ultrasmall conjugated polymer nanoparticles through polymer chain packing. *Nat. Commun.* **8,** 15256 (2017).

21. Collison, C. J., Rothberg, L. J., Treemaneekarn, V. & Li, Y. Conformational effects on the photophysics of conjugated polymers: A two species model for MEH-PPV spectroscopy and dynamics. *Macromolecules* **34,** 2346–2352 (2001).

22. Quan, S. *et al.* Solvent and concentration effects on fluorescence emission in MEH-PPV solution. *Eur. Polym. J.* **42,** 228–233 (2006).

23. Cadby, A. J. & Tolbert, S. H. Controlling optical properties and interchain interactions in semiconducting polymers by encapsulation in periodic nanoporous silicas with different pore sizes. *J. Phys. Chem. B* (2005). doi:10.1021/jp0536753

24. Köhler, A., Hoffmann, S. T. & Bässler, H. An Order–Disorder Transition in the Conjugated Polymer MEH-PPV. *J. Am. Chem. Soc.* **134,** 11594–11601 (2012).

25. Huang, Y.-S., Gierschner, J., Schmidtke, J. P., Friend, R. H. & Beljonne, D. Tuning interchain and intrachain interactions in polyfluorene copolymers. *Phys. Rev. B* **84,** 205311 (2011).

26. Tung, K.-P. *et al.* Large Enhancements in Optoelectronic Efficiencies of Nano-plastically Stressed Conjugated Polymer Strands. *ACS Nano* **5,** 7296–7302 (2011).

27. Schneider, J. A., Dadvand, A., Wen, W. & Perepichka, D. F. Tuning the Electronic Properties of Poly(thienothiophene vinylene)s via Alkylsulfanyl and Alkylsulfonyl Substituents. *Macromolecules* **46,** 9231–9239 (2013).

28. Matsumoto, T., Tanaka, K. & Chujo, Y. Synthesis and Characterization of Gallafluorene-Containing Conjugated Polymers: Control of Emission Colors and Electronic Effects of Gallafluorene Units on ?-Conjugation System. *Macromolecules* **48,** 1343–1351 (2015).

29. Tilley, A. J. *et al.* Synthesis and Fluorescence Characterization of MEHPPV Oligomers. *J. Org. Chem.* **76,** 3372–3380 (2011).

30. Ruiz Perez, J. D. & Mecking, S. Anisotropic Polymer Nanoparticles with Tunable Emission Wavelengths by Intersegmental Chain Packing. *Angew. Chemie - Int. Ed.* **56,** 6147–6151 (2017).

31. Van Iersel, M. M. Sensible Sonochemistry. (2008).

32. Suslick, K. S. Sonochemistry. *Science (80-.).* **247,** 1439–1445 (1990).

33. Luche, J. Synthetically useful sonochemical reactions in solution. *Ultrason. Sonochem.* **3,** S215–S221 (1996).

34. Mills, A. & Holland, C. Effect of ultrasound on the kinetics of oxidation of octan-2-ol and other secondary alcohols with sodium bromate, mediated by ruthenium tetraoxide in a biphasic system. *Ultrason. - Sonochemistry* **2,** 33–38 (1995).

35. Nakamura, E., Machii, D. & Inubushi, T. Homogeneous Sonochemistry in Radical Chain Reactions. Sonochemical Hydrostannation and Tin Hydride Reduction. *J. Am. Chem. Soc.* **111,** 6849–6850 (1989).

36. Price, G. J., Norris, D. J. & West, P. J. Polymerization of Methyl methacrylate Initiated by Ultrasound. *Macromolecules* **25,** 6447–6454 (1992).

37. Javed, T., Mason, T. J., Phull, S. S., Baker, N. R. & Robertson, A. Influence of ultrasound on the Diels-Alder cyclization reaction: synthesis of some hydroquinone derivatives and lonapalene, an anti-psoriatic agent. *Ultrason. - Sonochemistry* **2,** 3–4 (1995).

38. Meier, H., Stalmach, U. & Kolshorn, H. Effective conjugation length and UV/vis spectra of oligomers. *Acta Polym.* **48,** 379–384 (1997).

39. Landfester, K. *et al.* Semiconducting Polymer Nanospheres in Aqueous Dispersion Prepared by a Miniemulsion Process. *Adv. Mater.* **14,** 651–655 (2002).

40. Franke, M., Braeutigam, P., Wu, Z.-L., Ren, Y. & Ondruschka, B. Enhancement of chloroform degradation by the combination of hydrodynamic and acoustic cavitation. *Ultrason. Sonochem.* **18,** 888–894 (2011).

41. Wu, Z.-L., Ondruschka, B. & Bräutigam, P. Degradation of Chlorocarbons Driven by Hydrodynamic Cavitation. *Chem. Eng. Technol.* **30,** 642–648 (2007).

42. Maitra, D. *et al.* Mechanism of hypochlorous acid-mediated heme destruction and free iron release. *Free Radic. Biol. Med.* **51,** 364–373 (2011).

43. Bondarev, D., Trhlíková, O., Sedláček, J. & Vohlídal, J. Stability of MEH-PPV: Poly{[2-methoxy-5-(2-ethylhexyloxy)-1,4-phenylene]vinylene} in solutions exposed to air in the dark and at daylight at laboratory temperature. *Polym. Degrad. Stab.* **110,** 129–136 (2014).

44. Bronze-Uhle, E. S., Batagin-Neto, A., Lavarda, F. C. & Graeff, C. F. O. Ionizing radiation induced degradation of poly (2-methoxy-5-(2'-ethyl-hexyloxy) -1,4-

phenylene vinylene) in solution. *J. Appl. Phys.* **110,** 73510 (2011).

45. Wang, H., Tao, X. & Newton, E. Thermal degradation kinetics and lifetime prediction of a luminescent conducting polymer. *Polym. Int.* **53,** 20–26 (2004).

46. Bao, B. *et al.* A controllable approach to development of multi-spectral conjugated polymer nanoparticles with increased emission for cell imaging. *Chem. Commun.* **49,** 10623 (2013).

47. Sommerburg, O. *et al.* β-Carotene cleavage products after oxidation mediated by hypochlorous acid—a model for neutrophil-derived degradation. *Free Radic. Biol. Med.* **35,** 1480–1490 (2003).

48. Pennathur, S. *et al.* Potent antioxidative activity of lycopene: A potential role in scavenging hypochlorous acid. *Free Radic. Biol. Med.* **49,** 205–213 (2010).

49. Burroughes, J. H. *et al.* Burroughes1990 Light-emitting diodes based on conjugated polymers.pdf. *Nature* **347,** 539–541 (1990).

50. Pang, Y., Samoc, M. & Prasad, P. N. Third-order nonlinearity and two-photon-induced molecular dynamics: Femtosecond time-resolved transient absorption, Kerr gate, and degenerate four-wave mixing studies in poly (*p* -phenylene vinylene)/sol-gel silica film. *J. Chem. Phys.* **94,** 5282–5290 (1991).

51. Woo, H. S. *et al.* Optical-Spectra and Excitations in Phenylene Vinylene Oligomers. *Synth. Met.* **59,** 13–28 (1993).

52. Orion, I., Buisson, J. P. & Lefrant, S. Spectroscopic studies of polaronic and bipolaronic species in n -doped poly(paraphenylenevinylene). *Phys. Rev. B* **57,** 7050–7065 (1998).

53. Mulazzi, E., Ripamonti, A., Wery, J., Dulieu, B. & Lefrant, S. Theoretical and experimental investigation of absorption and Raman spectra of poly(paraphenylene vinylene). *Phys. Rev. B* **60,** 16519–16525 (1999).

54. Özyürek, M., Bekdeşer, B., Güçlü, K. & Apak, R. Resorcinol as a Spectrofluorometric Probe for the Hypochlorous Acid Scavenging Activity Assay of Biological Samples. *Anal. Chem.* **84,** 9529–9536 (2012).

55. Henglein, A. & Fischer, C.-H. Sonolysis of Chloroform. *Berichte der Bunsengesellschaft für Phys. Chemie* **88,** 1196–1199 (1984).

56. March, J. G. & Simonet, B. M. A green method for the determination of hypochlorite in bleaching products based on its native absorbance. *Talanta* **73,** 232–236 (2007).

57. Wu, C. & McNeill, J. Swelling-Controlled Polymer Phase and Fluorescence Properties of Polyfluorene Nanoparticles. *Langmuir* **24,** 5855–5861 (2008).

58. Landfester, K. *et al.* Semiconducting polymer nanospheres in aqueous dispersion prepared by a miniemulsion process. *Adv. Mater.* **14,** 651–655 (2002).

59. Becke, A. D. A new mixing of Hartree–Fock and local density-functional theories. *J. Chem. Phys.* **98,** 1372–1377 (1993).

60. Hehre, W. J., Ditchfield, R. & Pople, J. A. Self—Consistent Molecular Orbital Methods. XII. Further Extensions of Gaussian—Type Basis Sets for Use in Molecular Orbital Studies of Organic Molecules. *J. Chem. Phys.* **56,** 2257–2261 (1972).

61. Francl, M. M. *et al.* Self-consistent molecular orbital methods. XXIII. A polarization-type basis set for second-row elements. *J. Chem. Phys.* **77,** 3654–3665 (1982).

62. Hariharan, P. C. & Pople, J. A. The influence of polarization functions on molecular orbital hydrogenation energies. *Theor. Chim. Acta* **28,** 213–222 (1973).

63. Frisch MJ, Trucks GW, Schlegel HB, Scuseria GE, Robb MA, Cheeseman JR, Scalmani G, Barone V, Mennucci B, Petersson GA, N. H. Gaussian 09, Revision A, Gaussian. Inc., Wallingford CT. (2009).

64. Jeffrey P. Merrick, Damian Moran, *,† and & Radom*, L. An Evaluation of Harmonic Vibrational Frequency Scale Factors. (2007). doi:10.1021/JP073974N

65. Kortüm, G., Braun, W. & Herzog, G. Principles and Techniques of Diffuse-Reflectance Spectroscopy. *Angew. Chemie Int. Ed. English* **2,** 333–341 (1963).

66. Morris, J. V., Mahaney, M. A. & Huber, J. R. Fluorescence quantum yield determinations. 9,10-Diphenylanthracene as a reference standard in different solvents. *J. Phys. Chem.* **80,** 969–974 (1976).

CHAPTER

5

MEH-PPV OLIGOMERS IN PCMs FOR MULTIEMITTING MATERIALS

In chapter 3 has been proposed a temperature sensor based on the mixture PCM/MEH-PPV. The polymer has shown an excellent solubility exclusively in fatty acid PCM. The shorter chain of the MEH-PPV oligomers could favour a better solubility of such material also in paraffin PCM. Here, the oligomers, synthesised with the method showed in Chapter 4, are mixed with fatty acids and paraffin PCM to obtain material suitable for a temperature sensor. The advantages with respect to the system showed in Chapter 3 are: I) a more extensive range of PCM to be used for the mixture, increasing the variety of detectable temperature and the compatibility of the system with other materials, since paraffin are inert; II) the possibility to select desired emission wavelength, which can be used to build a multicolour emitting sensor. Moreover, having oligomers and polymer emitting in the red, green and blue region of the visible electromagnetic spectrum open to the possibility to fabricate white light emitting system.

5.1. INTRODUCTION

In *Chapter 3* we reported the successful fabrication of a temperature fluorescent sensor prototype based on the thermally and reversibly switchable fluorescence of the conjugated polymer MEH-PPV, as controlled by the solid-to-liquid transition of the phase change materials (PCM) in which the polymer is dissolved. However, the low solubility of the MEH-PPV polymer only allowed for the use of acidic PCMs, whose polarity guaranteed the required solubility. Aliphatic PCMs did not induce the emission changes, fact ascribed to the low solubility of the polymer in both, solid and liquid, states of the PCM. This limitation restricts the strategy.

Afterwards, in *Chapter 4*, we demonstrated ultrasonication of a $CHCl_3/H_2O$ solution of the MEH-PPV polymer resulted in its reproducible and controllable fragmentation into smaller oligomers exhibiting a progressive blue-shift of the absorption and emission properties.

Finally, it is the aim of this chapter to combine both approaches by using such oligomers as fluorescent molecular thermometers and/or white light emitting materials, using phase change materials of different melting temperatures. Next we summarized the state-of-the art and representative examples of both applications.

5.1.1. Temperature sensor

Temperature is a fundamental property of matter and its measurement is of great importance in research and industrial applications. Among the different materials and devices developed for this purpose, polymer sensors that exhibit a change in their fluorescence have been extensively studied in recent years. Indeed, through the many optical methods employed for sensing, fluorescence has attracted particular attention as it is a sensitive technique that can be optically measured even with a remote sensor. Main advantages over contact temperature sensors are in applications where the presence of a strong electromagnetic noise or the need of sophisticated and specific wiring circuits represents a real technical challenges.[1] Additional advantages of a luminescence-based thermometer are the usually fast response and the spatial resolution that can be achieved from the macroscale (in the case of luminescent paints) down to the nanoscale (such as in fluorescence microscopy).[2]

Fluorescent temperature sensors can be classified into four types:

1. heat-induced fluorescence enhancement,[3]
2. heat-induced fluorescence quenching,[4]
3. selective emission enhancement at a specific temperature range,[5]
4. selective emission shifting at a specific temperature range.[6]

For their application as a sensor, that can allow for the simple monitoring of the temperature in terms of fluorescence intensity and/or shift changes, fluorescence enhancement and emission-shift type are the best candidates thank to their high signal-to-noise ratio and ease detection. For instance, threshold temperature sensors, as visual indicators of thermal history for temperature-sensitive products, have already been obtained by Crenshaw *et al.* incorporating excimer-forming dyes into glassy amorphous or semicrystalline host polymers (Figure 5.1). Such sensors exhibit permanent changes of the material emission properties once the glass transition temperature of the host polymer is reached due to the irreversible formation of the dye aggregates.[6] One of the advantages of using a polymeric matrix is their flexibility, which makes such composites suitable for some technological advanced applications (e.g., skin multifunctional sensors, wearable electronics, measurements on complex surfaces, and so on).

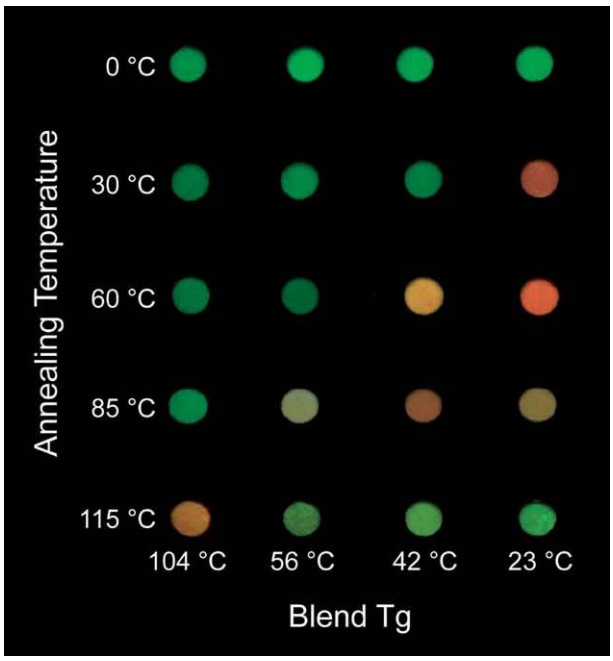

Figure 5.1. Poly(alkyl methacrylate) copolymers and oligo(p-phenylene vinylene)s blend films upon annealing for at least 15 h at the temperatures indicated. The samples are shown under illumination with 365 nm light. (Copyright Wiley-VCH Verlag GmbH & Co. KGaA, Weinheim).[6]

Pucci *et al.* fabricated thermoresponsive fluorophoric polymer blends based on the excimer forming stilbene dye BBS dispersed in ethylene/norbornene copolymers (at the concentration of 0.1 wt.%. When the copolymer is heated above its glass transition temperature (T_g = 64 ºC), the authors detected permanent optical changes due to the variation of the dye supramolecular structure, as shown in Figure 5.2.[7]

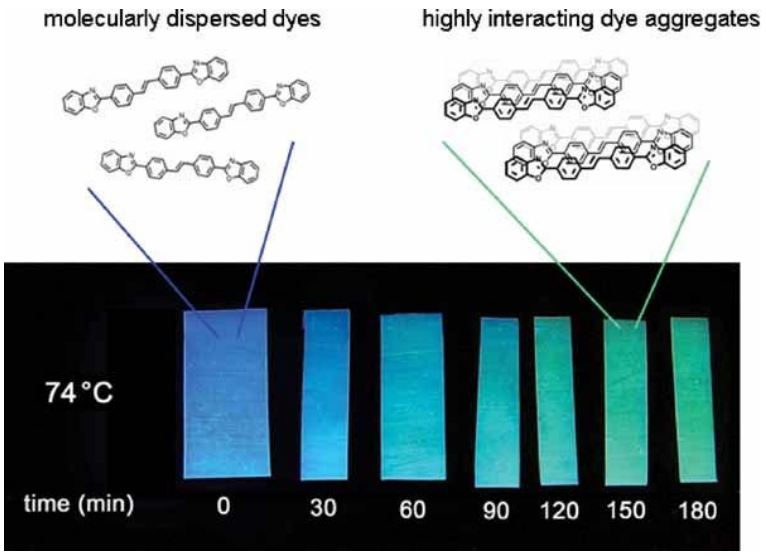

Figure 5.2. Picture of the BBS dye in ethylene/norbornene copolymer film taken under irradiation at 366 nm at different annealing time at 74 °C. The sketch depicts the change in the molecular aggregation of the dye with temperature. (Copyright © 2009 WILEY-VCH Verlag GmbH & Co. KGaA, Weinheim).[7]

The main limitation of these materials for their application is the irreversibility of the fluorescence switch once the target temperature is reached. Moreover, the detection temperature mechanism relies on the intrinsic physical properties of the polymers that act as a host, involving two main restrictions: I) the detection of different temperatures requires the synthetic modification of the polymers and II) it is difficult to obtain a sharp temperature transition (detection) with polymers, as they usually exhibit a wide T_g and III).

5.1.2. White light emitting diode (WOLED)

In the last decades, increasing attention has been directed towards the development of white organic light emitting devices (WOLED) according to its industrial relevance. These devices are based on organic molecules with high emitting efficiency. WOLEDs can be used as the backlight in flat-panels or to replace traditional incandescent white light sources. The last one represents an important energetic and environmental challenge as lighting consumes an important amount of electricity each year. For example, in the United States nearly 30 % of all the electricity produced for buildings is consumed by lighting. This consumption is

translated in a cost for the consumers to light their homes, offices, streets, and factories of almost $58 billion a year.[8] These data suggest that increasing the efficiency of lighting, even by a small amount, has the potential to generate enormous savings in both cost and energy. Incandescent lamps accounts for 42 % of the electrical energy consumed and their total power efficiency (η_t) is 3 times lower than the efficiency the OLED tested in laboratory (12-17 lm W^{-1} and 30-60 lm W^{-1} respectively).[9] Based on this increased efficiency, the US Department of energy estimated a 29 % decrease in the national energy consumption by 2025 if WOLEDs will be employed in solid-state lighting.[8]

Additional interest to use small molecules and organic polymers in electronic systems is motivated by the low cost and versatility of these materials. Organic films can be deposited on a variety of low-cost substrates (such as glass, plastic or metal foils) and are relatively ease to process and, potentially, do not require the addition of expensive and toxic metals.[10] Conjugated polymers present a further gain compared to small organic molecules. Large area fabrication of devices based on small molecules is a costly process, since it requires vacuum deposition, whereas conjugated polymers are solution processable, so large surface polymeric films can be easily made with low-cost deposition methods (such as spin-coating, ink-jet printing, screen printing, doctor-blade and roll-to-roll).

So far several examples of polymeric WOLED have been reported in the literature, following different strategies for the activation of the white light (such as polymer blend[11], exciplex forming polymers[12], single polymer forming aggregates[13] and polymers doped with dyes[14] or metal complexes[15]), obtaining in most of the cases luminance comparable to the small-molecules LEDs.[14] Among the different strategies, the trichromatic LED-based white light is the most investigated because of its several advantages. In this approach, emission from multiple monochromatic LEDs is additively mixed to generate white light.[16,17] Trichromatic LED-based devices offer white light sources characterised by a good colour rendering-index and high luminous efficiency, thanks to the possibility of fine-tuning of the spectral intensity and wavelength of individual LEDs. However, these types of sources are sensible to different parameters (such as maximum wavelengths, spectral widths and lumen outputs) which influence the spectrum of the white-light source and make difficult to maintain the desired white emission. Moreover, the light flux and the wavelength of a LED are affected by the variation of the temperature.[18] Since the temperature dependence of the flux and the wavelength are not precisely known, compensation and feedback control using thermal sensors are often not sufficient.

5.2. OBJECTIVES

According to the previous precedents, the main objective for this chapter is:

"To investigate the temperature dependence of the oligomers obtained in *Chapter 4* dissolved in different PCMs. Due to their shorter chain than MEH-PPV, oligomers are expected to offer better solubility in PCMs. The presence of the PCMs has also a double function: I) favour a better dissipation of the heat in the device avoiding overheating and II) it allows for a precise temperature dependence of the emission properties".

If successful, the sub-objectives would be:

- Build a temperature sensor with multichromatic light signalling thanks to their tuneable emission. For this a single oligomer will be studied in different PCMs.
- Selected oligomers will be combined to have a proper emission matching the RGB colour model as white light emitting systems on a single or various PCMs. The advantage of this system as WOLED is the possibility to fine control the emission properties of the conjugated oligomers and polymers with the temperature. As discussed above, trichromatic LED-based white light sources are susceptible to the temperature. With the PCMs/oligo-poly MEH-PPV system it could be possible to improve such sources.

5.3. RESULTS AND DISCUSSION

5.3.1. Temperature sensor

To establish a temperature sensor, we selected the sample MEH-s 4x (obtained following the sonochemical procedure reported in *Chapter 4*) and tested its temperature dependence in three PCMs: dodecanoic acid, eicosane, and hexadecane.

The solution of MEH-s 4X in PCM was prepared at two different concentrations following the procedure reported in *Chapter 3* for the sample DA/MEH. Briefly, a given amount of the synthesised oligomer MEH-s 4X dissolved in CH_2Cl_2 was added to the PCM and mixed. Then the organic solvent was evaporated, and the mixed solution of oligomers in PCM (hereafter named as DA/MEH-s 4X) was obtained at two different concentrations: 0.1 wt.% and 0.01 wt.% (see Experimental Section). The fluorescence of the solutions was studied at two different temperatures: below the T_m of the employed PCM for the solid state and above the T_m for the liquid state.

Dodecanoic acid

Given the switchable emission properties showed by the MEH-PPV polymer in DA, this PCM was the first used to investigate the behaviour of the oligomers.

Figure 5.1 show photograph of the cuvette with the solution of the oligomer MEH-s 4X dissolved in dodecanoic acid (hereafter named as DA/MEH-s 4X) at two concentrations (0.1 % in Figure 5.1a and 0.01% in Figure 5.1b). In both sample, the difference in the colour of the light emitted between the solid (left cuvette) and liquid (right cuvette) state is clearly visible. Moreover, the central photograph shows the sensibility of the system, which melt only in the part of the cuvette heated. Also the effect of the concentration on the emitted light is evident, with the less concentrated sample showing a bluish emission, while the most concentrated is greenish.

The fluorescence of the system DA/MEH-s 4X at a concentration of 0.1% is shown Figure 5.1c. In the solid state (blue line) the mixture presents a broad peak with a maximum at 581 nm. When the temperature is increased up to 60 °C, the PCMs melts and the emission from the oligomers presents a large hypsochromic shift of 43 nm (λ_{max} = 581→538 nm) while the intensity of the emission slightly increases.

The less concentrated sample, DA/MEH-s 4X 0.01%, in the solid state presented a broad peak with a maximum at 571 nm (Figure 5.1d), 10 nm blue-shifted from the concentrated sample. Once the PCM was melted, the emission slightly increased and the band shifted to a λ_{max} = 537 nm, close position to the one observed for the most concentrated solution. Compared to the behaviour of MEH-PPV dispersed in DA, the blue shift provided by the oligomer was more significant (43 nm versus 20 nm), while the intensity variation was less pronounced. Figure 5.3e-f also shows the normalised spectra of samples DA/MEH-s 4x 0.1% and 0.01% and the comparison with the sample MEH-s 4X dissolved in CH_2Cl_2 (dashed grey line). The emission properties of the liquid DA/MEH-s 4X 0.1% and DA/MEH-s 4X 0.01% were very similar. The solvation degree of the two solutions was similar enough to obtain the same stabilization of the electronic states of the polymer chains. Both DA/MEH-s emission, were blue-shifted (~14 nm) compared to the emission in DCM, probably due to the different polarity of the solvent.

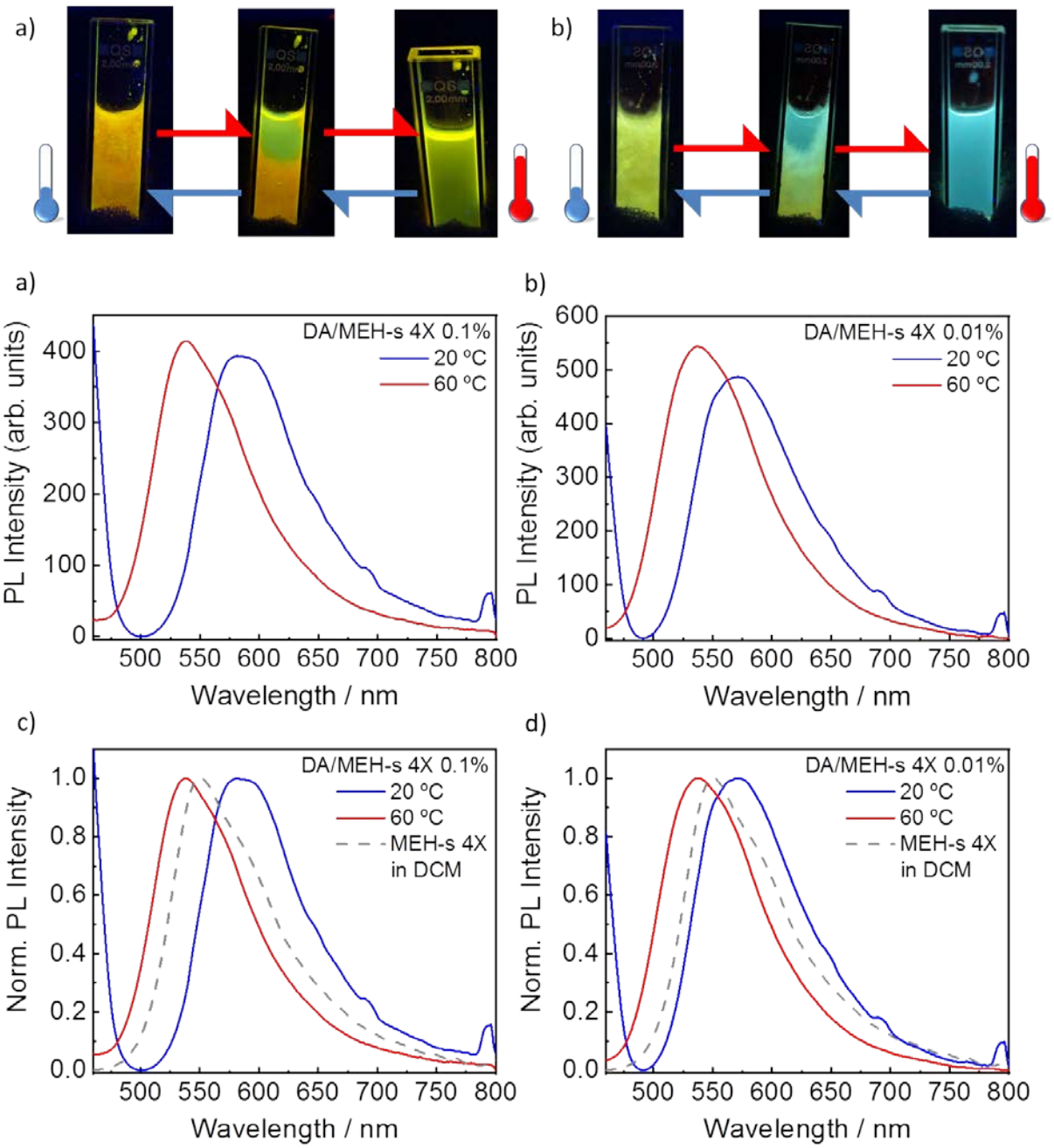

Figure 5.3. Digital camera images of *a)* DA/MEH-s 4X 0.1% and *b)* 0.01% in solid (right), liquid (left)state, and in the center the coexistence between the two phases; emission spectra of c*)* the sample DA/MEH-s 4X 0.1% and d*)* DA/MEH-s 4X 0.01% measured at 20 °C (blue line) and 60 °C (red line), e*)* normalised emission spectra of DA/MEH-s 4X 0.1% and *e)* DA/MEH-s 4X 0.01% measured at 20 °C (blue line) and 60 °C (red line) compared with the emission of MEH-s in dichloromethane (grey dash line). (Excitation at λ = 430 nm).

Eicosane

After studying the behaviour of the oligomer in solid/liquid DA, it was decided to investigate the fluorescence properties of the same oligomer in EC. In *Chapter 3* it was concluded that the lack of fluorescence switch of the MEH-PPV upon EC phase transition was due to the negligible solubility of the polymer in the PCM, in both solid and liquid state. The oligomers were tested in EC, hypothesizing that their solubility was much higher than the polymer.

During the preparation of the solutions it was observed that MEH-s 4X had a much higher solubility in EC than MEH-PPV and no phase segregation was observed. The emission of MEH-s 4X in solid EC at higher concentration (EC/MEH-s 4X 0.1%) is shown in Figure 5.4c (blue line), which is similar to the emission observed in solid DA, with a maximum at 578 nm. Upon heating, the emission increased its intensity and shifted to higher energy (λ_{max} = 532 nm). The second EC/MEH-s 4X 0.01% solution presented a similar behaviour. The emission increased its intensity upon melting and the increase was even larger than in the more concentrated sample. When the PCM is melted, the emission of MEH-s 4X 0.01% is blue-shifted from 554 to 521 nm. , a larger shift (~11 nm) than the one observed in the concentrated sample.

The normalised spectra of the two solutions (Figure 5.4e-d) compared the emission of the oligomer in EC with its emission in DCM. When the oligomer concentration is decreased, the emission in solid EC is blue-shifted. EC/MEH-s 4X 0.01% presented a maximum at 554 nm similar to the emission of the oligomer in CH_2Cl_2, indicating a good solubility of the oligomer in eicosane.

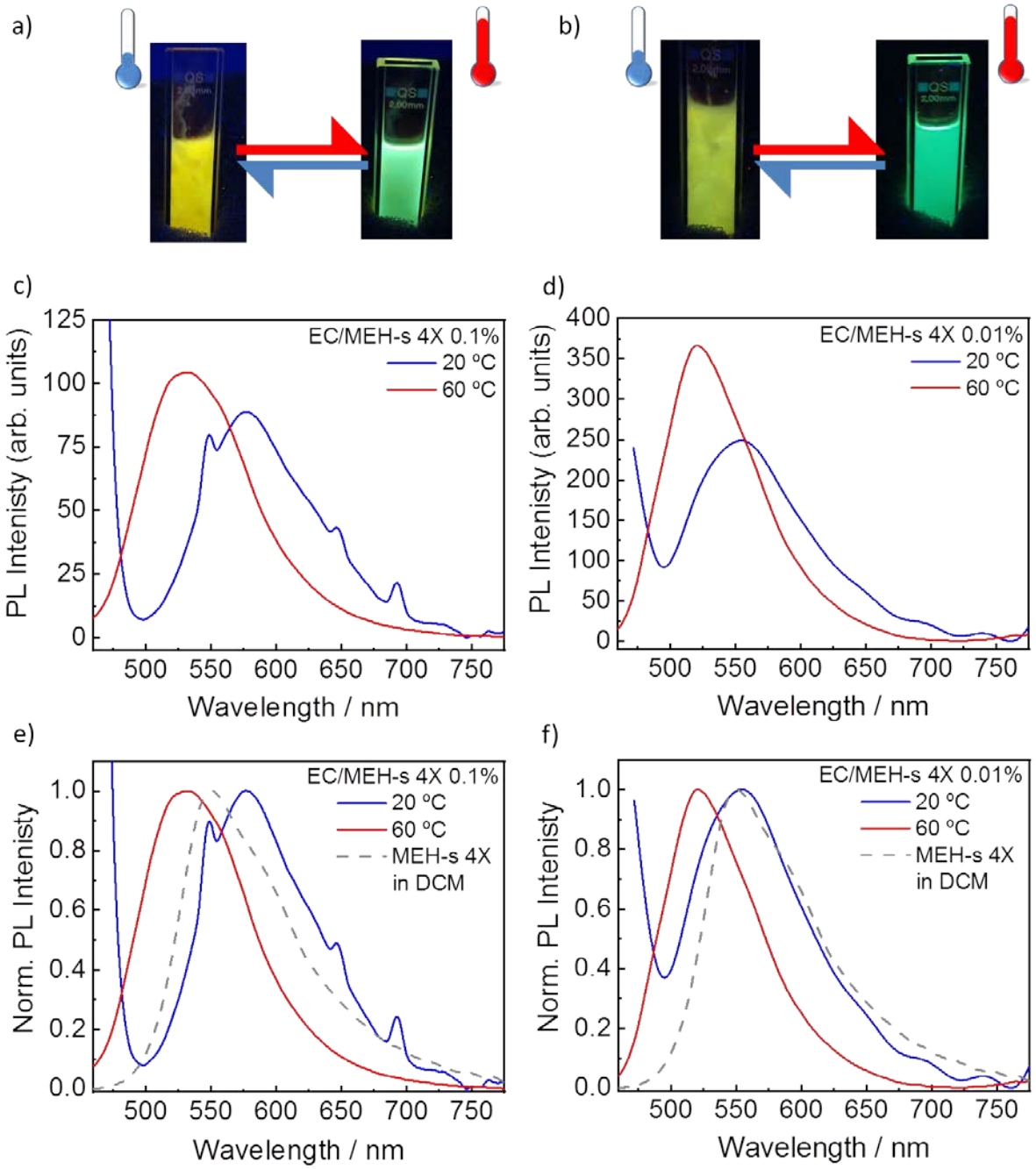

Figure 5.4. Digital camera images of *a)* EC/MEH-s 4X 0.1% and *b)* 0.01% in solid (right) and liquid (left) state *c)* emission spectra of the sample EC/MEH-s 4X 0.1% and d*)* EC/MEH-s 4X 0.01% measured at 20 °C (blue line) and 60 °C (red line), *e)* normalised emission spectra of EC/MEH-s 4X 0.1% and *f)* EC/MEH-s 4X 0.01% measured at 20 °C (blue line) and 60 °C (red line) compared with the emission of MEH-s in dichloromethane (grey dash line). (Excitation at λ=430 nm).

Hexadecane

MEH-s 4X was also tested in Hexadecane, lower T_m paraffin. The final mixed solution did not present evidence of aggregation nor phase segregation after solidification, as did occur for the pristine polymer MEH-PPV. The emission intensity of the oligomers in the most concentrated sample (HD/MEH-s 4X 0.1%) increases considerably (about three times, from 0.61×10^4 to 1.51×10^4 arb. units) on warming from 0 °C to 20 °C, with a main peak shift from 560 nm to 527 nm (Figure 5.5c). Also, the less concentrated solution was investigated (HD/MEH-s 4X 0.01%). The emission of MEH-s 4X did not change passing from the solid state (Figure 5.5d blue line) to the liquid state (red line). The intensity of the emission remains nearly the same and the blue-shifted observed in the previous samples is not present.

Figure 5.5e-f show the normalised spectra of HD/MEH-s 4x 0.1% and 0.01% compared with the emission of the oligomer dissolved in CH_2Cl_2. The emission band in solid HD/MEH-s 4X 0.1% is coincident with that found in CH_2Cl_2 (dashed grey line), with a shoulder at high energy (539 nm) is present. In sample HD/MEH-s 4X 0.01%, the main band is practically the same at 0 °C and 20 °C (523 nm and 521 nm respectively), the only difference is the weak shoulder at 551 nm present in the emission at 0 °C which disappears melting the HD. Additionally, the emission of the oligomer in both, liquid and solid, HD is blue-shifted compared with the emission in in CH_2Cl_2.

The difference between the two concentrations can be also appreciated by naked eyes, as shown by the photograph of the cuvettes with the two solutions (Figure 5.5a-b). The solid-to-liquid phase change induced an evident shift in the light emitted colour of the most concentrated sample (Figure 5.5a), while no change are present in the less concentrated (Figure 5.5b).

The comparison of the sample in PCM and DCM suggests that the oligomers in hexadecane have low tendency to aggregate, probably due to better solvation ascribing to the shorter C-atom chain of the alkane.

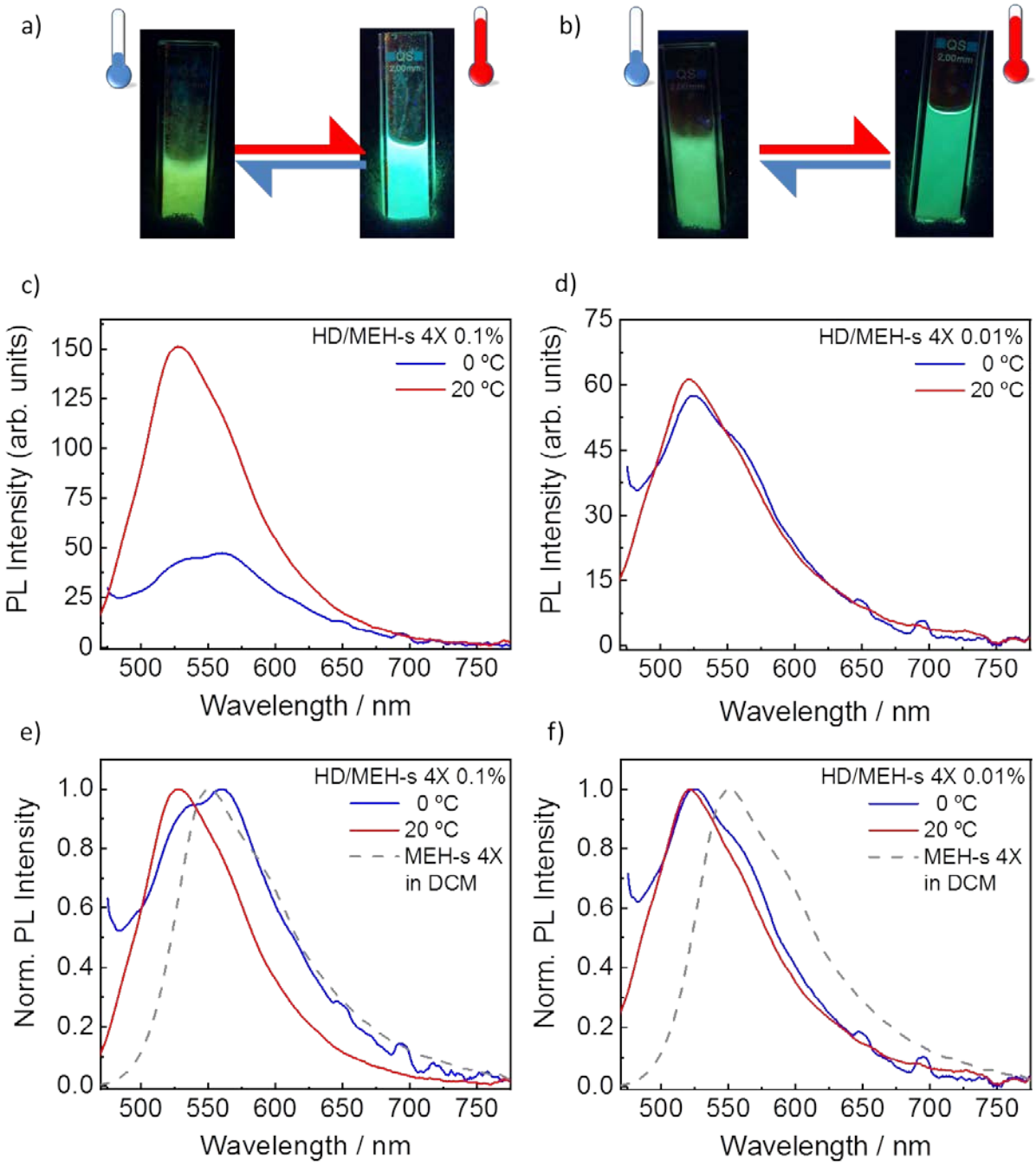

Figure 5.5. Digital camera images of *a)* HD/MEH-s 4X 0.1% and *b)* 0.01% in solid (right) and liquid (left) state *c)* emission spectra of the sample HD/MEH-s 4X 0.1% and *d)* HD/MEH-s 4X 0.01% measured at 20 °C (blue line) and 60 °C (red line); *e)* normalised emission spectra of HD/MEH-s 4X 0.1% and *f)* HD/MEH-s 4X 0.01% measured at 20 °C (blue line) and 60 °C (red line) compared with the emission of MEH-s in dichloromethane (grey dash line). (Excitation at λ=430 nm).

The change in the colour of the emitted light upon the heating of MEH-s 4X in PCMs is noticeable even at naked eyes. Figure 5.6 reports a picture where on the left there is a piece of cellulose filter paper soaked with the liquid samples EC/MEH-s 4X 0.1% and HD/MEH-s 4X 0.1%, then cooled to 4 ºC, while on the right there is a second piece of paper soaked with the samples heated above the corresponding T_m. The systems were chosen at 0.1 wt.% concentration because it was providing the largest shift in the emission properties of the MEH-s 4X, passing from solid to liquid. All samples were irradiated with a UV-lamp at 365 nm. The orange to green/yellow emission colour change, also observable at naked-eye, matched with the emission spectra of the corresponding systems in their solid (EC λ_{max} = 578 nm, Figure 5.4c and λ_{max} = 560 nm + 539 nm Figure 5.5c) and liquid state (EC λ_{max} = 532 nm, Figure 5.4c and HD λ_{max} = 527 nm Figure 5.5c). Upon heating and cooling the soaked cellulose filter paper, the green/yellow and orange emissions were repeatedly formed.

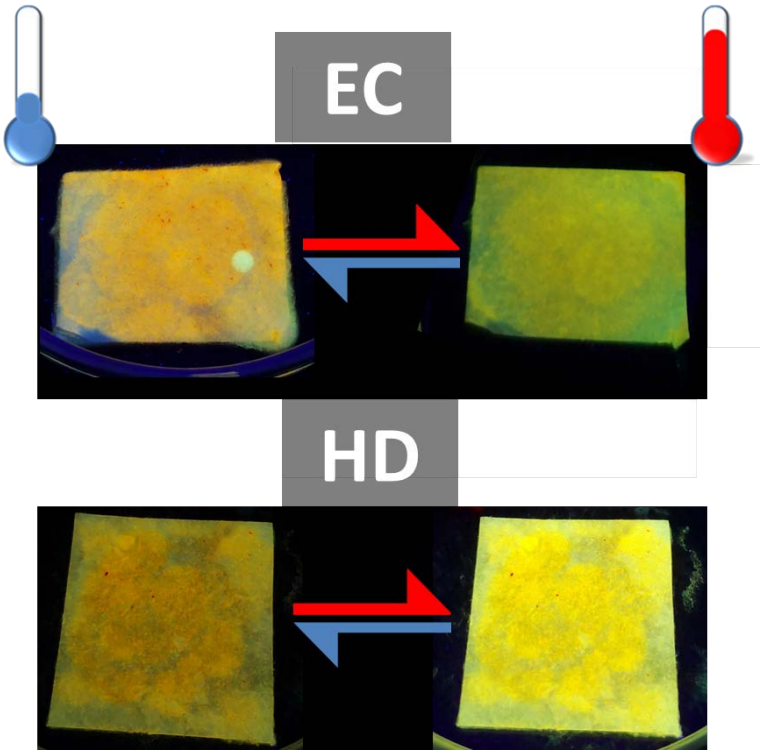

Figure 5.6 Digital camera image of four pieces of cellulose filter paper soaked with the mixture EC/MEH-s 4X 0.1% (top) and HD/MEH-s4X 0.1% (bottom). The piece on the left is kept at room temperature, while the one on the right is heated above T_m^{DA}. Both samples were irradiated with a UV-lamp at 365 nm.

Finally, the results obtained for the three different PCMs at two concentrations are summarized in Table 5.1 and analysed next. In almost all cases a large emission switch could be obtained upon melting of DA. Notably, the DA and EC mixtures of the oligomer MEH-s 4X provided larger switches than the MEH-PPV. The shifts of fluorescence found in DA and EC were very similar, with a blue shifts around 43-46 nm for the most concentrated samples

and 33-34 nm for the diluted ones. It seems to be a general tendency for the diluted sample to exhibit less marked shifts, mainly because the bands showed in the solid PCMs (DA and EC) are already more blue shifted (24 nm and 10 nm, respectively) than for the more concentrated samples. The blue shifts of the more diluted samples were related to the higher solubilisation of the oligomer and the reduction of aggregates or other types of interactions that generally produce red shifts of the bands.

The fact that in liquid EC a higher blue shift (11 nm) than in DA (1 nm) is observed for the differently concentrated solutions suggested a better solubility of the oligomer in eicosane rather than in dodecanoic acid. In the case of the HD, this is brought to the extreme condition that the two solutions (HD/MEH-s 4x 0.1% and HD/MEH-s 4x 0.01%) exhibited different behaviours. Specifically, while the HD/MEH-s 4x 0.1% showed a blue-shift of 33 nm, the less concentrated sample (HD/MEH-s 4x 0.1%) presented only 2 nm of shift. Again, similarly to what observed for EC, the negligible shift for the lower concentrated sample, was caused by the already blue shifted emission of the solid low-concentrated HD mixture. This negligible shift could be explained by a higher degree of solubility of this oligomer in HD, leading to practically no aggregates formation in the solid state at low concentration.

PCM	[Conc.]	λ_{em}^{solid} (nm)	T ºC	λ_{em}^{liquid} (nm)	T ºC	Blue-shift (nm)
Dodecanoic	0.1%	581	20	538	60	43
(T_m = 46.0 ºC)	0.01%	571		537		34
Eicosane	0.1%	578	20	532	60	46
(T_m = 36.5 ºC)	0.01%	554		521		33
Hexadecane	0.1%	560+539	0	527	20	33
(T_m = 18.2 ºC)	0.01%	523+551		521		2

Table 5.1. Emission maxima of the oligomer MEH-s dispersed in DA, EC, and HD with the oligomer concentration of 0.1% w/w, at two different temperatures to have the PCMs in liquid and solid state.

In any case, beyond all the considerations previously described, the blue-shift found for the higher concentration are high and robust enough as to establish a multi-temperature sensor. The main advantage with respect to the one described for MEH-PPV in *Chapter 3*, is the universality of this system as different PCMs of different families can be used.

5.3.2. Multiemitting devices

In the previous part, the oligomer MEH-s 4x was investigated in different PCMs. In almost all cases large spectral shifts were produced. Moreover, by changing the PCMs the switching temperature could be easily tuned. In addition of the experiments done with MEH-s 4X in different PCMs, we wanted to test other oligomers (MEH-s 2X and MEH-s 1.5X), each showing a different emission in CH_2Cl_2, in a single PCM family. It is expected that starting from oligomers of different emitting properties, multi-fluorescent switches could be obtained in different spectral regions.

MEH-s 2X

Solutions of MEH-s 2X in DA were prepared at two different concentrations of 0.1% and 0.01% w/w, following the procedure described above (for more details see Experimental Section). The emission properties of the resulting mixed solution (hereafter named DA/MEH-s 2X 0.1% and 0.01%, respectively) were investigated at two different temperatures of 20 °C and 60 °C. Figure 5.7a shows the emission spectra of the more concentrated sample DA/MEH-s 2X 0.1%. At the lowest temperature, (blue line) the system presents a broad peak with a maximum at 550 nm. When the temperature is increased up to 60 °C, the PCMs melts, and the emission from the oligomers (red line) presents a large hypsochromic shift of about 46 nm (550→504 nm) while the intensity of the emission increases considerably (approximately two times, from 3.78×10^4 to 6.38×10^4). The normalised spectra in Figure 5.7b compare the emission of the oligomer in the PCM (solid line) with the emission of the same oligomer in dichloromethane (dashed grey line). When the dodecanoic melts, the emission of MEH-s 2X (solid red line) is slightly blue shifted compared with the emission in DCM solution, similarly to what we have also observed in the previous oligomer studied. The fluorescence measurements of the less concentrated system showed similar results to sample DA/MEH-s 4X. In the solid state, the oligomers present a broad emission band with a maximum at 539 nm (Figure 5.7c blue line). Upon heating, the PCM melts and the fluorescence of the oligomers is blue-shifted to 503 nm and increase in intensity (Figure 5.7c red line). The normalised spectra reported in Figure 5.7d shows that the emission of MEH-s 2X in liquid dodecanoic acid (solid red line) is slightly blue shifted from the emission of MEH-s in DCM (dashed grey line). Moreover, the maximum is nearly at the same wavelength of the more concentrated sample (503 nm and 504 nm respectively).

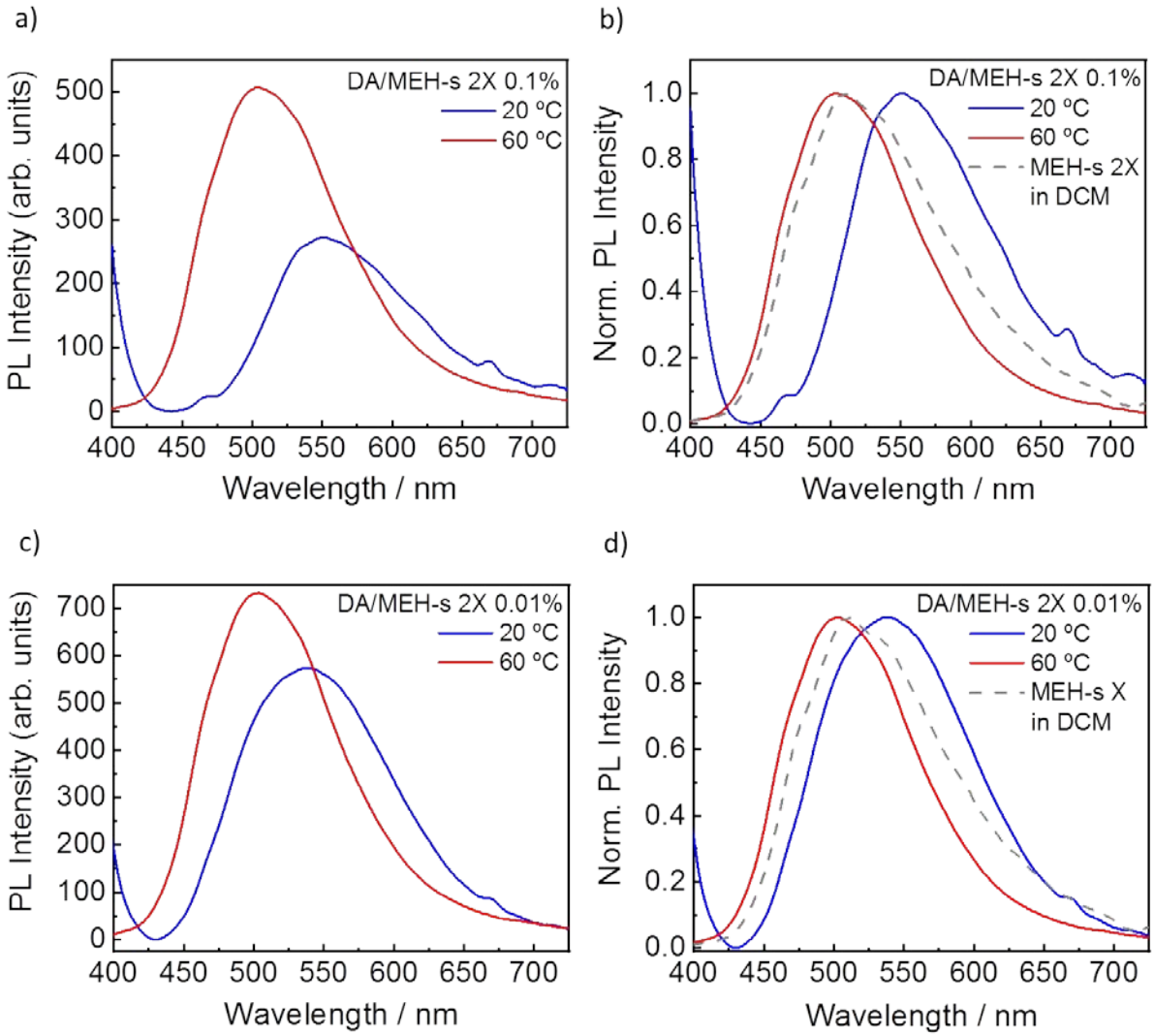

Figure 5.7. *a)* emission spectra and *b)* normalise emission spectra of the sample DA/MEH-s 2X 0.1% measured at 20 °C (blue line) and 60 °C (red line); *c)* emission spectra and *d)* normalise emission spectra of the sample DA/MEH-s 2X 0.01% measured at 20 °C (blue line) and 60 °C (red line). (Excitation at λ=390 nm).

MEH-s 1.5X

Finally, we also synthesise the shorter MEH-PPV oligomers presenting an emission in the blue region of the visible spectrum. The sample MEH-s 1.5X was obtained following the procedure described in *Chapter 2*, but varying the polymer concentration in order to match the desired blue emission (for more details see the experimental section). Nonanoic acid was selected as PCMs in order to test the oligomer in a fatty acid with the lower melting point.

The sample was characterised spectroscopically, measuring the fluorescence at room temperature and 0 °C. Figure 5.9a shows the drastic change in emission intensity passing from the solid state (blue line) to the liquid state (red line) where presents a 3-fold increase (from 0.31×10^4 to 0.98×10^4. The normalised spectra in Figure 5.9 b highlight the blue-

shifted in the oligomers emission moving from solid NA (solid blue line) with the maximum at 495 nm, to the liquid NA (solid red line) with the maximum at 478 nm. Figure 5.9b also shows that the oligomer MEH-s 1.5X in liquid nonanoic acid presents the emission at nearly the same wavelength of the oligomers dissolved in DCM (dash grey line), where the maximum is at 481 nm.

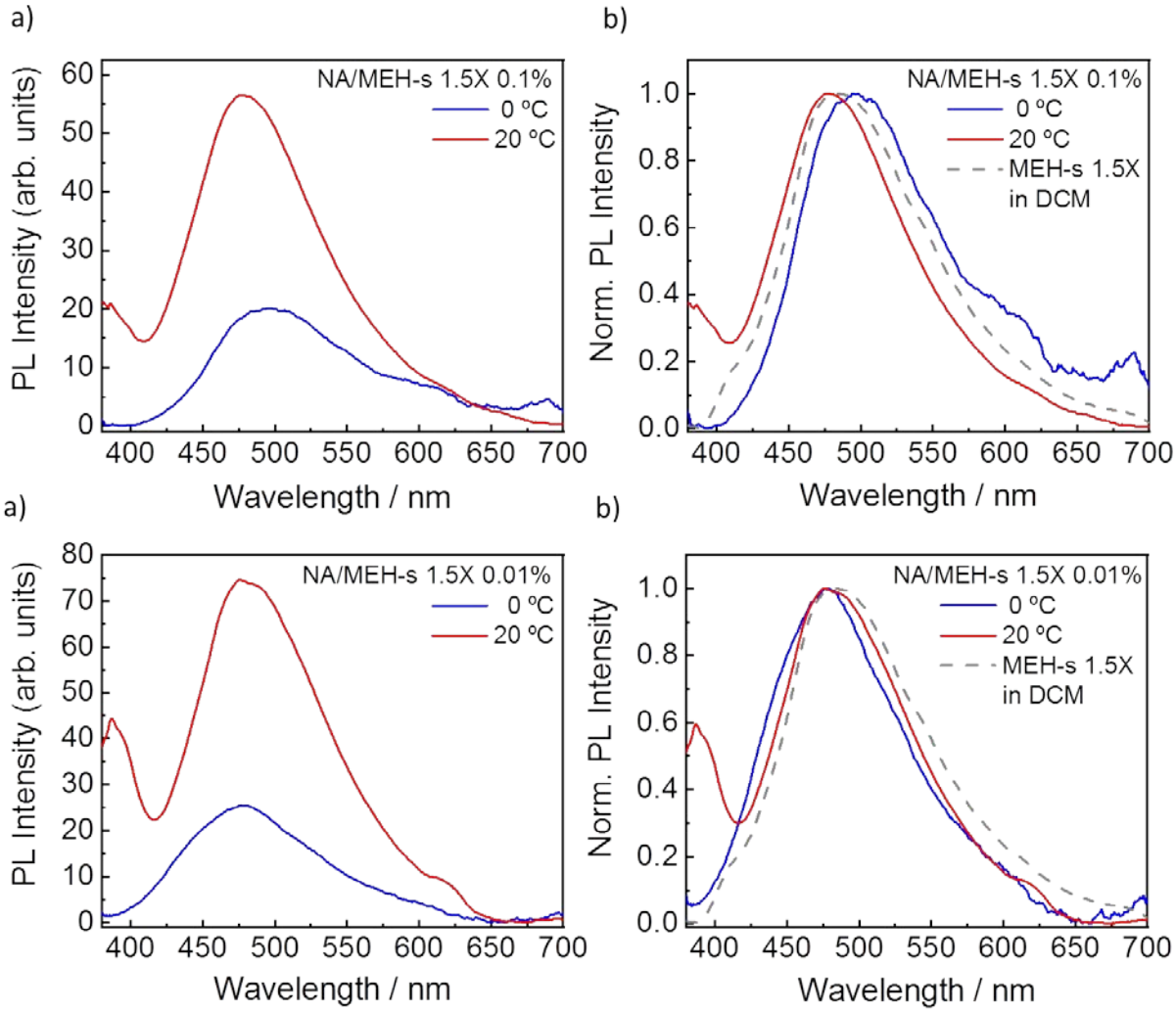

Figure 5.8. *a)* emission spectra and *b)* normalise emission spectra of the sample NA/MEH-s 1.5X 0.1% measured at 20 °C (blue line) and 60 °C (red line); *c)* emission spectra and *d)* normalise emission spectra of the sample NA/MEH-s 1.5X 0.01% measured at 20 °C (blue line) and 60 °C (red line). (Excitation at λ=365 nm).

A less concentrated solution, with oligomer content of 0.01% w/w (hereafter named as NA/MEH-s 1.5X 0.01%), was also studied. The changing in the intensity passing from the solid to the liquid phase follows the same trend of the sample NA/MEH-s 1.5X 0.1%, with an approximately 3-fold increase of the fluorescence intensity, as shown in Figure 5.9a. Contrary to what observed for the more concentrated sample, in NA/MEH-s 1.5X 0.01% the wavelength of the main peak of the emission in the liquid NA (red solid line, 475 nm) and

solid NA (blue solid line, 476 nm) coincide, as can be seen by the normalised spectra in Figure 5.9b. Interestingly, in this case, when the PCM is melted, a new band at high energies appears, with a maximum at 387 nm. A closer look at the emission spectra of MEH-s 1.5X in DCM shows a weak shoulder at higher energies which in liquid nonanoic acid becomes an intense band.

From the fluorescence spectra of the oligomers and the polymer in the respective PCMs, reported in Figure 5.9a, it can be noted that the PCMs/MEH-PPV and PCMs/MEH-s mixtures presented emission maxima compatible with the wavelengths necessary to have white emission, according to the RGB (red-green-blue) colour mode (Table 5.3). Indeed, at room temperature, SA/MEH, xx% HD/MEH-s 4X and NA/MEH-s 1.5X presents emissions in the red (619 -635 nm), green (527 nm) and blue (478 nm) regions of the spectrum, respectively. The combination of these 3 systems in the same material should provide a white emitting system. Considering that all emitting components could be achieved from the same commercially available starting material and that the solvents are based on low-cost PCM materials, this combination might have potential applicability in white emitting devices.
To do this we could hypothesise a strategy based on the encapsulation of the appropriate PCM/MEH mixtures and the embedment of these capsules inside a polymeric material, as the already showed for the model system in *Chapter 3*.

SAMPLE	CONC.	λ_{em}^{solid} (nm)	T ºC	λ_{em}^{liquid} (nm)	T ºC	Blue-shift (nm)
SA/MEH-PPV	0.1%	619	20	607+546	60	12
HD/MEH-s 4X	0.1%	560+539	20	527	60	33
NA/MEH-s 1.5X	0.1%	495	0	478	20	17

Table 5.2. Emission maxima of the sample DA/MEH-PPV, EC/MEH-s 4X, and NA/MEH-s 1.5X with the oligo-/polymer concentration of 0.1% w/w, at two different temperature to have the PCMs in liquid and solid state.

Colour	Range of λ	Optimal λ
Red	620-645 nm	627 nm
Green	520-550 nm	530 nm
Blue	460-490 nm	470 nm

Table 5.3. Wavelengths range and optimal value necessary for the RGB colour model.

Figure 5.9 reports the emission spectra of the three dispersions highlighting the appropriate wavelength of the maxima for the RGB system. Depositing the samples NA/MEH-s 0.5X, NA/MEH-s X and DA/MEH in three different microscope glass slides is possible to appreciate the colour of the light emitted from the three samples.

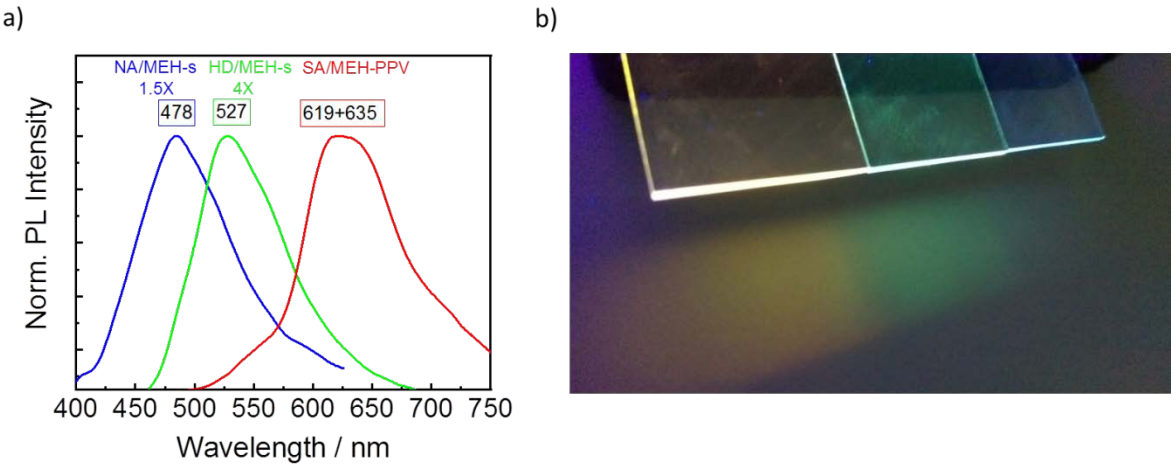

Figure 5.9. *a)* emission spectra of the oligomer MEH-s 1.5X in nonanoic acid (blue line) with a maximum at 478 nm, emission spectra of the oligomer MEH-s 4X in hexadecane (green line) with a maximum at 527 nm and emission spectra of the polymer MEH-PPV in stearic acid (red line) with a broad maximum between 619 nm and 635 nm. All the spectra were measured at room temperature, exciting to the absorption maximum of each molecule. *b)* Picture of the three samples deposited over glass microscope slides and excited with a UV-lamp (365 nm) to show the RGB emission.

However, the simultaneous use of oligomers with different temperature-tuneable emissions dissolved in PCMs presenting different melting points could be used to fabricate a multicolour temperature sensor. Such sensor could detect different specific temperatures which would be distinguished by the different colours of the light emitted and different emission shifts provided by the different oligomers. The versatility of the multicoloured oligomers offers an important advantage compared with the MEH-PPV, where all the samples exhibit similar emission with slight shifts (*Chapter 3*).

Figure 5.10 shows the sheets of filter papers where the mixture of SA/MEH 0.1%, DA/MEH 0.1%, EC/MEH-s 4X 0.1%, HD/MEH-s 1.5X 0.1% of the polymer and two different oligomers with different PCMs were deposited. The samples, heated at heated at 0 °C, 40 ºC and 70 ºC and irradiated with UV-lamp (365 nm), showed different emitted colours at each set temperature. Thanks to the combination of different PCMs and distinct oligomers and MEH-PPV the light emitted from the four different system sequentially shift from red-orange to yellow-green. Only the sample HD/MEH-PPV did not show a shift appreciable to naked eyes.

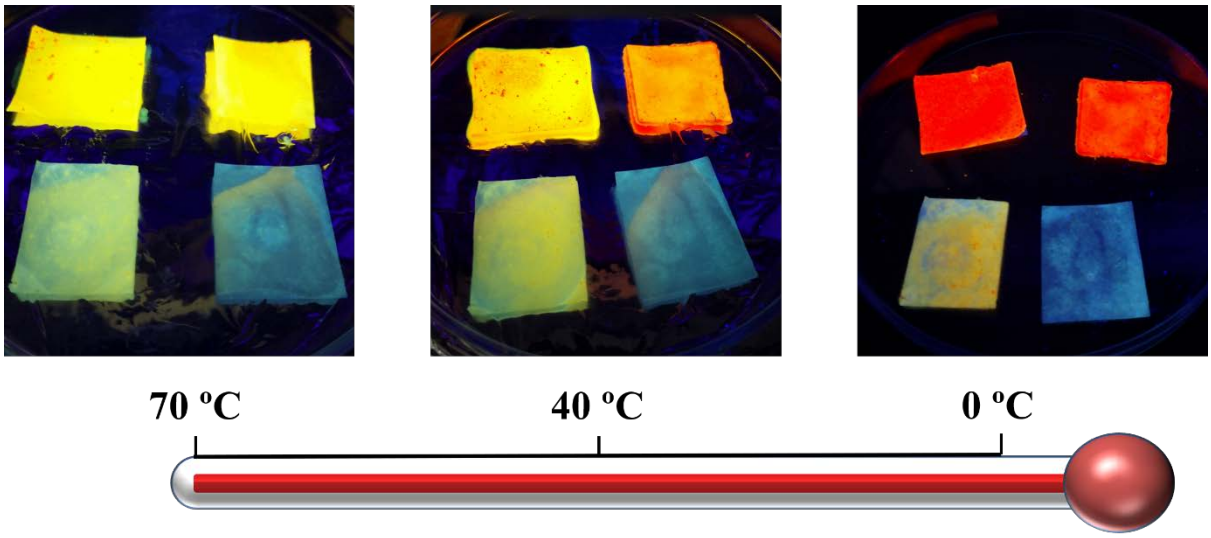

Figure 5.10. Picture of different mixtures of oligo PPV and MEH-PPV with PCMs deposited over pieces of filter paper. The samples were heated at 0 °C, 40 ºC, and 70 ºC and irradiated a 365 nm. On the top-left the sample deposited is the MEH-PPV in DA, on the top-right the sample deposited is the MEH-PPV in SA, on the bottom left the sample deposited is the MEH-s 4X in EC and bottom-right the sample deposited is the MEH-s 1.5X in HD. At the 0ºC, all the PCMs are in the solid phase, at 40ºC, all the PCMs are in the liquid phase except the stearic acid, at 70ºC, all the PCMs are in the liquid phase.

5.4. SUMMARY

In conclusion, the experiments with the oligomers MEH-s and PCMs showed a similar trend to the one already observed for PCMs/MEH-PPV. The emission of the sample MEH-s is blue-shifted passing from the solid to liquid phase of the PCMs, in particular, the sample MEH-s 4X and 2X exhibited an important shift of the emission maxima (higher than 30 nm). Moreover, the oligomers exhibited good solubility in both fatty acids and paraffins. These data confirmed the suitability of the PCMs/MEH-s system to be used as temperature sensors, and the different colour of the light emitted by the oligomers open the possibility to build a colourimetric temperature sensor.

A further application of these systems relies on the fine tune of the light emitted by the oligomers at known temperature combined with heat capacity of the PCMs which could be exploited for a white light system.

5.5. EXPERIMENTAL SECTION

PREPARATION OF THE DISPERSIONS

Preparation of the DA/MEH-s 4X mixture.

The oligomers MEH-s were obtained following the procedure already described in *Chapter 4*. MEH-PPV chloroform solutions (at the suitable concentration to obtain the specific oligomer, $3 \times 10^{-3} M$, 4 * 10^{-3} M, and 8 * 10^{-3} M) were sonicated in presence of Milli-Q® water, without the surfactant. The organic phase was collected and the solvent was evaporated under vacuum. The precipitated was dissolved in CH_2Cl_2 and filtered using a nylon syringe filter (0.2 µm pores) to remove aggregates. The final solution should contain approximately 1 mg/ml of MEH-s.

The solutions PCM/MEH-s 0.1% were prepared adding the oligomer solution (1 ml) to 1 g of PCM in a glass vial so to have a final concentration of 0.1% w/w. The PCM solutions of the oligomers were placed in a sonicating water bath for 30 minutes to improve the oligomer solubilisation. The organic solvent was evaporated placing the vial with the solution in a hot plate heating at 10 °C above the T_m^{PCM} and stirring overnight. The evaporation of the solvent led to a clear coloured liquid (the colour depended on the MEH-s) with no apparent formation of aggregates. Once the mixtures were cooled to 20 °C, those made by PCMs with T_m^{PCM} >

RT, turned solid without producing phase segregation between the oligomer and PCM. Those made by PCMs with T_m^{PCM} < RT gave homogenous liquid solution, without segregation. Upon cooling at T < T_m^{PCM}, no phase segregation was observed either.

The solutions PCM/MEH-s 0.01% were prepared, in a glass vial, adding 900 mg of PCM to 100 mg of the solution PCM/MEH-s 0.1%. Successively, 2 ml of DCM were added to the mixture to obtain a homogeneous mixture. The solution was placed in a sonicating water bath so to improve the dissolution of the oligomer in the PCM. Finally, the organic solvent was evaporated by heating at 10 ºC above the T_m^{PCM} and stirring the solution overnight.

5.6. REFERENCES

1. Wang, X. D. & Wolfbeis, O. S. Fiber-Optic Chemical Sensors and Biosensors (2013-2015). *Anal. Chem.* **88,** 203–227 (2016).

2. Baleizão, C. *et al.* An optical thermometer based on the delayed fluorescence of C70. *Chem. - A Eur. J.* **13,** 3643–3651 (2007).

3. Uchiyama, S., Matsumura, Y., De Silva, A. P. & Iwai, K. Fluorescent Molecular Thermometers Based on Polymers Showing Temperature-Induced Phase Transitions and Labeled with Polarity-Responsive Benzofurazans. *Anal. Chem.* **75,** 5926–5935 (2003).

4. Wang, S., Westcott, S. & Chen, W. Nanoparticle luminescence thermometry. *J. Phys. Chem. B* **106,** 11203–11209 (2002).

5. Shiraishi, Y., Miyamoto, R., Xuan, Z. & Hirai, T. Rhodamine-based fluorescent thermometer exhibiting selective emission enhancement at a specific temperature range. *Org. Lett.* **9,** 3921–3924 (2007).

6. Crenshaw, B. R., Kunzelman, J., Sing, C. E., Ander, C. & Weder, C. Threshold temperature sensors with tunable properties. *Macromol. Chem. Phys.* **208,** 572–580 (2007).

7. Donati, F., Pucci, A., Boggioni, L., Tritto, I. & Ruggeri, G. New cyclic olefin copolymer for the preparation of Thermally Responsive luminescent filmsa. *Macromol. Chem. Phys.* **210,** 728–735 (2009).

8. Navigant Consulting. *U.S. lighting market characterization; Volume I: National lighting inventory and energy consumption estimate*. *Renewable Energy* **I,** (2002).

9. D'Andrade, B. W. & Forrest, S. R. White organic light-emitting devices for solid-state lighting. *Adv. Mater.* **16,** 1585–1595 (2004).

10. Forrest, S. R. The path to ubiquitous and low-cost organic electronic appliances on plastic. *Nature* **428,** 911–918 (2004).

11. Granström, M. & Inganäs, O. White light emission from a polymer blend light emitting diode. *Appl. Phys. Lett.* **68,** 147–149 (1996).

12. Chao, C. I. & Chen, S. A. White light emission from exciplex in a bilayer device with two blue light-emitting polymers. *Appl. Phys. Lett.* **73,** 426–428 (1998).

13. Tsai, M. L., Liu, C. Y., Hsu, M. A. & Chow, T. J. White light emission from single component polymers fabricated by spin coating. *Appl. Phys. Lett.* **82,** 550–552 (2003).

14. Kido, J., Shionoya, H. & Nagai, K. Single-layer white light-emitting organic electroluminescent devices based on dye-dispersed poly(N-vinylcarbazole). *Appl. Phys. Lett.* **67,** 2281–2283 (1995).

15. Tanaka, I., Suzuki, M. & Tokito, S. White light emission from polymer electrophosphorescent light-emitting devices doped with iridium complexes. *Jpn. J. Appl. Phys.* **42,** 2737–2740 (2003).

16. Zukauskas, A., Vaicekauskas, R., Ivanauskas, F., Shur, M. S. & Gaska, R. Optimization of white all-semiconductor lamp for solid-state lighting applications. *Int. J. High Speed Electron. Syst.* **12,** 429–437 (2002).

17. Muthu, S., Schuurmans, F. J. P. & Pashley, M. D. Red, green, and blue LEDs for white light illumination. *IEEE J. Sel. Top. Quantum Electron.* **8,** 333–338 (2002).

18. Chhajed, S., Xi, Y., Li, Y. L., Gessmann, T. & Schubert, E. F. Influence of junction temperature on chromaticity and color-rendering properties of trichromatic white-light sources based on light-emitting diodes. *J. Appl. Phys.* **97,** (2005).

CHAPTER

6

THESIS CONCLUSIONS

The main conclusions of this thesis are:

1. PCMs have been successfully used to reversibly switch the emission of the MEH-PPV thanks to its differential interactions with the solid and liquid states, controlled by temperature changes. Though successful, the low solubility and the tendency to aggregate of this polymer in non-polar PCMs has restricted its activity to fatty acids PCMs. This limitation has been solved by replacing MEH-PPV polymer by its more soluble and miscible oligomers obtained by controlled ultrasonication.

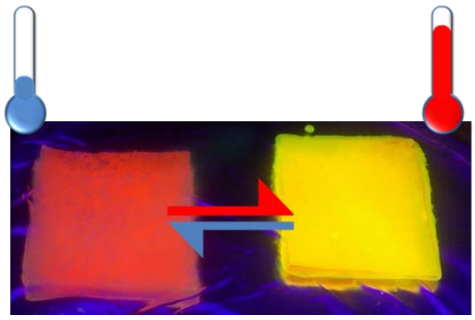

2. The reproducibility of the reversible temperature-induced fluorescence switch for MEH-PPV in three fatty acids of different melting temperatures was used to establish a temperature sensor that selectively discriminates between three well-defined temperature ranges. The use of selected oligomers with markedly different emission wavelengths allowed us to develop a related temperature sensor with multichromophoric responses.

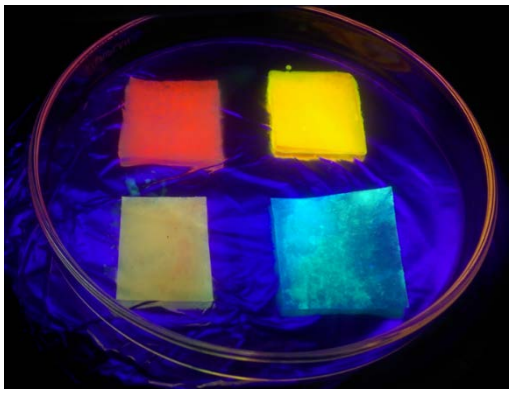

3. To integrate these systems into a free-standing film without compromising the switchable emission properties, we proposed to confine them PCM/MEH-PPV micro/nanostructures. Though many MEH-PPV/PCM encapsulation methodologies and conditions were attempted most of them revealed unsuccessful, except the microstructuration as solid lipid microparticles. Such could be incorporated into free-standing films retaining the reversible switchable properties bulk solutions.

4. Oligomers with different chain lengths were generated starting from a chloroform solution of the commercially available MEH-PPV polymer. We demonstrated that the shortening of the polymer chain and, consequently of the conjugation length, could be obtained upon the ultrasound-induced formation of the reactive hypochlorous acid in a water/chloroform mixed solution.

5. The oligomeric species can be nanostructured at the same time of their formation, by sonicating the water/chloroform mixed mixture in the presence of a surfactant that stabilizes the nanoemulsion. The resulting nanoparticles exhibited tuneable light emission spread from the red to the blue region (from λ_{max}= 597 nm to λ_{max}= 481) of the visible electromagnetic spectrum. The selection of the nanoparticles with the proper wavelength is of interest to explore future tuneable light emitting devices.

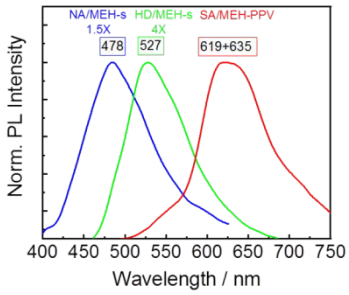

6. The resulting nanoparticles could be embedded in polymeric matrices to obtain flexible fluorescent polymeric films.

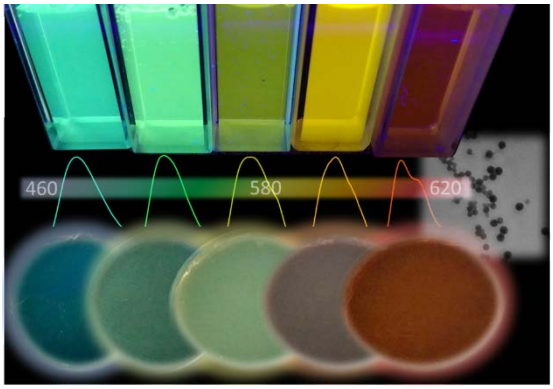

CHAPTER

7

CHARACTERISATION TECHNIQUES

Scanning electron microscopy (SEM).

SEM images were collected on the scanning electron microscope FEI Quanta 650 FEG at acceleration voltages between 2-10 kV. Samples were mounted on SEM metal stubs covered with aluminum or carbon tape and they were coated with a thin layer of platinum (~ 5 nm), except for samples whreon energy dispersive X-ray spectrometry (EDX) were performed. EDX analysis was carried out using secondary electron mode at acceleration voltage of 20 kV. Nanoparticles suspensions or sample solutions (100 μL) were deposited on the stub by drop casting, allowing solvent evaporation in air at room temperature. For solid powders approximately 1 mg of sample was deposited on the adhesive carbon tape.

Transmission electron microscopy (TEM).

TEM images were collected on the electron microscope Hitachi H-7000 operated at 75kV. The samples were prepared by dropcasting 10 μL of suspension on top of TEM grid (ultrathin carbon type-A, 400 mesh, copper, approx. grid hole size 42 μm) and allowing the water evaporating in air at room temperature.

UV−vis spectroscopy.

Absorption spectra of the organic solutions and water suspensions were registered in the Agilent Cary 60 spectrophotometer using a 1x1 cm quartz cuvette. The solvent was used as blank in each measurement. The CPNs_X-10X@PVA films were measured by placing the integrating sphere (Agilent Cary 60 remote diffuse reflectance accessory, DRA) directly on top of the film. For these measurements the reference sample consisted of the white polytetrafluoroethylene (PTFE) standard. The Kubelka-Munk equation ($F(R) = (1–R)^2/2R$)[65] was used to estimate the absorption spectra from the experimental diffused reflectance spectra.

Steady state emission.

Emission spectra of the organic solutions and water suspensions were recorded through the PTI QuantaMaster 300 phosphorescence/fluorescence spectrophotometer (Horiba

Ltd.). The measurements of the samples in solution were carried out in 1x1 cm square quartz cuvette. The CPNs_X-10X@PVA films were measured in front face mode, placing a portion of the film (1 cm x 2 cm) in the cuvette holder at 45 º respect to the incident radiation beam. The samples of polymer and oligomers in PCMs were measured in a triangular 1 x 1 cm cuvette, placed at 45º from exciting light source to detection direction. The sample temperature was controlled through a recirculating thermostat (Huber MPC-K6) coupled to the sample holder.

Fluorescence relative quantum yields (Φ_f).

Quantum yields of the oligomer $CHCl_3$ solutions (A_{355} = 0.05) were obtained recording the emission spectra with a custom-made spectrofluorometer (rectangle mode), where an Andor CCD camera is coupled to a spectrograph. The fluorescence quantum yields of water suspensions of CPNs were obtained measuring the emission spectra (front face mode) with the PTI QuantaMaster 300 phosphorescence/fluorescence spectrophotometer (Horiba Ltd.). In all cases an ethanol solution of DPA (Φ_f^{EtOH} = 0.95)[66] was used as reference.

FT-IR spectroscopy

FT-IR spectra of the sample powder (2 mg) were recorded by using a Tensor 27 (Bruker) spectrophotometer equipped with a single-reflection diamond window ATR accessory (MKII Golden Gate, Specac).

X-Ray photoelectron spectroscopy (XPS).

The spectra were recorded at room temperature on a high-resolution texture diffractometer (PANalyticalX′Pert PRO MRD) equipped with a CoKα radiation source (λ= 1.7903 Å) and operating in reflection mode. The solid samples were placed in an amorphous silicon oxide flat plate and measured directly.

Proton nuclear magnetic resonance spectroscopy (1H-NMR).

^{1}H-NMR spectra were performed from 10 mg of sample dissolved in $CDCl_3$ or THF-d_8. All samples were recorded at 298 K on a Bruker Avance spectrometer operating at 400

MHz (Bruker DPX400) for the proton signal acquisition. The spectra are given in chemical shifts, δ (ppm). The DOSY spectra were acquired with the ledbpgp2s pulse program from Bruker topspin software. The diffusion dimension of the 2D DOSY spectra and DOSY maps were processed by means of the Bruker topspin software (version 3.5). ^{1}H-NMR spectra were processed and visualized with MestReNova software.

Gel permeation chromatography (GPC).

The measurements were performed on an Agilent 1260 Infinity GPC/SEC system, with a guard column before the two analytical columns (PL Mixed gel C, 5 microm column and PL gel, 5 microm, 10.000 A column), using THF as solvent and a refractive index detection system. 40 μL of the sample were injected and eluted at a flow of 1 mL/min at 30 ºC. For calibration polystyrene standards were used.

FT-Raman spectroscopy.

FT-Raman spectra were recorded by using a FT-Raman accessory kit (RamII) of a Bruker Vertex 70 FT-IR interferometer and a continuous-wave Nd:YAG laser (λ_{exc} = 1064 nm). A germanium detector operating at liquid-nitrogen temperature was used and the Raman scattering radiation was collected in a back-scattering configuration with a 4 cm^{-1} spectral resolution. An average of 1000 scans was used in the reported spectra.

Differential Scanning Calorimetry (DSC).

DSC measurements were carried out in a TA Instruments Q20 differential scanning calorimeter. Approximately 5 mg of the sample were deposited on the 0.5 cm-indiameter aluminum pan. An empty pan was used as a reference. The scanning rate was 10 K/min for both the heating and cooling processes. The scanned temperature range depended on the sample

Dynamic Light Scattering (DLS).

The average particle size were performed with dynamic light scattering method using Malvern Zetasizer (Nano ZS, Malvern Instruments, U.K.). The particle size values were

obtained by averaging of 16 measurements for 3 cycles at an angle of 173° at 25 °C using glass cells.